Scattering resonances and Pseudospectrum : stability and completeness aspects in optical and gravitational systems

Lamis Al Sheikh

Université de Bourgogne Franche-Comté
Institut de Mathématiques de Bourgogne, UMR 5584, CNRS5
Ecole doctorale Carnot-Pasteur

THÈSE

pour l'obtention du grade de

Docteur de l'Université de Bourgogne
en Mathématiques

présentée et soutenue publiquement par

Lamis Al Sheikh

le 10 Janvier 2022

Scattering resonances:
stability and completeness aspects in optical and gravitational potentials

Directeur de thèse: **José Luis Jaramillo**

Rapporteurs

Prof. Jean-Philippe Nicolas

Prof. Carlos F. Sopuerta

Jury composé de

Dr.Yann Boucher

Prof. Dietrich Häfner

Dr. Rodrigo Panosso Macedo

Prof. Gérard Colas des Francs

Dr. Lysianne Hari

Prof. Carlos F. Sopuerta

This work is dedicated to my mother and to the memory of my father.

Acknowledgment

First of all I would like to thank Gitter. I discovered his work in the German notebook of Marcus Ansorg, he provided a full settings for the numerical work I followed. Then I would like to thank my supervisor Prof.José Luis Jaramillo for telling me after many months of working with Gitter that Gitter in German means grid, I simply thought it's a name of a person.
Seriously, let us start again.

I would like to express my genuine heartfelt gratitude to **José Luis Jaramillo** for the exceptional supervision work. Aside from disponibility, joyful passionate interesting discussions, guidance and support on all levels, I would not make it and present my work today without his persistence and patience, friendly attitude and management skills.
My profound thanks to all the members of my PhD jury for accepting being engaged and for the big effort and time.
Dr. Rodrigo Panosso Macedo has been of a big help and source of knowledge to this PhD, thank you Rodrigo for the good discussions, professionalism and patience.
I can not thank enough Yann Boucher for the constant inestimable support he has been providing since my master of photonics that he supervised. Thanks to you Yann also for being in the comité de suivi la thèse.. I am so thankful to Prof.Gérard Colas de Franks who followed this PhD work and had always his door open for all kind of discussions.
I would also like to express my sincere appreciation to Giuseppe Dito who was my teacher in the master of Mathematics in Dijon for being supportive and for the always finding time for questions and discussions.
My work in Bordeaux in LP2N was an essential part in my journey to validate finally this thesis. I am thankful to Kévin Vynck for his close kind supervision in my early steps in research there and of course many thanks to Philippe Lalanne from whom I learned a lot.

I would like to acknowledge Rémi Mokdad Mokdad and Edgar Gasperin Garcia for the good discussions and the friendly relationship.
I am also thankful to M.Jourani the lab director for assuring a positive work environment in Institut de Mathématiques de Bourgogne (IMB). Of course many thanks to Anissa Bellaassali, Magali Crochot, Françise léger and Aziz too.
A big thanks to Mr. Hans Jauslin the director of the Ecole doctorale of Carnot−Pasteur who was always there for any relevant issue and to the members of the interesting "groupe de travail" between IMB and ICB.
My profound thanks to PhD students in IMB. Sharing the office with Umar Mohammed and Helal Aldarak made the hardest moments funny. My sincere thanks to Mireille, Ajenkya, Oscar and Francisco for being good friends and for sharing nice moments.

I would like to express my deepest gratitude to my father who is a key stone to what I am today, unfortunately he passed away few months before. My limitless gratitude to my beloved great hearted mother. A big thanks to my kind elder brother Youssef. And of course to my old sister Waad, her husband Mussab Zneika. Both of them are behind opening me the opportunity to come to France to continue my studies, a punch of thanks for all the support they have been providing.
A particular thanks to my little sister Lujein who always succeed in making me smile even in hardest times, thanks for her confidence in me.

The sweetness thanks to my cute nieces, my little friends Naya and Nasha and to my polite nephews Aram and Karam.
My sincere thanks to my friends Samah, Yara and Yana in Damascus. A big thanks also to Hassan Darwich for being a good friend.
My sincere thanks to Tarek Kasmieh for his support and encouragement.
Many contributed positively in shaping my life till reaching this point, I am not able to mention all.

Abstract

The general context of this thesis is an effort to establish a bridge between gravitational and optical physics, specifically in the context of scattering problems using as a guideline concepts and tools taken from the theory of non-self-adjoint operators. Our focus is on Quasi-Normal Modes (QNMs), namely the natural resonant modes of open leaky structures under linear perturbations subject to outgoing boundary conditions. They also are referred to as scattering resonances.

In the conservative self-adjoint case the spectral theorem guarantees the completeness and spectral stability of the associated normal modes. In this sense, a natural question in the non-self-adjoint setting refers to the characterization and assessment of appropriate notions of QNM completeness and spectral stability in open non-conservative systems. This defines the general objective of this thesis. To this aim, and in contrast with the traditional approach to scattering resonances, we adopt a methodology in which QNMs are cast as a spectral problem of an appropriate non-self-adjoint operator. Specifically this methodology is based on following three ingredients:

(i) *Hyperboloidal approach:* The hyperboloidal slicing approach is already used in gravitational problems, we introduced it here to optical ones. The idea is to study the wave equation in hyperbolic slices instead of usually used Cauchy slices. The system of coordinates is more adapted to the problem of QNMs and its outgoing boundary conditions, in particular addressing the exploding modes in the Cauchy approach. The modes are normalizable in such coordinates and working in these slices eliminate the need of imposing the outgoing boundary conditions.

(ii) *Pseudospectrum of an operator:* the notion of ϵ-pseudospectrum allows to assess the (in)stability of eigenvalues of an operator in the complex plane due to a perturbation to the operator of order ϵ. This thesis introduces the notion of pseudospectrum in gravitational and optical physics in the vicinity of the eigenvalues.

(iii) *Numerical Chebyshev spectral methods:* On the technical level, spectral methods provides an efficient tool when translating the problem into a numerical one. In particular we used Chebyshev basis to expand our fields.

The results of this work touch three areas:

(i) *The instability of QNMs for some class of potentials.* The fundamental modes are stable specially under small "high frequency" perturbations, whereas overtones are sensitive to such perturbations. The instability of the overtones increases as their imaginary part grows.

(ii) *The universality of the asymptotic behaviour of QNMs and pseudospectrum.* We remark an asymptotically logarithmic behavior of pseudospectrum contour lines and bounding the opening QNMs branches from below.

(iii) *QNMs expansion.* We revisit Lax & Phillips asymptotic resonant expansions of a "scattered field" in terms of QNMs in our physical settings. In particular , we make use of Keldysh expansion of the generalizations of the expressions for normal modes of conservative systems, specifically in terms of normalizable QNM eigenfunctions and explicit expressions for the excitation coefficients.

Résumé

Le contexte général de cette thèse est un effort pour établir un pont entre la physique gravitationnelle et optique, spécifiquement dans le contexte des problèmes de diffusion à l'aide des concepts et des outils tirés de la théorie des opérateurs non auto-adjoints. Nous nous concentrons sur les modes quasi-normaux (MQN), appelés les modes de résonance naturels des structures à fuites ouvertes sous des perturbations linéaires soumises à des conditions de bords sortantes. Ils sont également appelés résonances de diffusion. Dans le cas auto-adjoint conservateur, le théorème spectral garantit la complétude et la stabilité spectrale des modes normaux associés. En ce sens, une question naturelle dans le cadre de non auto-adjoint est reliée à la caractérisation et à l'évaluation des notions appropriées de complétude de MQNs et de stabilité spectrale dans les systèmes ouverts non conservateurs. Ceci définit les objectifs de cette thèse. Pour ce faire, et contrairement à l'approche traditionnelle des résonances de diffusion, nous adoptons une méthodologie dans laquelle les MQNs sont présentés comme un problème spectral d'un opérateur approprié non auto-adjoint. Plus précisément, cette méthodologie est basée sur les trois ingrédients suivants :

(i) *L'approche hyperboloïdale:* L'approche en tranchant hyperboloïdales est déjà utilisée dans les problèmes gravitationnels, nous l'avons introduite dans les problèmes optiques. L'idée est d'étudier l'équation d'onde en tranches hyperboliques au lieu des tranches de Cauchy habituellement utilisées. Le système de coordonnées est plus adapté à la problématique des QNMs et de ses conditions aux limites sortantes, en particulier, aborder les modes explosifs dans l'approche de Cauchy. Les modes sont normalisables en de telles coordonnées et travailler dans ces tranches éliminent le besoin d'imposer les conditions de bords sortantes.

(ii) *Pseudospectre d'un opérateur:* la notion de ϵ-pseudospectre permet d'évaluer la (in)stabilité des valeurs propres d'un opérateur dans le plan complexe en raison d'une perturbation de l'opérateur d'ordre ϵ. Cette thèse introduit la notion de pseudospectre en physique gravitationnel et optique au voisinage des valeurs propres.

(iii) *Au niveau technique,* les méthodes spectrales fournissent un outil efficace pour traduire le problème en un problème numérique. En particulier, nous avons utilisé la base de Chebyshev pour l'expansion des nos champs.

Les résultats de ce travail touchent trois domaines :

(i) *L'instabilité des MQN pour certaines classes de potentiels.* Les modes fondamentaux sont stables spécialement sous de petites perturbations "à haute fréquence", alors que les harmoniques sont sensibles à de telles perturbations. L'instabilité des harmoniques augmente à mesure que leur partie imaginaire grandit.

(ii) *L'universalité du comportement asymptotique des MQNs et du pseudospectre.* Nous remarquons un comportement asymptotiquement logarithmique des lignes de contour du pseudospectre et délimitant les branches d'ouverture des MQNs par le bas.

(iii) *MQNs expansion.* Nous revisitons les expansions résonantes asymptotiques de Lax & Phillips d'un "champ diffusé" en termes de MQNs pour nos problèmes physiques. En particulier, nous utilisons le développement de Keldysh des généralisations des expressions pour les modes normaux des systèmes conservateurs, spécifiquement en termes de fonctions propres MQN normalisables et d'expressions explicites pour les coefficients d'excitation.

Contents

Part I

Part one: Conceptual mathematical and physical frame

Chapter 1

Scattering theory and resonators: problems and objectives

Contents

Quasi-normal modes (QNMs) is a subject of a big excitement nowadays. It makes an indispensable part of undergoing studies in many domains of physics. In particular in gravitational physics, optics, as well as in acoustics oceanography ... The huge interests that is carried to these QNMs in scientific world come from its importance and necessity to understand and describe phenomena related to open systems. Underneath the physics of QNMs in different domains, there is the same essential mathematical problem related in an ultimate manner to non-self adjoint operators, where QNMs are known in mathematics, specially in the community working on affine topics to spectral analysis as scattering resonances.
Simulations and numerical results in nano optics have shown the efficiency of describing a scattered field around a nano resonator as an expansion over QNMs. On the other hand, there still is lack of a rigorous mathematical understanding behind this efficiency. Many issues related to QNMs still wait answers and need to be regarded more rigorously. For example: what is the eventual error function for the expansion of the scattered field in terms of QNMs? Under which conditions and in which sense do these modes form a complete basis in some space endowed with some specific scalar product.
In the general relativity settings, this topic has received a lot of attention too. In astrophysical settings that is because of the strong dependence of the ringing down phase signal (when two black holes merge) on such modes. Motivations from mathematical relativity and gravity in high energy settings (such as the CFT/Ads conjecture) also stress the relevance of QNMs. Although the extensive rigorous work by Sjostrand, Zworski and others, unlike normal modes which are well known and studied in spectral theory, we do not have yet the same level of understanding QNMs because of the complicated structure of the resolvent of non-self-adjoint operators. In this thesis we are concerned about studying QNMs in specific physical settings that are either

having a gravitational potential as Pöschl-Teller one or as in Schwarzschild black holes, or having a permittivity that follows Lorentz model. Due to the leakage of energy from the resonant structures, that is defined by either a potential or a permittivity, and to the nature of light and gravitational waves in free space at infinities, the natural resonant modes suffer from outgoing boundary conditions. These conditions make the studied operator a non self-adjoint one and results in complex modes frequency that are QNM frequencies. In the following two sections we introduce the general physical settings in which we are casting QNM problem as an eigenvalue problem in the third one we will show the problem from a mathematical point of view and then we will state the thesis goals. The last section is to give a breif view of the chapters organization.

1.1 Optical scattering problems

The main interest of studying such a problem is to better understand the interaction between light and different media. In particular we are concerned in this thesis about the simplest geometrical model of a nano-particle as a resonator. That is to model a nano-particle as a one-dimensional cavity. Although this model received a lot of interests and well known in study books from a physical point of view, we still think that it is a good starting point in order to understand deeper its interaction with light on the mathematical level. In a more concrete way, the studied problem here is a 1-D cavity where the permittivity inside is a function of frequency and position $\epsilon(\omega, x)$. We consider air or vacuum outside the cavity for simplicity without loss of generalization.
A scattering problem would be: Having an electromagnetic source (or background incident field), what is the output i.e. what is the field that this nano-particle (1-D cavity) scatters?
The equation that describes this mechanism inside the cavity in Fourier domain is:

$$[\epsilon(\omega, x)\omega^2 + \partial_x^2]\phi(\omega, x) = S(\omega, x), \tag{1.1}$$

where $\phi(\omega, x)$ is the scattered field ans $S(\omega, x)$ is the source. To proceed we should consider the boundary conditions besides the equation. Having Dirichlet boundary conditions on the cavity, that is to consider the scattered field as zero at the boundaries of the cavities, it yields the problem to a well known one. The scattered field can be expanded perfectly in terms of the eigenfunctions of the homogeneous equation of 1.1 (with a zero source). These eigenfunctions are known as normal modes and the eigenvalues are real. In this thesis we are concerned about outgoing boundary conditions that is:

$$x \Rightarrow +\infty, \;\; \phi_s(\omega, x) \propto e^{-i\omega x} x \Rightarrow -\infty, \;\; \phi_s(\omega, x) \propto e^{+i\omega x} \tag{1.2}$$

Having these boundary conditions make the problem more complicated than the one of normal modes and the resonance modes in this case are known as Quasi-normal modes. Still the orientation in the scientific community is to asses the relation between a scattered field with these modes.
In this work we try to understand this relation in the light of the relevant mathematical tools. Moreover we establish a method in order to be able to normalize these modes and calculate them numerically. On the other hand, we raise a question about the stability of the calculated solutions to answer question such as: *What is the effect of a small perturbation of the permittivity on the eigenvalues (resonant frequencies)?*

1.2 Gravitational scattering problems

Quasi-normal modes in gravitational physics, being the resonant modes in black holes and neutron stars, have received lot of studies in the literature. The ringing down behavior of gravitational waves that emitted from the merger of two black holes can be described in terms of these modes.
Having spherical symmetry the problem can be reduced to a 1-D problem. We focus in this work on one dimensional model, where the propagating waves are the gravitational ones, and the "resonant structure" is described by a gravitational potential. For the general case of gravitational potential we do not consider any cavity or physical borders, since in general it is a smooth function in the space. Although in neutron stars one should a box and the problem become more similar to an optical one.
On the physical level, the main concern here is to study a Cauchy problem, that is having initial conditions on a scalar field $\phi(t,x)$: $phi_0 = \phi(0,x)$ and $phi_1 = \frac{\partial}{\partial t}\phi(t,x)|_{t=0}$ and having the equation that describes the physics behind how this field evolves with time, that is:

$$[-\partial_t^2 + \partial_x^2 - V(x)]\phi(t,x) = 0, \tag{1.3}$$

what are the solution as a function of space and time and what are the resonant frequencies. Under Laplace transform, 1.3 becomes:

$$[s^2 + \partial_x^2 - V(x)]\phi(s,x) = -s\phi_0 - \phi_1, \tag{1.4}$$

we can look at the terms: $-s\phi_0 - \phi_1$ as a source. As in the optical case one should consider outgoing boundary conditions too. Thus the problem described in 1.4 becomes very close to the one in 1.1 (having in mind a relation between Laplace symbole and Fourier one as: $s = i\omega$).
Here also we are interested in calculated the modes, use again Lax and Phillips theorem to assess the expansion of the field $\phi(t,x)$ in terms of modes (that are the solutions of 1.4 with a zero source) and studying the stability of these modes to answer questions like: *What is the effect of a small perturbation in the gravitational potential $V(x)$ on the eigenvalues (the resonant frequencies)* .

1.3 The mathematical problem

As we have seen in both previous paragraphs the equations behind both physical problems are close. Actually one general equation can describe both:

$$[-\epsilon(t,x) * \partial_t^2 + \partial_x^2 - V(x)]\phi(t,x) = 0, \tag{1.5}$$

which becomes in Fourier space:

$$[\epsilon(\omega,x)\omega^2 + \partial_x^2 - V(x)]\phi(\omega,x) = S(\omega,x). \tag{1.6}$$

To solve a QNMs problem we put the source to zero and the equation can be written as:

$$P\phi(\omega,x) = -\epsilon(\omega,x)\omega^2\phi(\omega,x), \tag{1.7}$$

where the operator $P = \partial_x^2 - V(x)$ and of course with the boundary conditions. The main mathematical problem arise because of that the outgoing boundary conditions spoil the adjointedness of the operator P. Even when ϵ does not depend on ω (the is no dispersion), still the

outgoing boundary conditions cause the operator to be a non-self-adjoint one, the eigenvalues to be complex and the modes not to be normalizable due to their explosion at infinities of space. To transform the problem to a one in a Hilbert space, many technical approaches were used in literature such as complex scaling. Here we are using a different approach, that is re-writing the wave equation in compactified space-time using hyperboloidal slicing approach. Using this slices make the modes belong to a Hilbert space and they can be normalized choosing a certain scalar product. We cast QNM problems as an eigenvalue problem in order to calculate them.

1.4 Objectives

Due to the non-self-adjoint (moreover non normal) nature of the problem, we loose the control on the completeness of eigenfunctions and on the stability of eigenvalues as well. Our main objectives in this work are:

i) Assessment of the asymptotic resonant QNMs in terms of QNMs eigenfunctions in a Hilbert space. Relation to Lax-Phillips results. Reduction to normal modes in the self-adjoint case and assessment of completeness.

ii) Assessment of the (in)-stability of the eigenvalues due to a small perturbation of the studied potentials or permittivity. In order to achieve the second goal intermediate objectives are :

   - Definition of an appropriate scalar product of the system in order to asses the perturbation size in an energy scale.
   - Application of pseudospectrum notion to scattering optical and gravitational problems.

iii) Introduction/redefinition of physical quantities motivated by the spectral theory of non-self-adjoint operators, in particular the pseudospectrum and related notions and application in in gravitational and optical scattering problems.

1.5 Chapters organization

Part 1 of this thesis presents and addresses the studies of the problem theoretically from different angles: gravitational physics, optics and mathematical one. After the introduction, we establish the physical settings. In chapter 2 we show briefly the theory behind the wave equation that we are going to treat, that is a wave equation with a gravitational potential and we provide some relevant concepts that are necessary to understand later our methodology. Chapter 3 is concerned about optics where the information of the scatterer is encompasses in the permittivity. Chapter 4 starts with a mathematical introduction about scattering theory of self-adjoint operators then introducing Quasi-normal modes and different ways in the literature to deal with its divergence at infinities of space. Chapter 5 is a core chapter that is concerned about different approaches to expand a scattered field in terms of QNMs.

Part 2 is dedicated to explain the main approaches and tools in order to calculate QNMs, study the spectrum and its stability, that are: well known auxiliary fields as a technical tool in chapter 6. The concept of pseudospectrum in chapter 7, which is the tool that we are using later to study the stability issues. The mathematics behind the numerical methods and discretization

we use later, chapter 8. Chapter 9 is dedicated to explain hyperboloidal slicing approach showing that this approach permit to deal in a simple way with the outgoing boundary conditions and provides a way to normalize the modes. In chapter 10 we go back to pseudospectrum and its related issues with numerics.

Part three mainly consists of three parts where each one is taken from an article. Chapter 11 and 12 are for gravitational problems while chapter 13 is for optical settings.

Chapter 6 explains the hyperboloidal slicing approach.

Chapter 2

Physical settings: Gravitational physics

Contents

In this section we give a brief idea about gravitational physics and the derivation behind a wave equation with gravitational potential, in particular the case of spherically symmetric black hole. Furthermore we mention the notions of conformal compactification and Penrose diagram that will help in explaining a main benefit of using hyperboloidal slices coordinates, that is the no need of imposing outgoing boundary conditions at the infinities.

2.1 General relativity

The general theory of relativity is one of two important pillars of modern physics, which studies gravitational interactions, other than the quantum field theory that explains the other three fundamental interactions in universe known till now (electromagnetic, weak, and strong). It is the theory which gives the most accurate calculations for the corresponding observations and experiments about gravitational interactions. Einstein's general theory of relativity provided a revolutionary view to understand the structure of space-time with relation to the gravitational fields. It was developed by Albert Einstein along many years till it was culminated on 1915. The connection he explained between the matter and the geometry of space-time makes it one of the most beautiful theories ever. To explain it i am borrowing John Wheeler's famous phrase: "Einstein's geometric theory of relativity can be summarized thus: space-time tells matter how to move; matter tells space-time how to curve". The theory describes the gravitational interaction in one compact equation, that can not be understood with out some of the notions of differential geometry. It is in its general form:

$$G_{\mu\nu} + \Lambda g_{\mu\nu} = \kappa T_{\mu\nu} \tag{2.1}$$

where $G_{\mu\nu}$ is Einstein tensor:

$$G_{\mu\nu} = R_{\mu\nu} - \frac{1}{2} R g_{\mu\nu} \tag{2.2}$$

Looking naively at his equation, one can note that the left hand side of the equation describes the geometry of space-time structure in particular how it curves. Whereas the right side is in relation with mass - energy and momentum expressed by Energy-momentum tensor.

16 is dedicated to make a brief reminder of some notions of differential geometry that are necessary to have the mathematical taste of the theory.
In the following subsections We shall discuss Schwarzschild solution and a sketch on the derivation of its metric. A subsection also is dedicated to conformal compactification and at the end we give a brief explanation of a black hole region.
We basically follow here two main references that are: [99] and [84].

2.1.1 Stationary spherical symmetric black holes: Schwarzschild solution

Schwarzschild solved the Einstein equations under the assumption of spherical symmetry in 1915, two years after their publication. We will give in this subsection a sketch on the derivation of Schwarzschild metric.

We will use here $(-,+,+,+)$ as a signature of the metric. The line element is:

$$ds^2 = g_{\mu\nu}dx^\mu dx^\nu \tag{2.3}$$

The solution we search is for:

- Spherical symmetry space-time. Thus it is invariant under rotation. The functions should not depend on θ nor on ϕ.
- Static i.e. it is unchanged under a time-reversal $t \Rightarrow -t$. Thus the metric components are not functions of time. Also, nor any of their derivatives with respect to time.
- A vacuum solution is one that satisfies the equation $T_{ab} = 0$. Using Einstein field equations, this implies that $R = 0$ and $R_{ab} = 0$.

Using the arguments in 2.1.1 and those in 2.1.1 make all the metric components which have cross terms between time and space covariant tensors vanish. Thus $g_{\mu\nu} = 0$, when $\mu \neq \nu$. Using again the same arguments we get: $g_{11} = A(r)$ and $g_{22} = B(r)$, where the line element is:

$$ds^2 = -g_{11}dt^2 + g_{22}dr^2 + g_{33}d\theta^2 + g_{44}d\phi^2 \tag{2.4}$$

Every hypersurface for $r = const$ should be the same of that in a flat space-time (to stay invariant under rotation), thus we can write: $g_{33} = r^2$ and $g_{44} = r^2\sin^2(\theta)$.
The line element could be written again as:

$$ds^2 = -A(r)dt^2 + B(r)dr^2 + r^2d\theta^2 + r^2\sin^2(\theta)d\phi^2. \tag{2.5}$$

The next step is to calculate Christoffel symbols for this metric and then Ricci scalar in terms of $A(r)$, $B(r)$. Making the equality between this form of Ricci scalar and zero (since we are searching for a vacuum solution) allows to deduce $A(r)$, and $B(r)$. Finally, Schwarzschild metric is for:

$$ds^2 = -f(r)dt^2 + (f(r))^{-1}dr^2 + r^2(d\theta^2 + \sin^2(\theta)d\phi^2), \tag{2.6}$$

where $f(r) = (1 - \frac{C}{r})$. Comparing with Newtonian mechanics results (as a limit of GR) $f(r)$ yields as $f(r) = (1 - \frac{2GM}{r})$, where M is the mass of the source.

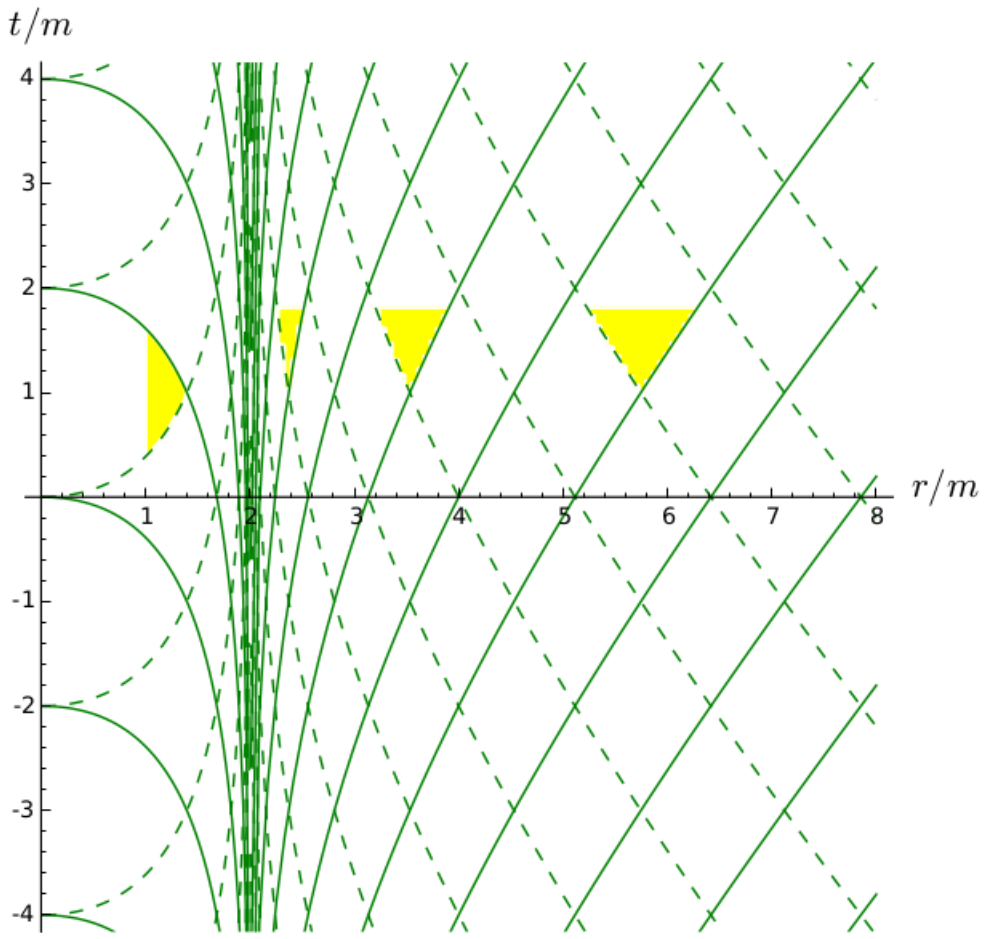

Figure 2.1: Causal structure of Schwarzschild, diagram in Schwarzschild coordinates [84].

Birkhoff theorem

Birkhoff's theorem in general relativity, states that the unique spherically symmetric solution of the vacuum field equations is Schwarzschild solution, thus it must be static and asymptotically flat.

Null geodisics, tortoise coordinate and effective potential

Actually the null geodesics are for:

$$\frac{dt}{dr} = \pm(f(r))^{-1} = \pm(1 - \frac{2GM}{r})^{-1}. \tag{2.7}$$

Figure 2.1.1 shows these trajectories with light cones in different regions.

Note that light cones at $r \Rightarrow \infty$ are as in Minkowski's, then they close more and more until arrive at $r = 2M$ where they completely close. Then transition to $r < 2M$ makes light cones open again but in different orientation, that makes the coordinate r a "time".

The tortoise coordinate $r*$ is defined:

$$r* = r + 2GM \log(\frac{r}{2GM} - 1) \tag{2.8}$$

so as to satisfy:

$$\frac{dr*}{dr} = (1 - \frac{2GM}{r})^{-1}). \tag{2.9}$$

Note that $r* \Rightarrow -\infty$ as $r \Rightarrow 2GM$ (Schwarzschild radius) and $r* \Rightarrow +\infty$ as $r \Rightarrow +\infty$. Note also that the line element in terms of the tortoise coordinate is:

$$ds^2 = -f(r)dt^2 + (f(r))^{-1}dr^2 + r^2(d\theta^2 + \sin^2(\theta)d\phi^2) \tag{2.10}$$

Let us now write massless Klein-Gordon equation:

$$\Box_g \phi = 0, \tag{2.11}$$

where $\Box_g = g^{\mu\nu}\nabla_\mu\nabla_\nu$ is the D'Alembertian operator associated with the metric g. More specifically:

$$\Box_g = \frac{1}{\sqrt{-g}}\partial_\mu(g^{\mu\nu}\sqrt{-g}\partial_\nu) \tag{2.12}$$

Using Schwarzschild metric leads to a wave equation with effective potential with either axial or polar parities, that is respectively Regger-Wheeler and Zerilli potentials. These potentials are given by the following equations:

$$V_\ell^{\mathrm{RW},s}(r) = \left(1 - \frac{2M}{r}\right)\left(\frac{\ell(\ell+1)}{r^2} + (1-s^2)\frac{2M}{r^3}\right) \ , \tag{2.13}$$

for the axial case, where $s = 0, 1, 2$ correspond to the scalar, electromagnetic and (linearized) gravitational cases, and

$$V_\ell^{\mathrm{Z}}(r) = \left(1 - \frac{2M}{r}\right) \left(\frac{2n^2(n+1)r^3 + 6n^2Mr^2 + 18nM^2r + 18M^3}{r^3(nr+3M)^2}\right) \ , \tag{2.14}$$

with

$$n = \frac{(\ell-1)(\ell+2)}{2} \ . \tag{2.15}$$

for the polar case.

2.1.2 Conformal compactification: future null infinity

Definitions

Conformal Considering two pseudo-Riemannian manifolds equipped respectively with g, h as metrics. These two metrics are said to be conformal if and only if $h = \lambda^2 g$, where λ is a real-valued smooth function defined on the manifold and is called the conformal factor. There is an equivalence class of such metrics which is called conformal class. The conformal relation between these metrics preserve angles on a conformal class.

Compactification The compactification of a topological space X is to embed it as a dense subset of a compact space. An important thing to do (when compactifying) is to control points that "go to infinity".
Conformal compactification A conformal compactification was first introduced by Penrose [150]. He added new boundary points to the manifold of compactified space-time. It can be defined as embedding of a non-compact Lorentzian manifold into a compact Lorentzian manifold as a dense open subspace, such that the embedding is a conformal map.
Assume having a Lorentzian physical manifold (M, g), whose boundaries are at infinity and its line element is ds^2, its conformal compactification is a compact manifold with boundaries whose line element is ds_2^2. Thus:

$$ds^2 = \Omega^2 ds_2^2, \tag{2.16}$$

where Ω is the conformal factor that diverge on the boundaries.
A basic example is R^n and its conformal comactification is the sphere S^n, where the inverse of this map is the stereographic projection.

Penrose diagram

It represents an extension of the Minkowski diagram which preserves the light cones slope at all points. Locally the metric is conformally equivalent to that of Minkowski's.In particular the casual structure, and therefore light propagation are the same of that of Minkowski's. Some important facts are

- It is compact but it represents the whole infinite space-time.
- It has what is called null infinities where the light starts (past null infinities) and finishes (future null infinities)

We get this diagram by starting from Minkowski diagram and we do three transformations for the coordinates. Let us start from (t, x) as coordinates of Minkowski diagram. The first transformation is:

$$\begin{aligned} u &:= t + x \\ v &:= t - x \end{aligned} \tag{2.17}$$

So we have the new coordinates along the light cones edges. The second is a conformal transformation:

$$\begin{aligned} p &:= tan^{-1}(u) \\ q &:= tan^{-1}(v) \end{aligned} \tag{2.18}$$

This is to compactify the space-time and the last is to go back to a space and time like axis:

$$\begin{aligned} T &:= p + q \\ X &:= p - q \end{aligned} \tag{2.19}$$

In all steps we have to keep track of the ranges. Actually step one and two are necessary to preserve the light cones slopes so the causality properties of space-time are preserved in a new compactified space-time. In step three there is a change to be made in the metric, so that when we draw a time-like or a space-like lines they will be as in the figure. Let us look at the

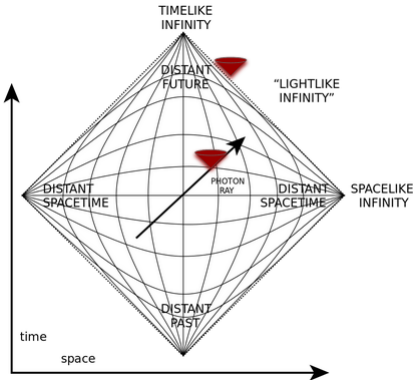

Figure 2.2: Penrose diagram of an infinite Minkowski universe, horizontal axis u, vertical axis v. Figure taken from Wikipedia

null infinities of Penrose diagram. Actually if we draw the light cones at any point of these null infinities, it will point outwards of the space-time that means that information set at any of these points will not affect what is going on inside the space-time. The characterizes null infinities as a "outgoing boundary" hypersurfaces. This is what we need to treat outgoing boundary conditions in a Quasi Normal Modes problem, since they are imposed at infinities. The bottom line is that if our surface $t = 0$ is set to intersect the null infinity, then outgoing boundary conditions are automatically imposed, since light cones are outgoing at null infinity. This provides a geometrical way of imposing the outgoing boundary conditions.

A second connection to Hyperboloidal slices approach

The idea is that certain coordinate systems are better adapted than others to address a given particular aspect of the problem. In this sense: The coordinates (t, x) of our Cauchy problem are badly adapted to say anything about null infinity because surfaces $t = const$ never meet null infinity when $x \to \infty$ Here we will choose coordinates (τ, y) that are well adapted to null infinity, so for $\tau = constant$ the limit $x \to \infty$ takes to null infinity, that is exactly what we want to address. So we need to make transformation along the light line to arrive to null infinities, we choose "Hyperbolic" transformations:

$$\begin{aligned} \tau &= t - ln(2cosh(x)) \\ y &= tanh(x) \end{aligned} \tag{2.20}$$

Note that the second line in the (2.20) leads to a compactification of the space. Also, when $x \to +\infty, \tau = t - x$ and when $x \to -\infty, \tau = t + x$

2.1.3 Black holes

An informal definition of a black hole is that a black hole is a region of space-time from which no particle can escape. This region is separated from the rest of the space time by a hypersurface called the event horizon which allows the movement of a particle just to the inside of the black hole region.
Another definition that is very well explained in [84] is: "Let (M, g) be a space-time with a

conformal completion at null infinity; the black hole region, or simply black hole, is the set of points of M that are not in the causal past of the future null infinity".

Chapter 3

Physical settings: Optics

Contents

Our interest in this chapter are optical resonators i.e. structures that have different optical properties than the surrounding material. We focus here on the permittivity as an optical property considering the permeability is the same of that of free space in the studied models. For sake of simplicity and to be able to focus more on the mathematical properties of our problem, we study 1D cavity which can be in its simplest case two parallel mirrors that are totally reflecting light. Such a cavity has Dirichlet boundary conditions (the fields are zeros on the both boundaries). Such a system is ideal and do not exchange any energy with the outside. A more practical example is a material that has ϵ as its permittivity surrounded by air with permittivity ϵ_0. Such a structure leaks energy and the boundary conditions are outgoing. In the first section we remind of wave equation of a scattered field followed by a small discussion showing that the source of the mathematical problem is the boundary conditions. In a later section we revise Drude model of permittivity and finally the famous Purcell factor and the importance of finding a way to normalize the modes.

3.1 Wave equation of a scattering field

We consider a nanoparticle modeled by 1D optical dispersive cavity with permittivity of $\epsilon(x,t)$. We assume that the nanoparticles is surrounded by air.

The scalar field of electromagnetism in one dimension for total field is described by

$$[\epsilon(x,t) * \frac{\partial^2}{\partial t^2} - \frac{\partial^2}{\partial x^2}]\phi_t(x,t) = 0. \tag{3.1}$$

Where $\epsilon(x,t)$ is the dielectric constant. And the equation of the background field is given by:

$$[\frac{\partial^2}{\partial t^2} - \frac{\partial^2}{\partial x^2}]\phi_b(x,t) = 0. \tag{3.2}$$

We define the scattered field as $\phi_t - \phi_b$, substituting 3.2 from 3.1, we get:

$$[\epsilon(x,t) * \frac{\partial^2}{\partial t^2} - \frac{\partial^2}{\partial x^2}]\phi_s(x,t) = [(1-\epsilon(x,t))\frac{\partial^2}{\partial t^2}]\phi_b(x,t). \tag{3.3}$$

Applying Fourier transformation, we get:

$$[\epsilon(x,\omega)\omega^2 + \frac{\partial^2}{\partial x^2}]\phi_s(x,\omega) = [(\epsilon(x,\omega)-1)\omega^2]\phi_b(x,\omega). \tag{3.4}$$

We define $[(\epsilon(x,\omega)-1)\omega^2]\phi_b(x,\omega)$ as a source $I(x,\omega)$, and the equation of the scattered field becomes:

$$[\epsilon(x,\omega)\omega^2 + \frac{\partial^2}{\partial x^2}]\phi_s(x,\omega) = I(x,\omega). \tag{3.5}$$

According to optics literature [114] modes to find the modes is to find the solutions to the homogeneous equation eq.3.5 (considering $I(x,\omega) = 0$) taking into consideration the boundary conditions. QNMs are the modes when the field (ϕ) have outgoing boundary conditions, that are:

$$\phi \sim e^{-i\omega x}, x \to +\infty, \tag{3.6}$$

$$\phi \sim e^{+i\omega x}, x \to -\infty, \tag{3.7}$$

We shall discuss in the following section two particular cases, one when we do not have such boundary conditions to show that they are the main responsible of loosing the well known properties of normal modes, the other is when having outgoing boundary conditions but with zero absorption.

3.1.1 Absorption with Dirichlet conditions

This little paragraph is to show that it is indeed the boundary conditions who spoil the adjointedness of the operator, and the absorption alone do not.
We consider Dirichlet boundary conditions, with the equation of modes:

$$\frac{\partial^2}{\partial x^2}\phi_n(x,\omega_n) = -\epsilon(x,\omega_n)\omega_n^2\phi_n(x,\omega_n) \tag{3.8}$$

In the case of ϵ does not depend on x we can write $\lambda = -\epsilon(\omega_n)\omega_n^2$. Having Dirichlet conditions makes the operator of this problem self-adjoint and the eigenfunctions form a basis for the solutions, eigenvalues are real and the solutions are stable. However our frequencies here (ω)s are not the eigenvalues. To calculate the frequencies, we calculate first λs, then by knowing the dependence of ϵ on ω the frequencies could be calculated.

3.1.2 Drude model with zero absorption

In this section we discuss a particular case of permittivity, considering a homogeneous wave equation and outgoing boundary conditions. Drude model describes the permittivity of a metal by the following equation:

$$\epsilon = \epsilon_\infty - \frac{\omega_p^2(x)}{\omega^2 + i\Gamma\omega}, \tag{3.9}$$

where ω_p is the plasmon frequency, Γ describes the absorption. There exist a range of frequencies for which Γ is negligible in comparison to ω. We will focus on this range and put Γ to zero. So our permittivity will be:

$$\epsilon = \epsilon_\infty - \frac{\omega_p^2(x)}{\omega^2}. \tag{3.10}$$

This permittivity encodes the scatterer information, and the equation of modes of resonance is:

$$(\frac{d^2}{dx^2} + \epsilon\omega^2)\phi(\omega, x) = 0. \tag{3.11}$$

By replacing ϵ by its value from (3.10) we get:

$$(\frac{d^2}{dx^2} + \epsilon_\infty\omega^2 - \omega_p^2(x))\phi(\omega, x) = 0. \tag{3.12}$$

We will identify $\omega_p^2(x)$ as the effective potential. We define $\epsilon_\infty\omega^2$ as $\bar{\omega}^2$. **Permittivity approximation in Drude model**
Drude model follows from Lorentz model by considering that most electrons in the material are free and not bounded to a nucleus, thus it is applied to metals generally. The formula of the permittivity as follows is given by:

$$\epsilon(\omega, x) = \epsilon_\infty(x) - \frac{\omega_p^2(x)}{\omega^2 + i\Gamma(x)\omega}\ , \tag{3.13}$$

where $\omega_p^2 = \frac{Nq^2}{\epsilon_0 m_e}$, and $\Gamma$is the absorption. We linearize the permittivity first order linearization, thus we get:

$$\epsilon(\omega) = \epsilon_\infty - \frac{\omega_p^2}{\omega^2}\left(1 - i\frac{\Gamma}{\omega}\right) \tag{3.14}$$

Inserting this expression in the time-independent wave equation of the scattered field 3.5, it becomes:

$$\left[\frac{\partial^2}{\partial x^2} - V(x) + \epsilon_0\left(\epsilon_\infty - \beta(x,\omega)\right)\omega^2\right]\phi_s(x,\omega) = I(x,\omega), \tag{3.15}$$

where $V(x) = \omega_p^2 > 0$, $\beta = \frac{i\Gamma\omega_p^2}{\omega^3} << \epsilon_\infty$.

Negligable absorption case
Considering the absorption to be zero or the quantity $\frac{i\Gamma\omega_p^2}{\omega^3}$ is negligible in front of ϵ_∞ for the range of visible light. We set β to zero in eq.3.15, the equation for finding the QNMs becomes:

$$\left[\frac{\partial^2}{\partial x^2} - V(x) + \epsilon_0\epsilon_\infty\omega_q^2\right]\phi_q(x,\omega) = 0. \tag{3.16}$$

We define $P_V = -\Delta + V(\vec{x})$, thus we can write eq.3.16 in the following way:

$$[P_V - \epsilon_0\epsilon_\infty\omega_q^2]\phi_q(x,\omega) = 0, \tag{3.17}$$

rescalling the frequency, we write:

$$[P_V - \omega_q^2]\phi_q(x,\omega) = 0, \tag{3.18}$$

Now we can see easily that following Drude model with $\Gamma = 0$ reduces the permittivity problem to a case with a potential. Thus what runs in the potential case holds for this special permittivity case. In particular the theory by Lax & Phillips 5.1.5 and the result of asymptotic expansion. However we must mention that such case is purely mathematical.

3.2 Purcell factor and the need of normalization

Studying lossy energy systems, it is indispensable to take about quality factor and mode volume, two major characteristics of resonances. These quantities contribute in Purcell factor computing, which describes the changes in spontaneous emission of a quantum particle. This change happens because of the cavity.

Spontaneous emission is the process in which a quantum mechanical system (such as a molecule, an atom or a subatomic particle) transits from an excited energy state to a lower energy state (e.g., its ground state) and emits a quantized amount of energy in the form of a photon. It arises due to interaction between the material and its local electromagnetic environment. A simple relevant example could be an electric dipole between two electrons of different energy levels. This system is represented by the dipole moment operator $\hat{\mu}$, where:

$$\hat{\mu} = \mu\hat{\sigma}^{+} + \mu^{*}\hat{\sigma}^{-}, \tag{3.19}$$

where $\hat{\sigma}^{+}$ and $\hat{\sigma}^{-}$ are the two level system (TLS) raising and lowering operators.

We denote by γ_p the decay rate of the excited state population in vacuum, where p stands for population. The rate of photon emission at time t is:

$$\xi(t) = \gamma_p < \hat{\sigma}^{+}\hat{\sigma}^{-} > \tag{3.20}$$

Energy conservation requires that the decrease of the TLS excitation should at any time be compensated by the increase of the photon number so that:

$$\partial_t < \hat{\sigma}^{+}\hat{\sigma}^{-} >= -\gamma_p < \hat{\sigma}^{+}\hat{\sigma}^{-} > \tag{3.21}$$

It follows that:

$$\gamma_p < \hat{\sigma}^{+}\hat{\sigma}^{-} >= e^{-\gamma_p t} \tag{3.22}$$

Hence during the so-called spontaneous emission, the excited state population $< \hat{\sigma}^{+}\hat{\sigma}^{-} >$ and the radiation rate both decay exponentially with the characteristic time $t_p = \gamma_p^{-1}$ The rate of spontaneous emission was described by Fermi's golden rule. But a key thing to keep here is that Fermi's golden rule describes transitions between eigenstates of some unperturbed Hamiltonian, and that these eigenstates are assumed to be **orthogonal** during its derivation. One of the proposed solutions is in the article "Theory of the Spontaneous Emission in Photonic and Plasmonic Nanoresonators", by Lalanne. This effect is defined as the modification of a quantum system's spontaneous emission rate by its environment (for example, there is a change in the spontaneous emission from a dipole between when being in a resonating optical cavity or in the vacuum).
Basically two were introduced by Purcell to quantify the maximum decay rate that can happen:

The quality factor (Q), and the mode volume (V).

Purcell factor F describes represents the maximum acceleration for an ideal coupling between the emitter and the cavity mode. It happens for perfect spectral, spatial, and polarization matching. Purcell factor F is given in terms of Q, and V:

$$F = \frac{3}{4\pi^2}(\frac{\lambda_0}{n})^3\frac{Q}{V} \tag{3.23}$$

where $\frac{\lambda_0}{n}$ is the resonance wavelength in the material surrounding the emitter.

Purcell factor F describes represents the maximum acceleration for an ideal coupling between

the emitter and the cavity mode. It happens for perfect spectral, spatial, and polarization matching. Once the mode field distribution is known, any deviation from perfect coupling can be calculated analytically. A usually used relation is:

$$\frac{\gamma}{\gamma_0} = F\frac{\omega_0^2}{\omega^2}\frac{\omega_0^2}{\omega_0^2 + 4Q^2(\omega - \omega_0)^2} \tag{3.24}$$

The quality factor Q can be seen as spectral energy density associated to the resonant mode. It describes how damped a resonance is, or equivalently, characterizes a resonance bandwidth relative to its center frequency. A higher Q indicates a lower rate of energy loss relative to the energy stored in the resonator; the oscillations of the temporal response die out more slowly and the resonator rings longer. The Q-factor of a resonance is often defined as 2π times the ratio of the time-averaged energy stored in the cavity to the energy dissipated per cycle.

$$Q = \frac{\omega_{re}}{2\omega_{im}} \tag{3.25}$$

High Q could be achieved using dielectric materials. The volume initially introduced by Purcell was a geometrical volume representing the spatial extent of the (microwave) resonator, but with the large amount of work devoted to optical micro-cavities in the 90s, the mode volume definition has evolved to the following expression:

$$V = \frac{1}{\epsilon_0 n^2}\int \epsilon(r)|E(r)|^2 d^3r \tag{3.26}$$

In his article Sauvan et al [162], they derive a new definition of V, and then to the rate between decay rate in a cavity and in a bulk material. However this derivation depends on the assumption that quasi normal modes (QNMs) (the natural modes in a natural optical cavity) are complete.

$$V = \frac{\int[\tilde{E}\cdot\frac{\partial\omega\epsilon}{\partial\omega}\tilde{E} - \tilde{H}\cdot\frac{\partial\omega\mu}{\partial\omega}\tilde{H}]}{2\epsilon_0 n^2[\tilde{E}(r_0)\cdot u]^2} \tag{3.27}$$

In order to calculate the integral that appears in eq.3.27 there is a need to normalization, in the same article of [162] a PML approach is used for this reason. The article of Stout et al. [175] also discuss the mode volume taking into consideration the existence of a non-resonant term in the expansion of Green function. Whatever a mode volume is defined, the need of having the field normalizable and overcome the divergence problem is undeniable. In 12 we follow hyperboloidal slices approach that is explained in 8.

Chapter 4

Scattering resonances: Quasi-Normal Modes (QNM)

Contents

This chapter is concerned about introducing Quasi-normal modes from different aspects. We start this chapter by revising some necessary definitions from functional analysis in order to explain the spectral theory of self-adjoint operators. In the second section we introduce scattering resonances namely Quasi-normal modes from physics of optics first and then from a more rigorous mathematical side. Section three is dedicated to explicit explanations of different approaches in literature to deal with these exploding modes at the space infinities. We finish by introducing a contact again with hyperboloidal slices approach.

4.1 Normal modes: spectral theorem

4.1.1 Self-adjoint operators

First of all we remind of some basic definitions from functional analysis. [188], [14].
Definition: If T be a linear operator in $\mathcal{H}$ (Hilbert space), then its adjoint T^* is defined as follows. The domain $D(T^*)$ consists of the vectors $u \in \mathcal{H}$ for which the map:
$D(T) \to \mathbb{C} : v \mapsto \langle u, Tv\rangle$ is bounded with respect to the $\mathcal{H}-$norm. For such u there exists, by the Riesz representation theorem, a unique vector denoted by T^*u such that $\langle u, Tv\rangle = \langle T^*u, v\rangle$ for all $v \in D(T)$.
T is called self-adjoint if $T = T^*$ and $D(T) = D(T^*)$.
Definitions: (Resolvent set, spectrum, eigenvalue, point spectrum). Let T be a linear operator in a Hilbert space $\mathcal{H}$. The resolvent set often denoted by $\rho(T)$ consists of the complex z for which the operator $T - z : D(T) \to \mathcal{H}$ is bijective and the inverse $(T - z)^{-1}$ is bounded. The spectrum $\sigma(T)$ of T is defined by $\sigma(T) := \mathbb{C} \setminus \rho(T)$.
An eigenvalue of T is a number $\lambda \in \mathbb{C}$ such that $Ker(T - \lambda) \neq 0$ (that means $\exists u \in D(T)|(T - \lambda)u = 0$), u is called an eigenvector.

Note the operator $T - \lambda I$ may not have an inverse, even if λ is not an eigenvalue. thus the spectrum of an operator always contains all its eigenvalues, but is not limited to them. The point spectrum $spec_p(T)$ is the set of the eigenvalues of T.
Definitions: (Closed set, bounded set, compact set, compact operator). A closed set is a set which contains all of its limit points. Therefore, a closed set A is one for which, $\forall x \notin A$, then x can always be isolated in some open set which doesn't touch A.
Given a topological vector space (X, τ) over a field $\mathbb{K}$, a subset B of X is called bounded in X if: $\forall (s_i)_{i=1}^{\infty}$ that converges to 0 and every sequence $(b_i)_{i=1}^{\infty}$ in B, the sequence $(s_i b_i)_{i=1}^{\infty}$ converges to 0 in X.
A subset is called compact if it is closed and bounded.
Compact operator: Let E and F be two Banach spaces. A linear map T is said to be compact if (equivelantely):
$\forall B \subset E$ with B bounded, $T(B)$ is relatively compact in F .
$\forall (u_n) \in E^N$, where (u_n) is a bounded sequence, (Tu_n) has a convergent subsequence.

Theorem (The Spectral theorem of self-adjoint operators). Suppose $T \in \mathcal{K}(H)$ (compact on H) be self-adjoint. Then there exists a system of orthonormal vectors ϕ_1, ϕ_2, ϕ_3, ϕ_4, ... of eigenvectors of T and corresponding distinct eigenvalues λ_1, λ_2, λ_3, λ_4, ... such that

$|\lambda_1| \leq |\lambda_2| \leq |\lambda_3| \leq |\lambda_4|$ ... , $Tx = \sum_k^{\infty} \lambda_k \langle x, \phi_k \rangle \phi_k$ for all $x \in H$. If (λ_n) is infinite, then $\lambda_n \to 0$ as $n \to \infty$. The series on the right hand side converges in the operator norm of $\mathcal{B}(H)$ (the space of all bounded operators on H).
The eigenfunctions of a such operator are called in physics problems normal modes. An eample from physics is a Fabry-Perot cavity with Dirichlet boundary conditions (where the field ϕ is 0 at boundaries).

However in physics waves problem, one frequently have to deal with boundary conditions where the resonator leaks energy to the outside, such conditions spoil the closeness of the resonator, which results in making the Laplacian in the wave equation to not be a self-adjoint operator any more with respect to the intuitive L_2 norm.

4.2 QNMs - scattering resonances

In physics quasi-normal modes are the natural modes of dissipated resonances for structures that leak energy to the outside via "outgoing boundary conditions". In optics and for a field satisfying Helmholtz equation, **Sommerfeld condition** plays a role in determining the boundary conditions at infinity. It says:
the sources must be sources, not sinks of energy. The energy which is radiated from the sources must scatter to infinity; no energy may be radiated from infinity into ... the field. Sommerfeld condition makes the only possible wave at infinity is an outgoing wave. When the field at infinities is proportional to $e^{\pm i\omega x}$, where x is the space coordinate and the singes in the sense of being outgoing at each infinity, then the boundary conditions are called outgoing boundary conditions. Similarly in gravitational waves, also acoustics, ocean waves nothing comes from infinity, and the outgoing boundary conditions are the natural condition at infinity in waves resonating problems. In these cases the resonance modes are called Quasi-normal modes (QNMs), and the resonance frequencies are called Quasi-normal frequencies (QNFs).
In mathematics scattering resonances is the formal name in this context. Scattering resonances

frequencies are known to be the poles of the resolvent in its meromorphic continuation in the complex plan. (equivalently in physics the poles of the Green function).

4.2.1 Resonance in Physics: the optical case

Normal modes are well studied phenomena. [162] For a system which is hermitian normal modes appears as a perfect solution to the resonance. Scattered field is consistent of super position of these normal modes. However if energy can escape to the outside, the system would be open and nonconservative, and the associated mathematical operator would not be hermitian in the usual sense. For lossy system (such as an open system with radiation loss or closed system with absorption loss), quasi normal modes (QNMs) are reported to be the response of such resonant structures. Quasi normal modes "known" to be in optics as the solutions of Maxwell equations without a source. The wave could be represented by the following expression:

$$e^{i(\omega t - \vec{k}.\vec{x})} \tag{4.1}$$

in QNMs to find solution w must be complex which means there is absorption $w = w0 + iwi$ So

$$e^{i\omega_0 t} e^{-\omega_i t - i(\frac{w}{c})x} \tag{4.2}$$

And the wave expression becomes:

$$e^{i\omega_0 t - i(\frac{\omega_0}{c})x} e^{-\omega_i t + (\frac{\omega_i}{c})x} \tag{4.3}$$

this means there is decay in time, but with larger x, it is larger and larger. and the mode volume is infinite

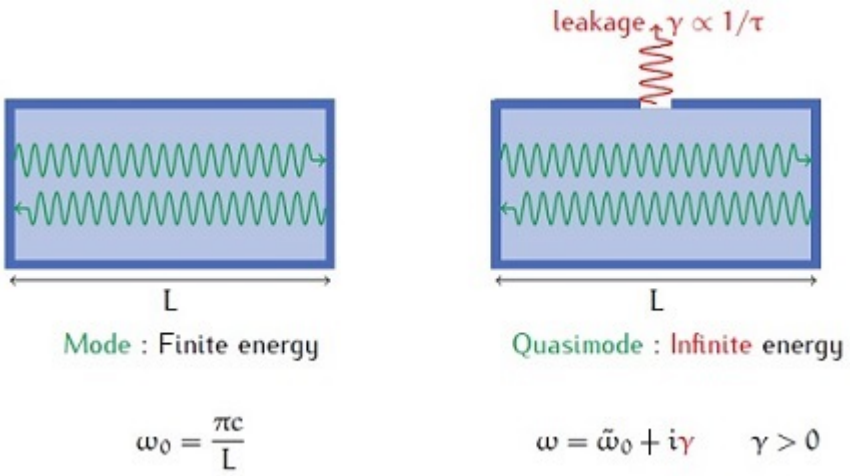

Figure 4.1: Normal modes vs Quasi normal modes in an optical cavity [136].

to understand this one can imagine that we need infinite energy to compensate this enlarging with x and here is the problem in calculations of QNMs But what really happens ? QNMs are the poles of the system (or the cavity) for which we have a maximum transmission when there is an incident wave, the cavity starts to resonate if the frequency of the wave is close to the real part of the complex frequency of QNMs the imaginary part describes the decay with time. Here

arises the question about completeness of the QNMs, and the physical meaning can we describe the scattered field as superposition of QNMs with coupling coefficients: α_n : $E_s = \Sigma \alpha_n E_{QNMs_n}$

Our focus: Nanoparticles

Nanoparticles have been of a growing interest in the few recent decades [8] [6] [5], thanks to the nanotechnology which allowed to fabricate such small particles with dimensions between 10 to 100 nm. Different shapes of nanoparticles of different materials could be fabricated. Shape, permittivity, surrounding medium permittivity, wavelength are all essential parameters to the optical response of the nanoparticle, thus they are essential in design nanostructures with different properties.

Nanostructures are used recently in many applications, some of them: Medicine, as delivering drugs to tumors. Manufacturing, as nanoparticles can be dispersed in industrial coatings to protect wood, plastic, and textiles from exposure to UV rays. Energy, where researchers have demonstrated that sunlight, concentrated on nanoparticles, can produce steam with high energy efficiency.

Although the wide range of nanoparticles applications, our understanding of how these particles behave under illumination is fuzzy. The frequency response is one of the most important optical properties. The developing of analytical expressions for the resonance frequencies is still missing lot of work. Although simulations now by softwares as Comsol could solve the problem, still to design and control nanostructures resonance, it would be easier and more powerfull to have analytical expressions.

The simplest way to say a nanoparticle is to consider it as a cavity which has its resonance at discrete set of frequencies which we are investigating in this work. We aim here to develop our knowledge about the resonance in optical cavities, which could lead and help to understand more general questions about the resonance in other cavities up to the black holes.

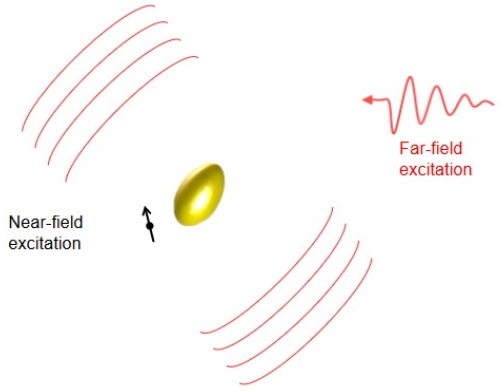

Figure 4.2: Excitation of nanoparticle. Image taken from [113]

Nanoparticles are particles between 1 and 100 nanometers in size. When an electromagnetic field is incidence, the nanoparticle could scatter and/or absorb the incident light. The power of extinction equals the sum of the power absorb and the scattered power. One of the most important quantities when studying the optical response of a nanoparticle is the scattering cross section. The scattering cross section σ_s is defined by the relation:

$$\frac{dP_s}{d\omega} = \frac{d\sigma_s}{d\omega} I_{i_{nc}}, \tag{4.4}$$

where Ps is the scattered power. I_{inc} is the intensity of incident light. ω is a solid angle. In the same way we can define the absorption and the extinction cross sections.

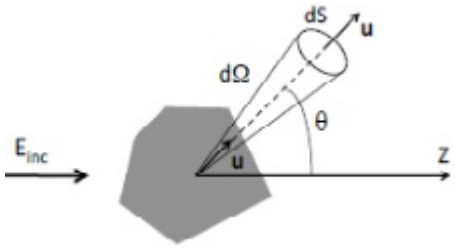

Figure 4.3: Scattering by a nanoparticle. Image taken from [44]

Peaks in the absorption happen at certain frequencies which are the resonance frequencies. The following figure shows the optical response of a disc made of silver with radius= $0.35\mu m$, and height= $0.30\mu m$

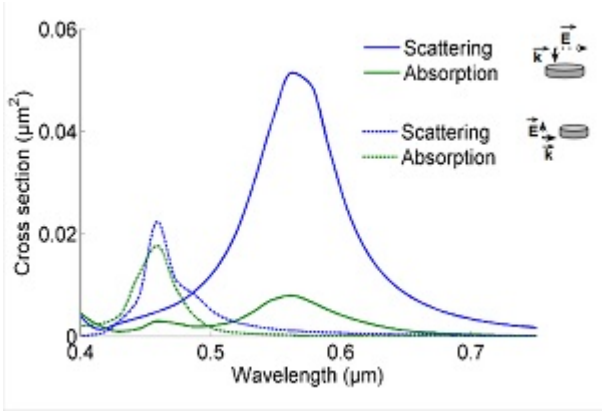

Figure 4.4: Silver nanodisk optical response

4.2.2 Resonances in Mathematics: Scattering resonances - spectral approach

We will show here the rigorous definition of a scattering resonance by [194] for a special case of a Cauchy problem where the potential is of compact support, with some results by the same author. The definition itself can be generalized to problems with a non-compact potential, and to problems with permittivity. Let us consider a one-dimensional scatterer defined by a potential $V(x)$.

Cauchy problem. Considering a Cauchy problem with initial data: $\phi_0 = \phi(0, x)$ and $\phi_1 = \partial_t \phi(0, x)$, where the field evolves with time according to the equation:

$$(\partial_t^2 - \partial_x^2 + V(x))\phi(t, x) = 0. \tag{4.5}$$

Under Laplace transformation to (4.5) we get:

$$(\partial_x^2 - s^2 - V(x))\phi_s(s, x) = s\phi_0 + \phi_1 = S_2(s, x). \tag{4.6}$$

To follow [194] consider $V(\mathbf{x})$ real, bounded and with support inside a ball of radius R_0,

- the operator P_V is given by $P_V = -\Delta + V$

- the resolvent $R_V(\omega)$ is given by $(P_V - \omega^2 I)^{-1}$

Theorem. The operator $R_V(\lambda)$ continues to a meromorphic family $R_V(\lambda) : L^2_{comp}(R^3) \to L^2_{loc}(R^3), \lambda \in C$. This gives a mathematical definition of scattering resonances:

Definitions.

- Suppose that $V \in L^\infty_{comp}(R)$ and that $R_V(\lambda)$ is the scattering resolvent of the previous Theorem. The poles of $\lambda \mapsto R_V(\lambda)$ are called *scattering resonances of* V . If λ_0 is a *scattering resonance* then, in this notation with $A(\lambda) = R_0(\lambda)$, *the multiplicity of* λ_0 is defined as $m(\lambda_0) = \mathrm{Dim}(span A_1(L^2_{comp}), , A_J(L^2_{comp}))$.

- We define $\lambda \neq 0$ as a scattering resonance of $P_V = -\partial_x^2 + V$, $V \in L^\infty_{comp}(\mathbb{R})$ iff
  1/ λ is an eigenvalue $u \in H^2_{loc}(\mathbb{R})$, $(P_V - \lambda^2)u = 0$
  2/ Outgoing boundary condition $u = a_\pm e^{\pm i\lambda x} \neq 0; \pm x \gg 1$.

- u is a resonant state for resonance λ_0, iff
  1/ It is an eigenfunction of the equation: $(P_V - \lambda_0^2)u = 0$.
  2/ It has outgoing boundary conditions: $\exists f \in L^2_{comp}(\mathbb{R}^n)$, $u = R_0(\lambda_0)f$

Resonance free regions

The logic behind the existence of a free zone is that the imaginary part of the resonant frequency determines the decay of a wave localized in frequency near the real parts of that resonant frequency. To have a wave that is resonating close to this real part value there will be constraints on the decay thus on the imaginary part, thus there is a limiting relation between the the real part and the imaginary part of the resonant frequency, which leads to have a region in the complex plan free of resonances.
high frequency resonance free regions are typically according to [194] of the form:

$$Im(\lambda) > -F(Re(\lambda)), Re(\lambda) > C, F(x) = \begin{cases} (a)e^{-\alpha x}, \alpha > 0 \\ (b)M \\ (c)M\log(x) \\ (d)\gamma x^\beta, \beta \in \mathbb{R}, \gamma > 0. \end{cases} \tag{4.7}$$

Where in the case of compactly supported potential the form of the free region follows (c) and (d): for bounded potentials [194]: (c), arbitrary M for smooth potentials (d)[262]. (a) for certain Gevery class of potential. We underline the relation between the form of the potential and the form of the free region zone.

4.3 Different approaches to QNMs

4.3.1 Heuristic definition in the Fourier formulation

Given the wave equation without source

$$\left(-\frac{1}{c^2}\frac{\partial^2}{\partial t^2} + \Delta - V\right)\phi = 0 \ , \tag{4.8}$$

where $\phi = \phi(t, \mathbf{x})$ is a scalar field defined on $\mathbb{R} \times \mathbb{R}^n$, Δ is the Laplacian in $\mathbb{R}^n$ and $V = V(\mathbf{x})$ is a potential (that will be taken non-negative, $V = V(x) \geq 0$). Quasi-normal modes correspond to solutions with purely outgoing boundary solutions, corresponding to the damped propagation of a perturbation of the system. Given the time independence of the potential V, we can consider a Fourier decomposition in time to study the behavior of each frequency mode ω

$$\phi(t, \mathbf{x}) = \frac{1}{2\sqrt{\pi}} \int_{-\infty}^{\infty} e^{i\omega t} \tilde{\phi}(\omega, \mathbf{x}) d\omega \ . \tag{4.9}$$

Each mode $\phi_\omega(t, \mathbf{x}) = e^{i\omega t}\tilde{\phi}(\omega, \mathbf{x})$ of fixed ω satisfies the equation

$$\left(\omega^2 + \Delta - V\right) \phi(\omega, \mathbf{x}) = 0 \ . \tag{4.10}$$

Normal modes. To motivate quasi-normal modes, let us first remind the notion of normal mode. If we solve (4.10) in a compact domain domain $D \subset \mathbb{R}^n$, imposing homogeneous Dirichlet or Neumann boundary conditions (more generally homogeneous Robin conditions) leads to the eigenvalue problem of a self-adjoint operator. Specifically, defining

$$P_V = -\Delta + V(\mathbf{x}) \ , \tag{4.11}$$

the homogeneous Dirichlet problem (analogoudly for the Neumann or Robin case)

$$P_V \phi_\lambda(\mathbf{x}) = \lambda \phi_\lambda(\mathbf{x}) \quad , \quad \phi_\lambda(\mathbf{x})|_{\partial D} = 0 \tag{4.12}$$

with $\lambda = \omega^2$, defines a selfadjoint operator where

a) Eigenvalues are real.

b) The modes ϕ_λ provide a orthonormal basis for the solutions of Eq. (4.10) in the appropriate functional space. In particular the expansion coefficients are determined by a projection through the underlying scalar product.

In a general setting, with P_V still self-adjoint but with domain in non-compact space, the spectrum of P_V is real with a pure point part $\sigma_p = \{\omega_n\}_{n\in\mathbb{N}}$ and a continuous part σ_c, and we can write

$$\phi(t, \mathbf{x}) = \sum_{n=0}^{\infty} c_n e^{i\omega_n t} \phi_n(\mathbf{x}) + \int_{\omega\in\sigma_c} c(\omega) e^{i\omega t} \phi(\omega, \mathbf{x}) \ . \tag{4.13}$$

Points a) and b) above contain, in a conservative case, the main elements we will be concerned with here, in a open dissipative context:

i) In an open dissipative system, outgoing boundary conditions spoil the self-adjoint character of P_V. Frequencies are generically complex and are refer to as "resonant" or "quasi-normal" frequencies.

ii) The corresponding "eigenmodes" (they are not normalizable) do not provide in general a basis in the space of solutions we are interested in. Assessing the conditions on $V = V(\mathbf{x})$ and D such that completeness is (in some sense to be specified) guaranteed is one of the underlying motivations for this work.

Quasi-normal modes: asymptotic conditions. Let us focus, for concreteness, on the 1-dimensional case

$$\left(-\frac{1}{c^2}\frac{\partial^2}{\partial t^2}+\frac{\partial^2}{\partial x^2}-V(x)\right)\phi(t,x)=0\ . \tag{4.14}$$

Taking the Fourier transform in time, every frequency mode ω

$$\phi_\omega(t,x)=e^{i\omega t}\phi(\omega,x)\ , \tag{4.15}$$

satisfies

$$\left(\frac{\omega^2}{c^2}+\frac{d^2}{dx^2}-V(x)\right)\phi(\omega,x)=0\ . \tag{4.16}$$

If $V=V(x)$ has compact support or, more generally, if it decays sufficiently fast, we can write, for $|x|\gg 1$

$$\left(\frac{\omega^2}{c^2}+\frac{d^2}{dx^2}\right)\phi(\omega,x)=0\ , \tag{4.17}$$

Writing $\phi(\omega,x)=e^{ikx}$, from the dispersion relation ω^2-k^2, it follows $k\pm x$, so that solutions in these regions write as a linear combination of rightwards-moving and leftwards-moving modes

$$e^{i\omega t}\phi(\omega,x)\sim a(\omega)e^{i\omega(t-x)}+b(\omega)e^{i\omega(t+x)}\ ,\quad |x|\gg 1\ . \tag{4.18}$$

Considering then outgoing boundary conditions amounts to impose

$$\begin{aligned} &x\to+\infty\ ,\quad b(\omega)=0 \quad\Leftrightarrow\ \phi(\omega,x)\sim e^{-i\omega x}\\ &x\to-\infty\ ,\quad a(\omega)=0 \quad\Leftrightarrow\ \phi(\omega,x)\sim e^{i\omega x}\end{aligned} \tag{4.19}$$

to be imposed in Eq. (4.16). As we have commented above, under these conditions the operator P_V is not self adjoint and, therefore, in general we have that solutions have complex frequencies

$$\omega=\omega^{\rm R}+i\omega^{\rm I}\ , \tag{4.20}$$

with $\omega^{\rm R}={\rm Re}(\omega)$ and $\omega^{\rm I}={\rm Im}(\omega)$. From a physics a perspective, an open system with a finite energy, we expect that the function $\phi(t,x)$ to decay in time. This determines the sign of $\omega^{\rm I}$. Indeed, wee see

$$x\to\pm\infty\ \ ,\ \ e^{i\omega x}\phi(\omega,x)\sim e^{i\omega(t\mp x)}=e^{i\omega t}e^{\mp i\omega x}=e^{i(\omega^{\rm R}+i\omega^{\rm I})t}e^{\mp i\omega x}=e^{i\omega^{\rm R}t}e^{-\omega^{\rm I}t}e^{\mp i\omega x}\ . \tag{4.21}$$

We must then impose

$$\omega^{\rm I}={\rm Im}(\omega)>0. \tag{4.22}$$

We are now in conditions to introduce a first heuristic notion of quasi-normal mode:[194]

Quasi-normal modes are solutions $\phi(\omega_{\rm QNM},x)$ to Eq. (4.16) satisfying outgoing boundary conditions (4.19). The corresponding quasi-normal mode frequencies $\omega_{\rm QNM}$ satisfy: ${\rm Im}(\omega_{\rm QNM})>0$.

We note that from (4.22) it the following asymptotic behavior in space follows

$$\begin{aligned} x \to +\infty \ , \quad & \phi(\omega, x) \sim e^{-i\omega x} = e^{-i\omega^{\mathrm{R}} x} e^{\omega^{\mathrm{I}} x} \\ x \to -\infty \ , \quad & \phi(\omega, x) \sim e^{i\omega x} = e^{i\omega^{\mathrm{R}} x} e^{-\omega^{\mathrm{I}} x} \end{aligned} \tag{4.23}$$

That is, from condition (4.22) it follows that the mode $\phi(\omega, x)$ is exponentially divergent at both ends asymptotic ends. This is a typical behavior of quasi-normal modes (in a Cauchy slice). In particular, we see that if an expansion of the wave field is to be found, the latter will essentially make sense in a bounded domain.

We can point out some issues in this Fourier approach to quasi-normal modes:

a) Relation to initial data:

   a.i) The Fourier analysis approach does not show light in the understanding of how quasi-normal modes are excited by initial data perturbations. More specifically, a normal-mode analysis relating the solution to their initial data, as in the self-adjoint case, is not available.

   a.ii) The divergence of the quasi-normal mode at spatial infinity is an artifact of having a mode existing in time since an infinite past: due to the decay behavior in time, the perturbation at past infinity must be arbitrarily large to survive at present time. The system accumulates an infinite amount of energy at spatial infinity. In this sense, a single quasi-normal mode is not a state of the system. One should rather think of perturbations that started at some finite time, and this leads to the need of controlling initial data.

4.3.2 Laplace approach

b) Outgoing boundary conditions in (4.19) are actually not enough to single out just a solution (in the generic case). The asymptotic expansion must be specified in a more refined manner in order to eliminate solutions that "hidden" under the exponential reminder [141] [139]. A more systematic and refined treatment is therefore needed.

The introduction of quasi-normal modes (or resonances) in section 4.3.1 through a heuristic considerations of asymptotic in a Fourier analysis setting presents some shortcomings related to the difficulty to make contact with initial data of propagating modes, on the one hand, and to the insufficient nature of boundary conditions (4.19) to completely determine the solution.

An approach based on the Laplace transform, rather than the Fourier transform, permits to address these issues. General introductions to this approach can be found in [105] [139]

As in the Fourier case, the treatment requires the consideration of time independent systems. We will consider initial data with a compact support: then the solution to equation (4.16) is bounded and admits a Laplace transform. The Laplace transform of $\phi(t, x)$, that will denote as $\mathcal{L}(\phi)(s, t)$ or $\hat{\phi}(t, x)$ is given by

$$\mathcal{L}(\phi)(s, t) = \hat{\phi}(t, x) = \int_0^\infty e^{-st} \phi(t, x) dt \ . \tag{4.24}$$

This is an analytical function as long as the (complex) parameter s satisfies $\mathrm{Re}(s) > 0$, as a consequence of the boundedness of $\phi(t, x)$.

In order to transform Eq. (4.14) under the Laplace transform we note that, given a function $f(t)$ with Laplace transform $\mathcal{L}(f)(s) = \hat{f}(s)$, integration by parts leads to the relations

$$\begin{aligned} \mathcal{L}(f')(s) &= s\hat{f}(s) - f(0) \\ \mathcal{L}(f'')(s) &= s^2\hat{f}(s) - sf(0) - f'(0) \end{aligned} \tag{4.25}$$

Then, applying these transformations to the dynamical Eq. (4.14), we get

$$s^2\hat{\phi}(s,x) - s\phi(0,x) - \frac{\partial}{\partial t}\phi(0,x) - \hat{\phi}''(s,x) + V\hat{\phi}(s,x) = 0 \ , \tag{4.26}$$

that can be rewritten as the inhomogeneous evolution equation

$$-\hat{\phi}''(s,x) + \left(V(x) + s^2\right)\hat{\phi} = I(s,x) \ , \tag{4.27}$$

with

$$I(s,x) = s\phi(0,x) + \frac{\partial}{\partial t}\phi(0,x) \ . \tag{4.28}$$

Given a solution $\hat{\phi}(s,x)$ to (5.1.4), we obtain the solution $\phi(t,x)$ to the original dynamical equation (4.14) with initial data

$$\phi(0,x), \frac{\partial}{\partial t}\phi(0,x) \ , \tag{4.29}$$

4.3.3 Dealing with exploding modes

Complex scaling approach to QNMs

When dealing with QNMs either analytically or numerically, one would face a problem in dealing with the exploding of the modes in both infinities. The complex scaling method was suggested first by [1], [15] and developed later to deal with a "black box" (compactly supported resonator). In [194] details were given to deal specially with QNMs of the problem of compactly supported potential. The advantage of this method is to allow an estimation of the resonances multiplicity, as it can be adopted to normalize the modes. It helps to translate the problem into another differential problem all over the space where the fields do not explode. This method can be used for compactly supported potentials, and also for exponentially decaying potentials.

The idea behind using complex scaling is to re-construct new non self-adjoint operator whose discrete spectrum is the same as the studied operator (P_V), but his eigen functions are different in both regions outside the support of the potential. To make that let us define a parametrization $\gamma : \mathbb{R} \to \Gamma \subset \mathbb{C}$, where Γ is a curve C^1,

Let Γ consists of three parts Γ^-, Γ', and Γ^+ are such in Fig.4.5

The support of V: $[-R,R] \subset \Gamma'$. We construct the operator $P_{V,z} = \partial_\Gamma^2 - V$ For example, let us take Γ as: $z = xe^\theta$, and θ is such that there is no resonances in the region below Γ^+. On $z \in [-R,R]$ the two operators are equal $P_{V,z} = P_V$. In both other regions Γ^-, and Γ^+ we consider the solution to $(P_{0,z} - \lambda)\Phi = 0$, $\Phi^+ = \alpha^+ e^{-i\lambda z}$, and $\Phi^- = \alpha^- e^{i\lambda z}$ (which are different from the solution of $(P_V - \lambda)\phi = 0$, where $\partial_x = e^{i\theta}\partial_z$)

Finally the considered modes over the whole space is:

$$\phi(x) = \begin{cases} \Phi^+(x), x > L \\ \phi(x), x \in [-R,R] \\ \Phi^-(x), x < -L \end{cases} \tag{4.30}$$

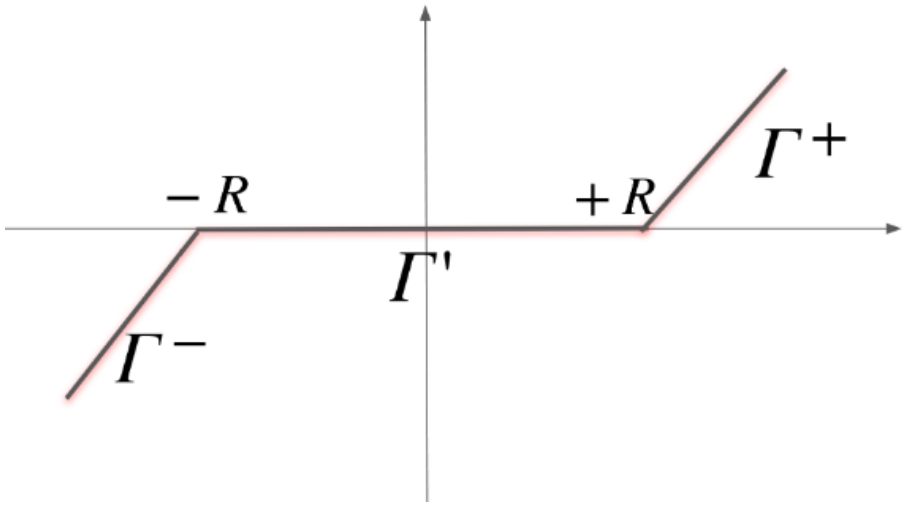

Figure 4.5: Here we show an example of a curve Γ

where they are eigenfunctions of the operator $P_{V,z}$. We have seen how the method of complex scaling helps to deal with the scattering resonance problem boundary conditions which cause the modes to explode at infinities. In technical simulations we do not need to treat the whole space, in particular we do not need to deal with infinities. On the other hand we need to mimic the physical world by assuring outgoing conditions in the far field zone. In the next paragraph we will show the widely used method to do so.

4.3.4 Perfectly matched layer (PML)

Perfectly matched layer (PML) method is a way to terminate infinite domain calculations. It could be seen from a physical point of view as adding a totally absorbent layer around a resonator in the far field region in order to absorb all the outgoing waves of the resonator and to not reflect any part of it (which is exactly what is required in scattering problems).
PML was proposed by Berenger to deal with electromagnetism problems. First he introduced an effective absorbent medium which needed for computations and simulations in 2D [18] and later in 3D.[19]
Considering an electromagnetic wave in free space with ($E_z = 0$). Maxwell equations can be written as:

$$\begin{aligned} \frac{\partial H_z}{\partial t} + \sigma^* H_z &= \frac{\partial E_x}{\partial y} - \frac{\partial E_y}{\partial x} \\ \frac{\partial E_y}{\partial t} + \sigma E_y &= -\frac{\partial H_z}{\partial x} \\ \frac{\partial E_x}{\partial t} + \sigma E_x &= \frac{\partial H_z}{\partial y}, \end{aligned} \tag{4.31}$$

where σ is the electric conductivity, and σ^* is the magnetic one. If $\sigma = \sigma^*$ then the impedance of the medium equals that of the vacuum, so if a wave is scattering from this medium to the vacuum, it will encounter no impedance and no reflection will occur. The genius work of Berenger suggests splitting the magnetic field H_z into $H_{zx} + H_{zy}$, so Maxwell equations can be re-written

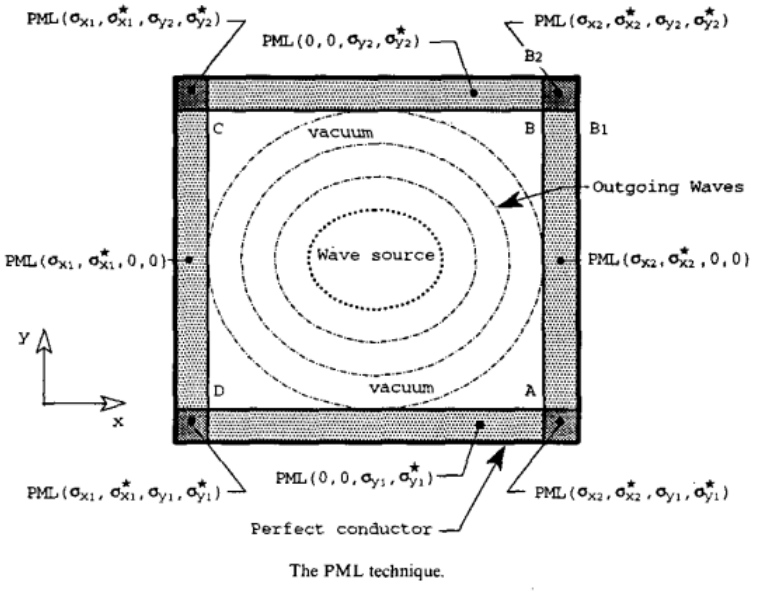

Figure 4.6: Perfectly match layer as it was proposed by Berenger at first time. [18]

as the following:

$$\begin{aligned}
\frac{\partial H_{zy}}{\partial t} + \sigma^*(y) H_{zx} &= \frac{\partial E_x}{\partial y} \\
\frac{\partial H_{zx}}{\partial t} + \sigma^*(x) H_{zx} &= -\frac{\partial E_y}{\partial x} \\
\frac{\partial E_y}{\partial t} + \sigma(x) E_y &= -\frac{\partial H_z}{\partial x} \\
\frac{\partial E_x}{\partial t} + \sigma(y) E_x &= \frac{\partial H_z}{\partial y}.
\end{aligned} \tag{4.32}$$

Imposing certain conditions on the relations between $\sigma(x)$, $\sigma(y)$, $\sigma^*(x)$ and $\sigma^*(y)$, allow to construct a medium with no reflection.

For example when $\sigma(y) = \sigma^*(y) = 0$ the medium can absorb a wave propagating along x and when $\sigma(x) = \sigma^*(x) = 0$ the medium can absorb a wave propagating along y. If the conductivities of these two mediums are equal, then the medium which has interface with both do not reflect any wave as the corners as in Fig.4.3.4.

Berenger method was derived in Cartesian coordinates for simply-shaped domains with straight (planar) artificial boundaries. Later many studies were made to improve PMLs and make it more flexible with respect to coordinated and the shape of the scatterer. [135], [187], [160], [112], [50], [51] A remarkable one is on a strong relation with complex scaling method. It depends on stretching coordinates by introducing a stretching function. It can also be regarded as changing the metric. For a TE case equivalently to Berenger PML, a change of variables could be made to have the same results.

$$x' = x + \frac{i}{\omega} \int_0^x \sigma(s) ds \tag{4.33}$$

The method of changing variables has advantages over Berenger's PML in curvilinear coordinates. It was shown by [52] that it gives much more accurate absorbing layer in polar and other

coordinates.

Other improvements are mentioned in the review of [152] Review and recent developments on the perfectly matched layer (PML) method for the numerical modeling and simulation of elastic wave propagation in unbounded domains

The method which we adopt here in this work depends also on coordinates transfer, but from a space-time perspective. It's called Hyperboloidal Slices Approach. It is a beautiful method that has some advantages especially when dealing with gravitational potentials problems that just vanish at infinities. Here we will focus on some technical details that allows the modes to not explode at both infinities as this is the objective of the current section.

4.3.5 A contact with hyperboloidal slices

Bizoń-Mach changing coordinates is written as:

$$\begin{aligned} \tau &= t - \ln(2\cosh(x)) \\ y &= \tanh(x) \end{aligned} \tag{4.34}$$

A field $\phi(t,x)$ (in the conventions we chose) is proportional to: $e^{i\omega t}\phi_x(x)$ in the Cartesian coordinates. The same field will be written as $e^{i\omega\tau}\phi_y(y)$ in the new coordinates.
Actually

$$e^{i\omega t}\phi_x(x) = e^{i\omega\tau}e^{+i\omega\ln(2\cosh(x))}\phi_x(x) = e^{i\omega\tau}\phi_y(y), \tag{4.35}$$

thus the relation between both considered fields in both coordinates systems is:

$$\phi_y(y) = e^{+i\omega\ln(2\cosh(x))}\phi_x(x) \tag{4.36}$$

Considering modes and as $\omega_n = \omega_n^R + i\omega_n^I$ then:

$$\phi_{yn}(y) = e^{-\omega_n^I\ln(2\cosh(x))}\phi_{xn}(x) \tag{4.37}$$

The part $e^{-\omega_n^I\ln(2\cosh(x))}$ introduce an attenuation to the mode so they do not explode at infinities. To be more explicit at infinities a QNM is written as:

$$\begin{aligned} \phi_{xn}(x) &\sim e^{-i\omega_n x} \text{ for } x \to +\infty \\ \phi_{xn}(x) &\sim e^{+i\omega_n x} \text{ for } x \to -\infty \end{aligned} \tag{4.38}$$

But the considered modes in (τ, y) coordinates are:

$$\begin{aligned} \phi_{yn}(y) &\sim e^{+i\omega_n\ln(2\cosh(x))}e^{-i\omega_n x} \text{ for } x \to +\infty \\ \phi_{yn}(y) &\sim e^{+i\omega_n\ln(2\cosh(x))}e^{+i\omega_n x} \text{ for } x \to -\infty \end{aligned} \tag{4.39}$$

This can be re-written as:

$$\begin{aligned} \phi_{yn}(y) &\sim e^{\omega_n^I(x-\ln(2\cosh(x)))} \text{ for } x \to +\infty \\ \phi_{yn}(y) &\sim e^{-\omega_n^I(x-\ln(2\cosh(x)))} \text{ for } x \to -\infty \end{aligned} \tag{4.40}$$

Both functions do not diverge, as $\lim_{x\Rightarrow\infty}(\ln(2\cosh(x))) = x$ and the term of attenuation compensate the divergence of modes in (t,x) coordinates.

Chapter 5

QNM: completeness and stability issues

Contents

This chapter touches one of the most QNMs issues debating points. In the first section that is about completeness and resonant expansion we pass by some different senses of defining QNMs completeness in literature then we introduce the most hitting theories and approaches related to this issue. At the end we give a starting point for the discussion of stability of resonance frequencies by mentioning the two keys we will be using later in results chapters, that are the pseudospectrum and conditioning number.

5.1 Completeness

5.1.1 Introduction

Quasi normal modes completeness was studied for different systems and with different definitions. We aim here at discovering some different points of view about what is meant by QNMs completeness. To start we need to have a clear vision about what are QNMs. It is widely believed especially in optics domain, that QNMs are the eigen solutions to the time independent wave equation with a zero source and subject to outgoing boundary conditions. However this definition is not Mathematically rigorous, where QNMs frequencies are known as scattering resonances and defined as the poles of the meromorphic continuation of the resolvent in the complex plan. In the field of gravitational physics, they are known nowadays by their mathematical definition. We adopt here this definition which was mentioned by Dyatlov et al..
Many works were done to assess the relation between the spectrum and the resolvent poles depending on identifying Fredholm operators. It is stated in the article [100], and then in [21], that if T is unbounded close operator then "T has a purely discrete spectrum if and only if T has a Riesz resolvent". For the particular case of a QNMs problem with a compactly supported potential in 1D, Dyatlov et al. [68] have proved that in this case the poles of the resolvent coincide with the points of the spectrum which is discrete. No similar work, up to our knowledge, was done for a compactly supported permittivity in the optical domain.

5.1.2 The evolved definition of completeness

- It seems from the old literature in gravitational physics (before 1970) that completeness sometimes was stated although no rigorous mathematical proof was given (similar to optical domain nowadays)(the is explained in [55].

- Also it is obvious from the article of [27] that it was believed in the equivalence relation between having a discrete spectrum, and the completeness in the sense of that the eigenfunctions form a basis of Hilbert space. In [27], it was written: ". All linear stability arguments in astrophysics concerning spherically symmetric stars depend crucially on the completeness of the eigenfunctions of the associated operators, which is equivalent to the fact that these operators have a pure point spectrum."

- In Beyer and Schmidt article they considered that the possible incompleteness in QNMs problems results from having a continuous part in the spectrum. The completeness they were describing is defined as the following: *On an initial hyper surface of the star one is given Cauchy data. Completeness means that a sum of modes can be constructed which agrees with these Cauchy data.*

- This was not the case anymore in [26], where their proof of the completeness in Pöschel teller case depended on knowing the exact QNMs frequencies, and then deducing QNMs functions and integrating in the complex plan. The definition of the completeness that was adopted, which is our interest here, is as the following, they wrote:
"let f be some complex-valued C^∞-function with compact support and let ϕ_f be the corresponding solution with initial values:

$$\phi_f(0,x)=0, \qquad \text{and} \quad \frac{d\phi_f}{dt}(0,x)=f(x). \tag{5.1}$$

For all real x. Denote by $\phi_{f,g}$ the following averaged function obtained from ϕ_f ,

$$\phi_{f,g}(t) := \begin{cases} \int g^*(x)\phi_f(x)dx & \text{if } t\geq 0 \\ 0 \text{ if} \quad t<0, \end{cases} \tag{5.2}$$

where g is some complex-valued C^∞ -function with compact support. *The quasi-normal modes of V are complete, in the sense that there is a family of complex numbers c_ω where $\omega \in q(A)$ (QNMs frequencies) such that for for a large enough t_0 and for every $t\in[t_0,\infty[$:*

$$\left(c_\omega \int_{-\infty}^{\infty} u_\omega(y')f(y')dy' \int_{-\infty}^{\infty} g^*(x')u_\omega(x')dx' e^{i\omega t} \right)_{\omega\in q(A)}, \tag{5.3}$$

is absolutely summable with sum $\phi_{g,f}(t)$. So the summation of this sequence (using any order of summation) gives the quasinormal mode expansion of $\phi_{g,f}(t)$ for large times".

- We would like to refer too to the completeness definition by [155] : "QN mode completeness means that the coefficients α_n and β_n can be chosen so that the sum:

$$\theta = \sum_{-\infty,odd}^{\infty} (\alpha_n + i\beta_n)(e^{i\omega_n x} - e^{-i\omega_n x})e^{-i\omega_n t}, \tag{5.4}$$

agrees with any specified Cauchy data at (say) $t = 0$. In terms of the functions $C(x) = \theta(x, t = 0)$, and $E(x) = \int_0^x \frac{\partial}{\partial t}\theta(x', t)|_{t=0}dx'$. "

- And finally in the article of Nollert et al. [140] completeness is about expressing the evolved field in time in term of QNMs, from the article: "A complete QNMs system, satisfies:
  - The solutions to the QNMs eigenvalue problem form a discrete spectrum and can be arranged in order of increasing $|\mathtt{Re}(\omega_{\mathtt{n}})|$.
  - We consider only Cauchy data that:
    * has support only within a compact region,
    * belongs to a specific continuity class C^p , where $p \in$ N depends on the nature of the problem,
    * results in a waveform which is square integrable in t, with $t \in [t_{min}, +\infty[$, (t_{min} is the moment that Cauchy initial data start to arrive to the observed point).
  - For such Cauchy data, the waveform $f(t)$ that evolves from any such allowed Cauchy data can be written as:
$$f(t) = \sum_n a_n e^{i\omega_n t}. \tag{5.5}$$

Apart from that we will discuss three different remarkable developments to approach the QNMs expansion.

5.1.3 Mittag-Leffler theorem

The Mittag−Leffler theorem on expansion of a meromorphic function (see ,) is one of the basic theorems in analytic function theory, giving for meromorphic functions an analogue of the expansion of a rational function into the simplest partial fractions. Let $\{a_n\}_{n=1}^{\infty}$ be a sequence of distinct complex numbers, $|a_1| \leq |a_2| \leq \dots$, with $\lim_{n\to\infty} a_n = \infty$, and let $g_n(z)$ be a sequence of rational functions of the form

$$g_n(z) = \sum_{k=1}^{I_n} \frac{1}{(z - a_n)^k}, \tag{5.6}$$

so that an is the unique pole of the corresponding function $g_n(z)$. Then there are meromorphic functions $f(z)$ in the complex $z-$plane C having poles at a_n, and only there, with given principal parts 5.6 of the Laurent series corresponding to the points an. All these functions f(z) are representable in the form of a Mittag-Leffler expansion

$$f(z) = h(z) + \sum_1^{\infty}[g_n(z) + p_n(z)], \tag{5.7}$$

where $p_n(z)$ is a polynomial chosen in dependence of an and $g_n(z)$ so that the series 5.7 is uniformly convergent (after the removal of a finite number of terms) on any compact set $K \in$ C and $h(z)$ is an arbitrary entire function. The Mittag-Leffler theorem implies that any given meromorphic function $f(z)$ in C with poles an and corresponding principal parts $g_n(z)$ of the Laurent expansion of $f(z)$ in a neighborhood of an can be expanded in a series 5.7 where the entire function $h(z)$ is determined by $f(z)$. Mittag-Leffler gave a general construction of the

polynomials $p_n(z)$; finding the entire function $h(z)$ relative to a given $f(z)$ is sometimes a more difficult problem. To obtain 5.7 it is possible to apply methods of the theory of residues.
As a result of this theorem if one knows that the scattered field is a meromorphic function in C and it has only simple poles, then it can be expanded over these poles.

5.1.4 Heuristic approach: Resonant expansions in Laplace

Considering again the equation (4.24). Through the inverse of the Laplace transform given by Bromwich intregal

$$\phi(t,x) = \frac{1}{2\pi i}\int_{c-i\infty}^{c+i\infty} e^{st}\hat{\phi}(s,x)ds \ , \tag{5.8}$$

where $c > 0$. In order to construct a solution to the inhomogeneous equation we consider the homogeneous equation:

$$-\hat{\Psi}''(s,x) + \left(V(x) + s^2\right)\hat{\Psi} = 0 \ , \tag{5.9}$$

Note that thus can be written as: $P_V\hat{\Psi}(s,x) = -s^2\hat{\Psi}(s,x)$
Which coincide with the one in the Fourrier approach. $P_V\hat{\Psi}(s,x) = \lambda\hat{\Psi}(s,x)$
Where the implicit relation: $s = iw$ is employed. Therefore points in the complex "s-space" are related $\pi/2$ with respect to points in the complex ω-space. The general solution of is given by the sum of the general solution to the homogeneous plus a particular solution:

$$\hat{\Psi}(s,x) = \hat{\Psi}_{ge}(s,x) + \hat{\Psi}_p(s,x). \tag{5.10}$$

Given two particular solutions of the homogeneous equation $\Psi_1(s,x)$, $\Psi_2(s,x)$, the general solution of the homogeneous is written by: $\Psi_a\hat{(s,x)} = a(s)\Psi_1 + b(s)\Psi_2$ On the other hand, the particular solution $\hat{\Psi}_p$ of the inhomogeneous equation can be constructed from an appropriate Green function $G(s,x,x')$:

$$\hat{\Psi}_p(s,x) = \int_{-\infty}^{+\infty} G(s,x,x')I(s,x')dx'. \tag{5.11}$$

In 1D Green function can be constructed from two linearly independent solutions to the homogeneous solution: $f_-(s,x)$ and $f_+(s,x)$ Then, it can be shown:

$$G(x,x') = \frac{1}{\mathbb{W}(s)}f_-(s,x_<)f_+(s,x_>) = \begin{cases} \frac{1}{\mathbb{W}(s)}f_-(s,x')f_+(s,x) & if x' < x, \\ \frac{1}{\mathbb{W}(s)}f_-(s,x)f_+(s,x') & if x' > x. \end{cases} \tag{5.12}$$

Where $x_< = min(x,x')$ and $x_> = max(x,x')$, and the Wronskian $\mathbb{W}(s) = f_-(s,x)f_+'(s,x) - f_-'(s,x)f_+(s,x)$. Note that the fact that $f_-(s,x)$ and $f_+(s,x)$ are solutions of the homogeneous equation implies the independence of $\mathbb{W}(s)$with respect to x.
In our treatment the initial conditions are fixed by the source $I(s,x)$.
The information about the homogeneous equation is fully encoded in the chosen Green function. We must determine the chosen $f_-(s,x)$ and $f_+(s,x)$. The criterion is given by the band charecter of $\Psi(t,x)$ i.e. in space-time. Thus implies that the Laplace transform must be also bounded in x.
For simplicity, let us assume that $V(x)$ is of compact support then i.e. $V(x) = 0x > x_max, x <$

$x_m in$. For $x > x_m ax$ the only solution to the homogeneous (up to a constant) that doesn't diverge at infinity is given by $f_+(x) = e^{-sx}(x > x_m ax)$thus fixes completely f_1. Likewise the only solution to the homogeneous diverge at $-\infty$ is e^{sx} (Here $s \in \mathbb{C}, \text{with} Re(s) > 0$) . The uniqueness of f_- bounded at $-\infty$ and f_+ at ∞ can be shown in general cases (for potentials decaying sufficiently fast). Therefore we have:

$$\lim_{x\to-\infty} f_-(x) = e^{sx} \ \Re(s) > 0, \tag{5.13}$$

$$\lim_{x\to+\infty} f_+(x) = e^{-sx} \ \Re(s) > 0. \tag{5.14}$$

$$\tag{5.15}$$

Which are completely fixed. Note that no "ad hoc" boundary condition have been imposed. These conditions follow from the natural requirement of boundedness of the $\Psi(t, x)$ defined in a Cauchy problem.

Quasi-normal modes Once the Laplace transform is calculated, we can have the space-time picture with inverse Laplace transform:

$$\Psi(t, x) = \frac{1}{2\pi i} \int_{c-i\infty}^{c+i\infty} e^{st} \hat{\Psi}(s, x) ds \quad c > 0. \tag{5.16}$$

In order to evaluate this integral we deform it in the complex plane, and applying Cauchy theorem:

$$\oint \hat{\Psi}(s, x) e^{st} ds = 2\pi i \Sigma_q Res[\hat{\Psi}(s, x) e^{st}, sq] \tag{5.17}$$

Under the following assumptions:

- The integral on the circular contour, when the radius becomes infinitely large, is infinitely small.
- There are no essential singularities.
- f_- and f_+ are analytic in s.

In this case we can write:

$$\Psi(t, x) = \frac{1}{2\pi i} \int_{c-i\infty}^{c+i\infty} e^{st} \int_{\infty}^{+i\infty} G(s, x, x') I(s, x') dx' ds \tag{5.18}$$

$$= \frac{1}{2\pi i} \oint e^{st} \frac{1}{\mathbb{W}(s)} \int_{-\infty}^{\infty} f_-(x <) f_+(x >) I(s, x') dx' ds. \tag{5.19}$$

The only non analycity is related to poles associated to zeros of $\mathbb{W}(s)$, so we have from Cauchy theorem:

$$\Psi(t, x) = \frac{1}{2\pi i} 2\pi i \Sigma_q e^{s_q t} Re[\frac{1}{\mathbb{W}(s)}, s_q] \int_{-\infty}^{+\infty} f_-(s, x_<) f_+(s, x_>) I(s_q, x') dx'. \tag{5.20}$$

For a simple pole:

$$Res(f, c) = \lim_{z\to c}(z - c) f(z). \tag{5.21}$$

If $f(z) = \frac{g(z)}{b(z)}$, with $g(z)$ and $b(z)$ analytic and $b(c) = 0$, $b^{'}(c) \neq 0$ Using l'hopital: $Res(f, c) = \lim_{z\to c}(z-c)f(z) = \lim_{z\to c}\frac{\frac{d}{dt}(z-c)g(z)}{\frac{d}{dt}b(z)} = \lim_{z\to c}\frac{g(z)+(z-c)g(z)}{b^{'}(z)} = \frac{g(c)}{b^{'}(c)}\cdot$ Therefore

$$\Psi(t,x) = \Sigma e^{s_q t}\frac{1}{\mathbb{W}(s_q)}\int_{-\infty}^{+\infty} f_-(s,x_<)f_+(s,x_>)I(s_q,x')dx'. \tag{5.22}$$

If the initial data have a compact support $[x_min, x_max]$ then, for $x > x_max$:

$$\Psi(t,x) = \Sigma e^{s_q t}\frac{1}{\mathbb{W}(s_q)}f_+(s_q,x)\int_{-\infty}^{+\infty} f_-(s,x')I(s_q,x')dx' \tag{5.23}$$

$$= \Sigma c_q^+ U_q^+(t,x). \tag{5.24}$$

Where

$$c_q^+ = \frac{1}{\mathbb{W}(s_q)}\int_{-\infty}^{+\infty} f_-(s,x')I(s_q,x')dx' \tag{5.25}$$

$$U_q^+(t,x) = e^{s_q t}f_+(s,x). \tag{5.26}$$

For $x < x_min$:

$$\Psi(t,x) = \Sigma e^{s_q t}\frac{1}{\mathbb{W}(s_q)}f_-(s_q,x)\int_{-\infty}^{+\infty} f_+(s,x')I(s_q,x')dx' \tag{5.27}$$

$$= \Sigma c_q^- U_q^-(t,x). \tag{5.28}$$

Where

$$c_q^- = \frac{1}{\mathbb{W}(s_q)}\int_{-\infty}^{+\infty} f_+(s,x')I(s_q,x')dx' \tag{5.29}$$

$$U_q^-(t,x) = e^{s_q t}f_-(s,x). \tag{5.30}$$

Zeros of the Wronskian can not occur for $Re(s) > 0$ indeed the solutions $f_+(s,x)$ and $f_-(s,x)$ are linearly independent, so the $\mathbb{W}(s) \neq 0$. Zeros of the Wronskian can occur for adequate potentials, of $Re(s) < 0$ corresponding to the analytic extension of $f_+(s,.)$ and $f_-(s,.)$ to $Re(s) < 0$ If the Wronskian equals zero $f_+(s,x)$ and $f_-(s,x)$ are proportional, as a consequence of the boundedness condition of the Laplace transform for $Re(s) > 0$ the analytic extension of $f(s_q,x) = f_-(s_q,x) = f_+(s_q,x)$ to the left half complex plane satisfy:
$\lim_{x\to-\infty} f_(s_q,x) = e^{sx}\ \Re s > 0,$

$\lim_{x\to+\infty} f_(s_q,x) = e^{-sx}\ \Re s < 0.$
Using $s = i\omega$ we recover the outgoing boundary condition:

$$\lim_{x\to-\infty} f_(s_q,x) = e^{+i\omega x}, \tag{5.31}$$

$$\lim_{x\to+\infty} f_(s_q,x) = e^{-i\omega x}, \tag{5.32}$$

with $Re(s) < 0$ so $Im(\omega) > 0$.

Both Leung et al. in [119], [118] and Nollert et al. in [140], [139] used the fact that a Green function can be written as the multiplication of two solutions of the homogeneous equation over their Wronskian.
Both also verified or set some conditions in order to assure the vanishing of the integral over the half circle.

Leung et al. work

In optics, the work by Leung et al. is widely used when referring to QNMs completeness. This is justified (in physics domain) by their statement: "The derivations presented in this paper conform to the usual standards of rigor in physics, but do not constitute a fully mathematical proof." In [119], they have treated a scattering problem with permittivity that only depends on x and not on ω. The homogeneous wave equation they studied is:

$$[\epsilon(x)\frac{\partial^2}{\partial t^2} - \frac{\partial^2}{\partial x^2}]\phi(t,x) = 0. \tag{5.33}$$

They have used WKB approximation and a certain inner product to show that having a cut in the potential (here permittivity) leads to a complete set of QNMs.
In [118] used a permittivity that depends on x and also on ω but in a certain way to assure the vanishing of the contour integral over the half circle.

$$\epsilon(\omega,x) = \epsilon_\infty(x) + \frac{c}{\omega} + ... \tag{5.34}$$

An important point is that they have just stated **Completeness inside the cavity**. Completeness in their articles means that we can expand the retarded Green function as a sum over the resonant frequencies.

$$G(x,y;t) = \frac{i}{2}\sum_{j>0}\frac{f_j(x)f_j(y)e^{-i\omega_j t}}{\omega << f_j|f_j >>}. \tag{5.35}$$

Or if

$$\delta(x-y) = Re[i\sum_{j>0}\frac{f_j(x)f_j(y)I_j(\tau)}{<< f_j|f_j >>}], \tag{5.36}$$

where f_j is a solution to the homogeneous equation, I_j is the source.

Nollert et al. work

Nollert et al. in [140] have treated a Cauchy problem for the following wave equation:

$$[\frac{\partial^2}{\partial t^2} - \frac{\partial^2}{\partial x^2} + V(x)]\phi(t,x) = 0. \tag{5.37}$$

They have assumed the condition in 5.1.2. and for a certain potential "spiked truncated dipole potential"

$$V_{STDP}(x) = V_{TDP}(x) + V_\delta\delta(x-x_\delta), \tag{5.38}$$

where

$$V_{TDP}(x) = \begin{cases} 0 & x < x_0 \\ \frac{1}{x^2} & x \geq x_0. \end{cases} \tag{5.39}$$

For this specific potential they have shown an asymptotic logarithmic behavior of the eigenvalues, then have shown the convergence of the following series: $\sum_{-n}^{n} a_k e^{s_k t}$ to the evolved field.

Application to 1D optical cavity

To build the Green function, we choose the independent solutions f_- and f_+ of the homogeneous equation, as in the figures.
Solution f_+:

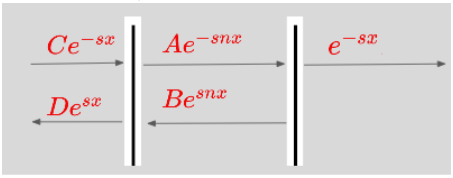

Solution f_-:

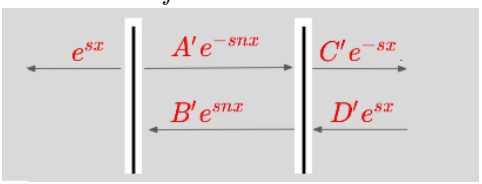

Coefficients are fixed from continuity of the field and its first derivative at the interfaces. The Wronskian is the same in the three regions, with value

$$W(s) = -2C. \tag{5.40}$$

That is zero for the complex frequencies of QNMs:

$$\left(\frac{n-1}{n+1}\right)^2 e^{-2ns_jL} = 1\ . \tag{5.41}$$

Completeness for Pösch-Teller potential

Beyer in [26] treated the a Cauchy problem with a Pöschel-Teller potential; that is:

$$V(x) := \frac{V_0}{cosh^2(x/b)}, x \in R. \tag{5.42}$$

"A main result is that after a large enough time t_0 , the solutions of this equation corresponding to C^∞-data with compact support can be expanded uniformly in time with respect to the quasi-normal modes, thereby leading to absolutely convergent series."
The sense of completeness is as in 5.1.2.

5.1.5 Resonant expansions: Spectral approach (Lax-Phillips to Zworski)

We discuss here a version of a theory stated first by [116], and adapted later by [192] to a theorem in $\mathbb{R}^n$ for odd dimensions, we consider $V(\mathbf{x})$ real, bounded and with support inside a ball of radius R_0 (i.e. $\text{supp}(V) \subset B(0, R_0)$), the operator P_V is given by $P_V = -\Delta + V$, and the resolvent $R_V(\omega)$ is given by $(P_V - \omega^2 I)^{-1}$.

Theorem [192]
Let us consider $\phi_s(t, \mathbf{x})$ be a solution of

$$\begin{cases} \left(\partial_t^2 + P_V\right)\phi_s(t,\mathbf{x}) = 0\ , \\ \phi(0,\mathbf{x}) = \phi_1(\mathbf{x}) \in H^1(B(0,R_1))\ , \\ \partial_t\phi(0,\mathbf{x}) = \phi_2(\mathbf{x}) \in L^2(B(0,R_2))\ , \end{cases} \tag{5.43}$$

where $R_1 \geq R_2$. Then for any $a > 0$

$$\phi_s(t, \mathbf{x}) = \sum_{\mathrm{Im}(\omega_j)<a} e^{i\omega_j t} u_j(\mathbf{x}) + E_a(t) \ , \tag{5.44}$$

where $\{\omega_j\}_{j=1}^{\infty}$ are the resonances of P_V and u_j are the corresponding resonant states

$$u_j = \mathrm{Res}_{\omega=\omega_j} \left(iR_V(\omega)\phi_2 + \omega R_V(\omega)\phi_1 \right) \tag{5.45}$$

and there exists a constant C_a depending on V and R_1 and a such that

$$\begin{aligned} &||E_a(t)||_{H^1(B(0,R_1))} \\ &\leq C_a e^{-ta} \left(||\phi_1||_{H^1} + ||\phi_2||_{L^2} \right) \ , \ t \geq 0 \ . \end{aligned} \tag{5.46}$$

Remarks

- Note that u_j in the expansion is the action of the resolvent on the initial data. The translation of that to a scattering problem would be the action of the resolvent on the source. We remind that u_j is a resonant state as defined in 4.2.2 [30].
- Note that u_j are not normalized, so the theory does not define coefficients for normalized resonant states.

Here are some remarks on the result of the theorem:
There is no guaranty that t. The only fact we have is that the error is smaller than Ce^{-ta}, where c is a function of a.

- If C is a constant then

$$\begin{aligned} &\forall a \in \mathbb{R}^+ \text{ and } \exists \lambda_0 \in \mathrm{Spec}(P_V) \text{ s.t. } -a < \lambda_0 :\Rightarrow \\ &\forall \epsilon > 0 : \exists t_0 \text{ s.t. } \forall t > t_0 \Rightarrow Ce^{-at} < \epsilon \Rightarrow \\ &||E_a(t)||_{H^1(B(0,R_1))} \leq \epsilon \\ &||\phi_s(t, \mathbf{x}) - \sum_{\mathrm{Im}(\omega_j)<a} e^{i\omega_j t} u_j(\mathbf{x})||_{H^1(B(0,R_1))} \leq \epsilon \end{aligned} \tag{5.47}$$

- If C is an increasing function but slower than e^{at} such that $\lim_{t\to\infty} \frac{C(a)}{e^{at}} = 0$ then also waiting a proper time then the error function vanishes for t large enough.
- If $\lim_{t\to\infty} \frac{C(a)}{e^{at}} = \infty$ the error will be growing when taking more modes into account.
- If $\lim_{t\to\infty} \frac{C(a)}{e^{at}} =$ *constant* this means that there is always an error of expansion that does not vanish by taking more modes, and the field is not converging exactly to the expansion.

5.1.6 Keldysh expansion

QNM Keldysh expansion

Keldysh's asymptotic expansion of the resolvent provides explicitly the possibility to write the resolvent $(L - \omega)^{-1}$ of an operator L as a sum over ω. That is in the case of non-selfadjoint

operators [102, 103, 129, 28, 29]. However this does not mean that the general expansion in Keldysh theorem is uniformly converging to the resolvent besides the existence of a holomorphic function to be added to the sum.

Let us consider a non-selfadjoint operator L and its adjoint $L^\dagger$ with respect to a given scalar product $\langle\cdot,\cdot\rangle$. Then, right- v_n and left- w_n (proper) eigenvectors are defined, respectively, as the eigenvectors of L and $L^\dagger$

$$Lv_n = \lambda_n v_n \quad , \quad L^\dagger w_n = \overline{\lambda}_n w_n \ . \tag{5.48}$$

Notice that v_n and w_n are normalizable vectors. Let us assume, for simplicity, that eigenvalues are simple. In this context, instead of a standard normalization, let us adopt the condition

$$\langle w_n, v_n\rangle = -1. \tag{5.49}$$

This condition can be generalized (see [102, 103, 129, 28, 29], in particular taking into account the Jordan decomposition of L). We can then normalize one of them, but in general not both. That is, in general v_n and w_n are not normalized: $\langle v_n, v_n\rangle \neq 1 \neq \langle w_n, w_n\rangle$. In this setting, we consider a bounded domain $\Omega_\lambda \in \mathbb{C}$. Under appropriate hypothesis (namely the discreteness and isolation of λ_n, guaranteed if $L-\lambda I$ is Fredholm), there is a finite number N of eigenvalues $\lambda_n \in \Omega$. In this setting, Keldysh's expansion [102, 103, 129, 28, 29] of the resolvent in $\lambda \in \Omega$ writes, in the "bra" , "ket" notation, as

$$(L-\lambda)^{-1} = \sum_{\lambda_n\in\Omega} \frac{|v_n\rangle\langle w_n|}{\lambda-\lambda_n} + H(\lambda) \ , \tag{5.50}$$

where $H(\lambda)$ is analytic in Ω (see full technical details of this case in [28]). Let us denote this formally as

$$(L-\lambda)^{-1} \sim \sum_{\lambda_n\in\Omega} \frac{|v_n\rangle\langle w_n|}{\lambda-\lambda_n} \ , \tag{5.51}$$

namely, the resolvent in (bounded) Ω is written as a finite sum of poles plus an analytical function.

Note that to write a more explicit Keldysh expansion is subject to the choice of the scalar product.
A QNMs expansion relevant to 5.1.5 and 5.1.6 will be discussed with details in 12.

5.2 QNM spectrum stability

The spectral theory of self-adjoint operators tells us that they are stable under small perturbation. This also can be extended to normal operators on some Hilbert space. That is if P is a normal operator with a spectrum $\sigma(P)$, then adding a small perturbation operator ϵE, where $||E|| = 1$ (the norm in the studied Hilbert space), will not displace the eigenvalues farer than a spectral distance of the same order of ϵ. More specifically, due to the well known resolvent estimate, one can write [166] : $(z-P)^{-1} \leq (\mathrm{dist}(z,\sigma(P)))^{-1}$.
However, for non-normal operators $(z-P)^{-1}$ may be very large even when z is far from the spectrum which makes the eigenvalues very unstable under small perturbations of the operator. Basically there are two mathematical tools that can help to estimate the instability. Those are the pseudospectrum which is a map over the complex plan (or a chosen region of the complex plan in practice) (see 9) and the conditioning number that can be calculated for a certain eigenvalue to estimate how unstable it is. Both will be discussed later in details in 9, 10.1.3 and in 10.1.2

Part II

Part two: Technical formalism

Chapter 6

Pseudospectrum

Contents

Stability investigation is an important issue when studying eigen value problem solutions such as when finding QNMs frequencies. ϵ-pseudospectrum is a powerful tool that can be calculated for different points of complex plan, this allows to visualize different degrees of (in)stabilities in different areas of the plan and know for an ϵ order perturbation of an operator, what are the possible values of perturbed eigenvalues. Here we introduce its notions, conditioning number and finally discussing the pseudospectrum contour lines in relation with random perturbation. The spectrum of a non-self-adjoint operator is potentially unstable under small perturbations of the operator. Let us consider a linear operator A on a Hilbert space with scalar product $\langle\cdot,\cdot\rangle$, and denote its adjoint by $A^\dagger$, satisfying $\langle A^\dagger u, v\rangle = \langle u, Av\rangle$. The operator A is called normal if and only if $[A, A^\dagger]=0$. In particular, a self-adjoint operator $A^\dagger = A$ is normal. In this setting, the 'spectral theorem' (under the appropriate functional space assumptions) states that a normal operator is characterized as being unitary diagonalizable. The eigenfunctions of A form an orthonormal basis and, crucially in the present discussion, the eigenvalues are stable under perturbations of A. The lack of such a 'spectral theorem' for non-normal operators entails a severe loss of control on eigenfunction completeness and the potential instability of the spectrum of the operator A. Here, we focus on this second aspect.

6.1 Spectral instability: the eigenvalue condition number

Let us consider an operator A and an eigenvalue λ_i. Left u_i and right v_i eigenvectors are characterized as [1]

$$A^\dagger u_i = \bar{\lambda}_i u_i \quad , \quad A v_i = \lambda_i v_i \ , \tag{6.1}$$

with $\bar{\lambda}_i$ the complex conjugate of λ_i. Let us consider, for $\epsilon > 0$, the perturbation of A by a (bounded) operator δA

$$A(\epsilon) = A + \epsilon\, \delta A \quad , \quad ||\delta A|| = 1 \ . \tag{6.2}$$

[1] In the matrix case $u_i^* A = \lambda_i u_i^*$, with $u^* = \bar{u}^t$, i.e. u_i are indeed left-eigenvectors.

The eigenvalues [2] in the perturbed spectral problem

$$A(\epsilon)v_i(\epsilon) = \lambda_i(\epsilon)v_i(\epsilon) \ , \tag{6.3}$$

satisfy

$$\begin{aligned} |\lambda_i(\epsilon) - \lambda_i| &= \epsilon \frac{|\langle u_i, \delta A v_i(\epsilon)\rangle|}{|\langle u_i, v_i\rangle|} = \epsilon \frac{|\langle u_i, \delta A v_i\rangle|}{|\langle u_i, v_i\rangle|} + O(\epsilon^2) \\ &\leq \epsilon \frac{||u_i||||\delta A v_i||}{|\langle u_i, v_i\rangle|} + O(\epsilon^2) \leq \epsilon \frac{||u_i||||v_i||}{|\langle u_i, v_i\rangle|} + O(\epsilon^2) \ , \end{aligned} \tag{6.4}$$

where the first line generalizes [101, 180] the expression employed (for self-adjoint operators, where $u_i = v_i$) in quantum mechanics first-order perturbation theory, the first inequality in the second line is the Cauchy-Schwartz inequality and in the second inequality we make explicit use of an operator norm $||\cdot||$ induced from that of the vector Hilbert space, so that $||\delta A v|| \leq ||\delta A||||v||$, and $||\delta A|| = 1$ in (6.2). Then, defining the condition number κ_i associated with the eigenvalue λ_i, we can write the bound for the perturbation of the eigenvalue λ_i

$$|\lambda_i(\epsilon) - \lambda_i| \leq \epsilon\kappa_i, \quad \kappa_i = \kappa(\lambda_i) := \frac{||u_i||\ ||v_i||}{|\langle u_i, v_i\rangle|} \ . \tag{6.5}$$

In the normal operator case, u_i and v_i are proportional (namely, since A and $A^\dagger$ commute they can be diagonalized in the same basis). Then, again by Cauchy-Schwartz, $\kappa_i = 1$ and we encounter spectral stability: a small perturbation of order ϵ of the operator A entails a perturbation of the same order ϵ in the spectrum. In contrast, in the non-normal case, u_i and v_i are not necessarily collinear. In the absence of a spectral theorem nothing prevents u_i and v_i to become close to orthogonality and κ_i can become very large: small perturbations of A can produce large deviations in the eigenvalues. The relative values of κ_i control the corresponding instability sensitivity of different λ_i's to an operator perturbation [3].

6.2 Pseudospectrum

A complementary approach to the study of the spectral (in)stability of the operator A under perturbations consists in considering the following questions:

Given the operator A and its spectrum $\sigma(A)$, which is the set of complex numbers $\lambda \in \mathbb{C}$ that are actual eigenvalues of "some" small perturbation $A + \delta A$, with $||\delta A|| < \epsilon$? Does this set extend in $\mathbb{C}$ far *from the spectrum of A?*

In this setting, if we are dealing with an operator that is spectrally stable, we expect that the spectrum of $A + \delta A$ will not change strongly with respect to that of A, so that the set of $\lambda \in \mathbb{C}$ corresponding to the first question above will not be far from $\sigma(A)$, staying in its vicinity at a maximum distance of order ϵ. On the contrary, if we find a tiny perturbation δA of order $||\delta A|| < \epsilon$ such that the corresponding eigenvalues of $A + \delta A$ actually reach regions in $\mathbb{C}$ at distances far apart from $\sigma(A)$, namely orders of magnitude above ϵ, we will conclude that our operator suffers of an actual spectral instability.

[2] Specifically, we consider "proper eigenvalues" in the sense of belonging to the point spectrum $\sigma_p(A)$ of A, in particular not being part of the continuum spectrum $\sigma_c(A)$ of the operator. For simplicity, we consider eigenvalues of multiplicity one.

[3] Still, certain eigenvalues of a non-normal operator (but not all) can have condition number equal to one. A 'normal eigenvalue' is defined as an eigenvalue λ with $\kappa(\lambda) = 1$. This notion can be helpful in the study of particular stable eigenvalues in the possibly unstable spectrum of a non-normal operator.

6.2.1 Pseudospectrum and operator perturbations

The previous discussion is formalized in the notion of pseudospectrum, leading to its following (first) definition [4].

Definition 1 (Pseudospectrum: perturbative approach). Given $A \in M_n(\mathbb{C})$ and $\epsilon > 0$, the ϵ-pseudospectrum $\sigma^\epsilon(A)$ of A is

$$\begin{aligned} &\sigma^\epsilon(A) \\ &= \quad \{\lambda \in \mathbb{C}, \exists\, \delta A \in M_n(\mathbb{C}), ||\delta A|| < \epsilon : \lambda \in \sigma(A + \delta A)\}. \end{aligned} \tag{6.6}$$

This notion of ϵ-pseudospectrum $\sigma^\epsilon(A)$ is a crucial one in our study of eigenvalue instability since it implies that points in $\sigma^\epsilon(A)$ are actual eigenvalues of some ϵ-perturbation of A: if $\sigma^\epsilon(A)$ extends far from the spectrum $\sigma(A)$ for a small ϵ, then a small physical perturbation δA of A can produce large actual deviations in the perturbed physical spectrum. The pseudospectrum becomes a systematic tool to assess spectral (in)stability, as illustrated in the hydrodynamics context [179].

Although the characterization (6.6) of $\sigma^\epsilon(A)$ neatly captures the notion of (in)stability of A, from a pragmatic perspective it suffers from the drawback of not providing a constructive approach to build such sets $\sigma^\epsilon(A)$ for different ϵ's (see however subsection 6.3 below, for a further qualification of this question in terms of random perturbation probes).

6.2.2 Pseudospectrum and operator resolvent

To address the construction of pseudospectra, another characterization of the set $\sigma^\epsilon(A)$ in (6.6) of Definition 1 is very useful. Such second characterization is based on the notion of the resolvent $R_A(\lambda) = (\lambda \mathrm{Id} - A)^{-1}$ of the operator A.

An eigenvalue λ of A is a complex number that makes singular the operator $(\lambda \mathrm{Id} - A)$. More generally, the spectrum $\sigma(A)$ of A is the set $\{\lambda \in \mathbb{C}\}$ for which the resolvent $R_A(\lambda)$ does not exist as a bounded operator (cf. details and subtleties on this notion in e.g. [101, 169]). This spectrum concept is a key notion for normal operators but, due to spectral instabilities discussed above, $\sigma(A)$ is not necessarily the good object to consider for non-normal operators, in our context. The notion of ϵ-pseudospectrum enters then in scene. Specifically, an equivalent characterization of the ϵ-pseudospectrum set $\sigma^\epsilon(A)$ in Definition 1 is given by the following definition [180, 169].

Definition 2 (Pseudospectrum: resolvent norm approach). Given $A \in M_n(\mathbb{C})$, its resolvent $R_A(\lambda) = (\lambda \mathrm{Id} - A)^{-1}$ and $\epsilon > 0$, the ϵ-pseudospectrum $\sigma^\epsilon(A)$ of A is characterised as

$$\sigma^\epsilon(A) \quad = \quad \{\lambda \in \mathbb{C} : ||R_A(\lambda)|| = ||(\lambda \mathrm{Id} - A)^{-1}|| > 1/\epsilon\}. \tag{6.7}$$

This characterization captures that, for non-normal operators, the norm of the resolvent $R_A(\lambda)$ can be very large far from the spectrum $\sigma(A)$. This is in contrast with the normal-operator case, where (in the $||\cdot||_2$ norm)

$$||R_A(\lambda)||_2 \leq \frac{1}{\mathrm{dist}(\lambda, \sigma(A))}\ . \tag{6.8}$$

[4] For the sake of simplicity and clarity, we dwell at the matrix level [180]. For the discussion in general Hilbert spaces, cf. [169].

In the non-normal case, one can only guarantee (e.g. [180])

$$||R_A(\lambda)||_2 \leq \frac{\kappa}{\text{dist}(\lambda, \sigma(A))} \ , \tag{6.9}$$

where κ is also a condition number, different but related to the eigenvalue condition numbers κ_i in (6.5) (κ, associated with the matrix diagonalising A, provides an upper bound to the individual κ_i's; see [180] for details). In the non-normal case, κ can become very large and ϵ-pseudospectra sets can extend far from the spectrum of A for small values of ϵ. The extension of $\sigma^\epsilon(A)$ far from $\sigma(A)$ is therefore a signature of strong non-normality and indicates a poor analytic behavior of $R_A(\lambda)$.

The important point here is that the characterization of the ϵ-pseudospectrum in Definition 2, namely Eq. (6.7), provides a practical way of calculating $\sigma^\epsilon(A)$. If we calculate the norm of the resolvent $||R_A(\lambda)||$ as a function of $\lambda = \text{Re}(\lambda) + i\text{Im}(\lambda) \in \mathbb{C}$, this provides a real function of two real variables $(\text{Re}(\lambda), \text{Im}(\lambda))$: the boundaries of the $\sigma^\epsilon(A)$ sets are just the 'contour lines' of the plot of this function $||R_A(\lambda)||$. In particular, ϵ-pseudospectra are nested sets in $\mathbb{C}$ around the spectrum $\sigma(A)$, with ϵ decreasing towards the 'interior' of such sets and such that $\lim_{\epsilon \to 0} \sigma^\epsilon(A) = \sigma(A)$.

6.2.3 Pseudospectrum and quasimodes

For completeness, we provide a third equivalent characterization of the pseudospectrum in the spirit of characterising λ's in the ϵ-pseudospectrum set $\sigma^\epsilon(A)$ as 'approximate eigenvalues' of A, 'up-to an error' ϵ, with corresponding 'approximate (right) eigenvectors' v. Specifically, it holds [180, 169] that $\sigma^\epsilon(A)$ can be characterised also by the following (third) definition.

Definition 3 (Pseudospectrum: quasimode approach). Given $A \in M_n(\mathbb{C})$ and $\epsilon > 0$, the ϵ-pseudospectrum $\sigma^\epsilon(A)$ of A and its associated ϵ-quasimodes $v \in \mathbb{C}^n$ are characterised by

$$\sigma^\epsilon(A) = \{\lambda \in \mathbb{C}, \exists v \in \mathbb{C}^n : ||Av - \lambda v|| < \epsilon\} \ . \tag{6.10}$$

This characterisation introduces the notion of "ϵ-quasimode" v (referred to as "pseudo-mode" in [180]), a key notion in the semiclassical analysis approach to the spectral study of A [169]. On the other hand, this third characterization also clearly indicates the numerical difficulty that may occur when trying to determine the actual eigenvalues of A, since round-off errors are unavoidable. This signals the need of a careful treating, whenever addressing numerically the spectral problem of a non-normal operator A.

6.2.4 Pseudospectrum and choice of the norm

In this subsection we have presented the ϵ-pseudospectrum as a notion that may be more adapted to the analysis of non-normal operators than that of the spectrum. We must emphasize however, that the notion of spectrum $\sigma(A)$ is intrinsic to the operator A, whereas the ϵ-pseudospectrum $\sigma^\epsilon(A)$ is not, since it also depends on the choice of an operator norm. This is crucial, since it determines what we mean by 'big/small' when referring to the perturbation δA, and therefore critically impacts the assessment of stability: a small operator perturbation δA in a given norm, can be a large one when considering another norm. In the first case, from a large variation $\delta\lambda$ in the eigenvalues we would conclude instability, whereas in the second case such variation could be consistent with stability.

In this sense, from a mathematical perspective, the study of spectral (in)stability through pseudospectra amounts, in a good measure, to the identification of the proper scalar product determining the norm, that is, to the identification of the proper Hilbert space in which the operator A acts. However, from a physical perspective we might not have such a freedom to choose a mathematically conveniently rescaled norm, since what we mean by large and small may be fixed by the physics of the problem, e.g. by the size of involved amplitudes, intensities or the energy contained in the perturbations. Then, the choice of an appropriate norm, both from a mathematical and physical perspective, is a fundamental step in the analysis (cf. discussion in [81]). This is the rationale behind the choice of the energy norm $||\cdot||_{\text{E}}$ in (8.20). Once the norm is chosen, the equivalent characterizations in Definitions 1, 2 and 3, respectively Eqs. (6.6), (6.7) and (6.10), emphasize complementary aspects of the ϵ-pseudospectrum notion and the $\sigma^\epsilon(A)$ sets.

6.3 Pseudospectrum and random perturbations

When considering the construction of pseudospectra, we have presented the characterization of $\sigma^\epsilon(A)$ in terms of the resolvent $R_A(\lambda)$ in Definition 2, Eq. (6.7), as better suited than the one in terms of spectra of perturbed operators in Definition 1, Eq. (6.6). The reason is that the former involves only the unperturbed operator A, whereas the latter demands a study of the spectral problem for *any* perturbed operator $A + \delta A$ with small δA: a priori, the difficulty to explicitly control such space of possible δA perturbations hinders an approach based on such characterisation in Definition 1.

But the very nature of the obstacle suggests a possible solution, namely to consider the systematic study of the perturbed spectral problem under random perturbations δA as an avenue to explore ϵ-pseudospectra sets. This heuristic expectation actually withstands a more careful analysis and constitutes the basis of a rigorous approach to the analysis of pseudospectra [169]. From a practical perspective, the systematic study of the spectral problem of $A + \delta A$ with (bounded) random δA with $||\delta A|| \leq \epsilon$, has proven to be an efficient tool to explore the 'migration' of eigenvalues through the complex plane (inside the ϵ-pseudospectra) [180]. This is complementary to (and 'technically' independent from) the evaluation of $\sigma^\epsilon(A)$ from the contour-lines of the norm $||R_A(\lambda)||$ of the resolvent. Such complementarity of approaches will prove key later in our analysis of Nollert & Price's high-frequency perturbations of the Schwarzschild's potential and the related QNMs.

Two important by-products of this random perturbation approach to the pseudospectrum are the following:

i) Random perturbations help identifying instability-triggering perturbations: ϵ-pseudospectra and condition numbers κ_i are efficient in identifying the instability of the spectrum and/or a particular eigenvalue λ_i, respectively. However, they do not inform on the specific kind of perturbation actually triggering the instability. This can be crucial to assess the physical nature of the found instability. The use of families of random operators adapted to specific types of perturbations sheds light on this precise point. We will make critical use of this in our assessment of Schwarzschild's (in)stability.

ii) Random perturbations improve analyticity: a remarkable and apparently counter-intuitive effect of random perturbations is the improvement of the analytic behaviour of $R_A(\lambda)$ in $\lambda \in \mathbb{C}$ [169]. In particular, the norm $||R_A(\lambda)||$ gets reduced away from $\sigma(A)$, as for normal

operators [cf. Eq. (6.8)], so that the ϵ-pseudospectra sets pattern becomes "flattened" (a signature of good analytic behaviour) below the random-perturbation scale ϵ.

To complement this perspective on the relation between the two given approaches to spectral (in)stability, namely perturbation theory and ϵ-pseudospectra, respectively subsections 6.1 and 6.2, let us connect eigenvalue condition numbers $\kappa(\lambda_i)$ with ϵ-pseudospectra $\sigma^\epsilon(A)$. The question we want to address is: how far can the ϵ-pseudospectrum $\sigma^\epsilon(A)$ get away from the spectrum $\sigma(A)$? The κ_i's provide the answer.

Let us define the 'tubular neighbourhood' $\Delta_\epsilon(A)$ of radius ϵ around the spectrum $\sigma(A)$ as

$$\Delta_\epsilon(A) = \{\lambda \in \mathbb{C} : \mathrm{dist}\,(\lambda, \sigma(A)) < \epsilon\}\ , \tag{6.11}$$

which is always contained in the ϵ-pseudospectrum $\sigma^\epsilon(A)$ [180]

$$\Delta_\epsilon(A) \subseteq \sigma^\epsilon(A)\ . \tag{6.12}$$

The key question is about the inclusion in the other direction. Normal operators indeed satisfy [180]

$$\sigma_2^\epsilon(A) = \Delta_\epsilon(A)\ , \tag{6.13}$$

where $\sigma_2^\epsilon(A)$ indicates the use of a $||\cdot||_2$ norm. That is, a ($||\delta A|| < \epsilon$) perturbed eigenvalue of a normal operator can move up to a distance ϵ from $\sigma(A)$. This is what we mean by spectral stability: an operator perturbation of order ϵ induces an eigenvalue perturbation also of order ϵ. However, in the non-normal case, where $\kappa(\lambda_i) > 1$, it holds (for small ϵ) [180]

$$\sigma^\epsilon(A) \subseteq \Delta_{\epsilon\kappa}(A) := \bigcup_{\lambda_i \in \sigma(A)} \Delta_{\epsilon\kappa(\lambda_i)+O(\epsilon^2)}(\{\lambda_i\})\ , \tag{6.14}$$

so that $\sigma^\epsilon(A)$ can extend into a much larger tubular neighbourhood of radius $\sim \epsilon\kappa(\lambda_i)$ around each eigenvalue, signaling spectral instability if $\kappa(\lambda_i) \gg 1$. This bound is the essential content of the Bauer-Fike theorem relating pseudospectra and eigenvalue perturbations (cf. [180] for a precise formulation).

Chapter 7

Spectral Chebyshev methods

Contents

7.1 Introduction

The goal in this chapter is to explain the tools we used to calculate numerically QNMs and its corresponding frequencies. In particular, we used spectral methods. There are various numerical methods that deal with partial differential equation problem. Weighted residuals methods used in applied mathematics normally give insight into the operator. These methods are finite difference method (FDM), finite element method (FEM), and spectral methods. Such methods depend on discretization the studied domain I and search for numerical solution that satisfies the equation with a least possible error. The solution in these methods (also called the trial function) is expanded in terms of basis functions (also called approximating functions). A test function also is used in order to achieve the least error of the approximation, by minimizing the residual in the differential equation that is generated by using the trial function instead of the exact solution. Finite difference method is known to be the simplest method, but it provides a point wise approximation. Finite element method is widely used to solve physical and engineering problems, due to its flexibility of handling complex geometries. It depends on dividing the studied domain into many sub domains, and find the suitable expansion in each, this makes the approximating functions local and not infinitely differentiable. Spectral methods is known to provide the most efficient tools to solve numerically ordinary and partial differential equations, as well as eigenvalues problems for a required accuracy.

They are known to be global methods, as they expand the solution into a basis over the whole domain. Actually the value of the derivative of a function at a point depends on the value of the

function at all other points. Being global methods make the resulting solutions global smooth functions.

There are sub methods (collocation, Galerkin, tau) regarding to the test function. Tau method enforce that the product of the residual resulting from a basis function the as many as possible basis functions is zero. While in Galerkin the product of such a residue is enforced to be as zero with as many as possible of a recombined basis. So when dealing with a non-self adjoint operator one needs to study and choose a proper scalar product. Collocations method avoid such a problem, it chooses test functions to be delta functions at a selected set of points (collocation points) and guaranty that the residue of each of the basis functions is zero at these points.
The use of collocations method were made first for spatially periodic problems by Kreiss and Oliger (1972) [109] and by Orszag (1972) [144]. Orszag's work in a series of articles started by 1969 [143] is considered to be the basic work in developing spectral methods in general. Many studies were made to compare the efficiency and accuracy of different methods using different models of differential equations. All found that the collocations method is at the same efficiency or the most efficient one. [144], [70], [92], [95], [121].

Regarding the basis functions, it is natural to choose Fourier basis for periodic systems. While for non-periodic ones we need algebraically polynomials such as Chebyshev polynomials. The work in this chapter is inspired by the book of Canuto, Hussaini, Quarteroni and Zang [38] (the same authors of a landmark book in 1988 about modern spectral methods), and the famous book of Trefethen [178], which put these methods in practice showing examples, and software codes. As it follows closely the detailed work by Marcus Ansorg (2013) [9], which is the main reference to this chapter. This chapter contains an introduction to differential matrices, then we move to the particular case of Chebyshev, explaining different grids that could be used and its differentiation matrices, then we shall finish by introducing the numerical method of integrating using Chebyshev polynomials.

7.1.1 Introduction to differential matrices

Let us have a differential equation in some finite domain I in which the solution $\tilde{\phi}$ depends on the variable x. We will call the solution we are searching to find: ϕ, and will denote x_i to the grid points that discretize I, ψ_i give the values of the derivative of ϕ at the points of the grid x_i. First we shall consider a grid where it is equally sparse. h gives the step: $h = x_{i+1} - x_i$. The second order finite difference approximation is:

$$\psi_i = \frac{\phi_{i+1} - \phi_{i-1}}{2h}. \tag{7.1}$$

If the problem is periodic then

$$\psi_0 = \frac{\phi_1 - \phi_N}{2h}, \tag{7.2}$$

and

$$\psi_N = \frac{\phi_0 - \phi_{N-1}}{2h}. \tag{7.3}$$

And the differentiation matrix will be as in the following equation:

$$\begin{bmatrix} \psi_0 \\ \\ \vdots \\ \\ \psi_N \end{bmatrix} = h^{-1} \begin{bmatrix} 0 & \frac{1}{2} & & & -\frac{1}{2} \\ -\frac{1}{2} & 0 & \ddots & & \\ & & \ddots & & \\ & & \ddots & 0 & \frac{1}{2} \\ \frac{1}{2} & & & -\frac{1}{2} & 0 \end{bmatrix} \begin{bmatrix} \phi_0 \\ \\ \vdots \\ \\ \phi_N \end{bmatrix}. \tag{7.4}$$

Let us suppose that the problem is not periodic and we have homogeneous Dirichlet boundary conditions. We will have $\phi_{-1} = \phi_{N+1} = 0$. And the differential matrix becomes as in the equation:

$$\begin{bmatrix} \psi_0 \\ \\ \vdots \\ \\ \psi_N \end{bmatrix} = h^{-1} \begin{bmatrix} 0 & \frac{1}{2} & & & 0 \\ -\frac{1}{2} & 0 & \ddots & & \\ & & \ddots & & \\ & & \ddots & 0 & \frac{1}{2} \\ 0 & & & -\frac{1}{2} & 0 \end{bmatrix} \begin{bmatrix} \phi_0 \\ \\ \vdots \\ \\ \phi_N \end{bmatrix}. \tag{7.5}$$

Making this point, we stress here the effect of the boundary conditions on the differential matrix. Another way to write ψ_i is to consider polynomials p_i, where $p_i(x_j) = \phi_j$, and $\psi_i = p_i'(x_i)$. We can write p_i such that:

$$p_i(x) = \phi_{i-1} a_{-1}(x) + \phi_i a_0(x) + \phi_{i+1} a_1(x), \tag{7.6}$$

where:

$$\begin{aligned} a_{-1}(x) &= \frac{(x - x_i)(x - x_{i+1})}{2h^2} \\ a_0(x) &= -\frac{(x - x_{i-1})(x - x_{i+1})}{2h^2} \\ a_1(x) &= \frac{(x - x_{i-1})(x - xi)}{2h^2} \end{aligned} \tag{7.7}$$

Differentiate $p_i(x)$ and evaluate it at x_i gives ψ_i. I have introduced the last method in order to generalize it from two aspects:

- A second-order approximation for the derivative of ϕ was used. Spectral methods theoretically takes this order to infinity. practically to a big number of order as possible, which makes the derivative at one point depends on the function at all other points (global methods).
- p_i are polynomials used to expand the solution. It could be trigonometric, such as Fourier basis polynomials, which is used for periodic problems. As it could be algebraic, such as Chebyshev polynomials.

The next sections discuss the choice of the grid as well as the choice of the polynomial used to expand the solution.

7.2 The choice of Chebyshev polynomials

7.2.1 Conditions for choosing a basis

We want to approximate a function $\phi(x)$ by using basis functions $\phi_i(x)$, so The expansion in terms of basis functions should verify:

- The partial sum $\sum_{k=0}^{N} c_k \phi_i(x)$ should converges fast to the function itself as $N \to \infty$
- Given a function, the calculation of the coefficients c_k should be easy. As reconstructing a function knowing the coefficients should be easy too.
- Given a function $\phi(x)$ approximated by $\sum_{k=0}^{N} c_k \phi_i(x)$, it should be easy to find another set of coefficients a_k such that: the derivative $\phi'(x)$ can be approximated by $\sum_{k=0}^{N} a_k \phi_i(x)$.

Chebyshev polynomials meet all the three requirements, the choice of the grid, and the requirements of our problem which is solving eigenvalue problem in a non-periodic settings.

7.2.2 Chebyshev polynomials of the first kind

Chebyshev polynomials of the first kind are defined through the identity :

$$T_k(cos\theta) = \cos(k\theta) \tag{7.8}$$

It can be written also for $|x| < 1$ as:

$$T_k(x) = \cos(k\, arccos(x)) \tag{7.9}$$

The following lines gives the few first Chebyshev polynomials:

$$\begin{aligned} T_0(x) &= 1 \\ T_1(x) &= x \\ T_2(x) &= 2x^2 - 1 \\ T_3(x) &= 4x^3 - x \end{aligned} \tag{7.10}$$

Here are a few of their important properties, which will help for the rest of the chapter:

- **Recursion relation**
  Because of:$\cos((k+1)\phi) + \cos((k-1)\phi) = 2\cos(k\phi)\cos(\phi)$ Then Chebyshev polynomials satisfy the following recursion relation:

$$T_{k+1} = 2xT_k(x) - T_{k-1}(x) \tag{7.11}$$

- **Orthogonality relation**
  Chebyshev polynomials are orthogonal with respect to the weighting function $\frac{1}{\sqrt{(1-x^2)}}$, on the interval $[-1, -1]$ they verify:

$$< T_n, T_m >_w = \int_{-1}^{+1} \frac{T_n(x)\, T_m(x)}{\sqrt{(1-x^2)}} = \int_0^{\pi} \cos(n\phi)\ \cos(m\phi) d\phi = \begin{cases} 0 & m \neq n \\ \frac{\pi}{2} & m = n \neq 0 \\ \pi & m = n = 0 \end{cases} \tag{7.12}$$

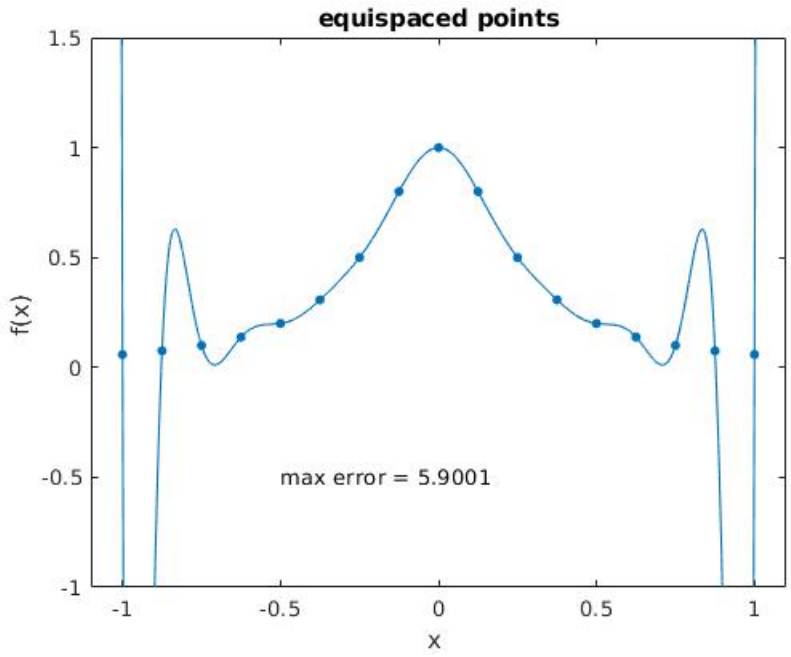

Figure 7.1: Runge phenomena

- **Expansion**
  Let $\psi(x) \in \mathbb{L}^2_w([-1,+1])$, then it can be written as:

$$\psi(x) = \frac{c_0^\psi}{2} + \sum_1^\infty c_k^\psi T_k(x) \tag{7.13}$$

7.3 Chebyshev grids: Gauss, Lobatto, Radau

Keeping in mind that our problem is not a periodic one, to choose a grid, the first idea that might comes to mind is to choose equally spaced points. However Carl Runge discovered in 1901 that a problem of oscillations at the boundaries might happen in this context when a smooth function is interpolated by polynomials [161]. To understand this phenomena we choose here the same function in Trefethen book:

$$f(x) = \frac{1}{1+16x^2}, \tag{7.14}$$

Then will calculate the values of this function at equally spaced grid, and finally interpolate a function that fits these values (using software). The result of that is shown in Fig.7.1. Obviously the problem appears near the edges, to avoid that a standard choice is Chebyshev nodes, since the density of the collocation points will be more near the edges choosing this kind of grid. In the following illustrations (as Ansorg did) we consider a domain $[-1,+1]$. Obviously this can be mapped to any other single domain. Essentially Three types of grids can be taken into account. That depends on what boundary points to consider or not, so it depends on the application:

- Chebyshev-Gauss grid, where the points corresponds to the roots of Chebyshev polynomial.

$$x_j = \cos(\frac{\pi(j+\frac{1}{2})}{N+1}) : j = 0, 1, 2, ..., N \tag{7.15}$$

And $\phi_j = \frac{\pi(j+\frac{1}{2})}{N+1}$. Note that this grid contains no boundary points, $x_0 = \cos(\frac{\pi}{2N+2}) < 1$, and $x_N = -\cos(\frac{\pi}{2N+2}) > -1$.

- Chebyshev-Lobatto grid, where the points are the extrema of Chebyshev polynomial:

$$x_j = cos(\frac{j\pi}{N}) : j = 0, 1, 2, ..., N \tag{7.16}$$

Note that this grids contain the two boundary points, $x_0 = +1$, and $x_N = -1$.

- Right Chebyshev-Radau grid. Its points correspond to the following formula:

$$x_j = \cos(\frac{2\pi j}{2N+1}) : j = 0, 1, 2, ...N \tag{7.17}$$

This corresponds to the Fourier points: $\phi_j = \frac{2\pi j}{2N+1}$. So this grid contains the right boundary edge $x_0 = +1$ but not the left one $x_0 = \cos(\frac{2\pi N}{2N+1}) > -1$.

- Left Chebyshev-Radau grid. Its points correspond to the following formula:

$$x_j = -\cos(\frac{2\pi j}{2N+1}) = \cos(\frac{\pi(2N+1-2j)}{2N+1}) : j = 0, 1, 2, ...N \tag{7.18}$$

This corresponds to the Fourier points: $\phi_j = \pi - \frac{2\pi j}{2N+1}$. So this grid contains the left boundary edge $x_0 = -1$ but not the right one $x_0 = \cos(\frac{\pi}{2N+1}) < 1$.

Fig.7.2 shows the interpolation over Chebyshev points for the same function eq.7.14, using Chebyshev-Lobatto grid. The error here is defined as the norm of the difference of the function values at equally spaced grid and the value of the interpolated function at these values. Fig.7.3 shows the convergence of the error using Chebyshev grid.

7.4 Chebyshev expansion coefficients

Writing eq.7.13 for the points of a Chebyshev grid, and till a certain N one gets:

$$\psi(x_j) = \frac{c_0^\psi}{2} + \sum_1^N c_k^\psi T_k(x_j) = \frac{c_0}{2} + \sum_1^N c_k \cos(k\phi_j) \tag{7.19}$$

With $\chi_j = \chi(\phi_j) = \psi(x_j) = \psi(\cos\phi_j)$, one gets:

$$\chi_j = \sum_{k=-N}^{+N} \gamma_k e^{ik\phi_j} \tag{7.20}$$

Thus: $\gamma_k = \frac{c_k}{2}$

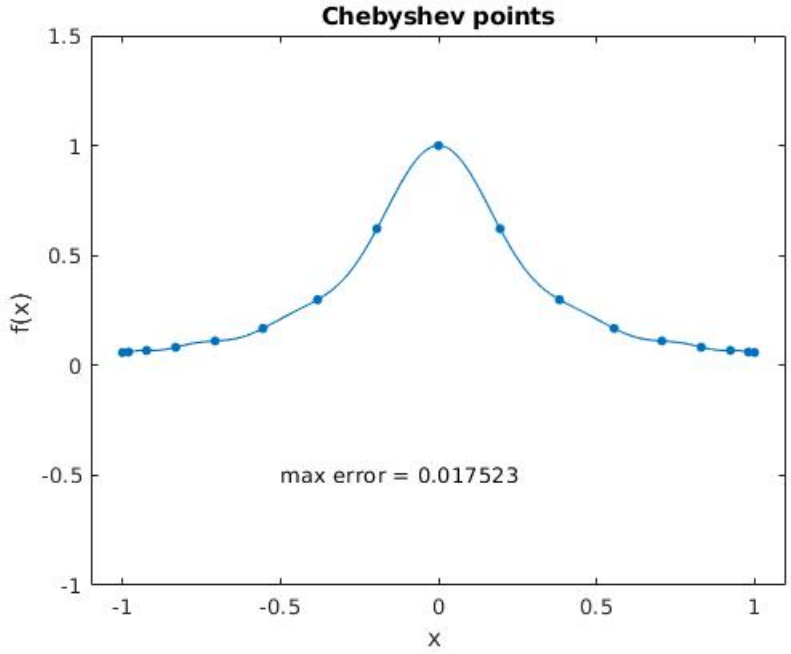

Figure 7.2: Interpolating a function using Chebyshev grid

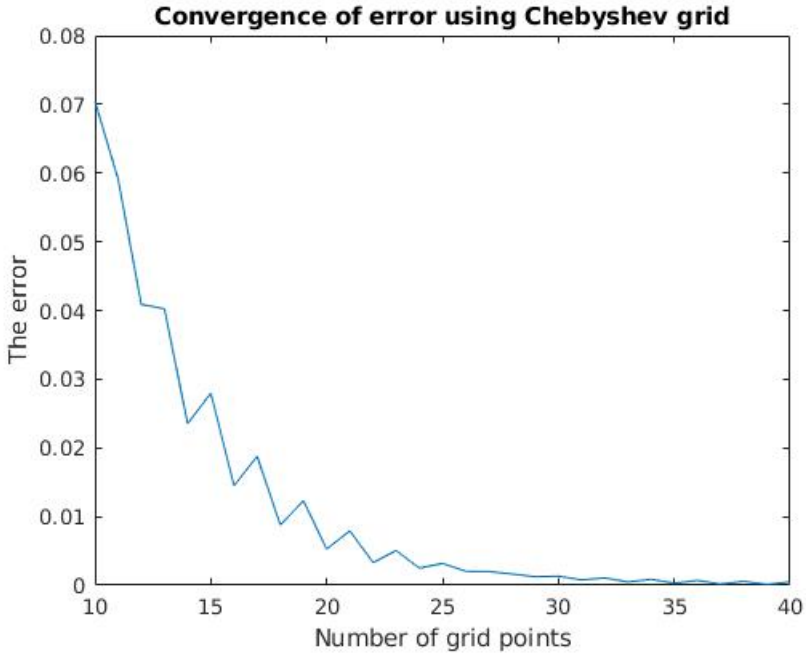

Figure 7.3: Error of interpolating a function using Chebyshev grid

The coefficients for different grids

- Coefficients in Gauss grid:

$$c_m = \frac{2}{N+1}\sum_{j=0}^{N}\psi(x_j)T_m(x_j) \tag{7.21}$$

- Coefficients in Lobatto grid:

$$c_m = \frac{2-\delta_{mN}}{4N}(\psi(1)+(-1)^m\psi(-1)+2\sum_{j=1}^{N-1}\psi(x_j)T_m(x_j)) \tag{7.22}$$

- Coefficients in Right-Radau grid:

$$c_m = \frac{4}{2N+1}(\frac{\psi(1)}{2}+\sum_{j=1}^{N}\psi(x_j)T_m(x_j)) \tag{7.23}$$

- Coefficients in Left-Radau grid:

$$c_m = \frac{4}{2N+1}(\frac{(-1)^m\,\psi(-1)}{2}+\sum_{j=1}^{N}\psi(x_j)T_m(x_j)) \tag{7.24}$$

7.5 Chebyshev differential matrix

7.5.1 Right Radau

$$D^1_{mj} = \begin{cases} \frac{N}{3}(N+1) & m=j=0 \\ (-1)^j\frac{\sqrt{2(1+x_j)}}{(1-x_j)} & m=0, j\neq 0 \\ \frac{(-1)^{m+1}}{\sqrt{2}(1-x_m)\sqrt{1+x_m}} & m\neq 0, j=0 \\ \frac{-1}{2(1-x_m^2)} & m=j\neq 0 \\ \frac{(-1)^{m-j}}{x_m-x_j}\sqrt{\frac{1+x_j}{1+x_m}} & 0\neq m\neq j\neq 0 \end{cases} \tag{7.25}$$

and those of the second order differentiation matrix:

$$D^2_{mj} = \begin{cases} \frac{1}{15}(N-1)N(N+1)(N+2) & m = j = 0 \\ (-1)^j \frac{2\sqrt{2}\sqrt{1+x_j}}{3(1-x_j)^2}[N(N+1)(1-x_j)-3] & m = 0, j \neq 0 \\ \frac{(-1)^{m+1}(2x_m+1)}{\sqrt{2}(1-x_m)^2(1+x_m)^{\frac{3}{2}}} & m \neq 0, j = 0 \\ \frac{-N(N+1)}{3(1-x_m^2)} - \frac{x_m}{(1-x_m^2)^2} & m = j \neq 0 \\ \frac{(-1)^{m-j}(2x_m^2 - x_m + x_j - 2)}{(x_m - x_j)^2(1-x_m^2)}\sqrt{\frac{1+x_j}{1+x_m}} & 0 \neq m \neq j \neq 0 \end{cases} \tag{7.26}$$

7.5.2 Left Radau

$$D^1_{mj} = \begin{cases} \frac{-N}{3}(N+1) & m = j = 0 \\ (-1)^{j+1}\frac{\sqrt{2(1+x_j)}}{(1-x_j)} & m = 0, j \neq 0 \\ \frac{(-1)^m}{\sqrt{2}(1-x_m)\sqrt{1+x_m}} & m \neq 0, j = 0 \\ \frac{1}{2(1-x_m^2)} & m = j \neq 0 \\ \frac{(-1)^{m-j}}{x_j - x_m}\sqrt{\frac{1+x_j}{1+x_m}} & 0 \neq m \neq j \neq 0 \end{cases} \tag{7.27}$$

and those of the second order differentiation matrix:

$$D^2_{mj} = \begin{cases} \frac{1}{15}(N-1)N(N+1)(N+2) & m = j = 0 \\ (-1)^j \frac{2\sqrt{2}\sqrt{1+x_j}}{3(1-x_j)^2}[N(N+1)(1-x_j)-3] & m = 0, j \neq 0 \\ \frac{(-1)^{m+1}(2x_m+1)}{\sqrt{2}(1-x_m)^2(1+x_m)^{\frac{3}{2}}} & m \neq 0, j = 0 \\ \frac{-N(N+1)}{3(1-x_m^2)} - \frac{x_m}{(1-x_m^2)^2} & m = j \neq 0 \\ \frac{(-1)^{m-j}(2x_m^2 - x_m + x_j - 2)}{(x_m - x_j)^2(1-x_m^2)}\sqrt{\frac{1+x_j}{1+x_m}} & 0 \neq m \neq j \neq 0 \end{cases} \tag{7.28}$$

7.5.3 Gauss

$$D^1_{mj} = \begin{cases} \frac{x_m}{2(1-x_m^2)} & m = j \\ (-1)^{m-j}\frac{\sqrt{1-x_j^2}}{(x_m - x_j)\sqrt{1-x_m^2}} & m \neq j \end{cases} \tag{7.29}$$

and those of the second order differentiation matrix:

$$D^2_{mj} = \begin{cases} \frac{x_m}{(1-x_m^2)^2} - \frac{N(N+2)}{3(1-x_m^2)} & m = j \\ (-1)^{m-j}\frac{\sqrt{1-x_j^2}}{(x_m - x_j)\sqrt{1-x_m^2}}(\frac{x_m}{(1-x_m^2)} - \frac{2}{x_m - x_j}) & m \neq j \end{cases} \tag{7.30}$$

7.5.4 Lobatto

$$D^1_{mj} = \begin{cases} -\frac{2N^2+1}{6} & m = j = 0 \\ \frac{2N^2+1}{6} & m = j = N \\ \frac{-x_j}{2(1-x_j^2)} & m = j \neq 0, N \\ \frac{\kappa_m}{\kappa_j}\frac{(-1)^{m-j}}{(x_m - x_j)} & m \neq j \end{cases} \tag{7.31}$$

and those of the second order differentiation matrix:

$$D^2_{mj} = \begin{cases} \dfrac{N^2-1}{15} & m = j = 0, N \\ \dfrac{-1}{(1-x_j^2)^2} - \dfrac{N^2-1}{3(1-x_j^2)} & m = j \neq 0, N \\ \dfrac{2}{3}\dfrac{(-1)^j}{\kappa_j}\dfrac{(2N^2+1)(1-x_j)-6}{(1-x_j)^2} & 0 = m \neq j \\ \dfrac{2}{3}\dfrac{(-1)^{N+j}}{\kappa_j}\dfrac{(2N^2+1)(1+x_j)-6}{(1+x_j)^2} & N = m \neq j \\ \dfrac{(-1)^{m-j}}{\kappa_j}\dfrac{x_m^2+x_m x_j-2}{(x_m-x_j)^2(1-x_m^2)} & 0 \neq m \neq N, j \neq m \end{cases} \tag{7.32}$$

where:

$$\kappa_j = \begin{cases} 1 & 0 < j < N \\ 2 & j = 0, N \end{cases} \tag{7.33}$$

Example

To show the accuracy of these differential matrix, we have followed the Trefethen by calculating the derivative of different functions using the differentiation matrix in Gauss grid. Fig.7.4 shows the error for different number of points of Gauss grid.

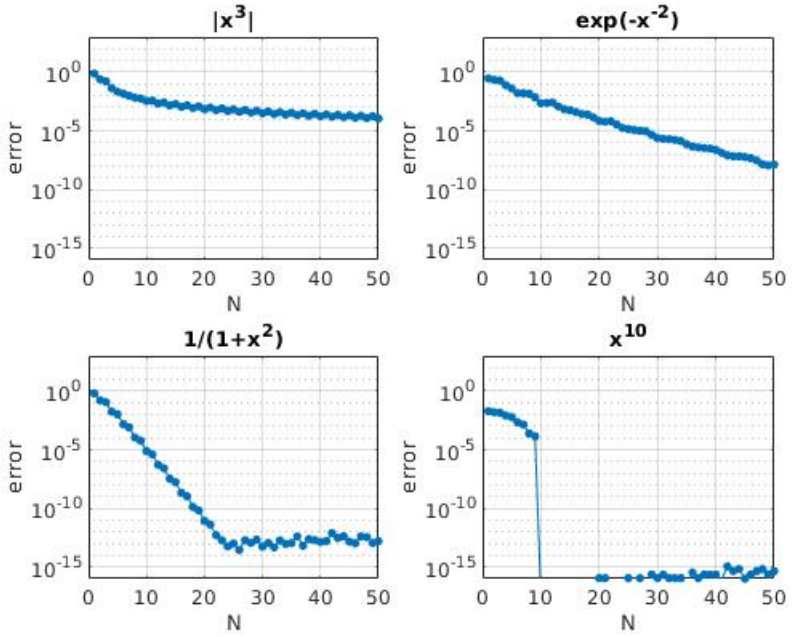

Figure 7.4: Error of differentiating a function using Chebyshev differential matrix

7.6 Chebyshev integration formula

General relation for all Chebyshev grids
Following Ansorg, we shall show here the integration of a function in a general Chebyshev grid

$$\mathrm{I} = \int_{-1}^{+1} \psi_N(x)\mathrm{dx} = \int_{-1}^{+1} [\frac{c_0}{2} + \sum_{k=1}^{N} c_k T_k(x)]\mathrm{dx} \tag{7.34}$$

So

$$\begin{aligned}
\mathrm{I} &= c_0 + \sum_{k=1}^{N} c_k \int_{-1}^{+1} T_k(x)\mathrm{dx} \\
&= c_0 + \sum_{k=1}^{N} c_k \int_{0}^{\pi} \sin(\phi)\cos(k\phi)\mathrm{d}\phi \\
&= c_0 + \frac{1}{2}\sum_{k=1}^{N} c_k \int_{0}^{\pi} \sin[(k+1)\phi] - \sin[(k-1)\phi]\mathrm{d}\phi \\
&= c_0 + \frac{1}{2}\sum_{k=1}^{N} c_k [\frac{-\cos[(k+1)\phi]}{k+1} + \frac{\cos[(k-1)\phi]}{k-1}]_0^{\pi} \\
&= c_0 + \frac{1}{2}\sum_{k=1}^{N} c_k [-\frac{(-1)^{k+1}-1}{k+1} + \frac{(-1)^(k-1)-1}{k-1}] \\
&= c_0 + \sum_{k=1}^{[\frac{N}{2}]} c_{2k} [\frac{1}{2k+1} - \frac{1}{2k-1}]
\end{aligned} \tag{7.35}$$

and finally:

$$\mathrm{I} = c_0 - 2\sum_{k=1}^{[\frac{N}{2}]} c_{2k} [\frac{1}{4k^2-1}] \tag{7.36}$$

where $[x]$ is the rounding function, i.e. the largest integer which is less or equal x. Using the expression of c_k for Gauss grid and inserting it in the previous equation, we get the integral in this grid as: **Gauss**

$$\begin{aligned}
\mathrm{I} &= \frac{2}{N+1}\sum_{j=0}^{N} \psi(x_j)T_0(x_j) - \frac{4}{N+1}\sum_{j=0}^{N} \psi(x_j) \sum_{k=1}^{[\frac{N}{2}]} [\frac{T_{2k}(x_j)}{4k^2-1}] \\
&= \frac{2}{N+1}\sum_{j=0}^{N} \psi(x_j)[T_0(x_j) - 2\sum_{k=1}^{[\frac{N}{2}]} \frac{T_{2k}(x_j)}{4k^2-1}]
\end{aligned} \tag{7.37}$$

7.7 Chebyshev scalar product matrix

To be more precise, a scalar product between η_1, and η_2 with respect to L_2-norm is:

$$\langle \zeta_1, \zeta_2 \rangle = \int \zeta_1^*(x)\zeta_2(x)dx, \tag{7.38}$$

where ζ^* is the conjugate transpose of ζ. On the level of numerics, using Chebyshev spectral methods, let us name the discretized version of ζ as η, to perform the integration according to eq.7.36, (and then eq.7.37 for Gauss grid, and the same for the other grids), we need to sum over $\eta_1^*\eta_2$. Here we write the explicit formulas for the integration matrix in each of the four grids.

Gauss The proper scalar product in the case of a Gauss grid is:

$$\langle \eta_1, \eta_2 \rangle = \frac{2}{N+1} \sum_{j=0}^{N} \eta_1^*(x_j)\eta_2(x_j)[T_0(x_j) - 2\sum_{k=1}^{[\frac{N}{2}]} \frac{T_{2k}(x_j)}{4k^2-1}] \tag{7.39}$$

This can be performed by constructing a diagonal matrix IM, and calculating the scalar product as the following:

$$\langle \eta_1, \eta_2 \rangle = \eta_1^* \times IM \times \eta_2, \tag{7.40}$$

where IM in the case a of **Gauss** grid (using eq.7.39 , and eq.7.40) is:

$$IM_{ij} = \begin{cases} T_0(x_j) - 2\sum_{k=1}^{[\frac{N}{2}]} \frac{T_{2k}(x_j)}{4k^2-1} & i = j \\ 0 & i \neq j \end{cases} \tag{7.41}$$

Running the same calculations for the other grids, one gets an integration matrix in each, as the following:

- **Lobatto**

$$IM_{ij} = \begin{cases} 0 & i \neq j \\ \frac{1}{2N}[1 - \sum_{k=1}^{[\frac{N}{2}]}(2-\delta_{2k,N})\frac{1}{4k^2-1}] & i = j = 0, N \\ \frac{1}{N}[1 - \sum_{k=1}^{[\frac{N}{2}]}(2-\delta_{2k,N})\frac{T_{2k}(x_j)}{4k^2-1}] & others \end{cases} \tag{7.42}$$

- **Right Radau**

$$IM_{ij} = \begin{cases} 0 & i \neq j \\ \frac{2}{2N+1}[1 - 2\sum_{k=1}^{[\frac{N}{2}]}\frac{1}{4k^2-1}] & i = j = 0 \\ \frac{4}{2N+1}[1 - 2\sum_{k=1}^{[\frac{N}{2}]}\frac{T_{2k}(x_j)}{4k^2-1}] & others \end{cases} \tag{7.43}$$

- **Left Radau** Exactly as in right Radau

$$IM_{ij} = \begin{cases} 0 & i \neq j \\ \frac{2}{2N+1}[1 - 2\sum_{k=1}^{[\frac{N}{2}]}\frac{1}{4k^2-1}] & i = j = 0 \\ \frac{4}{2N+1}[1 - 2\sum_{k=1}^{[\frac{N}{2}]}\frac{T_{2k}(x_j)}{4k^2-1}] & others \end{cases} \tag{7.44}$$

To conclude having a scalar product defined by the eq.7.38, is performed numerically as in eq.7.40. For a more general scalar product, the scalar product matrix IM could become non-diagonal, for example for the following definition of a scalar product:

$$\langle \zeta_1, \zeta_2 \rangle = \int (\partial_x \zeta_1)^*(x)(\partial_x \zeta_2(x))dx, \tag{7.45}$$

The new scalar product matrix G will incorporate the differentiation matrix, as the following:

$$G = D^* \times IM \times D \tag{7.46}$$

where D is the first order differentiation matrix, and D^* its conjugate transpose.

7.8 Chebyshev Adjoint matrix

For the numerics case, where we are dealing with a finite dimensional spaces, and for the sake of simplicity, we shall be concerned in this section about the adjoint definition restricted to our case.
Let V, W be finite dimensional spaces and $T \in L(V, W)$.
The adjoint of T is the unique element $T^* \in L(W, V)$ satisfying the identity: $\langle v, T^* w \rangle = \langle Tv, w \rangle$.
Coming back to matrices, the adjoint matrix of A is A^* such that:

$$\langle A\eta_1, \eta_2 \rangle = \langle \eta_1, A^* \eta_2 \rangle \tag{7.47}$$

In the previous section, it is explains that a scalar product, could be numerically calculated using:

$$\langle \eta_1, \eta_2 \rangle = \eta_1^{\dagger t} \times G \times \eta_2. \tag{7.48}$$

where $\eta^{\dagger t}$ is the conjugate transpose of η (not to be mixed with $*$ here which means the adjoint that can be defined in other ways). Applying eq.7.48 to eq.7.47, leads to:

$$\eta_1^{\dagger t} A^{\dagger t} \times G \times \eta_2 = \eta_1 \times G \times A^* \eta_2 \tag{7.49}$$

which leads to have:

$$A^{\dagger t} \times G = G \times A^* \tag{7.50}$$

and finally, the adjoint is:

$$A^* = G^{-1} \times A^{\dagger t} \times G \tag{7.51}$$

Chapter 8

Hyperboloidal approach to QNM

A key pillar of the general methodology we are using to study different wave equations is to write them in hyperboloidal slices coordinates. In this chapter we explain this approach explicitly.

8.1 Hyperboloidal approach: a heuristic introduction

Our approach to QNMs strongly relies on casting the discussion in terms of the spectral problem of a (non-selfadjoint) operator. In our scheme, this is achieved by means of a so-called hyperboloidal approach to wave propagation, that provides a systematic framework exploiting the geometric asymptotics of the spacetime, in particular enforcing the relevant outgoing boundary conditions in a geometric way. We start with a heuristic discussion of the basics, aiming at providing an intuitive picture and explicitly sacrificing rigor.

The notion of wave zone is a familiar concept in physics. It describes a region far away from a source where the degrees of a freedom of a given field (non-necessarily linear) propagate as a free wave, independently of their interior sources and obeying the superposition principle. Roughly speaking, this region is characterised by $r/R \gg 1$, where r is the location of a distant observer and R is a typical length scale of the source. This concept is addressed formally by taking appropriate limits $r \to \infty$ or $1/r \to 0$. From a spacetime perspective, however, such a limit must be carefully understood.

To fix ideas, let us consider a physical scenario in spherical symmetry, where a wave propagating at finite speed is described in a standard spherical coordinate system (t, r, θ, φ) (for simplicity, let us consider momentarily a flat spacetime where we ignore gravity effects). The retarded time coordinate $u = t - r$ corresponds to the time at which an outgoing wave, passing by the observer at r at time t, was emitted by a source located at the origin. Crucially, "light rays" propagate along (characteristic) curves satisfying $u = \text{const}$. In this setting, and as illustrated in Fig. 8.1, taking the limit $r \to \infty$ corresponds to completely different geometric statements depending on whether one stays at the hypersurface $t = \text{const}$ or rather on $u = \text{const}$. The limit attained by 'spacelike' (geodesic) curves satisfying the former condition ($t = \text{const}$) is referred to as 'space-like infinity' and denoted i^0, whereas lightlike or null (future geodesic) curves satisfying the latter condition ($u = \text{const}$) attain a limit referred to as future null infinity, denoted as $\mathtt{I}^+$. It is future null infinity $\mathtt{I}^+$ that formally captures the intuitive notion of outgoing wave zone.

Other alternatives to the $t = \text{const}$ and $u = \text{const}$ hypersurfaces are possible, something natural in a general relativistic context implementing coordinate choice freedom. A particularly convenient possibility in our present problem consists in choosing a third alternative: to keep

space-like hypersurfaces defined as level sets of an appropriate time function τ, while reaching future null infinity as $r \to \infty$ so as to enforce the outgoing character of the radiation. Such a third option is displayed in Fig. 8.1 as a $\tau =$ const hypersurface. The asymptotic geometry of such hypersurfaces is that of a hyperboloid, a feature giving name to the resulting hyperboloidal approach.

The previous heuristic picture of spacetime asymptotics is formalised in the geometric notion of conformal infinity [149, 82, 12, 13, 183, 76, 111], that provides a rigorous and geometrically well-defined strategy to deal with radiation problems of compact isolated bodies. A conformal compactification maps the infinities of the physical spacetime into a finite region delimited by the boundaries of a conformal manifold. Specifically, $\mathtt{I}^+$ corresponds to the future endpoints of null geodesics, whereas a time function τ will be referred to as hyperboloidal if hypersurfaces $\tau =$ const intersect $\mathtt{I}^+$, being therefore adapted to the geometrical structure at the infinitely far away wave zone.

The hyperboloidal formulation has proved to be a powerful tool in mathematical and numerical relativity, permitting to obtain existence results in the non-linear treatment of Einstein equations, as illustrated in the semiglobal result in [75], or providing a natural framework for the extraction of the GW waveform in numerical dynamical evolutions of GW sources. Together with those fully non-linear studies, over the last decade the hyperboloidal approach has been successfully applied to problems defined on fixed spacetime backgrounds (see e.g. [147] and references therein). In particular, [189] proposes a hyperboloidal approach to BH perturbation theory.

This is our setting for QNMs, where the hyperboloidal framework permits to implement geometrically the outgoing boundary conditions at $\mathtt{I}^+$, in a strategy first proposed by Schmidt in [164]. The adopted (compactified) hyperboloidal approach provides a geometric framework to study QNMs, that characterizes resonant frequencies in terms of an eigenvalue problem [189, 164, 69, 186, 10, 148, 147, 85, 79, 78, 80, 31]. As explained above, the scheme geometrically imposes QNM outgoing boundary conditions by adopting a spacetime slicing that intersects future null infinity $\mathtt{I}^+$ and, in the BH setting, penetrates the horizon. Since light cones point outwards at the boundary of the domain, outgoing boundary conditions are automatically imposed for propagating physical degrees of freedom. Along these lines, our scheme to address the BH QNM (in)stability problem strongly relies on the hyperboloidal approach, since it provides the rationale to define the non-selfadjoint operator on which a pseudospectrum analysis is then performed.

8.2 Wave equation in the compactified hyperboloidal approach

We focus on the propagation and, more generally, the scattering problem of (massless) linear fields on stationary spherically symmetric BH backgrounds. For concreteness, let us first consider a scalar field Φ, satisfying the wave equation

$$\Box\Phi = \nabla^a\nabla_a\Phi = 0 \ . \tag{8.1}$$

We adopt standard Schwarzschild coordinates

$$ds^2 = -f(r)dt^2 + f(r)^{-1}dr^2 + r^2\left(d\theta^2 + \sin^2\theta d\varphi^2\right) \ , \tag{8.2}$$

and emphasize that $t =$ const slices correspond to Cauchy hypersurfaces intersecting both the horizon bifurcation sphere and spatial infinity i^0. If we consider the rescaling

$$\Phi = \frac{1}{r}\phi \ , \tag{8.3}$$

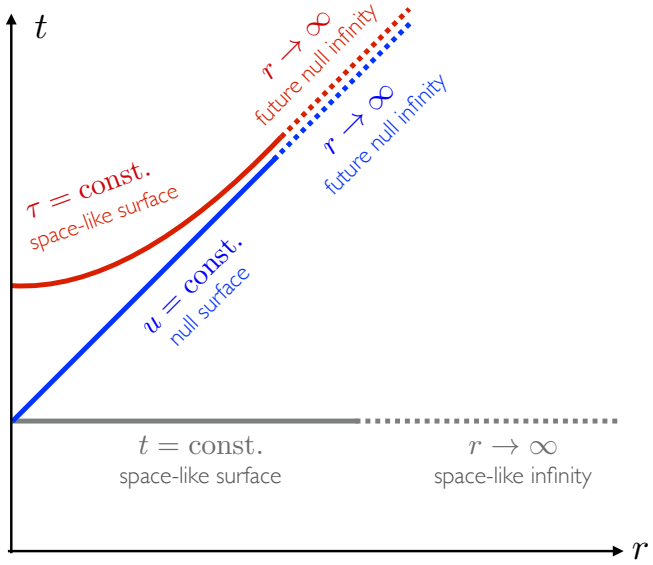

Figure 8.1: Schematic representation of the different "$r \to \infty$" limits along curves within different types of spacetime hypersurfaces. Cauchy hypersurfaces, of spacelike character and represented by the "$t = \text{const}$" condition in the figure, are such that this limit attains the so-called spatial infinity i^0, whereas in null hypersurfaces satisfying rather "$u = \text{const}$" (with $u = t - r$ a null 'retarded time') the limit attains the outgoing wave zone modelled by future null infinity $\mathtt{I}^+$. The hyperboloidal approach offers an intermediate possibility, where the limit is taken along spacelike hypersurfaces, formally represented by the "$\tau = \text{const}$", but still reaching $\mathtt{I}^+$ asymptotics.

then Eq. (8.1) rewrites, expanding ϕ in spherical harmonics with $\phi_{\ell m}$ modes and using the tortoise coordinate defined by $\dfrac{dr}{dr_*} = f(r)$ (with the appropriate integration constant), as

$$\left(\frac{\partial^2}{\partial t^2} - \frac{\partial^2}{\partial r_*^2} + V_\ell\right)\phi_{\ell m} = 0 \ , \tag{8.4}$$

where now $r_* \in \,]-\infty, \infty[$. Remarkably, when considering electromagnetic and (linearized) gravitational fields, the respective geometric wave equations corresponding to Eq. (8.1) can be cast in the form of Eq. (8.4) for appropriate effective scalar potentials. Specifically, two scalar fields with different parity can be introduced, satisfying Eq. (8.4) with suitable potentials V_ℓ. In the gravitational case, the axial parity is subject to the so-called Regge-Wheeler potential, whereas the polar one is controlled by the Zerilli potential (cf. e.g [45, 105, 125]).

The BH event horizon and (spatial) infinity correspond, respectively, to $r_* \to -\infty$ and $r_* \to +\infty$. We extend the domain of r_* to $[-\infty, \infty]$ and introduce the dimensionless quantities

$$\bar{t} = \frac{t}{\lambda} \ , \quad \bar{x} = \frac{r_*}{\lambda} \ , \quad \hat{V}_\ell = \lambda^2 V_\ell \ , \tag{8.5}$$

for an appropriate length scale λ to be chosen in each specific setting. More importantly, we consider coordinates (τ, x) that implement the compactified hyperboloidal approach

$$\left\{ \begin{array}{rcl} \bar{t} & = & \tau - h(x) \\ \bar{x} & = & g(x) \end{array} \right. . \tag{8.6}$$

Specifically (see Fig. 8.2):

i) The height function $h(x)$ implements the hyperboloidal slicing, i.e. $\tau = \text{const}$ is a horizon-penetrating hyperboloidal slice Σ_τ intersecting future $\mathtt{I}^+$.

ii) The function $g(x)$ introduces a spatial compactification from $\bar{x} \in [-\infty, \infty]$ to a compact interval $[a, b]$.

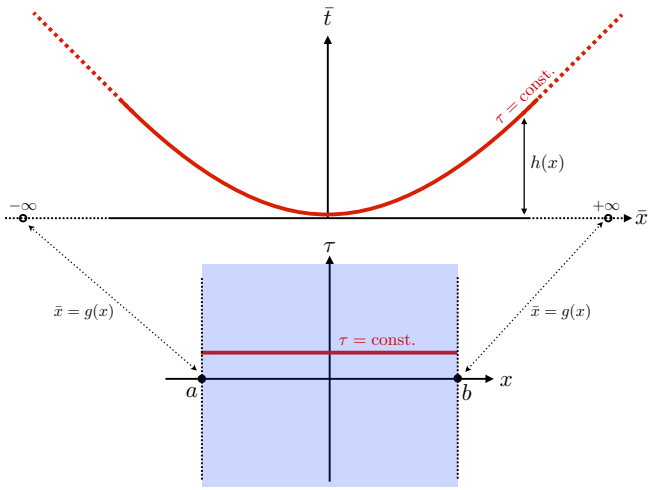

Figure 8.2: Schematic representation of the hyperboloidal coordinate transformation in Eq. (8.6). *Top panel:* Dimensionless Schwarzschild time and tortoise coordinates $(\bar{t}, \bar{x})$. The height function $h(x)$ bends the time slices so that future null infinity (and/or black-hole horizon) is reached in the limit $\bar{x} \to \pm\infty$. *Bottom panel:* Spatially compactified hyperboloidal coordinates (τ, x). The compactification function $g(x)$ maps the infinite domain $\bar{x} \in]-\infty, \infty[$ onto the finite interval $x \in]a, b[$. Points b and a are added at the boundary, representing null infinity $\mathtt{I}^+$ and/or the BH horizon. The blue stripe shows the domain of integration of the wave equation in Eq. (8.7) in these compactified hyperboloidal coordinates, namely $(\tau, x) \in]-\infty, +\infty[\times[a, b]$, corresponding to the full original domain $(\bar{t}, \bar{x}) \in \mathbb{R}^2$ of Eq. (8.4).

We note that the compactification is performed only in the spatial direction along the hyperboloidal slice, and not in time, so that the latter can be Fourier transformed in a unbounded domain. The relevant compactification here is a partial one, and not the total spacetime compactification leading to Carter-Penrose diagrams. The choice of $h(x)$ and $g(x)$ is, as we comment below, subject to certain restrictions. Under transformation (8.6), the wave equation (8.4) writes

$$\left[\left(1-\left(\frac{h'}{g'}\right)^2\right)\partial_\tau^2 - \frac{2}{g'}\left(\frac{h'}{g'}\right)\partial_\tau\partial_x - \frac{1}{g'}\left(\frac{h'}{g'}\right)'\partial_\tau \right.$$
$$\left. -\frac{1}{g'}\partial_x\left(\frac{1}{g'}\partial_x\right) + \hat{V}_\ell\right]\phi_{\ell m} = 0\,, \tag{8.7}$$

where the prime denotes derivative with respect to x. Admittedly, expression (8.7) appears more intricate than Eq. (8.4). However, this change encodes a neat geometric structure and, as we shall argue, it plays a crucial role in our construction and discussion of the relevant spectral problem.

8.3 First-order reduction in time and spectral problem

The structure in Eq. (8.7) is made more apparent by performing a first-order reduction in time, by introducing

$$\psi_{\ell m} = \partial_\tau \phi_{\ell m} \quad , \quad u_{\ell m} = \begin{pmatrix} \phi_{\ell m} \\ \psi_{\ell m} \end{pmatrix} \ . \tag{8.8}$$

Then, Eq. (8.7) becomes

$$\partial_\tau u_{\ell m} = i L u_{\ell m} \ , \tag{8.9}$$

where the operator L is defined as

$$L = \frac{1}{i} \left(\begin{array}{c|c} 0 & 1 \\ \hline L_1 & L_2 \end{array} \right) \ , \tag{8.10}$$

with

$$\begin{aligned} L_1 &= \frac{1}{w(x)} \big(\partial_x \left(p(x) \partial_x \right) - q_\ell(x) \big) \\ L_2 &= \frac{1}{w(x)} \big(2\gamma(x) \partial_x + \partial_x \gamma(x) \big) \ , \end{aligned} \tag{8.11}$$

and

$$\begin{aligned} & w(x) = \frac{g'^2 - h'^2}{|g'|} \quad , \quad p(x) = \frac{1}{|g'|} \quad , \quad q_\ell(x) = |g'| \, \hat{V}_\ell \\ & \gamma(x) = \frac{h'}{|g'|} \ . \end{aligned} \tag{8.12}$$

The structure of L_1 is that of a Sturm-Liouville operator. In particular, functions $h(x)$ and $g(x)$ are chosen such that they guarantee the positivity of the weight function $w(x)$, namely $w(x) > 0$. The operator L_2 has also a neat geometric/analytic structure adapted to the integration by parts, being symmetric in the following form: $L_2 = \frac{1}{w(x)} \Big(\gamma(x) \partial_x + \partial_x (\gamma(x) \cdot) \Big)$.

A key property of coordinate transformation (8.6) is that it preserves, up to the overall constant λ, the timelike Killing vector t^a controlling stationarity

$$t^a = \partial_t = \frac{1}{\lambda} \partial_{\bar{t}} = \frac{1}{\lambda} \partial_\tau \ . \tag{8.13}$$

In this sense functions t and $\lambda\tau$ "tick" at the same pace, namely they are natural parameters of t^a, i.e. $t^a(t) = t^a(\lambda\tau) = 1$ (the role of the constant λ being just that of keeping proper dimensions). This is crucial for the consistent definition of QNM frequencies by Fourier (or Laplace) transformation from Eqs. (8.4) and (8.7), since variables ω respectively conjugate to t and τ then coincide (up to the constant $1/\lambda$). In other words: the change of time coordinate in Eq. (8.6) does not affect the values of the obtained QNM frequencies.

Performing then the Fourier transform in τ in the first-order (in time) form (12.38) of the wave equation (with standard sign convention for the Fourier modes, $u_{\ell m}(\tau, x) \sim u_{\ell m}(x) e^{i\omega\tau}$) we arrive at the spectral problem for the operator L

$$L\, u_{n,\ell m} = \omega_{n,\ell m}\; u_{n,\ell m} \ , \tag{8.14}$$

or, more explicitly

$$\left(\begin{array}{c|c} 0 & 1 \\ \hline L_1 & L_2 \end{array}\right) \begin{pmatrix} \phi_{\ell m} \\ \psi_{\ell m} \end{pmatrix} = i\omega_{n,\ell m} \begin{pmatrix} \phi_{n,\ell m} \\ \psi_{n,\ell m} \end{pmatrix} \ . \tag{8.15}$$

8.3.1 Regularity and outgoing boundary conditions

As emphasized at the beginning of this section, a major motivation for the adopted hyperboloidal approach is the geometric imposition of outgoing boundary conditions at future null infinity and at the event horizon: being null hypersurfaces with light cones pointing outwards from the integration domain, the physical causally propagating degrees of freedom (as the scalar fields we consider here) should not admit boundary conditions, as long as they satisfy the appropriate regularity conditions. How does this translate into the analytic scheme resulting from the change of variables (8.6)?

The key point is that transformation (8.6) must be such that $p(x)$ in the Sturm-Liouville operator L_1 in Eq. (8.11) vanishes at the boundaries of the compactified spatial domain $[a, b]$

$$p(a) = p(b) = 0 \ . \tag{8.16}$$

This will be illustrated explicitly in the study cases discussed later. Then the elliptic operator L_1 is a 'singular' Sturm-Liouville operator, this impacting directly on the boundary conditions it admits. Specifically, if (appropriate) regularity is enforced on eigenfunctions, then L_1 does not admit boundary conditions. Moreover, such absence of boundary conditions extends to the full operator L in the hyperbolic problem. In brief: if sufficient regularity is imposed on the space of functions $u_{n,\ell m}$, then wave equations (8.7), (12.38) and the spectral problem (8.14) do not admit boundary conditions, as a consequence of the vanishing of $p(x)$ at the boundaries of $[a, b]$.

This is the analytic counterpart of the geometric structure implemented in the compactified hyperboloidal approach. QNM boundary conditions are in-built, as regularity conditions, in the 'bulk' of the operator L in Eqs. (8.14) and (8.15).

8.4 Scalar product: QNMs as a non-selfadjoint spectral problem

The outgoing boundary conditions in the present setting define a leaky system, with a loss of energy through the boundaries — null infinity and the black hole horizon — so that the system is not conservative. This suggests that the infinitesimal generator of the evolution in Eq. (8.7), namely the operator L, should be non-selfadjoint. This requires the introduction of an appropriate scalar product in the problem. Moreover, such identification of the appropriate Hilbert space for solutions is also key for the regularity conditions evoked above.

Eq. (8.7) describes the evolution of each mode $\phi_{\ell m}$ in a background 1+1-Minkowski spacetime with a scattering potential V_ℓ. A natural scalar product in this reduced problem (cf. [81] for an extended discussion in terms of the full problem), both from the physical and the analytical point of view, is given in terms of the energy associated with such scalar field mode. In the

context of the spectral problem (8.14), we must consider generically a complex scalar field $\phi_{\ell m}$, for which the associated stress-energy tensor writes (dropping (ℓ, m) indices) is

$$T_{ab} = \frac{1}{2}\left(\nabla_a\bar{\phi}\nabla_b\phi - \frac{1}{2}\eta_{ab}\nabla^c\bar{\phi}\nabla_c\phi + V_\ell\bar{\phi}\phi + \text{c.c}\right) , \tag{8.17}$$

where η_{ab} denotes the Minkowski metric in arbitrary coordinates and "c.c" indicates "complex − conjugate". In a stationary situation, the "total energy" contained in the spatial slice Σ_τ and associated with the mode ϕ is given [183] by

$$E = \int_{\Sigma_\tau} T_{ab}(\phi, \nabla\phi)t^a n^b d\Sigma_\tau , \tag{8.18}$$

where t^a is again the timelike Killing vector associated with stationarity and n^a denotes the unit timelike normal to the spacelike slice Σ_τ. Writing explicitly the energy in the compactified hyperboloidal coordinates (τ, x) in (8.6), we get

$$\begin{aligned} E(\phi, \partial_\tau\phi) &= \int_{\Sigma_\tau} T_{ab}(\phi, \partial_\tau\phi)t^a n^b d\Sigma_\tau \\ &= \frac{1}{2}\int_a^b \left[(g'^2 - h'^2)\partial_\tau\bar{\phi}\partial_\tau\phi + \partial_x\bar{\phi}\partial_x\phi + g'^2\hat{V}_\ell\bar{\phi}\phi\right]\frac{1}{|g'|}dx , \end{aligned} \tag{8.19}$$

where we identify the functions appearing in the definition of the L_1 operator in (8.11) and (8.12). In particular, if $g'^2 - h'^2 > 0$ (as we have required above) and $\hat{V}_\ell > 0$ (this is required for positivity of the norm) then, identifying $\partial_\tau\phi = \psi$ as in (12.37), we can write the following norm for the vector u in (12.37)

$$\begin{aligned} ||u||_E^2 &= \left|\left|\begin{pmatrix}\phi\\ \psi\end{pmatrix}\right|\right|_E^2 := E(\phi, \psi) \\ &= \frac{1}{2}\int_a^b \left(w(x)|\psi|^2 + p(x)|\partial_x\phi|^2 + q_\ell(x)|\phi|^2\right)dx . \end{aligned} \tag{8.20}$$

We refer in the following to this norm as the "energy norm". We notice that $\gamma(x)$ in Eq. (8.12), associated with L_2 does not enter in the norm, that is, in the energy. This norm comes indeed from a scalar product. Rewriting, for making its role more apparent, the $q_\ell(x)$ function as the rescaled potential $\tilde{V}_\ell$

$$\tilde{V}_\ell := q_\ell(x) = |g'(x)|\hat{V}_\ell = \frac{\hat{V}_\ell}{p(x)} , \tag{8.21}$$

and under the assumption above $\tilde{V}_\ell > 0$, we can introduce the "energy scalar product" for vector functions u in Eq. (12.37), as

$$\begin{aligned} \langle u_1, u_2\rangle_E &= \left\langle \begin{pmatrix}\phi_1\\ \psi_1\end{pmatrix}, \begin{pmatrix}\phi_2\\ \psi_2\end{pmatrix}\right\rangle_E \\ &= \frac{1}{2}\int_a^b \left(w(x)\bar{\psi}_1\psi_2 + p(x)\partial_x\bar{\phi}_1\partial_x\phi_2 + \tilde{V}_\ell\bar{\phi}_1\phi_2\right)dx , \end{aligned} \tag{8.22}$$

and, by construction, it holds $||u||_E^2 = \langle u, u\rangle_E$. This will be the relevant scalar product in our discussion.

The full operator L in (8.14) is not selfadjoint in the scalar product (8.22). In fact, the first-order operator L_2 stands for a dissipative term encoding the energy leaking at $\mathtt{I}^+$ and the BH horizon [81]. One could, at a first look, consider that this is related to the first-order character of L_2, which makes it antisymmetric when integrating by parts with a $L^2([a,b], w(x)dx)$ scalar product on ψ, in contrast with the selfadjoint character of the Sturm-Liouville operator L_1 in $L^2([a,b], w(x)dx)$ for ϕ functions. However, this is misleading and actually would suggest a wrong 'bulk' dissipation mechanism. When calculating the formal adjoint $L^\dagger$ of the full operator L with the scalar product (8.22), one gets

$$L^\dagger = L + L^\partial \ , \tag{8.23}$$

where L^∂ is an operator with support only on the boundaries of the interval $[a,b]$, that we can formally write as

$$L^\partial = \frac{1}{i}\left(\begin{array}{c|c} 0 & 0 \\ \hline 0 & L_2^\partial \end{array}\right) \ , \tag{8.24}$$

with L_2^∂ given by the expression

$$L_2^\partial = 2\frac{\gamma(x)}{w(x)}\left(\delta(x-a) - \delta(x-b)\right) \ , \tag{8.25}$$

where $\delta(x)$ formally denotes a Dirac-delta distribution. This is just a formal expression, that underlines precisely the need of a more careful treatment on the involved functional spaces, but it has the virtue of making apparent that the obstruction to selfadjointness lays at the boundaries, as one expects in our QNM problem, and not in the bulk, as one could naively conclude from the presence of a first-order operator L_2 (cf. discussion above): L_2^∂ explicitly entails a boundary dissipation mechanism. In particular, we note that L is selfadjoint in the non-dissipative $L_2 = 0$ case, as expected, but that this has required the introduction of quite a non-trivial scalar product.

As a bottomline, in this section we have cast the QNM problem as the eigenvalue problem of a non-selfadjoint operator. In the following section we discuss the implications of this.

8.5 Hyperboloidal in 3 regions

For the case of a compact scatterer, the wave equation differs inside the scatterer (a cavity) from the outside. So one way of solving that is to divide the space (one dimensional in the studied case) into three regions, write the wave equation in each, and then impose continuity conditions of the field and its derivative at each boundary between two regions, and finally solve the whole system of equations. Doing that does not prevent from still using auxiliary fields, or hyperboloidal slice. Actually the eq.8.15 is still valid inside the cavity taking into account the potential (which is indeed what indicate the existence of a scatterer), while outside the cavity assuming that it is a free space the same equations work but with a zero potential. Let us name the field as ϕ_I , ϕ_{II}, and ϕ_{III} in the three regions respectively from left to right, and the corresponding used auxiliary

field in each region ψ_I, ψ_{II}, and $\psi_I II$. Then we can write:

$$\begin{bmatrix} I & 0 & 0 & 0 & 0 & 0 \\ 0 & I & 0 & 0 & 0 & 0 \\ 0 & 0 & I & 0 & 0 & 0 \\ 0 & 0 & 0 & I & 0 & 0 \\ 0 & 0 & 0 & 0 & 1 & 0 \\ 0 & 0 & 0 & 0 & 0 & I \end{bmatrix} \partial_\tau \begin{bmatrix} \phi_I \\ \psi_I \\ \phi_{II} \\ \psi_{II} \\ \phi_{III} \\ \psi_{III} \end{bmatrix} = \begin{bmatrix} 0 & 1 & 0 & 0 & 0 & 0 \\ L_{I1} & L_{I2} & 0 & 0 & 0 & 0 \\ 0 & 0 & 0 & 1 & 0 & 0 \\ 0 & 0 & L_{II1} & L_{II2} & 0 & 0 \\ 0 & 0 & 0 & 0 & 0 & 1 \\ 0 & 0 & 0 & 0 & L_{III1} & L_{III2} \end{bmatrix} \begin{bmatrix} \phi_I \\ \psi_I \\ \phi_{II} \\ \psi_{II} \\ \phi_{III} \\ \psi_{III} \end{bmatrix} \tag{8.26}$$

Still the continuity conditions should be imposed. Using Chebyshev discretization, one can model the three regions as three grids maped to $y_1 : -1 \to tanh(-1)$, $x : tanh(-1) \to tanh(1)$, and $y_2 : tanh(-1) \to -1$. The number of points in each grid is $N + 1$. Regarding the type of the grid; the one for the cavity (scatterer) in the middle could be Lobatto, while the two grids of y_1 and y_2 are Right Radau, and left Radau. As the fields in the three regions is expressed using the same coordinates system, the continuity of the field could be expressed by:

$$\begin{aligned} \phi_I(y_1 = tanh(-1)) &= \phi_{II}(x = tanh(-1)) \\ \phi_{II}(x = tanh(1)) &= \phi_{III}(y_2 = tanh(1)) \\ \tfrac{\mathrm{d}}{\mathrm{dy_1}}\phi_I(y_1 = tanh(-1)) &= \tfrac{\mathrm{d}}{\mathrm{dx}}\phi_{II}(x = tanh(-1)) \\ \tfrac{\mathrm{d}}{\mathrm{dx}}\phi_{II}(x = tanh(1)) &= \tfrac{\mathrm{d}}{\mathrm{dy_2}}\phi_{III}(y_2 = tanh(1)) \end{aligned} \tag{8.27}$$

And the discretized version of the last set of equations is:

$$\begin{aligned} \phi_I(y_1(N)) &= \phi_{II}(x(0)) \\ \phi_{II}(x(N)) &= \phi_{III}(y_2(0)) \\ D_{y_1}[N,:]\phi_I &= D_{y_1}[0,:]\phi_{II} \\ D_x[N,:]\phi_{II} &= D_{y_2}[0,:]\phi_{III} \end{aligned} \tag{8.28}$$

To inserting these equations in the descretized version of 8.26, we modify 4 lines in it.

Chapter 9

Pseudospectrum in the energy norm

In this chapter we explain issues that are using knowledge from different previous chapters. To find the pseudospectrum for a problem with a non-self-adjoint operator such as QNM problem there is a key need to define a suitable scalar product, the later induces a norm. However there is a gap between an analytical definition of a scalar product and a its numerical implemented one. Using grids such as Chebyshev's requires additional attention to the implemented formulas. We derive here the relevant expressions for the construction of pseudospectra in the discretised version of the energy norm.

9.1 Scalar product and adjoint

Let us consider a general hermitian-scalar product in $\mathbb{C}^n$ as

$$\langle u, v\rangle_G = (u^*)^i G_{ij} v^j = u^* \cdot G \cdot v \ , \tag{9.1}$$

with G a positive-definite Hermitian matrix

$$G^* = G \quad , \quad x^* \cdot G \cdot x > 0 \ \text{ if } \ x \neq 0 \ , \tag{9.2}$$

where * denotes conjugate-transpose, i.e. $u^* = \bar{u}^t$ and $G^* = \bar{G}^t$ (we notice that in the problem studied in this work, the Hermitian positive-definite matrix G is actually a real symmetric positive-definite matrix $G^t = G$, but we keep the discussion in full generality). Using (9.1) and (9.2) in the relation

$$\langle A^\dagger u, v\rangle_G = \langle u, Av\rangle \ , \tag{9.3}$$

characterising the adjoint $A^\dagger$ of A with respect to the scalar product (9.1), we immediately get

$$A^\dagger = G^{-1} A^* G \ . \tag{9.4}$$

9.2 Induced matrix norm from a scalar product norm

The (vector) norm $||\cdot||_G$ in $\mathbb{C}^n$ associated with the scalar product $\langle\cdot,\cdot\rangle_G$ in (9.1), namely

$$||v||_G = (\langle v, v\rangle_G)^{\frac{1}{2}} \ , \tag{9.5}$$

induces a matrix norm $||\cdot||_G$ in $M_n(\mathbb{C})$ defined as

$$||A||_G = \max_{||x||=1, x\in\mathbb{C}^n} \{||Ax||_G\} \ , \ A \in M_n(\mathbb{C}) \ . \tag{9.6}$$

A more useful characterisation of this L^2 induced matrix norm is given in terms of the spectral radius $\rho(A^\dagger A)$ of $A^\dagger A$, where

$$\rho(M) = \max_{\lambda\in\sigma(M)} \{|\lambda|\} \ . \tag{9.7}$$

Indeed, we can write

$$\begin{aligned} ||A||_G^2 &= \left(\max_{||x||=1, x\in\mathbb{C}^n} \left\{ (\langle Ax, Ax\rangle_G)^{\frac{1}{2}} \right\} \right)^2 \\ &= \max_{||x||_G=1, x\in\mathbb{C}^n} \{\langle Ax, Ax\rangle_G\} \\ &= \max_{||x||_G=1, x\in\mathbb{C}^n} \left\{ \langle A^\dagger Ax, x\rangle_G \right\} \ . \end{aligned} \tag{9.8}$$

The rest of the argument essentially follows from Rayleigh-Ritz formula for self-adjoint operators. Explicitly, the (self-adjoint) matrix $A^\dagger A$ is unitarily diagonalisable and non-negative definite (that is, $\langle x, A^\dagger Ax\rangle_G \geq 0, \forall x \in \mathbb{C}^n$), so that we can find an orthonormal basis of eigenvectors $\{e_i\}$

$$A^\dagger A e_i = \lambda_i e_i \quad , \quad \langle e_i, e_j\rangle_G = \delta_{ij} \ , \tag{9.9}$$

with real non-negative eigenvalues λ_i that we order as

$$0 \leq \lambda_1 \leq \lambda_2 \ldots \leq \lambda_n \ . \tag{9.10}$$

Expanding $x = \sum_i x^i e_i$ for an arbitrary $x \in \mathbb{C}^n$, we write

$$\langle A^\dagger Ax, x\rangle_G = \sum_i \lambda_i |x^i|^2 \leq \lambda_n \sum_i |x^i|^2 = \lambda_n ||x||_G^2 \ , \tag{9.11}$$

that we can recast as

$$\left\langle A^\dagger A \frac{x}{||x||_G}, \frac{x}{||x||_G} \right\rangle_G \leq \lambda_n = \rho(A^\dagger A) \ . \tag{9.12}$$

Inserting this in Eq. (9.8), we conclude

$$||A||_G^2 \leq \rho(A^\dagger A) \ . \tag{9.13}$$

To prove that the inequality is actually saturated, it suffices to show that there exits a vector x, $||x||_G = 1$, that realizes the equality, i.e. $||Ax, Ax||_G^2 = \rho(A^\dagger A)$. If we consider $x = e_n$

$$\begin{aligned} ||Ae_n||_G^2 &= \langle Ae_n, Ae_n\rangle_G = \langle A^\dagger Ae_n, e_n\rangle_G \\ &= \lambda_n = \rho(A^\dagger A) \ , \end{aligned} \tag{9.14}$$

and we can finally conclude

$$||A||_G = \left(\rho(A^\dagger A)\right)^{\frac{1}{2}} \ . \tag{9.15}$$

9.3 Characterization of the pseudospectrum

Given an invertible matrix $A \in M_n(\mathbb{C})$ and a non-vanishing eigenvalue λ, then $1/\lambda$ is an eigenvalue of A^{-1} and

$$\max_{\lambda\in\sigma(A^{-1})} \{|\lambda|\} = \left(\min_{\lambda\in\sigma(A)} \{|\lambda|\}\right)^{-1} . \tag{9.16}$$

Then, for an invertible $M \in M_n(\mathbb{C})$, we can write for the squared norm $||\cdot||_G$ of its inverse M^{-1}

$$\begin{aligned} ||M^{-1}||_G^2 &= \rho\left((M^{-1})^\dagger M^{-1}\right) = \rho\left(\left(MM^\dagger\right)^{-1}\right) \\ &= \left(\min_{\lambda\in\sigma(MM^\dagger)} \{\lambda\}\right)^{-1} = \left(\min_{\lambda\in\sigma(M^\dagger M)} \{\lambda\}\right)^{-1} , \end{aligned} \tag{9.17}$$

where in the passage from the first line to the second we have used (9.16) and the definition (9.7) of the spectral radius, whereas in the last equality we have used that a matrix AB has the same eigenvalues as the matrix BA.

We consider now the ϵ-pseudospectrum characterisation in Definition 2, namely Eq. (6.7), applied to the discretised energy norm $||\cdot||_G$

$$\sigma_G^\epsilon(A) = \{\lambda \in \mathbb{C} : ||(\lambda \mathrm{Id} - A)^{-1}||_G > 1/\epsilon\} . \tag{9.18}$$

Using (9.17), with $M = \lambda\mathrm{Id} - A$, we can write

$$||(\lambda \mathrm{Id} - A)^{-1}||_G > 1/\epsilon \Leftrightarrow \epsilon > \left(\min_{\lambda\in\sigma(M^\dagger M)} \{\lambda\}\right)^{\frac{1}{2}} . \tag{9.19}$$

Finally, $\sigma_G^\epsilon(A)$ can be written as

$$\sigma_G^\epsilon(A) = \{\lambda \in \mathbb{C} : s_G^{\min}(\lambda\mathrm{Id} - A) < \epsilon\} , \tag{9.20}$$

where $s_G^{\min}(M)$ is the minimum of a set of "generalized singular values" of M, related to the $\langle\cdot,\cdot\rangle_G$ scalar product

$$s_G^{\min}(M) := \min\{\sqrt{\lambda} : \lambda \in \sigma(M^\dagger M)\} . \tag{9.21}$$

When choosing the energy scalar product in section 9.4, that is with $G = G^E$ (see explicit expression in appendix 14), we recover expression (9.26) for $\sigma_E^\epsilon(A)$. When using the canonical L^2 product we recover the standard $\sigma_2^\epsilon(A)$ in (9.23), where

$$s_2^{\min}(M) = \min\{\sqrt{\lambda} : \lambda \in \sigma(M^* M)\} =: \sigma^{\min} , \tag{9.22}$$

is the smallest of the singular values $\sigma_i(M) = \sqrt{\lambda_i}$, $\lambda_i \in \sigma(M^*M)$, in the standard singular value decomposition of M.

9.4 Numerical approach

The present work is meant as a first assessment of BH QNM (in)stability by using pseudospectra. At this exploratory stage, we address the construction of pseudospectra in a numerical approach. As indicated in section 6.2.3, the study of the spectral stability of non-normal operators is a challenging problem that demands high accuracy. Spectral methods provide well-adapted tools for these calculations [180, 178, 38].

We discretize the differential operator L in (12.38)-(8.14) via Chebyshev differentiation matrices, built on Chebyshev-Lobatto n-point grids, producing L^N matrix approximates (we note systematically $n = N + 1$ in spectral grids). Once the operator is discretized, the construction of the pseudospectrum requires the evaluation of matrix norms. A standard practical choice [180, 178] involves the matrix norm induced from the Euclidean L^2 norm in the vector space $\mathbb{C}^n$ that, starting from Eq. (6.7) in the Definition 2 of the pseudospectrum, leads to the following rewriting [180, 178]

$$\sigma_2^\epsilon(A) = \{\lambda \in \mathbb{C} : \sigma^{\min}(\lambda \mathrm{Id} - A) < \epsilon\} \ , \tag{9.23}$$

where $\sigma^{\min}(M)$ denotes the smallest singular value of M, that is, $\sigma^{\min}(M) = \min\{\sqrt{\lambda} : \lambda \in \sigma(M^*M)\}$, with $M \in M_n(\mathbb{C})$ and M^* its conjugate-transpose $M^* = \overline{M}^t$.

Although Eq. (9.23) captures the spectral instability structure of A, the involved L^2 scalar product in $\mathbb{C}^n$ is neither faithful to the structure of the operator L in Eq. (12.38), nor to the physics of the BH QNM problem (cf. discussion in section 6.2.4). Instead, we rather use the natural norm in the problem, specifically the Chebyshev-discretrised version of the 'energy norm' (8.20), following from the Chebyshev-discretised version of the scalar product (8.22). Specifically, we write the discretised scalar product in an appropriate basis as (we abuse the notation, since we use $\langle \cdot, \cdot \rangle_{_E}$ as in (8.22), although this is now a scalar product in a finite-dimensional space $\mathbb{C}^n$)

$$\langle u, v \rangle_{_E} = (u^*)^i G^E_{ij} v^j = u^* \cdot G^E \cdot v \quad , \quad u, v \in \mathbb{C}^n \ , \tag{9.24}$$

where G^E_{ij} is the Gram matrix corresponding to (8.22) (cf. appendix 14 for its construction) and we note $u^* = \bar{u}^t$. The adjoint $A^\dagger$ of A with respect to $\langle \cdot, \cdot \rangle_{_E}$ writes then

$$A^\dagger = \left(G^E\right)^{-1} \cdot A^* \cdot G^E \ . \tag{9.25}$$

The vector norm $||\cdot||_{_E}$ in $\mathbb{C}^n$ associated with $\langle \cdot, \cdot \rangle_{_E}$ in Eq. (9.24) induces a matrix norm $||\cdot||_{_E}$ in $M_n(\mathbb{C})$ (again, we abuse notation by using the same symbol for the norm in $\mathbb{C}^n$ and in $M_n(\mathbb{C})$). Then, the ϵ-pseudospectrum $\sigma^\epsilon_{_E}(A)$ of $A \in M_n(\mathbb{C})$ in the norm $||\cdot||_{_E}$ writes

$$\sigma^\epsilon_{_E}(A) = \{\lambda \in \mathbb{C} : s^{\min}_{_E}(\lambda \mathrm{Id} - A) < \epsilon\} \ , \tag{9.26}$$

where $s_{_E}$ is the smallest of the "generalized singular values"

$$s^{\min}_{_E}(M) = \min\{\sqrt{\lambda} : \lambda \in \sigma(M^\dagger M)\} \ , \tag{9.27}$$

with $M \in M_n(\mathbb{C})$ and its adjoint $M^\dagger$ given by Eq. (9.25).

Part III

Part three: Methodology, Implementation, and Results

This part show parts of the main three articles that this PhD contributed to.

Chapter 10

Quasi-Normal Modes in Gravity

Contents

10.1 A toy model: Pöschl-Teller potential

In our study of BH QNMs and their (in)stabilities, we exploit the geometrical framework of the hyperboloidal approach to analytically impose the physical boundary conditions at the BH horizon and at the radiation zone (future null infinity). As discussed in section 8, a crucial feature of such a strategy is that it allows us to cast the calculation of the QNM spectrum explicitly as the spectral problem of a non-selfadjoint differential operator, which is then the starting point for the tools assessing spectral instabilities presented in section 6, namely the construction of the pseudospectrum and the analysis of random perturbations. Finally, spectral methods discussed in section 7 are employed to study these spectral issues through a discretisation for the derivative operators. Prior to the study of the BH case, the goal of this section is to illustrate this strategy in a toy model, namely the one given by the Pöschl-Teller potential.

10.1.1 Hyperboloidal approach in Pöschl-Teller

The Pöschl-Teller potential [1], given by the expression

$$V(\bar{x}) = \frac{V_o}{\cosh^2(\bar{x})} = V_o \,\mathrm{sech}^2(\bar{x}) \quad , \quad \bar{x} \in]-\infty, \infty[\, , \tag{10.1}$$

has been widely used as a benchmark for the study of QNMs in the context of BH perturbation theory (e.g. [73, 26, 128]). Interestingly, QNMs of this potential have been very recently revisited to illustrate, on the one hand, the hyperboloidal approach to QNMs in a discussion much akin to the present one (cf. [31], cast in the setting of de Sitter spacetime) or, on the other hand, functional analysis key issues related to the selfadjointness of the relevant operator [72]. Our interest in Pöschl-Teller stems from the fact that it shares the fundamental behavior regarding

[1] Also known as Eckart, Rosen-Morse, Morse-Feshbach potential, see [35] for a discussion of the terminology.

QNM (in)stability to be encountered later in the BH context, but in a mathematically much simpler setting. In particular, Pöschl-Teller presents weaker singularities than the Regge-Wheeler and Zerilli potentials in Schwarzschild, that translates in the absence of a continuous part of the spectrum of the relevant operator L (corresponding to the "branch cut" in standard approaches to QNMs).

Let us consider the compactified hyperboloids given by Bizoń-Mach coordinates [32, 66] mapping $\mathbb{R}$ to $]-1,1[$

$$\begin{cases} \tau &= \bar{t} - \ln(\cosh \bar{x}) \\ x &= \tanh \bar{x} \end{cases} , \tag{10.2}$$

or, equivalently

$$\begin{cases} \bar{t} &= \tau - \frac{1}{2}\ln(1-x^2) \\ \bar{x} &= \operatorname{arctanh}(x) \end{cases} . \tag{10.3}$$

In the spirit of the conformal compactification along the hyperboloids described in section 8.2, we add the two points at (null) infinity (no BH horizon here), namely $x = \pm 1$, so that we work with the compact interval $[a,b] = [-1,1]$. Under this transformation the wave equation (8.4) reads

$$\Big((1-x^2)\left(\partial_\tau^2 + 2x\partial_\tau\partial_x + \partial_\tau + 2x\partial_x - (1-x^2)\partial_x^2\right) + V\Big)\phi = 0 \ , \tag{10.4}$$

namely the version of Eq. (8.7) corresponding to the transformation (10.2). We notice that angular labels (ℓ, m) are not relevant in the one-dimensional Pöschl-Teller problem. If $x \neq 1$ we can divide by $(1-x^2)$ and, defining

$$\tilde{V}(x) = \frac{V}{(1-x^2)} \ , \tag{10.5}$$

we can write

$$\left(\partial_\tau^2 + 2x\partial_\tau\partial_x + \partial_\tau + 2x\partial_x - (1-x^2)\partial_x^2 + \tilde{V}\right)\phi = 0 \ . \tag{10.6}$$

This expression is formally valid for any given potential $V(\bar{x})$ (although analyticity issues may appear if the asymptotic decay is not sufficiently fast, as it is indeed the case for Schwarzschild potentials at $\mathtt{I}^+$). If we now insert the Pöschl-Teller expression (10.1) and notice $\operatorname{sech}^2(\bar{x}) = 1 - x^2$, we get a remarkably simple effective potential $\tilde{V}$, actually a constant

$$\tilde{V}(x) = V_o \ . \tag{10.7}$$

In particular, the Pöschl-Teller wave equation (10.6) exactly corresponds to Eq. (4) in [31], so that the Pöschl-Teller problem is equivalent to the Klein-Gordon equation in de Sitter spacetime with mass $m^2 = V_o$. In the following, we choose $\lambda = 1/\sqrt{V_o}$ in the rescaling (8.5), so that we can set

$$\tilde{V} = 1 \ . \tag{10.8}$$

Performing now the first-order reduction in time (12.37)-(12.38) we get for $w(x)$, $p(x)$, $q(x)$ and $\gamma(x)$ in Eq. (8.12) the values

$$\begin{aligned} &w(x) = 1 \quad , \quad p(x) = (1-x^2) \quad , \quad q(x) = \tilde{V} = 1 \\ &\gamma(x) = -x \ , \end{aligned} \tag{10.9}$$

and therefore the operators L_1 and L_2 building the operator L in Eq. (8.10) write, in the Pöschl-Teller case, as

$$\begin{aligned} L_1 &= \partial_x \left((1-x^2)\partial_x\right) - 1 \\ L_2 &= -\left(2x\partial_x + 1\right) \ . \end{aligned} \tag{10.10}$$

As discussed in section 8.3.1, the function $p(x) = 1-x^2$ vanishes at the boundaries of the interval $[a,b] = [-1,1]$, defining a singular Sturm-Liouville operator. This is at the basis of the absence of boundary conditions, if sufficient regularity is enforced on the eigenfunctions of the spectral problem. Regularity therefore encodes the outgoing boundary conditions (see below). Finally, the scalar product (8.22) writes in this case as

$$\begin{aligned} \langle u_1, u_2 \rangle_E &= \left\langle \begin{pmatrix} \phi_1 \\ \psi_1 \end{pmatrix}, \begin{pmatrix} \phi_2 \\ \psi_2 \end{pmatrix} \right\rangle_E \\ &= \frac{1}{2}\int_{-1}^{1} \left(\bar{\psi}_1\psi_2 + (1-x^2)\partial_x\bar{\phi}_1\partial_x\phi_2 + \bar{\phi}_1\phi_2\right)dx \ . \end{aligned} \tag{10.11}$$

10.1.2 Pöschl-Teller QNM spectrum

Exact Pöschl-Teller QNM spectrum

Pöschl-Teller QNM spectrum can be obtained by solving the eigenvalue problem (8.14)-(8.15) with operators L_1 and L_2 given by Eq. (10.10). As commented above, no boundary conditions need to be added, if we enforce the appropriate regularity. In this particular case, this eigenvalue problem can be solved exactly. The resolution itself is informative, since it illustrates this regularity issue concerning boundary conditions.

If we substitute the first component of (8.15) into the second or, simply, if we take the Fourier transform in τ in Eq. (10.6) (with $\tilde{V} = 1$ from the chosen λ leading to Eq. (10.8)), we get

$$\left[(1-x^2)\frac{d^2}{dx^2} - 2(i\omega+1)x\frac{d}{dx} - i\omega(i\omega+1) - 1\right]\phi = 0 \ , \tag{10.12}$$

This equation can be solved in terms of the hypergeometric function ${}_2F_1(a,b;c;z)$, with $z = \dfrac{1-x}{2}$. In particular, for each value of the spectral parameter ω we have a solution that can be written as a linear combination of linearly independent solutions obtained from ${}_2F_1(a,b;c;z)$. Discrete QNMs are obtained only when we enforce the appropriate regularity, that encodes the outgoing boundary conditions. In this case, this is obtained by enforcing the solution to be analytic in $x \in [-1,1]$ (corresponding in z to analyticity in the full closed interval $[0,1]$), which amounts to truncate the hypergeometric series to a polynomial. We emphasize that such a need of truncating the infinite series to a polynomial, a familiar requirement encountered in many

different physical settings, embodies here the enforcement of outgoing boundary conditions. In sum, this strategy leads to the Pöschl-Teller QNM frequencies (cf. e.g. [26, 35])

$$\omega_n^{\pm} = \pm\frac{\sqrt{3}}{2} + i\left(n+\frac{1}{2}\right) \ , \tag{10.13}$$

with corresponding QNM eigenfunctions in this setting

$$\phi_n^{\pm}(x) = P_n^{(i\omega_n^{\pm}, i\omega_n^{\pm})}(x) \ , \ x \in [-1,1] \ , \tag{10.14}$$

where $P_n^{(\alpha,\beta)}$ are the Jacobi polynomials (see appendix 15). Two comments are in order here:

i) *QNMs are normalizable*: QNM eigenfunctions $\phi_n^{\pm}(x)$ are finite and regular when making $\bar{x} \to \pm\infty$, corresponding to $x = \pm 1$. This is in contrast with the exponential divergence of QNM eigenfunctions in Cauchy approaches, where the time slices reach spatial infinity i^0. This is a direct consequence of the hyperboloidal approach with slices reaching $\mathtt{I}^+$. The resulting normalizability of the QNM eigenfunctions can be relevant in e.g. resonant expansions (cf. e.g. discussion in [114]).

ii) *QNM regularity and outgoing conditions*: In the present case, namely Pöschl-Teller in Bizoń-Mach coordinates, analyticity (actually polynomial structure) implements the regularity enforcing outgoing boundary conditions. Analyticity is too strong in the general case. But asking for smoothness is not enough (see e.g. [10]). In Refs. [79, 78, 80] this problem is approached in terms of Gevrey classes, that interpolate between analytic and (smooth) C^∞ functions, identifying the space of $(\sigma, 2)$-Gevrey functions as the proper regularity notion. The elucidation of the general adequate functional space for QNMs, tantamount of the consistent implementation of outgoing boundary conditions, is crucial for the characterization of QNMs in the hyperboloidal approach.

Numerical Pöschl-Teller QNM spectrum

Fig. 10.1 shows the result of the numerical counterpart of the Pöschl-Teller eigenvalue calculation, whose exact discussion has been presented above, by using the discretised operators L, L_1 and L_2 described in section 7

$$L^N v_n^{(N)} = \omega_n^{(N)} v_n^{(N)} \ . \tag{10.15}$$

This indeed recovers numerically the analytical result in Eq. (10.13) (we drop the "$\pm$" label, focusing on one of the branches symmetric with respect the vertical axis).

We stress that the remarkable agreement between the numerical values from the bottom panel of Fig. 10.1 (see also Fig. 10.5 later) and the exact expression (10.13) is far from being a trivial result, as already illustrated in existing systematic numerical studies. This is in particular the case of Ref. [30] (where Pöschl-Teller is referred to as the Eckart barrier potential), where the fundamental mode $\omega_0^{\pm}$ in (10.13) is stable and accurately recovered, whereas *all* overtones $\omega_{n\geq 1}^{\pm}$ suffer from a strong instability (triggered, according to the discussion in [30, 192], by the C^1-regularity of the approximation modelling the Pöschl-Teller potential) and could not be recovered.

In our setting, a convergence study of the numerical values shows that the relative error

$$\mathcal{E}_n^{(N)} = \left| 1 - \frac{\omega_n^{(N)}}{\omega_n} \right| \ , \tag{10.16}$$

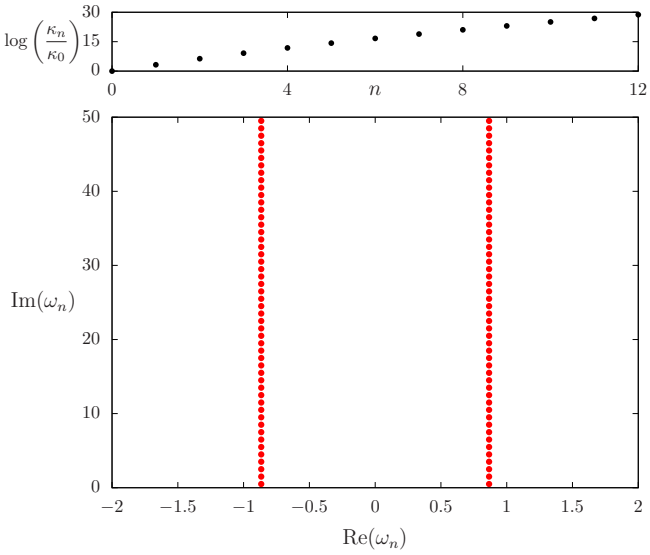

Figure 10.1: Pöschl-Teller QNM problem. *Bottom panel*: QNM spectrum for the Pöschl-Teller potential, calculated in the hyperboloidal approach described in section 10.1.1, with Chebyshev spectral methods and enhanced machine precision. *Top panel*: ratios of condition numbers κ_n of the first QNMs over the condition number κ_0 of the fundamental QNM, indicating a growing spectral instability compatible with the need of using enhanced machine precision.

between the exact QNM ω_n and the corresponding numerical approximation $\omega_n^{(N)}$ (obtained at a given truncation N of the differential operator) actually *increases* with the resolution. This is a first hint of the instabilities to be discussed later. Indeed, the top panel of Fig. 10.2 displays the error for the fundamental mode $n = 0$ and the first overtones $n = 1, \ldots, 4$ when the eigenvalue problem for the discretised operator is naively solved with the standard machine roundoff error for floating point operations (typically, $\sim 10^{-16}$ for double precision).

It is astonishing how, despite the simplicity of the exact solution, the relative error grows significantly already for the first overtones and, crucially, more strongly as the damping grows with higher overtones. To mitigate such a drawback, one needs to modify the numerical treatment in order to allow for a smaller roundoff error in floating point operations. The bottom panel Fig. 10.2 shows the error $\mathcal{E}_n^{(N)}$ when the calculations are performed with an internal roundoff error according to $5\times$`Machine Precision`, i.e. $\sim 10^{-5\times 16}$. In this case, the fundamental QNM $n = 0$ is "exactly" calculated at the numerical level (i.e. the difference between its exact value and the numerical approximation vanishes in the employed precission). The error for the overtones still grows, but in a safe range for all practical purposes. The values displayed in the bottom panel of Fig. 10.1 were obtained with internal roundoff error set to $10\times$`Machine Precision` and we can assure that the errors of all overtones are smaller than 10^{-100}.

Condition numbers of QNM frequencies

The growth in the relative error as we move to higher overtones in Fig. 10.2, suggests an increasing spectral instability in n of eigenvalues $\omega_n^{\pm}$, triggered by numerical errors related to machine precision, so that this instability can be reduced (but not eliminated) by improving the internal roundoff error.

At the level of the non-perturbed spectral problem (10.15), and in order to assess more

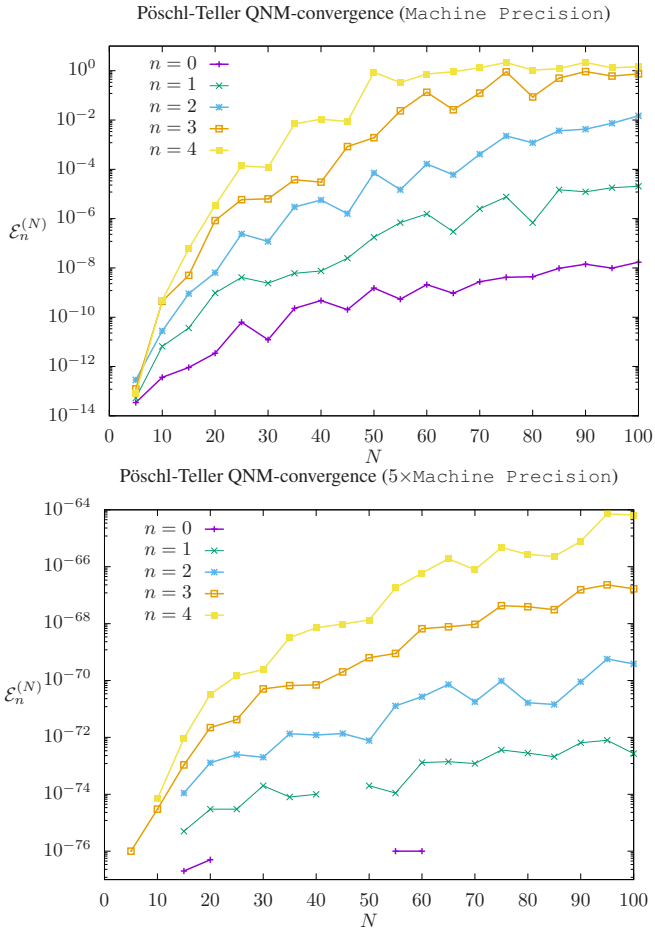

Figure 10.2: Convergence test for the Pöschl-Teller QNM. *Top panel*: double floating point operations with internal round-off error set to `Machine Precision`. *Bottom panel*: double floating point operations with internal round off error set to 5×`Machine Precision`. Note that missing points for $n = 0$ correspond to errors that exactly vanish at the employed machine precision.

systematically such spectral instability, we can apply the discussion in section 6.1 to the Pöschl-Teller approximates L^N. Namely, solving the right-eigenvector problem (10.15) together with left-eigenvector one

$$\left(L^N\right)^\dagger u_n^{(N)} = \bar{\omega}_n^{(N)} u_n^N \ , \tag{10.17}$$

we can compute the condition numbers $\kappa_n^{(N)} = \kappa(\omega_n^{(N)}) = ||v_n^{(N)}||_E ||u_n^{(N)}||_E / |\langle v_n^{(N)}, u_n^{(N)} \rangle_E|$ introduced in Eq. (6.5). Notice that this is quite a non-trivial calculation, since it involves: first, the construction of the adjoint operator $\left(L^N\right)^\dagger = \left(G^E\right)^{-1} \cdot (L^N)^* \cdot G^E$ and, second, the calculation of scalar products $\langle \cdot, \cdot \rangle_E$ and (vector) energy norms $|| \cdot ||_E$. These calculations involve the determination of the Gram matrix G^E associated with the energy scalar product (10.11) by implementing expression (14.12). These expressions are quite non-trivial and in the following section we provide a strong test to the associated analytical and numerical construction.

The result is shown in the top panel of Fig. 10.1. The ratio of the condition numbers κ_n, relative to the condition number of the fundamental mode κ_0, grows strongly with n. This indi-

cates a strong and increasing spectral instability consistent with the error convergence displayed in Fig. 10.2. The rest of this section is devoted to address this spectral stability issue.

10.1.3 Pöschl-Teller pseudospectrum

Motivating the pseudospectrum

As the previous discussion makes apparent, a crucial question that arises after obtaining the QNM spectrum of the operator L in Eq. (8.10), with L_1 and L_2 in (10.10) is whether such QNM eigenvalues are stable under small perturbations of L. More specifically for QNM physics, and in the context of the wave equation (8.4), whether the QNM spectrum is stable under small perturbations of the potential V. The latter is the specific type of perturbation we are assessing in this work.

In the numerical approach we have adopted, perturbations in the spectrum under small pertubations in L may arise either from numerical noise resulting from the chosen discretisation strategy, or they can originate from "real-world sources", namely small physical perturbations of the considered potential V. Ultimately, in the BH setting for which Pöschl-Teller provides a toy model, such physical perturbations could stem from a "dirty" environment surrounding a black hole, and/or emergent fluctuations from quantum-gravity effects. Therefore, the question of whether QNM spectrum instability is a structural feature of the operator L — i.e. not just an artifact of a given numerical algorithm — is paramount for our understanding of the fundamental physics underlying the problem.

A pragmatic approach to address this question consists in explicitly introducing families of perturbations [2], and study their effect on the QNM spectra themselves [120, 16, 42, 94, 54, 124, 156]. We will make contact with this approach later in section 10.1.4, but before that, we apply the pseudospectrum approach described in section 6.2 to the Pöschl-Teller problem. Indeed, one of the main goals of our present work is to bring attention to and emphasise the fact that the *unperturbed* operator already contains crucial information to assess such (in)stability features. We have already encountered this fact in the evaluation of the condition numbers κ_n in Fig. 10.1, that only depends on the unperturbed operator L, but we develop this theme further with the help of the pseudospectrum notion. Indeed, pseudospectrum analysis provides a framework to identify the (potential) spectral instability, which is oblivious to the particular perturbation employed. Then, in a second stage, actual perturbations of the operators with a particular emphasis on random perturbations along the lines in section 6.3, can be used to complement and refine such pseudospectrum analysis.

Fig. 10.3 shows the pseudospectrum for the Pöschl-Teller potential in the energy norm of Eq. (8.20) associated with the scalar product (10.11). Let us explain the content of such a figure. According to the characterization in the Definition 1, namely Eq. (6.6), of the ϵ-pseudospectrum of the operator L, the set $\sigma^\epsilon(L)$ is the collection of all complex numbers $\omega \in \mathbb{C}$ that are actual eigenvalues for some operator $L + \delta L$, where δL is a small perturbation of "size" smaller than a given $\epsilon > 0$. Consequently and crucially, adding a perturbation δL with $||\delta L||_E < \epsilon$ entails an actual ("physical") change in the eigenvalues ω_n that can reach up the boundary of the $\sigma^\epsilon(L)$ set, marked in white lines in Fig. 10.3. The key question is to assess if ϵ-pseudospectra for

[2] In fact, as far as we are aware of the historical development, the path towards the interest in QNM instability followed the opposite way: concerns about BH QNM spectra stability were raised only after modifications/approximations of the potential gave rise to unexpected results [138, 140] (Nollert's study being itself motivated by developments in QNMs of leaky optical cavities [118, 119, 48], namely the study of QNM completeness).

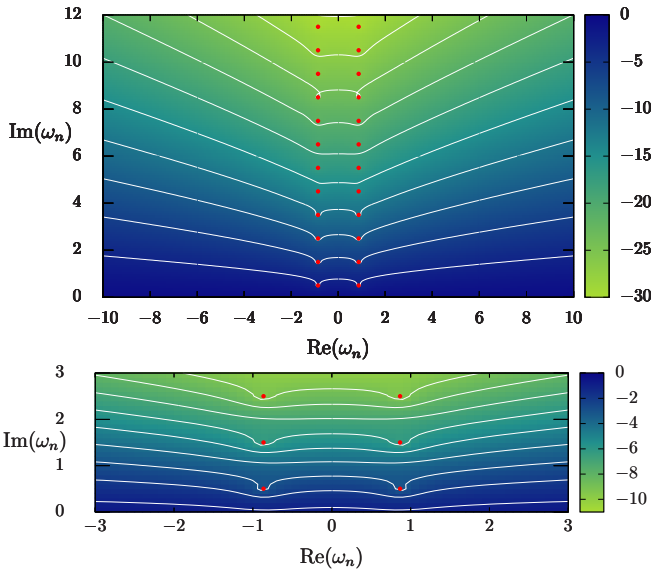

Figure 10.3: *Top panel*: Pseudospectrum for the Pöschl-Teller potential. QNMs (red circles) from Fig. 10.1 are superimposed for reference on their (in)stability. The color log-scale corresponds to $\log_{10}\epsilon$, white lines indicating the boundaries of ϵ-pseudospectra sets σ^ϵ, whose interior extends upwards in the ω-complex plane. *Bottom panel*: Zoom into the region around the fundamental QNM and first overtones.

small ϵ can extend in large areas of $\mathbb{C}$ or not. This is tightly related to condition numbers κ_n controlling eigenvalue spectral (in)stabilities, as explicitly estimated by the Bauer-Fike relation (6.14) between ϵ-pseudospectra sets and 'tubular neighbourhoods' $\Delta_{\kappa\epsilon}$ of radii $\epsilon\kappa_n$ around the spectrum. Let us first discuss a selfadjoint test case and, in a second stage, the actual non-selfadjoint case [3].

Pseudospectrum: selfadjoint case

As discussed in section 8.4, setting $L_2 = 0$ in Eq. (8.10) —while keeping L_1 as in Eq. (10.10)— leads to a selfadjoint operator L [4]. Therefore the associated spectral problem is, cf. section 6.1, stable. A typical pseudospectrum in the selfadjoint (more generally 'normal') case is illustrated by Fig. 10.4: a "flat" pseudospectrum with large values of ϵ for ϵ-pseudospectra sets, when moving "slightly" (in the $\mathbb{C}$-plane) from the eigenvalues. Note also, in this case, the horizontal contour lines far from the spectrum, indicating that all eigenvalues share the same stability properties in the energy norm.

Let us describe Fig. 10.4 in more detail. Boundaries of ϵ-pseudospectra $\sigma^\epsilon(A)$ are marked in white lines, with ϵ's corresponding to the values in the color log-scale. Pseudospectra $\sigma^\epsilon(L)$ are, by construction, "nested sets" around the spectrum (red points in Fig. 10.4), the latter corresponding to the "innermost set" $\sigma^\epsilon(L)$ when $\epsilon \to 0$. In this selfadjoint case, condition

[3] More properly and generally [180], one should distinguish the "normal" (indeed selfadjoint in the particular discussion in the present work) and the "non-normal" operator cases.

[4] Such an operator is relevant by itself, since it corresponds actually to the azymuthal mode $m = 0$ of a wave propagating on a sphere with a constant unit potential, indeed a conservative system. The eigenfunctions are nothing more than the Legendre polynomials $\phi_n(x) = P_n(x)$, with real eigenvalues $\omega_n^\pm = \pm\sqrt{1+\ell(\ell+1)}$. This provides a robust test case.

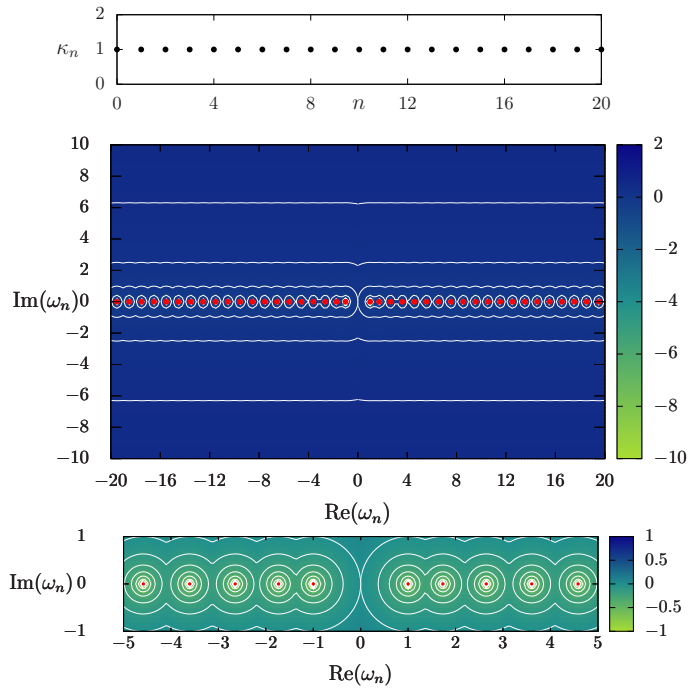

Figure 10.4: Pseudospectrum and eigenvalue condition numbers of a self-adjoint operator (Pöschl-Teller with $L_2 = 0$). *Top panel*: Condition numbers: $\kappa_n = 1$ for ω_n ($0 \leq n \leq 20$). *Middle panel*: Pseudospectrum: "flat" pattern typical of a spectrally stable (normal) operator. *Bottom panel*: Zoom near the spectrum, with concentric circles ("radius ϵ" tubular regions around eigenvalues) characteristic of stability.

numbers in (6.5) must satisfy $\kappa_n = 1$, as we have verified and explicitly shown in the top panel of Fig. 10.4. Then, and consistently with Eq. (6.13), the corresponding nested sets $\sigma^\epsilon(L)$ are actually tubular regions $\Delta_\epsilon(L)$ of "radius ϵ" around the spectrum, so that a change δL with a norm of order ϵ in the operator L entails a maximum change in the eigenvalues of the same order ϵ. Specifically, ϵ-pseudospectra sets show concentric circles around the spectra that quickly reach large-epsilon values, i.e. $\epsilon \sim O(1)$, when moving away from eigenvalues. As a consequence, one would need perturbations in the operator of the same order to dislodge the eigenvalues slightly away from their original values: we say then that L is spectrally stable. Pseudospectra sets with small ϵ are then "tightly packed" in "thin throats" around the spectrum, so that light green colors are indeed so close to spectrum "red points" that they are not visible in the scale of Fig. 10.4, giving rise to a typical "flat" pseudospectrum figure of a "single color".

Horizontal boundaries of ϵ-pseudospectra, when far from the spectrum, is a consequence (in this particular problem) of the use of the energy norm. If another norm is used, e.g. the standard one induced from the L^2 norm in $\mathbb{C}^n$, the global "flatness" of the pseudospectrum is still recovered, especially when comparing with the corresponding scales in Fig. 10.3, indicating already a much more stable situation than the general $L_2 \neq 0$ case. But when refining the scale, one would observe that pseudospectra contour lines far from the spectrum are not horizontal but present a slope growing with the frequency. This indicates that, under perturbations of the same size in that L^2 norm, higher frequencies can move further that low frequencies, this being in tension with the equal stability of all the eigenvalues. What is going on is the effect commented in section 6.2.4 concerning the impact of the norm choice on the notions of "big/small": when using

the L^2 norm, we would be marking with the same "small" ϵ different perturbations among which there exist δL instances that actually excite strongly the high frequencies, but such a feature is blind to the L^2 norm. If using however a norm sensitive to high-frequency effects, as it is the case of the energy norm that has a H^1 character incorporating derivative terms, those same perturbations δL would have a norm much larger than ϵ, the derivative terms in the energy norm indeed weighting more as the frequency grows. What in the L^2 norm was a small perturbation δL, turns out to be a big one in the energy one, so stronger modifications in the eigenvalues are indeed consistent with stability. In practice, in order to construct a given ϵ-pseudospectrum set, such "high-energy" perturbations δL need to be renormalized to keep ϵ fixed, something that the energy norm does automatically. This is a neat example of how the choice of the norm affects the assessment of spectral stability and, in particular, of the importance of the energy norm in the present work, namely for high-frequency issues.

Fig. 10.4 may appear as a boring figure, but it is actually a tight and constraining test of our construction, both at the analytical and numerical level. First of all, panels in Fig. 10.4 correspond to different calculations: the top panel results from an eigenvalue calculation (actually two, one for L and another for $L^\dagger$), whereas the "map" in the middle and bottom panels is the result of calculating the energy norm of the resolvent $R_L(\omega) = (\omega \mathrm{Id} - L)^{-1}$ at each point $\omega \in \mathbb{C}$. Both calculations depend on the construction of the Gram matrix G^E, but are indeed different implementations. The $\kappa_n = 1$ values in the top panel constitute a most stringent test, since modifications in either the analytical structure of the scalar product (10.11) or the slightest mistake in the discrete counterpart (14.12) spoil the result. As discussed at the end of section 10.1.2, this provides a strong test both of the analytical treatment and the numerical discretization of the differential operator and scalar product. On the other hand, the plain flatness of the pseudospectrum in the middle panel is a strong test of the selfadjoint character of L when $L_2 = 0$ that, given the subtleties of the spectral discretization explained in 7, provides a reassuring non-trivial test to the whole numerical scheme.

Non-selfadjoint case: Pöschl-Teller pseudospectrum

In contrast with the selfadjoint case, when considering the actual $L_2 \neq 0$ of the Pöschl-Teller case, pseudospectra sets $\sigma^\epsilon(L)$ with small ϵ extend in Fig. 10.3 into large regions of $\mathbb{C}$ (with typical sizes much larger than ϵ) and therefore the operator L is spectrally unstable: very small (physical) perturbations δL, with $||\delta L||_E < \epsilon$, can produce large variations in the eigenvalues up to the boundary of the now largely extended region $\sigma^\epsilon(L)$. Such strong variations of the spectrum are not a numerical artifact, related e.g. to machine precission, but they rather correspond to an actual structural property of the non-perturbed operator. Indeed, large values of the condition numbers κ_n in the top panel of Fig. 10.1 entail that the tubular sets $\Delta_{\epsilon\kappa}(L)$ in Eq. (6.11) extend now into large areas in $\mathbb{C}$. This fact on κ_n's is consistent with the large regions in Fig. 10.3 corresponding to $\sigma^\epsilon(L)$ sets with very small ϵ's. Such an non-trivial pattern of ϵ-pseudospectra is a strong indication of spectral instability, although without a neat identification of the actual nature of the perturbations triggering instabilities.

Reading pseudospectra: "topographic maps" of the resolvent

In practice, if one wants to read from pseudospectra —such as those in Fig. 10.3 or Fig. 10.4— the possible effect on QNMs of a physical perturbation of (energy) norm of order ϵ, one must first determine the "white-line" corresponding to that ϵ (using the log-scale). Then, eigenvalues can move potentially in all the region bounded by that line (namely, the ϵ-pseudospectrum set

for the non-perturbed operator L) that, in Fig. 10.3, corresponds to the region "above" white lines.

Pseudospectra can actually be seen as a "map" of the analytical structure of the resolvent $R_L(\omega) = (\omega \mathrm{Id} - L)^{-1}$ of the operator L, taken as a function of ω. This corresponds to the characterization in Definition 2 of the pseudospectrum, Eq. (6.7), which it is indeed the one used to effectively construct the pseudospectrum (specifically, its realisation (9.26) in the energy norm; cf. section 9.3 for details). In this view, the boundaries of the ϵ-pseudospectra (white lines in Figs. 10.3 and 10.4) can be seen as "contour lines" of the "height function" $||R_L(\omega)||_E$, namely the norm of the resolvent $R_L(\omega)$. In quite a literal sense, the pseudospectrum can be read then as a topographic map, with stability characterised by very steep throats around eigenvalues fastly reaching flat zones away from the spectrum, whereas instability corresponds to non-trivial "topographic patterns" extending in large regions of the map far away from the eigenvalues.

In sum, this "topographic perspective" makes apparent the stark contrast between the flat pattern of the selfadjoint case of Fig. 10.4, corresponding to stability, and the non-trivial pattern of the (non-selfadjoint) Pöschl-Teller pseudospectrum in Fig. 10.3, in particular indicating a (strong) QNM sensitivity to perturbations that increases as damping grows.

10.1.4 Pöschl-Teller perturbed QNM spectra

Pseudospectra inform about the spectral stability and instability of an operator, but do not identify the specific type of perturbation triggering instabilities. Therefore, in a second stage, it is illuminating to complement the pseudospectrum information with the exploration of spectral instability with "perturbative probes" into the operator, always under the perspective acquired with the pseudospectrum. A link between both pseudospectra and perturbation strategies is provided by the Bauer-Fike theorem [180], as expressed in Eq. (6.14).

Physical instabilities: perturbations in the potential V

Not all possible perturbations of the L operator are physically meaningful. An instance of this, in the setting of our numerical approach, are machine precision error perturbations δL^N to the L^N matrix. As discussed in section 10.1.2, machine precision errors indeed trigger large deviations in the spectrum, consistently with the non-trivial pattern of the pseudospectrum in Fig. 10.3, but clearly we should not consider such effects as physical. They are a genuine numerical artifact, since the structure of the perturbation δL^N does not correspond to any physical or geometrical element in the problem.

The methodology we follow to address this issue is: i) given a grid resolution N, we first set the machine precision to a value sufficiently high so as to guarantee that all non-perturbed eigenvalues are correctly recovered, and ii) we then add a prescribed perturbation with the specific structure corresponding to the physical aspect we aim at studying.

In the present work we focus on a particular kind of perturbation, namely perturbations to the potential V and, more specifically, perturbations $\delta\tilde{V}$ to the rescaled potential $\tilde{V}$ in (8.21). This is in the spirit of studying the problem in [138]. That is, we consider perturbations δL to the L operator of the form

$$\delta L = \left(\begin{array}{c|c} 0 & 0 \\ \hline \delta\tilde{V} & 0 \end{array}\right) . \tag{10.18}$$

We note that, at the matrix level, the $\delta\tilde{V}$ submatrix is just a diagonal matrix. Therefore, the structure of δL in Eq. (10.18) is a very particular one. The pseudospectrum in Fig. 10.3 tells us that L is spectrally unstable, and we know that machine precision perturbations trigger such instabilities, but nothing guarantees that L is actually unstable under a perturbation of the particular form (10.18). It is a remarkable fact, crucial for our physical discussion, that L is indeed unstable under such perturbations and, therefore, under perturbations of the potential V.

Random and high-frequency perturbations in the potential V

We have considered two types of generic, but representative, perturbations δL of the form given in Eq. (10.18):

i) *Random perturbations* $\delta\tilde{V}_{\rm r}$: we set the perturbation according to a normal Gaussian distribution on the collocation points of the grid. This is, by construction, a high-frequency perturbation. Random perturbations are a standard tool [180] to explore generic properties of spectral instability and there exists indeed a rich interplay between pseudospectra and random perturbations [169].

ii) *Deterministic perturbations* $\delta\tilde{V}_{\rm d}$: we have chosen

$$\delta\tilde{V}_{\rm d} \sim \cos(2\pi k\, x)\ , \tag{10.19}$$

in order to address the specific impact of high and low frequency perturbations in QNM spectral stability, by exploring the effect of changing the wave number k.

Perturbations $\delta\tilde{V}$ are then rescaled so as to guarantee $||\delta L||_{_E} = \epsilon$. The impact on QNM frequencies resulting from adding these perturbations is shown in Fig. 10.5. In both random and deterministic cases, the sequence of images in Fig. 10.5 shows a high-frequency instability of QNM overtones, that "migrate" towards new QNM branches. The fundamental (slowest decaying) QNM is however stable under these perturbations. More generally, such QNM instability is sensitive with respect to both perturbations' "size"and frequency.

Before we further discuss the details of the QNM instability, namely the nature of the new QNM branches, an important point must be addressed: whether the values obtained correspond to the actual eigenvalues of the new, perturbed operator $L+\delta L$, or whether they are an artifact of some numerical noise. As in the non-perturbed case discussed in section 10.1.2, and as explained above when introducing the employed methodology, results are obtained with a high internal accuracy (10×`Machine Precision`), so that any numerical noise is below the range of showed values. Proceeding systematically, Fig. 10.6 presents the convergence tests for a few eigenvalues resulting from the deterministic perturbation (random perturbations do not admit this kind of test) with norm $||\delta\tilde{V}_{\rm d}||_{_E} = 10^{-8}$ and frequency $k = 20$ (bottom right panel of Fig. 10.5). The relative error is calculated as

$$\mathcal{E}_n^{(N)} = \left| 1 - \frac{\omega_n^{(N)}}{\omega_n^{(N=400)}} \right| , \tag{10.20}$$

i.e., in the absence of exact results, we take as reference the values with a high resolution $N = 400$. As representative QNMs, we have chosen:

a) The last "unperturbed" overtone, whose value is actually very close to the (truly) unperturbed QNM ω_4.

b) The first new QNM on the imaginary axis.

c) Three QNMs along the new branch with values spread in $1 \lesssim \mathrm{Re}(\omega_n) \lesssim 10$ and $5 \lesssim \mathrm{Im}(\omega_n) \lesssim 8$.

One observes a systematic convergence, with the relative error dropping circa 10 orders of magnitudes when the numerical resolution increases [5] from $N = 150$ to $N = 400$. This result confirms that the spectrum corresponds indeed to the new, perturbed operator, and is not a numerical artifact. This neatly shows the unstable nature of the QNM spectrum of the unperturbed Pöschl-Teller operator: eigenvalues indeed migrate to new branches under very small perturbations.

Perturbed QNM branches and pseudospectrum

High-frequency perturbations trigger the migration of QNM overtone frequencies to new perturbed QNM branches. Fig. 10.7 displays the perturbed QNM spectra on the top of the pseudospectra for the unperturbed operator. The remarkable "predictive power" of the pseudospectrum becomes apparent: perturbed QNMs "follow" the boundaries of pseudospectrum sets. That is, QNM overtones "migrate" to new branches closely tracking the ϵ-pseudospectra contour lines. This happens for both random and deterministic high-frequency perturbations. Crucially, no such instability is observed for low-frequency deterministic perturbations, with small wave number k. Consequently, we shall refer in the following to this effect as an ultraviolet instability of QNM overtones.

Remarkably, such high-frequency QNM instability is not limited to highly damped QNMs but indeed reaches the lowest overtones, the random perturbations being more effective in reaching the slowest decaying overtones for a given norm $||\delta V||_{_E} = \epsilon$. This result is qualitatively consistent with analyses in [140, 94] for Dirac-delta potentials (compare e.g., perturbed QNM branches in Fig. 10.7 here with Fig. 1 in Ref. [94]). These findings advocate the use of pseudospectra to probe QNM instability, demonstrating its capability to capture it already at the level of the non-perturbed operator. At the same time, pseudospectra are oblivious to the nature of the perturbation triggering instabilities. A complementary perturbation analysis, in particular through random perturbations, has been then necessary to identify the high-frequency nature of the instability, confirming its physicality in the sense of being associated with actual perturbations of the potential V.

High-frequency stability of the slowest decaying QNM

The high-frequency instability observed for QNM overtones is absent in the fundamental QNM. The slowest decaying QNM is therefore ultraviolet stable. Such stability is already apparent in the pseudospectrum in Fig. 10.3, where the order of the ϵ's corresponding to ϵ-pseudospectra sets around the fundamental QNM reaches the values in the stable self-adjoint case in Fig. 10.4. This high-frequency stability is then confirmed in the perturbation analysis. Indeed, Fig. 10.7 demonstrates the need of large perturbations in the operator in order to reach the fundamental QNM, namely (random) perturbations with a 'size' $||\delta\tilde{V}||_{_E}$ of the same order as the induced variation in $\omega_0^{\pm}$. This behaviour is a tantamount of spectral stability.

[5] Compare this decrease of the error as numerical resolution increases (the "expected" behaviour) with the anomalous growth in Fig. 10.2. This reflects that the "perturbed operator" has indeed improved spectral stability properties, as compared with the spectrally unstable "unperturbed" Poeschl-Teller operator.

The contrast between the high stability of $\omega_0^{\pm}$ and the instability of overtone resonances $\omega_{n\geq 1}^{\pm}$ has already been evoked in 10.1.2, when referring to the large condition number ratios κ_n/κ_0, in particular referring to Bindel & Zworski's discussion in [30, 192]. This high-frequency stability of the fundamental mode is in tension with the instability found by Nollert in [138] for the slowest decaying mode for Schwarzschild. We will revisit this point in section 10.2.4. For the time being, we simply emphasize that the observed stability relies critically on the faithful treatment of the asymptotic structure of the potential, that is in-built in the adopted hyperboloidal approach permitting to capture the long-range structure of the potential up to null infinity $\mathtt{I}^+$. It is only when we enforce a modification of the potential at "large distances" that the "low frequency" fundamental QNM is affected. This is illustrated in Fig. 10.8 (see also [156, 3]), corresponding to a Pöschl-Teller potential set to zero beyond a compact interval $[x_{\min}, x_{\max}]$: such "cut" introduces high frequencies that make migrate the overtones to the new branches and, crucially, alters the asymptotic structure so that the fundamental QNM is also modified. Such "infrared" effect is however compatible with the spectral stability of the fundamental QNM, since such "cut" of the potential does not correspond to a small perturbation in δL.

Regularization effect of random perturbations

Before proceeding to discuss the BH case, let us briefly comment on an apparently paradoxical phenomenon resulting from the interplay between random perturbations and the pseudospectrum. In contrast with what one might expect, the addition of a random perturbation to a spectrally unstable operator L does not worsen the regularity properties of L but, on the contrary, it improves the analytical behaviour of its resolvent $R_L(\omega)$ [86, 88, 87, 89, 36, 131, 37, 130, 182, 142, 169]. This is illustrated in Fig. 10.9, that shows a series of pseudospectra corresponding to random perturbations of the Pöschl-Teller potential with increasing $||\delta\tilde{V}_{\rm r}||_E$. In addition to the commented migration of QNM overtones towards pseudospectra contour lines, we observe two phenomena: i) ϵ-pseudospectra sets with $\epsilon > ||\delta\tilde{V}_{\rm r}||_E$ are not affected by the perturbation, whereas ii) the pseudospectrum structure for $\epsilon < ||\delta\tilde{V}_{\rm r}||_E$ is smoothed into a "flat pattern". As we have discussed in Fig. 10.4, such flat pseudospectra patterns are the signature of spectral stability, a tantamount of regularity of the resolvent $R_L(\omega)$. The resulting improvement in the spectral stability of $L+\delta L$, as compared to L, is indeed consistent with the convergence properties of the respective QNM spectra, as illutrated by the contrast between the corresponding convergence tests in Figs. 10.6 and 10.2. In sum, random perturbations improve regularity, an intriguing effect seemingly related intimately to a Weyl law occurring in the large-n asymptotics of QNMs [192, 170], with suggestive physical implications in the QNM setting, e.g. in (semi)classical limits to smooth spacetimes from (random) structures at Planck scales.

10.2 Schwarzschild QNM (in)stability

We address now the physical BH case, namely the stability of QNMs in Schwarzschild spacetime. Whereas the previous section has been devoted, to a large extent, to discuss some of the technical issues in QNM stability, the spirit in this section is to focus more on the physical implications, in particular in the perspective of assessing the pioneering work in [138, 140].

10.2.1 Hyperboloidal approach in Schwarzschild

The attempt to implement the QNM stability analysis in the coordinate system employed for Pöschl-Teller, namely the Bizoń-Mach chart (10.2), is unsuccessful. The reason is the bad analytic behaviour at null infinity of Schwarzschild potential(s) in the corresponding coordinate x. Instead of this, we resort to the 'minimal gauge' slicing [10, 148, 146], devised to improve regularity in the Schwarzschild(-like) case.

We start by considering standard Schwarzschild (t, r) coordinates in the line element (8.2), with $f(r) = (1 - 2M/r)$ and BH horizon at $r = 2M$. "Axial" and "polar" Schwarzschild gravitational parities are described by the wave equation (8.4) with, respectively, Regger-Wheeler $V_\ell^{\mathrm{RW},s}(r)$ and Zerilli $V_\ell^{\mathrm{Z}}(r)$ potentials [159, 190, 45, 105, 125]. Specifically, we have

$$V_\ell^{\mathrm{RW},s}(r) = \left(1 - \frac{2M}{r}\right)\left(\frac{\ell(\ell+1)}{r^2} + (1-s^2)\frac{2M}{r^3}\right) \ , \tag{10.21}$$

for the axial case, where $s = 0, 1, 2$ correspond to the scalar, electromagnetic and (linearized) gravitational cases, and

$$V_\ell^{\mathrm{Z}}(r) = \left(1 - \frac{2M}{r}\right) \left(\frac{2n^2(n+1)r^3 + 6n^2Mr^2 + 18nM^2r + 18M^3}{r^3(nr+3M)^2}\right) \ , \tag{10.22}$$

with

$$n = \frac{(\ell-1)(\ell+2)}{2} \ . \tag{10.23}$$

for the polar case.

To construct horizon-penetrating coordinates reaching null infinity, one defines a height function h in (8.6) by first considering an advanced time coordinate built on the rescaled tortoise coordinate $\bar{x} = r^*/\lambda$, with $r_* = r + 2M\ln(r/2M - 1)$, so that the BH horizon is at $\bar{x} \to -\infty$, and then enforcing a deformation of the Cauchy slicing into a hyperboloidal one through the choice of a 'minimal gauge', prescribed under the guideline of preserving a good analytic behavior at $\mathtt{I}^+$. In a second stage, the function g in (8.6) implementing the compactification along hyperboloidal slices is implicitly determined by (note that instead of x in (8.6), we rather use σ for the spatial coordinate, so as to keep the standard usage in [10, 148, 146])

$$r = \frac{2M}{\sigma} \ . \tag{10.24}$$

Choosing $\lambda = 4M$ in the rescaling $\bar{x} = r^*/\lambda$ of Eq. (8.5), the steps above result (see details in [10, 148, 146]) in the 'minimal gauge' hyperboloidal coordinates for the transformation (8.6)

$$\begin{cases} \bar{t} &= \tau - \frac{1}{2}\left(\ln\sigma + \ln(1-\sigma) - \frac{1}{\sigma}\right) \\ \bar{x} &= \frac{1}{2}\left(\frac{1}{\sigma} + \ln(1-\sigma) - \ln\sigma\right) \end{cases} \ , \tag{10.25}$$

that, upon addition of the BH horizon and $\mathtt{I}^+$ points, maps $\bar{x} \in [-\infty, \infty]$ to the compact interval $\sigma \in [a, b] = [0, 1]$, with the BH horizon at $\sigma = 1$ and future null infinity at $\sigma = 0$.

Implementing transformation (10.25) in the first-order reduction in time in Eqs. (12.37)-(12.38), we get for $w(\sigma)$, $p(\sigma)$, $q_\ell(\sigma)$ (now explicitly depending on ℓ) and $\gamma(\sigma)$ in Eq. (8.12)

$$\begin{aligned} w(\sigma) &= 2\,(1+\sigma) \quad , \quad p(\sigma) = 2\sigma^2(1-\sigma)\,, \\ q_\ell(\sigma) &= \frac{(4M)^2 V_\ell}{2\sigma^2(1-\sigma)} \quad , \quad \gamma(\sigma) = 1-2\sigma^2\,, \end{aligned} \tag{10.26}$$

leading to the L_1 and L_2 operators building L in Eq. (8.10)

$$\begin{aligned} L_1 &= \frac{1}{2(1+\sigma)}\left[\partial_\sigma\left(2\sigma^2(1-\sigma)\partial_\sigma\right) - \tilde{V}_\ell\right] \\ L_2 &= \frac{1}{2(1+\sigma)}\left(2(1-2\sigma^2)\partial_\sigma - 4\sigma\right)\,, \end{aligned} \tag{10.27}$$

where the rescaled potential $\tilde{V}_\ell(\sigma) := q_\ell(\sigma)$ results, in the respective axial and polar cases, in the explicit expressions

$$\begin{aligned} \tilde{V}_\ell^{\mathrm{RW},s} &= 2\Big(\ell(\ell+1) + (1-s^2)\sigma\Big) \\ \tilde{V}_\ell^{\mathrm{Z}} &= 2\left(\sigma + \frac{2n}{3}\left(1 + 4n\frac{3+2n}{(2n+3\sigma)^2}\right)\right)\,. \end{aligned} \tag{10.28}$$

Finally, from Eqs. (10.26) and (8.22), the energy scalar product is

$$\begin{aligned} \langle u_1, u_2\rangle_{_E} &= \left\langle \begin{pmatrix}\phi_1\\ \psi_1\end{pmatrix}, \begin{pmatrix}\phi_2\\ \psi_2\end{pmatrix} \right\rangle_{_E} \\ &= \int_0^1 \left((1+\sigma)\bar{\psi}_1\psi_2 + \sigma^2(1-\sigma)\partial_x\bar{\phi}_1\partial_x\phi_2 + \frac{\tilde{V}_\ell}{2}\bar{\phi}_1\phi_2\right)d\sigma\,, \end{aligned} \tag{10.29}$$

where the weight $\tilde{V}_\ell$ is fixed by Eq. (10.28) for each polarization.

10.2.2 Schwarzschild QNM spectrum

As discussed in section 8.3.1, outgoing boundary conditions have been translated into regularity conditions on eigenfunctions. Specifically, as we have seen in the Pöschl-Teller case, the operator L_1 in (10.27) is a singular Sturm-Lioville operator, namely the function $p(\sigma) = \sigma^2(1-\sigma)$ vanishes at the boundaries of the interval $[a,b] = [0,1]$ consistently with Eq. (8.16). This translates into the fact that no boundary conditions can be imposed if enough regularity is required.

But there is a key difference between the Pöschl-Teller and the BH case: whereas in Pöschl-Teller the function $p(x) = (1-x)(1+x)$ vanishes linearly at the boundaries, and therefore $x = \pm 1$ are regular singular points, in Schwarzschild this is true for $\sigma = 1$ (BH horizon) but not for $\sigma = 0$ ($\mathtt{I}^+$), due to the quadratic σ^2 term. Null infinity is then an irregular singular point. This is the counterpart, in our compactified hyperboloidal formulation, of the power-law decay of Schwarzschild potentials responsible for the branch cut in the Green function of Eq. (8.4), with its associated "tails" in late decays of scattered fields. In the context of our spectral problem for the operator L, this translates into the appearance of a ("branch cut") continuous part in the spectrum. This has an important impact on the numerical approach, since the continuous

branch cut is realized in terms of actual eigenvalues of the discretised approximates L^N. Such eigenvalues are not QNMs and can indeed be unambiguously identified, but their presence has to be taken into account when performing the spectral stability analysis, that becomes a more delicate problem than in Pöschl-Teller. In this context, the latter becomes a crucial benchmark to guide the analysis in the BH case.

The Schwarzschild (gravitational) QNM spectrum (for $\ell = 2$) is shown in Fig. 10.10, that presents the result of the numerical calculation of the spectrum of the L operator defined by (10.26). This is obtained either for the Regge-Wheeler or the Zerilli rescaled potentials in (10.28), corresponding respectively to potentials (10.21) and (10.22). This provides a crucial internal consistency check for the analytical and numerical construction, since both potentials are known to be QNM-isospectral (see below in section 10.2.4). The branch cut structure is apparent in the eigenvalues along the upper imaginary axis. Such "branch cut" points can be easily distinguished from the special QNM corresponding to $\omega_{n=8}$, also in the imaginary axis, simply by changing the resolution: branch points move "randomly" along the vertical axis, whereas $\omega_{n=8}$ stays at the same frequency (see later 10.2.4 for a more systematic approach to establish the "non-branch" nature of $\omega_{n=8}$, when we will consider high-frequency perturbations to QNMs). Moreover, eigenfunctions associated with algebraically special modes are polynomials, as shown in the detailed studies of these modes for Schwarzschild and Kerr in [10, 53].

Due to the lack of an exact expression for the Schwarzschild QNMs, one must compare the obtained values against those available in the literature via alternative approaches — see, for instance [105, 139, 25, 107, 24, 39, 93, 174]. An estimative for the errors when QNMs are calculated with the methods from this work is found in Ref. [146]. From the practical perspective, and regardless of the numerical methods, it is well known that the difficulty to accurately calculate numerically a given QNM overtone $\omega_n^{\pm}$ increases significantly with n. For instance, convergence and machine precision issues similar to the ones commented above are reported in Refs. [122, 96, 74], a control of the internal roundoff accuracy being required. Alternatively, iterative algorithms such as Leaver's continued fraction method [117] require an initial seed relatively near a given QNM, which must be carefully adapted when dealing with the overtones [185]. The bottomline is that the calculation of BH QNM overtones is a challenging and very delicate issue.

In our understanding, the latter challenge is not a numerical hindrance but the consequence of a structural feature of the underlying analytical problem, namely the spectral instability of the Schwarzschild QNM problem. This is manifested already at the present stage of analysis, namely the calculation of QNM frequencies of non-perturbed Schwarzschild, in the eigenvalue condition numbers κ_n's shown in the top panel of Fig. 10.10: we encounter again the pattern found in the Pöschl-Teller case, cf. Fig. 10.1, with a growth of the spectral instability as the damping increases, with the notably anomaly of an enhanced stability for the algebraically special QNM frequency, with $n = 8$. We devote the rest of the section to explore this spectral instability with the tools employed for Pöschl-Teller.

10.2.3 Schwarzschild pseudospectrum

The pseudospectrum of Schwarzschild is presented in Fig.10.11. As illustrated in Pöschl-Teller, the pseudospectrum provides a systematic and global tool to address QNM spectral instability, already at the level of the unperturbed potential. A "topographic map" of the analytic structure of the resolvent, where regions associated with small ϵ-pseudospectra (light green) correspond to strong spectral instability, whereas regions with large ϵ (namely $O(\epsilon) \sim 1$, dark blue) indicate spectral stability. The superposition of the QNM spectrum shows the respective spectral stability

of QNM frequencies.

We can draw the following conclusions from Fig. 10.11:

i) The Schwarzschild pseudospectrum indicates a strong instability of QNM overtones, an instability that grows fast with the damping. White-line boundaries corresponding to ϵ-pseudospectra with very small ϵ's extend in large regions of the complex plane. This is compatible with the results in [138], providing a rationale —already at the level of the unperturbed potential— for the QNM overtone instability discovered by Nollert.

ii) The slowest decaying QNM is spectrally stable. Fig. 10.11 tells us that changing the fundamental QNM frequency requires perturbations in the operator of order $||\delta L||_E \sim 1$. This corresponds to spectral stability and is in tension with the results in [138], where the fundamental QNM is found to be unstable. We will address this point below.

iii) Schwarzschild and Pöschl-Teller potentials show qualitatively the same pseudospectrum pattern, with large "green regions" producing patterns in stark contrast with the flat self-adjoint case. On the one hand, this reinforces the usage of Pöschl-Teller as a convenient guideline for understanding the stability structure of BH QNMs and, on the other hand, it points towards an instability mechanism independent, at least in a certain measure, on some of the details of the potential.

We can conclude that Fig. 10.11 demonstrates —at the level of the unperturbed operator— the main features of the stability structure of the BH QNM spectrum, namely the QNM overtone instability and the stability of the fundamental QNM. However, the pseudospectrum does not inform us about the particular type of the perturbations that trigger the instabilities. This is addressed in the following subsection.

10.2.4 Perturbations of Schwarzschild potential

Once the Schwarzschild pseudospectrum, together with the condition numbers κ_n, have presented evidence of QNM spectral instability at the level of the unperturbed operator, in this section we address the question about the actual physical character of perturbations triggering such instabilities.

Ultraviolet instability of BH QNM overtones

The qualitative agreement between Pöschl-Teller and Schwarzschild pseudospectra, cf. Figs. 10.3 and 10.11, together with the experience gained in the study of Pöschl-Teller perturbations regarding the high-frequency instability of all QNM overtones and the stability of the fundamental QNM, guide our steps in the analysis of the BH setting.

Random perturbations: spoils from the "branch cut". The presence of a "branch cut" in the Schwarzschild spectrum, discussed in section 10.2.2, translates into a methodological subtlety when considering random perturbations in the BH case, as compared with the Pöschl-Teller one. The difficulty stems from the fact that not only the QNM eigenvalues, but also the eigenvalues associated with the discretized version of the branch cut, are sensitive to random perturbations $\delta\tilde{V}_{\rm r}$ of the potential. As a consequence, the possible contamination from eigenvalues from the branch cut complicates the analysis of the impact of random perturbations on QNM frequencies. This is an artifact of our particular numerical approach, and not a problem of the differential

operator itself, but it limits our capability to assess the triggering by random perturbation of the QNM migration to new branches, that was observed in the Pöschl-Teller case (cf. left column of Fig. 10.5). Other tools, either numerical refinements and/or analytical methodologies, are required to address this specific issue in Schwarzschild.

This does not mean that random perturbations have no use in our BH discussion. An illustrative example is the study of the stability of the algebraically special Schwarzschild QNM $\omega_{n=8}$. Whereas random perturbations move "branch cut" eigenvalues away from the imaginary axis, the algebraically special QNM stays stable. This methodology provides a powerful and efficient tool to probe the "physicality" of specific eigenvalues in very general settings (cf. e.g. Fig. 4 in [33]).

Deterministic perturbations. Given the limitations for random $\delta\tilde{V}_{\rm r}$'s, in the present study we have focused on the class of deterministic perturbations to the potential $\delta\tilde{V}_{\rm d}$ provided by Eq. (10.19). Crucially, such perturbations do not perturb the "branch eigenvalues" as (much as) random $\delta\tilde{V}_{\rm r}$ do, by-passing then the associated spectral instability contamination. Despite their simplicity, they provide a good toy-model to explore the effects of astrophysically motivated perturbations (assessment of "long range/low frequency" versus "small scale/high frequency" perturbations), as well as those arising from generic approaches to quantum gravity ("small scale/high frequency" effective fluctuations). They are, therefore, conveniently suited to address these instability issues.

The left column in Fig. 10.12 depicts (with $||\delta\tilde{V}_{\rm d}||_{_E} \sim 10^{-8}$) the stability of the first overtones against low frequency perturbations ($k = 1$, top-left panel) in contrast with the instability resulting from high-frequency perturbations ($k = 20$, bottom-left panel). Pushing along this line, the right column in Fig. 10.12 zooms in to study the very first overtones, which are paramount for the incipient field of black-hole spectroscopy. Assessing the (in)stability of the very first overtones is therefore crucial for current research programs in gravitational astronomy. It becomes apparent that the first overtones, this including the very first overtone, are indeed affected without any extraordinary or fine tuned perturbations $\delta\tilde{V}_{\rm d}$. In particular, and taking the left column as a reference, the first overtone is reached: i) either by considering a "slightly" more intense perturbation ($||\delta\tilde{V}_{\rm d}||_{_E} \sim 10^{-4}$, $k = 20$), or ii) perturbations with sufficiently high frequency ($||\delta\tilde{V}_{\rm d}||_{_E} \sim 10^{-8}$, $k = 60$).

From this perturbation analysis of the BH potential we conclude: i) all QNM overtones are ultraviolet unstable, as in Pöschl-Teller, the instability reaching the first overtone for sufficiently high frequency; ii) QNMs are stable under low frequency perturbations, this illustrating that spectral instability does not mean instability under "any" perturbation, in particular long-wave perturbations not affecting the QNM spectrum; iii) the slowest decaying QNM is ultraviolet stable, a result in tension with the instability of the fundamental QNM found in [138]. We revisit this point in section 10.2.4 below.

Isospectrality loss: axial versus polar spectral instability

Regge-Wheeler and Zerilli potentials for axial and polar perturbations are known to be isospectral in the QNM spectrum (cf. [46, 45, 7, 83]; see also [125]). In particular, Chandrasekhar identified (cf. point 28 in [45]) a necessary condition for two (one-dimensional) potentials $V_1(\bar{x})$ and $V_2(\bar{x})$, with $\bar{x} \in]-\infty, \infty[$ as the rescaled tortoise coordinate, to have the same transmission amplitude and present the same QNM spectrum. Specifically, both potentials must render the same values

when evaluating an infinite hierarchy of integrals

$$C_n = \int_{-\infty}^{\infty} v_n(\bar{x}) d\bar{x} \ , \tag{10.30}$$

with

$$\begin{aligned} v_1 &= V \ , \ v_3 = 2V^3 + V'^2 \\ v_5 &= 5V^4 + 10VV'^2 + V''^2 \ , \ v_{2n+1} = \dots \end{aligned} \tag{10.31}$$

These quantities turn out to be the conserved quantities of the Korteweg-de Vries equation and connect the Schwarzschild QNM isospectrality problem to integrability theory through the inverse scattering transform of Gelfand-Levitan-Marchenko (GLM) theory (cf. [67]; see [83] for an alternative approach in terms of Darboux transformations).

The key point for our spectral stability analysis of L is that axial and polar QNM isospectrality is the consequence of a subtle and "delicate" integrability property of stationary BH solutions, so we do not expect it to be robust under generic perturbations of V. In particular, given the non-linear dependence in V of the conserved quantities C_n in (10.30), we would expect either random $\delta\tilde{V}_{\rm r}$ or deterministic $\delta\tilde{V}_{\rm d}$ perturbations to render different values of C_n, therefore resulting in a loss of QNM isospectrality. Fig. 10.13 confirms this expectation: whereas the fundamental QNM mode remains stable under high-frequency perturbations, isospectrality is broken for the overtones with a slight, but systematic, enhanced damping in the axial case. Other mechanisms for BH isospectrality loss have been envisaged, e.g. in the study of the imprints of modified gravity theories [42], ultraviolet QNM overtone instability providing a possible mechanism inside general relativity. In sum, isospectrality loss provides an interesting probe into QNM instability, with potential observable consequences and will be the subject of a specifically devoted study elsewhere.

"Infrared instability" of the fundamental QNM

Both the pseudospectrum and the explicit perturbations of the potential indicate a strong spectral stability of the slowest decaying Schwarzschild QNM. This is tension with the results in [138, 140], where the instability affects the whole QNM spectrum, this including the slowest decaying QNM. This is a fundamental point to establish, since it directly impacts the dominating frequency in the late BH ringdown signal.

In our understanding, and as it was the case of the Pöschl-Teller potential discussed in section 10.1.4, the instability of the fundamental QNM frequency found by [138] is an artifact of the implemented perturbations, namely step-like approximations to the Schwarzschild potential (in particular Regge-Wheeler, but the same applies for Zerilli) that modify the potential at large distances. Specifically, V_ℓ is set to zero beyond $[x_{\rm min}, x_{\rm max}]$, fundamentally altering the long-range nature of Schwarzschild potential that becomes of compact support. What we observe in Fig. 10.12 is that keeping a faithful treatment of the asymptotic structure at infinity through the compactified hyperboloidal approach keeps spectral stability.

To test this idea (cf. also the recent [156], as well as [3]), and as we did in Pöschl-Teller, we have implemented a "cut Schwarzschild" potential in our hyperboloidal approach, setting the potential to zero from a given distance (both towards null infinity and the BH horizon). The result is shown in Fig. 10.14, showing a similar qualitative behaviour to Pöschl-Teller in Fig. 10.8. Overtones are strongly perturbed into the QNM branches already observed in Fig. 10.12, consistently with the high-frequencies introduced by the Heaviside cut. But, crucially, now the

fundamental QNM is indeed also modified, in contrast with its stable behaviour under high-frequency perturbations. This reinforces the understanding of this effect as a consequence of the "suppression" of the large-scale asymptotics of the potential [6]. However, the observed modification of the fundamental QNM frequency is not as dramatic as the one in [138]. We do not have a good explanation for this, but it may relate to the fact that the analysis in [138, 140] deals directly with Eq. (8.4), in particular in the setting of a Cauchy slicing getting to spatial infinity i^0. Such asymptotic framework may be more sensitive to the modification of the potential that the hyperboloidal one, related to null infinity $\mathtt{I}^+$. In this setting, and lacking a better expression, we refer to this effect as an "infrared instability" of the fundamental QNM.

Enforcing the compact support nature of V is naturally motivated in physical contexts such as optical cavities, and will be studied systematically in such settings [3]. In gravitation the physicality of such an effect is more difficult to assess, since gravity is a long-range interaction that, in contrast to the electromagnetic one, is not screened. In any case, insofar as a pertinent gravitational scenario may be envisaged for a such "cut potential", then the "infrared instability" shown for the first time in [138] would constitute a physical effect.

10.2.5 Nollert-Price BH QNM branches: instability and universality

We revisit the results in [138, 140] (see also [54, 156]), under the light of the elements introduced for the study of QNM spectral stability. Fig. 2 in [138] presents the migration of Schwarzschild QNMs to new branches, as the result of perturbing the (Regge-Wheeler) Schwarzschild potential with a step-like approximation with an increasing number "N_{st}" of steps (cf. Fig. 1 in [138]). A salient feature of Nollert's Fig. 2, further analysed with Price in [140], is that the new QNM branches distribute in a perfectly structured family of lines in the complex plane, unbounded in the real part of the frequency, that "move down" in the complex plane as N_{st} (i.e. the frequency in the perturbation) increases [7]. A comparison with Schwarzschild's pseudospectrum in our Fig. 10.11 shows two remarkable features: i) the pattern of the new branches found and studied by Nollert and Price is qualitatively similar to the contour lines of ϵ-pseudospectra, ii) the effect of increasing the frequency perturbation indeed corresponds to an increment in the ϵ of the corresponding contour line (namely the "energy size" of the pertubation that, as a H^1 norm, includes the frequency). In other words, Nollert and Price's BH QNM branches seem indeed to be closely related to ϵ-pseudospectrum contour lines.

In order to test this picture, we bring our perturbation analysis in section 10.2.4 into scene. Fig. 10.15 presents the superposition of perturbed QNM spectra in Fig. 10.12 onto the Schwarzschild pseudospectrum in Fig. 10.11. As in the Pöschl-Teller case, perturbed QNMs closely track ϵ-pseudospectra lines, demonstrating the insight gained above on Nollert's QNM instability by using the pseudospectrum: Nollert-Price QNM branches are identified as actual probes into the analytical structure of the non-perturbed wave operator. Moreover, the correlation of ϵ-contour lines with the "size/frequency" of the perturbations, endows the pseudospectrum not only with an explicative but also with a predictive power, as a tool to calibrate the relation between space-time perturbations and QNM frequency changes. The conceptual frame encoded in Fig. 10.15 is, in our understanding, the main contribution in this work.

[6] Such suppression must be stronger than exponential, since Poeschl-Teller shows stability of the fundamental QNM.

[7] The Nollert case $N_{\text{st}} = 1$ in his method "iii)" seems special. It corresponds precisely to the "cut potential" in section 10.2.4 and may require a separate discussion. It connects also with section 10.1.4, since method "iii)" in [138] "regularizes" Schwarzschild with a Poeschl-Teller factor, cf. Eq. (7) in [138].

QNM structural stability, universality and asymptotic analysis

Building on Nollert and Price's work, our analysis strongly suggests that BH QNM overtones are indeed structurally unstable under high-frequency perturbations: BH QNM branches migrate to a qualitatively different class of QNM branches. Noticeably and in contrast with this, the pseudospectrum analysis combined with the perturbation tools also suggests that the new class of "Nollert-Price BH QNM branches" presents structural stability features pointing to a kind of 'universality' in the QNM overtone migration pattern.

"Universality" in the high-frequency perturbations. The QNM migration pattern seems independent of the detailed nature of the high-frequency perturbation in the Schwarzschild potential. First, such universality is manifested by the similar QNM perturbation pattern produced by very different perturbations: step-like perturbations in [138], the sinusoidal deterministic ones showed in Fig. 10.15 and also random perturbations (not presented here due to "blurring" issues, consequence of the "branch cut" contamination). Second, the new branches follow closely the pseudospectra contour lines, a key point in this universality discussion, since it is completely prior to and independent of perturbations.

"Universality" in the potential. Perhaps more importantly, universality seems to go beyond the insensitivity to the nature of the perturbation: it seems to be shared by a whole class of potentials. First, the same pattern of perturbed branches is found in Pöschl-Teller, cf. Fig. 10.7. More dramatically, Nollert and Price's analysis in [140] is particularly illuminating in this respect. They considered a toy model capturing the effect of a (Dirac-delta) high-frequency perturbation on a BH-like potential, referred to as "truncated dipole potential" (TDP), that contains only two QNMs. Adding the singular (high-frequency) "spike" creates an infinite number of QNMs, again following a QNM branch pattern compatible with our pseudospectra contour lines (cf. Fig. 5 in [140] and see below).

But more noteworthy, and again noticed by Nollert [138], beyond the BH setting the new BH QNM branches are strikingly similar to (curvature) w-modes in neutron-star QNMs (cf. e.g. Fig. 3 in [105] and the systematic study in Ref. [191]). This is remarkable, suggesting that exact but unstable BH QNMs migrate to perturbed but stable QNMs branches whose qualitative pattern may be shared by generic compact objects [8].

Asymptotic analysis and universality. How to address systematically a possible universality in the qualitative pattern of the perturbed QNM branches? Asymptotic analysis provides a sound approach. The study of the spiked TDP QNMs by Nollert and Price [140] provides an excellent illustration, with the identification of the large-n asymptotic form of perturbed QNM branches, according to the logarithm dependence

$$\mathrm{Im}(\omega_n) \sim C_1 + C_2 \ln\left(\mathrm{Re}(\omega_n) + C_3\right) \quad , \quad n \gg 1 \ , \tag{10.32}$$

[8] Beyond w-modes of compact objects, such perturbed BH 'universal' branches share also features with QNMs of convex obstacles, where the asymptotic form of QNM branches (under a 'pinched curvature assumption') can be established [171, 193] as $\mathrm{Im}(\omega_n) \sim K|\mathrm{Re}(\omega_n)|^{\frac{1}{3}} + C$, for $n \gg 1$. Focusing on the spherical obstacle case [173] (see also [194, 68]), if considering all angular ℓ's modes and taking ℓ as the spectral parameter (while keeping n fixed), the similar qualitative pattern between the corresponding branches and the perturbed BH QNM branches raises an intriguing question about a possible duality between QNM and Regge poles (cf. e.g. [61, 62, 157, 65] in a complex angular momentum setting). In particular, the asymptotic logarithm pattern of perturbed-BH [140] and compact object [191] QNMs is exactly recovered for Regge poles of compact objects in [145] (cf. [58] for related asymptotics).

with C_1, C_2 and C_3 appropriate constants (note that C_3 can be put to zero for sufficiently high n, as in [140], since $\mathrm{Re}(\omega_n) \to \infty$ as $n \to \infty$; we prefer to keep it to account for intermediate asymptotics [97]). It is suggestive that this makes direct contact with the possible universality of perturbed BH QNMs and (non-perturbed) QNMs of compact objects evoked above. Indeed, as shown in Ref. [191], w-modes of (a class of) neutron stars present exactly this logarithm pattern [9]. Even more, this makes (an unexpected) contact with Pöschl-Teller, where the spectral instability discussed in section 10.1.2 is explained [30, 192, 194, 68] in terms of so-called broad "Regge resonances" (not to confuse with "Regge poles"), precisely described by such a logarithmic dependence [158] and explained in terms of the loss of continuity at a p-th order derivative, i.e. in terms of an underlying reduced C^p regularity (with $p < \infty$). Along these lines of C^p regularity, and in a WKB semiclassical analysis, such logarithmic branches have been also recovered in [156] in their recent discussion of Nollert's original work [138]. It would be therefore tempting to refer to the perturbed BH QNM branches as Nollert-Price-(Regge) QNMs, but this requires an elucidation of the role of the reduced C^p regularity in the generic perturbations we have studied here, that in particular include C^∞ regular (high-frequency) sinusoidal deterministic perturbations (10.19). In sum, the asymptotic pattern (10.32) provides a starting point to probe, in gravitational wave signals, the physical properties (e.g. energy, frequency) of small scale perturbations [97].

Beyond specific models, this kind of universal behaviour, independent of the high-frequency perturbation detailed nature and for a large class of potentials, invites for systematic semiclassical analyses of highly-damped scattering resonances, in terms of the wave operator principal part [10], including boundary behaviors. In the spirit adopted in this work, we expect asymptotic tools in the semiclassical analysis of the pseudospectrum to provide a systematic approach to assess the universality of perturbed BH QNM branches [11].

Overall perspective on Schwarzschild QNM instability

The main result of this article is summarized in Fig. 10.15. Specifically, it combines Figs. 10.10, 10.11 and 10.12 to demonstrate QNM spectral (in)stability through their respective three distinct calculations: i) the calculation of the eigenfunctions of the exact spectral problem to calculate condition numbers κ_n's, ii) the evaluation of operator matrix norms to generate the pseudospectrum, and iii) the calculation of eigenvalues of the perturbed spectral problem. Calculations i) and ii) work at the level of the unperturbed problem, whereas iii) deals with the perturbed problem. The three calculations fit consistently through the Bauer-Fike theorem that constrains through Eq. (6.14) the relation between the pseudospectrum and the tubular regions around the spectrum. They lead to these main results:

i) QNM overtones:

i.1) *QNM overtones are ultraviolet unstable, including the lowest overtones.* The pseudospectrum provides a systematic explanatory and predictive framework for QNM spectral instability, confirming the result by Nollert and Price [138, 140]. Such instability is indeed realised by physical high-frequency perturbations in the effective potential V, reaching the first overtone for sufficiently high frequencies and/or amplitudes in the perturbation.

[9] We thank B. Raffaelli for signaling this and also Ref. [145].

[10] We thank N. Besset for signaling this point.

[11] Such an approach is very much in the spirit of the "asymptotic reasoning" advocated in [17], where asymptotic analysis is understood as an efficient and systematic tool to unveil structurally stable patterns underlying universality behaviour.

i.2) *QNM overtones are stable under low frequency perturbations.* No instability appears for low/intermediate frequency perturbations of V, consistently with studies [73, 120, 16, 42, 94] on astrophysical BH environments.

ii) Slowest decaying (fundamental) QNM:

ii.1) *The slowest decaying QNM is ultraviolet stable.* This holds, in Schwarzschild, for each ℓ-fixed branch. This feature critically relies on keeping a faithful description of the asymptotic structure at infinity through the compactified hyperboloidal approach. This result is in contrast with conclusions in [138, 140], but no contradiction appears since the latter implement a step-potential approximation fundamentally modifying V at large distances, resulting rather in an "infrared probe" into QNMs.

ii.2) *The slowest decaying QNM is stable under low and intermediate frequency perturbations in the potential.* This property is shared by the whole QNM spectrum.

ii.3) *The slowest decaying QNM is "infrared unstable".* The instability of the fundamental QNM observed in [138, 140] is physical inasmuch as fundamental modifications of the large-distance structure of the potential are allowed.

iii) Structural stability and QNM isospectrality.

iii.1) *'Nollert-Price BH QNM branches' track pseudospectrum contour lines.* The QNM BH spectrum is ultraviolet structurally unstable, migrating to perturbed branches tracking ϵ-contour lines of pseudospectra. Such migration pattern is largely independent of the detailed nature of high-frequency perturbations and potential. Once on such 'Nollert-Price branches', QNMs are spectrally stable. These structural stability properties result in the universality of perturbed QNM branches.

iii.1) *QNM isospectrality ultraviolet loss.* High-frequency perturbations spoil the integrability of Regge-Wheeler and Zerilli potentials, resulting in a slightly enhanced damping of axial modes with respect to polar ones.

10.3 Conclusions and perspectives

10.3.1 Conclusions

We have demonstrated: i) fundamental BH QNMs are stable under high-frequency (ultraviolet) perturbations, while unstable under (infrared) modifications of the asymptotics, the latter consistent with [138]; ii) (all) BH QNM overtones are unstable under high-frequency (ultraviolet) perturbations, quantifiable in terms of the energy content (norm) of the perturbation, extending results in [138, 140] to show isospectrality loss; and iii) pseudospectrum contour lines provide the rationale underlying the structurally stable pattern of perturbed 'Nollert-Price QNM BH branches'. Pseudospectra, together with tools from the analysis of non-selfadjoint operators, have revealed the analytic structure underlying such (in)stability properties of BH QNMs, offering an integrating and systematic approach to encompass a priori disparate phenomena. The soundness of the results relies on the use of a compactified hyperboloidal approach to QNMs, with the key identification of the relevant scalar product in the problem as associated with the physical energy, combined with accurate spectral numerical methods.

Caveats in the current approach to QNM (in)stability

Beyond the soundness of the results, key questions remain:

i) How much does the instability depend on the hyperboloidal approach? In other words, is the instability a property of the equation or rather of the employed scheme to cast it? This is a legitimate and crucial question, requiring specific investigation. In spite of this, we are confident in the soundness of our conclusions: as discussed in detail, the same qualitative behaviour is found systematically by other studies not relying on the hyperboloidal approach, in particular Nollert and Price's pioneer work. Details may change from scheme to scheme, but the (in)stability properties seem robust.

ii) A numerical demonstration is not a proof. Moreover, numerical discretizations introduce their own difficulties and limitations. In particular, spectral issues in the passage from matrix approximations to the actual differential operator is a most delicate question. Again, we are confident in our results, as a consequence of mutual consistency of existing results and non-trivial tests like the ones described in the text. Definitely, proofs will require the use of other methods and techniques.

iii) Could the observed QNM spectral instability be an effect of regularity loss, namely a C^p effect? It may be, but it is difficult to conclude at this stage. C^p regularity provides indeed a sufficient condition for logarithmic branches (10.32) that can be traced to works by Regge [158], Berry [22, 23] or Zworski [192] and manifests in our setting in Nollert & Price's analysis of BH QNM instability [140] (complemented in [156]), broad "Regge resonances" in Pöschl-Teller QNM instability [30, 194, 68], or in neutron star w-modes [191] (cf. also [145] in related Regge poles). But we also attest the same instability phenomenon for regular sinusoidal perturbations of sufficiently high-frequency. Moreover, the pseudospectrum already informs of the instability (cf. contour lines) at the unperturbed "regular" stage. If high-frequency is actually the basic mechanism, then C^p would provide a sufficient, but not necessary condition for QNM instability. This point must be addressed.

10.3.2 Perspectives

While the pseudospectrum framework is already employed in physics (cf. e.g. [179, 180, 110, 169, 49]), there seems to be (up to our knowledge) no systematic application in the gravitational context. The introduction of pseudospectra in gravitational physics opens an avenue to interbreed the study of (in)stability and transients with other domains in physics (and beyond), by using pseudospectrum analysis as a common methodological frame. In the following we mention some possible lines of exploration in different gravitational settings, from astrophysics and fundamental gravity physics to mathematical relativity, closing the discussion with a perspective beyond gravity.

Astrophysics and cosmology

The astrophysical status of the ultraviolet QNM overtone instability, that reaches the lowest overtones for generic perturbations of sufficiently high frequency and energy, requires to assess whether actual astrophysical (and/or fundamental spacetime) perturbations are capable of triggering it. Some problems in which this question is relevant are the following:

a) *BH spectroscopy.* If such instability is actually present, this should be taken into account in current approaches to BH spectroscopy. The stability of the slowest decaying QNM guarantees that the dominating ringdown frequency is unaltered. But regarding QNM overtones, note that in we have not referred at all to late time ringdown frequencies, but to QNM frequencies: since such two sets of frequencies can actually decouple [138, 140, 104, 41, 108, 54, 106, 156] and, as already noticed by Nollert [138], the propagating (scattered) field itself is not much affected by high-frequency perturbations, finding the signature of perturbed QNMs in the gravitational wave signal may pose a very challenging problem [97]. Awareness of this potential effect in the GW signal may however lead to specifically tailored data analysis tools.

b) *BH environment.* The arrangement of perturbed QNM branches along (a priori known) ϵ-contour lines of pseudospectra opens the possibility of probing, in an 'inverse scattering' spirit, environmental BH perturbations. One can envisage to read the "size" of the physical perturbations by comparing observational QNM data with the "a priori" calibrated pseudospectrum. This may help to assess "dry" versus "wet" BH mergers, a point of cosmological relevance in LISA science.

c) *Universality of compact object QNMs.* The combination of the "universality" of the perturbed "Nollert-Price QNM BH branches" with Nollert's remark on their similarity to neutron star "w-modes", together with the demonstrated loss of BH QNM axial/polar isospectrality, poses a natural question: do QNM spectra of all generic compact objects share a same pattern?

   Schemes such as [124] may provide a systematic frame for the analysis of the astrophysical implications.

d) *BH QNM (in)stability in generic BHs.* A natural and necessary extension of the present work is the study of QNM (in)stability in the full BH Kerr-Newman family, in particular understanding how it intertwines with superradiance instability and the approach to extremality.

Fundamental gravitational physics

We note some possible prospects at the fundamental level:

a) *(Sub)Planckian-scale physics.* Planck scale spacetime fluctuations seem a robust prediction of different models of quantum gravity. They represent "irreducible" ultraviolet perturbations potentially providing a probe into Planck scale physics that, given the universality of BH QNM overtone instability, may be 'agnostic' to an underlying theory of quantum gravity. Such a search of quantum gravity signatures in BH gravitational wave physics is akin to [2]. Actually, it would suffice that a Planck scale "cut-off" induces an effective C^p regularity in the otherwise smooth low-energy description, to trigger the instability phenomenon. BH QNM instability might then provide a particular probe into 'discreteness' of spacetime (e.g. [151] are references therein).

b) *QNMs and (strong) cosmic censorship.* In the setting of cosmological BHs, the assessment of the extendibility through the Cauchy horizon in Reissner-Nordström de Sitter is controlled by the parameter $\beta = \alpha/\kappa_-$, where α is the spectral gap (the imaginary part of the fundamental QNM in our setting) and κ_- is the surface gravity of the Cauchy

horizon [91, 40]. Therefore, a good understanding in this setting of the (in)stability properties of the slowest decaying QNM, and more generally of the QNM spectrum, may be enlightening in the assessment of the thresholds for Cauchy horizon stability.

c) *Random perturbations and spacetime semiclassical limit.* The "regularization effect" of random perturbations [86, 88, 87, 89, 36, 131, 37, 130, 182, 142, 169] in the scattering Green's function is an intriguing phenomenon that may play a role in the transition to a semiclassical smooth effective description of fundamental gravitational degrees of freedom described in a more basic (quantum) theory, possibly including an irreducible randomness ingredient. Again, the universality of the phenomenon may play a key role.

Mathematical relativity

The presented numerical evidences need to be transformed into actual proofs. Some mathematical issues to address are:

a) *Regularity conditions and QNM characterization.* The mathematical study of QNMs entails subtle functional analysis issues. In the present hyperboloidal approach this involves, in particular, the choice of appropriate regularity conditions and the associated functional space. This connects our pseudospectrum study with the identification in [10] of the full upper-complex plane as the actual QNM spectrum, if general C^∞ eigenfunctions are allowed. More regularity must therefore be enforced. An analysis along the lines in [79, 78, 80], where Gevrey classes are identified as the proper functional spaces to define QNMs, is therefore required. Likewise, a systematic comparison with QNM stability in the framework of [91, 85] is needed (cf. also [194, 68]).

b) *Semiclassical analysis and QNM (in)stability.* The interest of asymptotic tools, in the study of QNM stability, is twofold. On the one hand, an "asymptotic reasoning" [17] built on the semiclassical analysis of QNMs (a subject taken to full maturity in Sjöstrand's works [90, 167, 64, 63, 60]) with a small parameter defined in terms of highly-damped QNM frequencies, can help to assess universality patterns of perturbed Nollert-Price BH QNM branches. On the other hand, asymptotic analysis provides powerful tools to prove rigorously spectral instability and non-trivial pseudospectra (cf. e.g. [59]). In particular, the recent work [34] provides an explicit example of scattering resonance (or QNM) instability, sharing much of the spirit of the discussion in this work.

Beyond gravitation:"gravity as a crossroad in physics"

The disclosure of BH QNM instability [138] resulted from the fluent interchange between gravitational and optical physics [118, 119, 48, 47, 120], again a key 'flow channel' in our work, e.g. to understand the 'infrared' instability of the fundamental QNM [3]. In this spirit, the present work can offer some hints for further boosting such kind of transversal research in physics.

The hyperboloidal approach, with its explicit formulation of the dynamics in terms of a non-selfadjoint operator, provides a scheme of interest whenever dealing with an open physical system with losses at a radiation zone, a recurrent situation throughout physics (e.g. in optics, acoustics, physical oceanography, to cite some settings). A specific lesson of the present work, to be exported to other physical contexts, is the identification of the relevant scalar product in terms of the system's energy, thus casting an a priori technical issue into neat physical terms. Moreover, when studying QNMs, the normalizability of the QNM eigenfunctions in the hyperboloidal approach

may open an alternative avenue to the characterization of the so-called 'mode volume' V_n of a QNM. This is relevant e.g. in the setting of photonic/plasmonic resonances [114]: together with the notion of 'quality factor' Q_n, given in terms of the ratio between the real and imaginary parts of a QNM (see e.g. [153] for its connection with BH gravity physics), it characterizes the Purcell factor $F_n \sim Q_n/V_n$ controlling the enhancement of spontaneous emission of a quantum system, a key notion in 'cavity quantum electrodynamics' [184].

Regarding the pseudospectrum, this notion is relevant whenever a non-Hermitian (or more generally non-selfadjoint operator) enters into scene, as it is typically the case in open systems [11]. In the context of non-Hermitian quantum mechanics, it has been proposed [110] to endow the pseudospectrum with a guiding central role in the theory, in a setting in which spectral instability makes insufficient the standard notion of spectrum to fully characterize the relevant operators. Apart from spectral instability, the pseudospectrum underlies purely dynamical phenomena [179, 180], in particular accounting for so-called nonmodal instability [163] in the setting of hydrodynamic stability theory and turbulence. Beyond hydrodynamics, the latter feature turns the pseudospectrum into a powerful tool for studying both spectral and dynamical stability issues in (open) physical systems that "trace" over a part of the total degrees of freedom and, as a result, are governed by non-selfajoint operators. Such systems occur all over physics (e.g. condensed matter, optics, plasmonics, acoustics, nanophysics... [11]), offering a natural arena for extending the already large range of applications of pseudospectra [71].

Gravitational physics is remarkable in its capacity to "provide a framework that calls for the interchange of ideas, concepts and methodologies from very different communities" [4] in physics. The hyperboloidal approach and the pseudospectrum here discussed realize an instance of this understanding of "gravity as a crossroad in physics" [4].

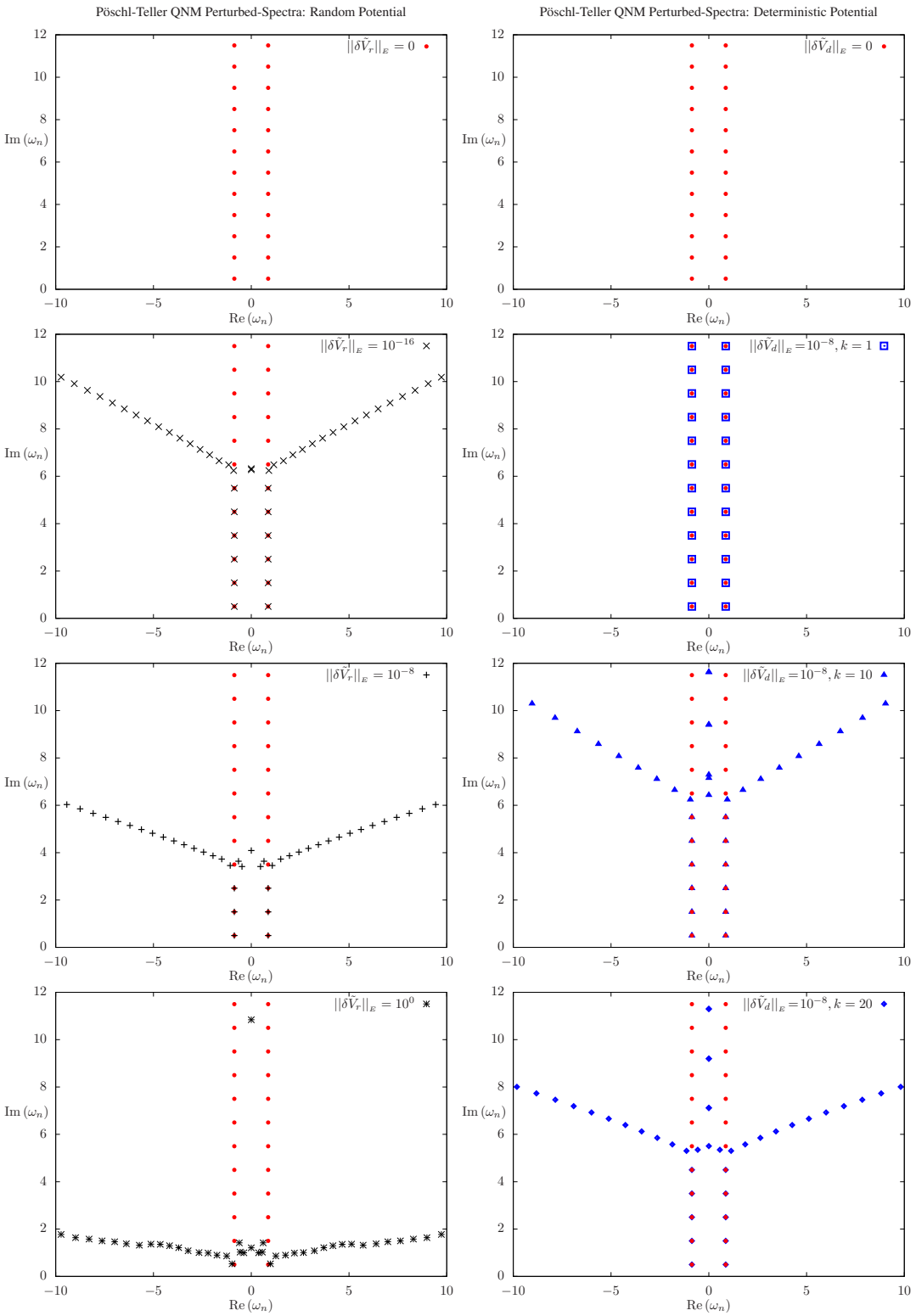

Figure 10.5: *Left column*: Sequence of QNM spectra for the Pöschl-Teller potential subject to a random perturbation $\delta\tilde{V}_{\rm r}$ of increasing "size" (in energy norm). The sequence shows how "switching on" a perturbation makes the QNMs migrate to a new branch (that actually follows closely a pseudospectrum contour line, compare with Fig. 10.3), in such a way that the instability starts appearing at highly-damped QNMs and descends in the spectrum as the perturbation grows (unperturbed values, in red, are kept along the sequence for comparison). The top panel corresponds to the non-perturbed potential shown in Fig. 10.1, the second panel shows how a random perturbation of with (energy) norm $||\delta\tilde{V}_{\rm r}||_E = 10^{-16}$ already reaches the 6th QNM overtone, whereas in the third panel a perturbation with $||\delta\tilde{V}_{\rm r}||_E = 10^{-8}$ already reaches the 3rd overtone. This confirms the instability already detected in the pseudospectrum, indicating its high-frequency nature. Crucially, to reach the fundamental mode, a perturbation of the same order $O(1)$ as the variation of the eigenvalue is required, this demonstrating the stability of the fundamental QNM in agreement with the pseudospectrum in Fig. 10.3. *Right panel*: Sequence of QNM spectra for Pöschl-Teller subject to a deterministic perturbation $\delta\tilde{V}_{\rm d} \sim \cos(2\pi k\, x)$. The

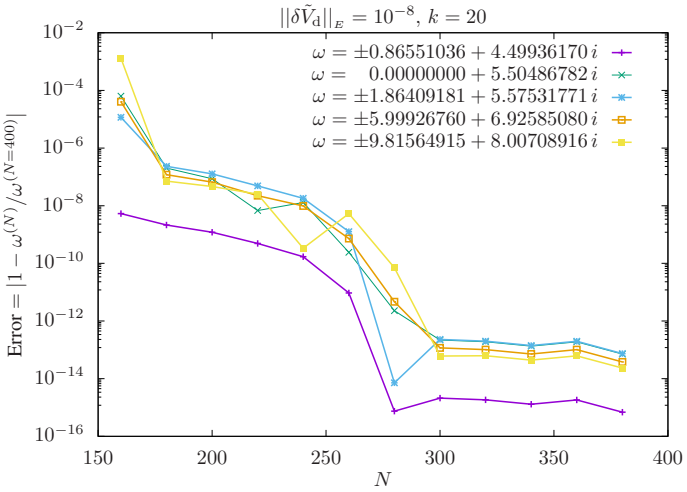

Figure 10.6: Convergence test for five significant QNMs of Pöschl-Teller perturbed under a deterministic high-frequency perturbation $\delta\tilde{V}_{\rm d}$ (cf. text). This demonstrates that the large QNM "migrations" observed in Fig. 10.5 are not a numerical artifact, but actually very small perturbations of the potential can result in large variations of the QNM spectrum, consistently with the pseudospectrum in Fig. 10.3.

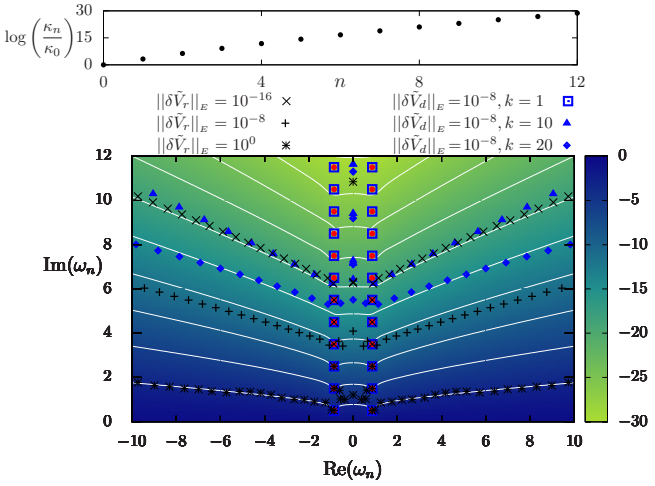

Figure 10.7: QNM spectral instability of Pöschl-Teller potential. Combination of Figs. 10.1, 10.3 and 10.5, corresponding to three independent calculations, respectively: condition numbers ratios κ_n/κ_0 (*top panel*), pseudospectrum and perturbed QNM spectra (*bottom panel*). The bottom pannel demonstrates the high-frequency nature of the spectral instability, as well as the migration of Pöschl-Teller QNMs towards pseudospectrum contour lines under high-frequency perturbations.

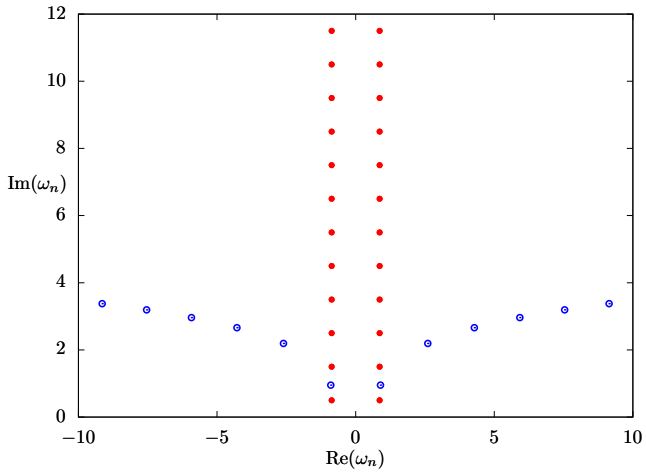

Figure 10.8: QNMs of Pöschl-Teller "cut" potential. Setting Pöschl-Teller potential to zero outside an interval $[x_{\min}, x_{\max}]$ introduces high-frequency perturbations that make QNM overtones migrate towards pseudospectrum contour lines, as well as an "infrared" modification that alters the fundamental QNM frequency. Whereas the latter tends to the non-perturbed Pöschl-Teller value as $x_{\min} \to -\infty$ and $x_{\max} \to \infty$, QNM overtones remain always strongly perturbed.

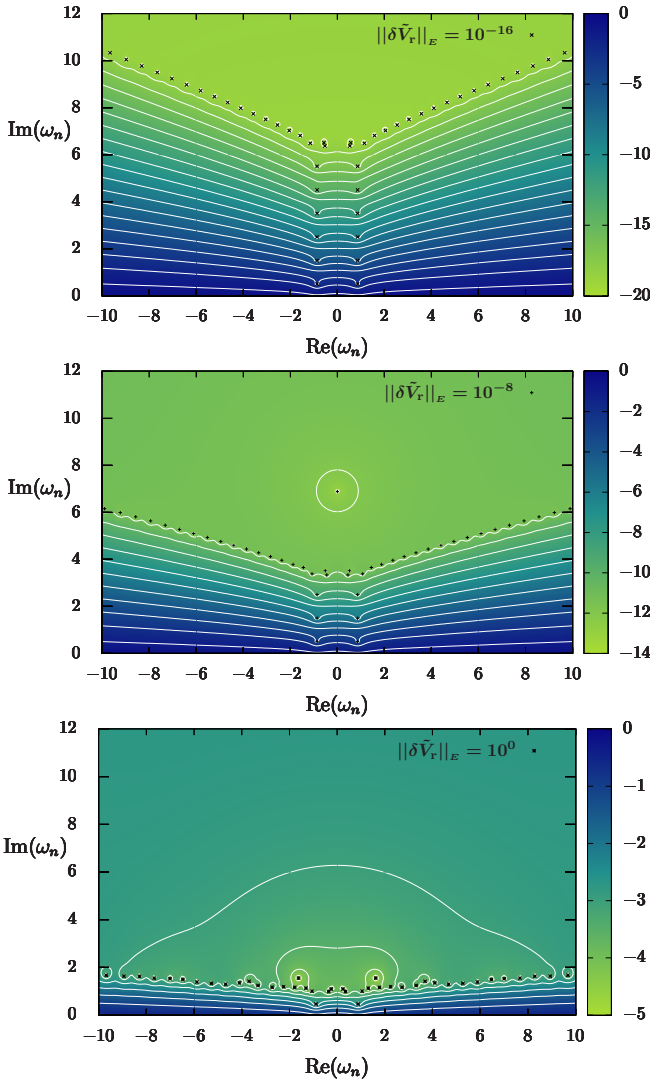

Figure 10.9: Pseudospectra of Pöschl-Teller under random perturbations $\delta\tilde{V}_{\rm r}$ of increasing norm, demonstrating the "regularizing" effect of random perturbations: pseudospectra sets σ^{ϵ} bounded by that "contour line" reached by perturbed QNMs become "flat", a signature of improved analytic behaviour of the resolvent, as illustrated in Fig. 10.4. Pseudospectra sets not attained by the perturbation remain unchanged. Regularization of $R_{L+\delta L}(\omega)$ increases as $||\delta\tilde{V}_{\rm r}||_E$ grows.

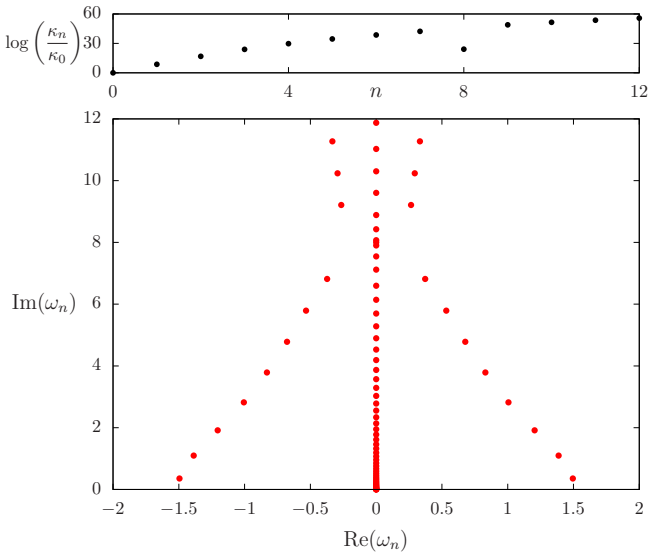

Figure 10.10: Schwarzschild QNM problem. *Bottom panel*: QNMs for the $\ell = 2$ axial and polar gravitational modes of Schwarzschild spacetime, corresponding respectively to the (isospectral) Regge-Wheeler and Zerilli potentials (eigenvalues along the imaginary upper half-line are the numerical counterpart of the Schwarzschild branch cut, but also the algebraically special QNM $\omega_{n=8}$; see [10] for a discussion of this). Note the normalization $4M\omega_n$, consistent with $\lambda = 4M$ after Eq. (10.24). *Top panel*: condition numbers κ_n normalized to the condition number κ_0 of the fundamental QNM. Note the relative enhanced stability of the algebraically special QNM.

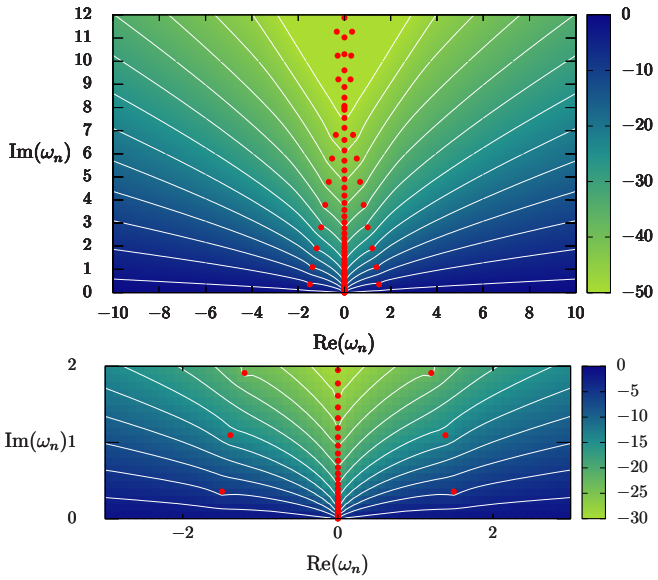

Figure 10.11: *Top panel*: Pseudospectrum of Schwarzschild spacetime ($\ell = 2$ gravitational modes, from Regger-Wheeler potential, similar for Zerilli). Again, QNM frequencies (red circles) from Fig. 10.10 are superimposed for reference on their (in)stability. The pattern of ϵ-pseudospectra sets σ^ϵ is qualitative similar to the Pöschl-Teller one (cf. Fig. 10.3), though presenting an enhanced spectral instability indicated by the smaller ϵ values of ϵ-pseudospectra contour lines (cf. range in color log-scale for $\log_{10}\epsilon$ in Fig. 10.3). *Bottom panel*: Zoom into the region around the fundamental QNM and first overtones.

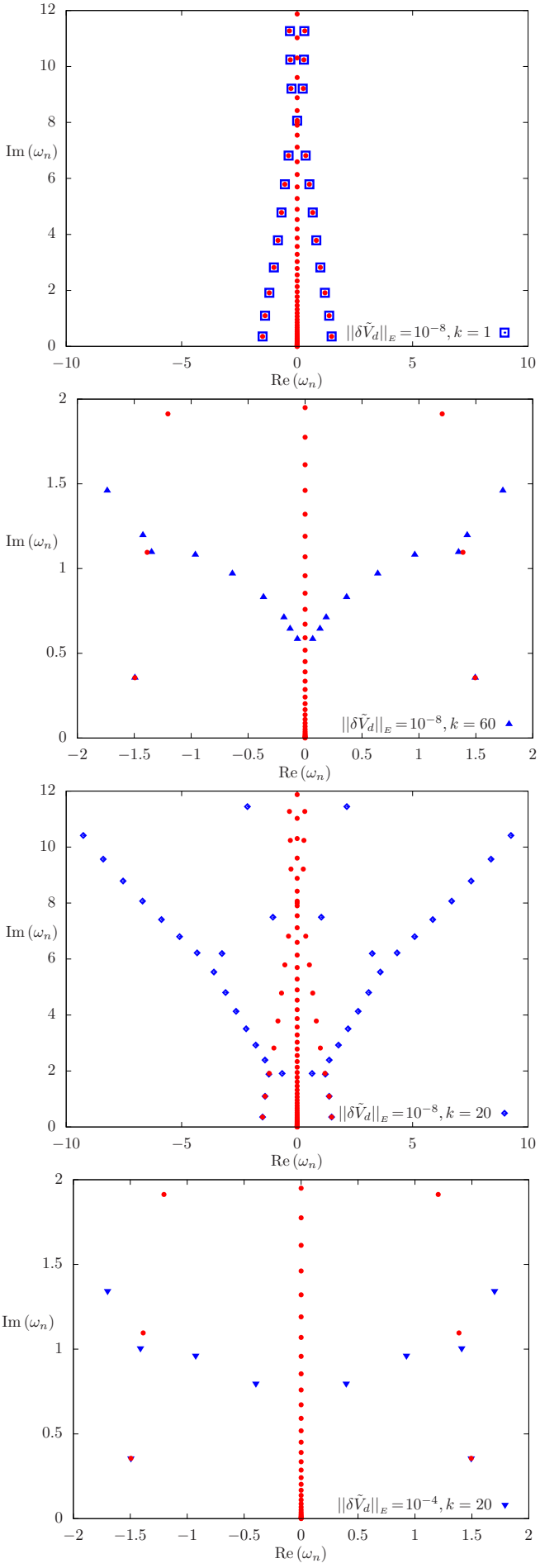

Figure 10.12: QNM spectra for deterministic perturbations $\delta\tilde{V}_{\rm d}$ of Schwarzschild $\ell = 2$ gravitational modes (here Regge-Wheeler, similar behaviour for Zerilli, cf. Fig. 10.13), superimposed over the unperturbed values (red). *Left column*: stability under low frequency perturbation (top panel) versus high-frequency instability of QNM overtones (bottom panel). *Right column*: zoom

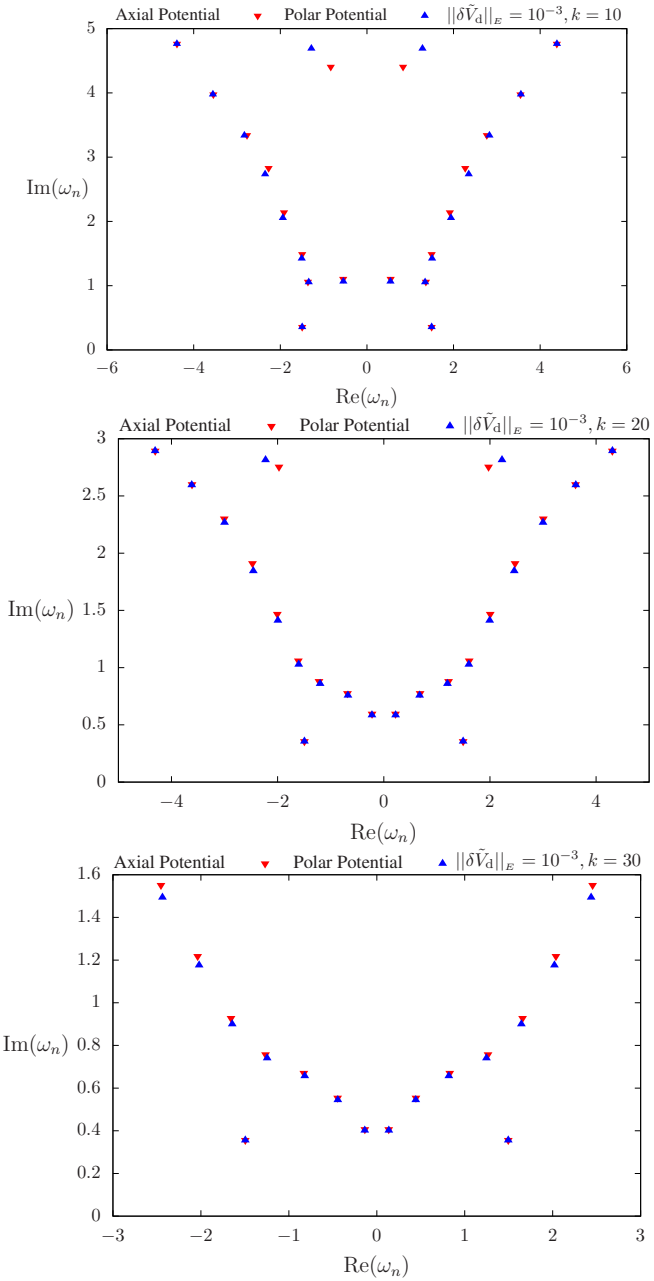

Figure 10.13: Loss of isospectrality in Schwarzschild, under high-frequency perturbations. The sequence of figures shows a zoom into the perturbation of lowest $\ell = 2$ axial and polar QNM overtones (the branch cut has been removed), with $\delta\tilde{V}_{\rm d}$ fixed to a value reaching the first overtone, and then increasing the frequency. The breaking of axial and polar isospectrality is demonstrated, with perturbed axial overtones slightly more damped than polar perturbed counterparts, though both laying over the same perturbed QNM branches (actually tracking the pseudospectra contour lines, cf. Fig. 10.15 below). The fundamental QNM remains unchanged, consistently with its stability, so the dominating ringdown frequency remains "isospectral".

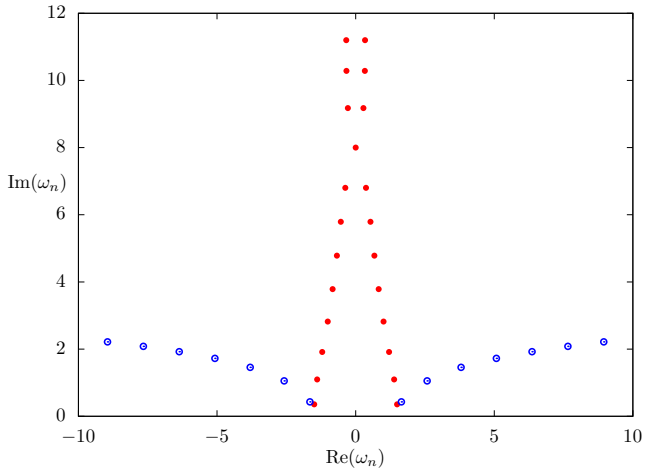

Figure 10.14: "Infrared" modification of the Schwarzchild fundamental QNM. As in the Pöschl-Teller case, cutting the Schwarzschild potential ($\ell = 2$, either Regge-Wheeler or Zerilli) outside a compact interval $[x_{\min}, x_{\max}]$ modifies the fundamental QNM, this accounting for its "instability" found in [138]. All QNM overtones are strongly perturbed due to the high-frequencies in the Heaviside cut, whereas (only) the fundamental QNM is recovered as $x_{\min}, x_{\max} \to \mp\infty$.

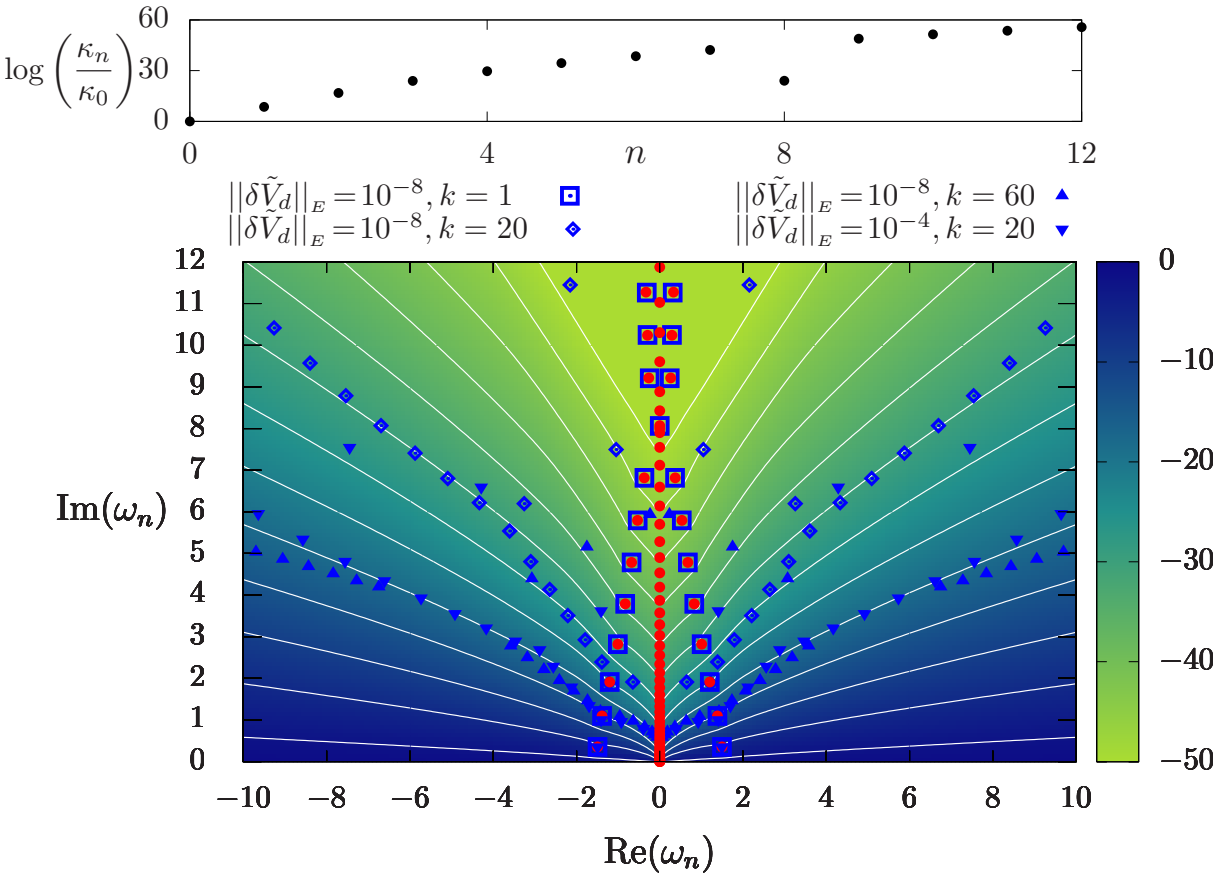

Figure 10.15: Gravitational QNM spectral (in)stability in Schwarzschild spacetime (here, $\ell = 2$ axial case corresponding to the Regge-Wheeler potential, same behaviour for polar modes with Zerilli potential). The figure shows the superposition of the pseudospectrum of Fig. 10.11, perturbed QNM spectra in Fig. 10.12, together with exact QNMs and condition numbers κ_n from Fig. 10.10. Employed norms follow from the energy scalar product in Eq. (10.29), i.e. energy defines "big" and "small". The pseudospectrum pattern, with ϵ-pseudospectra sets with small ϵ extending into large regions of the complex plane, indicates spectral instability of QNM overtones, consistently with the fastly growing κ_n's. Perturbations in the potential demonstrate the high-frequency (ultraviolet) instability of all overtones and their stability under low-frequency perturbations. Both pseudospectrum and perturbations in the potential show the ultraviolet stability of the fundamental QNM. Ultraviolet instability induce QNM overtones to migrate towards ϵ-pseudospectra contour lines, a pattern consistent with "Nollert-Price QNM branches" [138, 140] here illustrated up to the lowest overtone. Universality of this pattern is further supported by comparison with Pöschl-Teller in Fig. 10.7.

Chapter 11

More results in gravitational physics

After assessing the perturbed QNM in the GW signal, we address potential consequences enlarging BH spectroscopy into the BH astrophysical environment and fundamental physics. This entails, though, great accuracy in the observations and challenges in the data analysis techniques.

The so-called ϵ-pseudospectrum (see ref. [98] for a detailed discussion) determines the boundaries of QNM-free regions in the complex plane. Specifically, it provides the maximal region in $\mathbb{C}$ that QNMs can reach under (arbitrary) perturbations in the operator. Thus, a pseudospectrum analysis of the *unperturbed* operator provides a global picture of QNM spectral (in)stability [98]. Consistent with general results in the mathematical literature [158, 116, 115, 181, 168, 127, 172, 68, 30], our BH QNM-free regions are asymptotically logarithmic: $\omega_n^{\rm I} \sim C_1 + C_2 \ln(\omega_n^{\rm R} + C_3)$.

QNMs from discontinuous potentials at the pth-derivative (C^p) are 'optimal' in reaching the logarithmic QNM-free region boundaries. Their real $\omega_n^{\rm R}$ and imaginary $\omega_n^{\rm I}$ parts follow a 'Regge-QNM' [159, 30, 194, 68, 30] asymptotic log-pattern

$$\omega_n^{\rm R} = \pm \frac{\pi}{L^{\rm R}} \left(n + \tilde{\gamma}\right), \; \omega_n^{\rm I} = \frac{1}{L^{\rm R}} \left[\gamma \ln\left(\left|\omega_n^{\rm R}\right| + \gamma'\right) - \ln S\right], \tag{11.1}$$

shown first for C^p compact-support potentials [159, 192] and extended to BH-like potentials [138, 140, 156, 123] and w-modes of (a class of) neutron stars [191] (cf. also [22, 23]). Reverberation in chambers of 'Regge' length scale $L^{\rm R}$ is the mechanism behind the opening to less damped branches [159, 192, 22], modulated by 'regularity' $\gamma, \tilde{\gamma}, \gamma'$ and 'strength' S parameters.

The spectra distribution within the QNM-free regions for smooth (C^∞) potentials is not known a priori, but *the QNM must always lay above the logarithmic curves*. QNM move towards logarithmic pseudospectrum lines as k increases, we conjecture they reach them in the $k \to \infty$ limit, as instanced by Regge branches (11.1). The potentials for axial and polar parities under perturbation characterized by (ϵ, k) provide a testbed for the perturbed QNM distributions and isospectrality loss identified in [98]. We observe three different regimes, separated by the "internal" QNMs discussed sec. 2. We label their location by critical values $n_i(\epsilon, k)$ in the overtone number n with $n_1(10^{-3}, 10) = 2$ and $n_2(10^{-3}, 10) = 8$. The top panel of fig. 11.1 illustrate the three different regimes for $k = 10$. Migrated QNMs are stable for further perturbations.

(i) *Stable region:* for $n \lesssim n_1(\epsilon, k)$, perturbed polar/axial QNMs stay at a distance ϵ from their original values. $\Delta_n^{\rm iso}(k, \epsilon) := |\omega_n^{\rm a}(k, \epsilon) - \omega_n^{\rm p}(k, \epsilon)| = C_n(k)\epsilon$, with $C_n(k) = C_n(k + k_n)^{\alpha_n}$., with constants C_n, k_n and α_n. Near-future astrophysical observations shall measure $\Delta_n^{\rm iso}$ in lowest overtones $n \lesssim n_1(\epsilon, k)$, constraining theories via model-dependent $C_n(k)$. The fundamental QNM may discriminate the mechanism yielding the isospectrality-loss (e.g. [42, 124]).

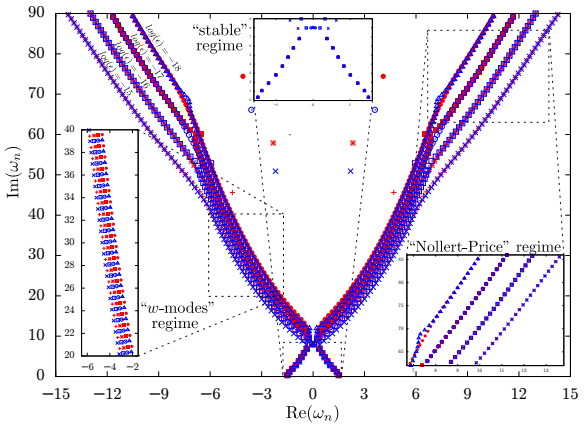

Figure 11.1: *Left Panel:* Regimes of axial/polar isospectrality loss ($k = 10$ and $\epsilon = 10^{-15}$-10^{-18}). As ϵ increases, $n_1(\epsilon, k)$ and $n_2(\epsilon, k)$ decrease: the "Nollert-Price" regime eats up the "w-modes", whereas the latter eat up the "stable" regime, finally reduced to the fundamental QNM (cf. Fig. 15 in [98]). *Right Panel:* Effective measures accounting for perturbed QNMs' distribution into "Nollert-Price" branches. QNMs' density lead to a BH QNM Weyl Law's length L^{W} (top) and branch opening $\mathcal{G}$ (bottom) with $\mathcal{G} = 0$ (Schwarzschild) and $\mathcal{G} = 1$ (C^p-potentials).

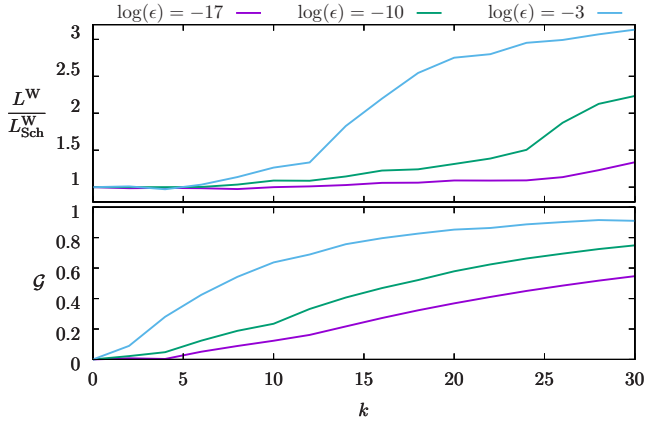

(ii) *Alternating axial/polar "w-modes":* QNMs drastically separate for $n_1(\epsilon, k) \lesssim n \lesssim n_2(\epsilon, k)$ with $\Delta_n^{\mathrm{iso}}(k, \epsilon) \sim O(1)$. Here it holds $\omega_n^{\mathrm{R}} \sim \ln(\omega_n^{\mathrm{I}}), \omega_n^{\mathrm{I}} \sim n$, 'opposed' to Regge-QNMs eq. (11.1). QNMs place themselves in an alternating pattern along the branch, as neutron star "w-modes" do [105, 191]. Isospectrality loss is most accessible in this regime, where BHs appear as compact star mimickers. The alternating behaviour is abruptly cut at $n_2(\epsilon, k)$, where isospectrality loss is enhanced since "internal" QNMs are very parity-sensitive.

(iii) *Nollert-Price regime:* For $n \gtrsim n_2(\epsilon, k)$ QNMs migrate further away from unperturbed ones, to branches $\omega_n^{\mathrm{I}} \sim \omega_n^{\mathrm{R}} \sim n$ (linear relation improving with larger ϵ), a stronger instability than for alternating "w-modes". Yet, isospectrality loss is linear in ϵ, as in the stable regime (i), a feature to be studied.

Increasing ϵ or k, both $n_1(\epsilon, k)$ and $n_2(\epsilon, k)$ diminish. The "stable" region shrinks, as the "w-mode" region starts at lower overtones. Regime (ii) also becomes smaller with the Nollert-Price going down in $\mathbb{C}$ as well. Eventually, region (iii) extends up to the fundamental QNM [98]. New regimes are not excluded, but their numerical study is challenging. Indeed, high values of

(ϵ, k) produce not only new Nollert-Price branches tracking pseudospectrum lines, but also an intricate pattern on the "internal" QNMs, whose distribution and significance requires further study. Notably, they impact the Weyl law below.

11.1 Effective parameters, asymptotics and Weyl law

We introduce QNM effective parameters for a phenomenological characterisation of spacetime perturbations in GW data. Observing QNMs following the logarithmic pattern (11.1) is a very strong indication of an underlying C^p-discontinuous potential. For large k perturbations, this suggests introducing for each ω_n: a 'n-Regge length scale' $L^{\rm R}_n := \pi/|\Delta\omega^R_n|$, a 'small-scale' $\gamma_n := L^{\rm R}_n \Delta\omega^{\rm I}_n/\Delta \ln \omega^{\rm R}_n$, and a 'perturbation strength' $\ln S_n := \gamma_n (L^{\rm R}_n)^{-1} \ln(\omega^{\rm R}_n) - \omega^{\rm I}_n$ effective parameters [1].

Such parameters are not generally adapted for low-k smooth perturbations, although 'asymptotic reasoning' [17] suggests that they may capture relevant patterns beyond its validity range. This is the case for $L^{\rm R}_n$ in regime (iii): $\omega^{\rm R}_n \sim n$ implies that $\Delta\omega^R_n$ is constant along the branch, defining a Regge length $L^{\rm R} := \pi/|\Delta\omega^R|$. As in neutron stars (eq. (2.7) in [191]), this is valid beyond the eq. (11.1) setting, suggesting reverberation at length scales $L^{\rm R}(k,\epsilon)$ as the mechanism making QNMs less damped and opening BH QNM branches [2]

We estimate such QNM branch opening with the quality factor Q_n, namely $(2Q_n)^{-1} = |\omega^I_n/\omega^R_n| =: \tan(\theta_{_{Q_n}})$ [114, 153]. Introducing $\mathcal{G} = \omega^{\rm R}_n/|\omega_n| = \cos(\theta_{_{Q_n}})$ (as $n \gg 1$), Schwarzschild QNMs' asymptotics [137] gives $\mathcal{G} = 0$, whereas eq. (11.1) yields $\mathcal{G} = 1$. Fig. 11.1's bottom-right panel shows the monotonic increase of $\mathcal{G} \in [0,1]$ (for several ϵ's) with k. Pseudospectra's logarithmic boundaries are attained for $k \to \infty$.

QNM asymptotics satisfies a Weyl's law, providing another length scale $L^{\rm W}$. Denoting by $N(\omega)$ the number of QNMs within the radius $|\omega_n| < \omega$ ($\omega \in \mathbb{R}$), QNM Weyl's law for $d = 1$-dimensional compact-support potentials [192] states: $N(\omega) \sim 2(L^{\rm W}/\pi)\omega$ (twice the Laplacian's Weyl law in compact manifolds [20]), with $L^{\rm W}$ the potential's support 'length'. Non-compact C^p potentials also follow this law (cf. eq.(11.1)), though the general non-compact case is more open [77, 165, 170].

Remarkably, though, BH QNMs do follow a Weyl law. From Schwarzschild's QNM asymptotics [137], $N_\ell(\omega)$=$8M\omega$, entailing a Weyl's length $L^{\rm W}_{\rm Sch}$=$4\pi M$. Writing $R = 2M$, $L^{\rm W}_{\rm Sch} = 2\pi R$ suggests QNMs created by waves 'creeping' [171] along the 'horizon circumference', akin to QNMs from Regge's poles [61, 62, 157, 65] in a membrane paradigm [56, 57, 154, 177]. Complementarily, the asymptotics $\Delta|\omega_n|\sim(4M)^{-1} = \kappa$ [132, 133, 134] in Weyl's counting, fits the factor [126] in the horizon area quantization $\Delta A = 8\pi L^2_{\rm Planck}$, suggesting a connection with BH thermodynamics, $N(\omega) \sim (T^{\rm W}_{\rm Sch}/\pi)\omega$, with a thermalizing bouncing time $T^{\rm W}_{\rm Sch} = 2L^{\rm W}_{\rm Sch} = 2\pi/\kappa = (T_{\rm Hawking})^{-1}$.

Beyond such heuristics, Weyl Law's remains valid for perturbed BH potentials and $L^{\rm W}$ is always robustly defined. $L^{\rm W}$ changes with perturbations, but not because of branch opening. For instance, Fig. 11.1's upper-right panel, shows $\mathcal{G} \sim 0.5$, for $\log(\epsilon) \sim -17$ and $k = 25$, but it still has $L^{\rm W}/L^{\rm W}_{\rm Sch} \sim 1$. Actually, branches open without changing $|\Delta\omega_n|$ along them. This permits, when $L^{\rm R}$ is defined, to link Regge's and Weyl's lengths through the quality factor:

[1] For instance, the spiked truncated dipole potential [140] yields $L \sim x_\delta - x_0$, $\gamma = 3/2$ and $S \sim V_\delta$ (delta-function coefficient). Polytropic neutron stars [191] have $L \sim r^*$ (star's radius), $\gamma \sim \mathcal{N}$ (polytropic index) and $S \sim$ "potential's discontinuity jump.

[2] At the last stage of the writing of this article, we became aware of ref. [123], where the authors identify precisely the scale $T = 2L^{\rm R} = \lim_{n\to\infty} 2\pi/|\Delta\omega^{\rm R}_n|$ and demonstrate its key role as the relevant period for 'echoes' [43] happening in C^p potentials.

$L^{\rm R}/L^{\rm W} = \cos(\theta_Q) = 2Q(1+4Q^2)^{-1/2} = \mathcal{G}$. In a $k \to \infty$ limit to Regge branches (11.1), $Q \to \infty$ ($\mathcal{G} \to 1$) so $L^{\rm R} \sim L^{\rm W}$. Changes in $L^{\rm W}$ actually respond to the 'activation' of new 'degrees of freedom', namely "internal" QNMs appearing at critical values $n_i(\epsilon, k)$ at branch regime borders: Fig. 11.1 shows a 'phase transition' with 'order parameter' $L^{\rm W}/L^{\rm W}_{\rm Sch}$ going from 1 to $O(3)$, due to "internal" QNMs becoming densely populated.

Finally, summing $N_\ell(\omega)$ over all (ℓ, m) gives $N(\omega) \sim \omega^3$, consistently with QNM Weyl's law in d dimensions [170], $N(\omega) \sim C_d \mathrm{Vol}_d \omega^d$. This may provide a strategy to probe the (effective) dimension of spacetime by counting QNMs.

11.2 Conclusions

- Confirming the potential presence of high-frequency perturbed QNM overtones [98] in the GW signal, for ℓ-fixed modes.
- We have presented a consistent picture for the QNM migration pattern to branches opening always above pseudospectrum logarithm curves, limit attained at ultraviolet frequencies with (C^p) regularity loss.
- Reverberation at Regge's length scales $L^R(\epsilon, k)$ is proposed as underlying mechanism, with multiple reflections decreasing QNM damping.
- Perturbed branches are stable and share basic features with generic compact object QNMs.
- We have described the patterns of isospectrality loss and introduced effective parameters to probe the physics of BH perturbations. A BH QNM Weyl's law has been introduced, with hints into classical/quantum BH physics, expressing the 'reverberation scale' in terms of a 'degrees-of-freedom-counting' Weyl's length $L^W(\epsilon, k)$ and QNM quality factors Q.
- The detection of perturbed QNMs (a highly degenerate inverse problem) poses a data analysis challenge, but insights and patterns here presented may provide keys for successful schemes, enlarging BH spectroscopy with a probe into the BH environment or the effective regularity of spacetime.

Chapter 12

Quasi-Normal Modes in Optics

12.1 Electromagnetic problem in hyperboloidal slices

According to Lorentz model the interaction electron-nucleus is represented by a harmonic oscillator. The equation for the electron-nucleus distance r is:

$$\frac{\partial^2 \mathbf{r}}{\partial t^2} + \Gamma \frac{\partial \mathbf{r}}{\partial t} + \omega_0^2 \mathbf{r} = -\frac{e\mathbf{E}}{m}, \tag{12.1}$$

where Γ is the damping loss rate, represents the absorption, ω_0 is the characteristic frequency of the harmonic oscillator, m is the mass of the electron, and $\mathbf{E}$ is is the local electric field acting on the electron. Then defining $\mathbf{P} = -Ne\mathbf{r}$ as the polarization, we can write the equation in terms of $\mathbf{P}$ as the following:

$$\frac{\partial^2 \mathbf{P}}{\partial t^2} + \Gamma \frac{\partial \mathbf{P}}{\partial t} + \omega_0^2 \mathbf{P} = \omega_p^2 \epsilon_0 \mathbf{E}, \tag{12.2}$$

where $\omega_p^2 = \frac{Ne^2}{m\epsilon_0}$, and N is electron density.

From Maxwell equations, we get:

$$\begin{aligned} \frac{\partial \mathbf{H}}{\partial t} &= -\frac{1}{\mu_0} \nabla \times \mathbf{E} \\ \frac{\partial \mathbf{E}}{\partial t} &= \frac{1}{\epsilon_0} (\nabla \times \mathbf{H} - \frac{\partial \mathbf{P}}{\partial t}) \end{aligned} \tag{12.3}$$

So we get the following equation for $\mathbf{E}$:

$$\frac{\partial^2 \mathbf{E}}{\partial t^2} = \frac{1}{\epsilon_0} (-\frac{1}{\mu_0} \triangle \mathbf{E} - \frac{\partial^2 \mathbf{P}}{\partial t^2}) \tag{12.4}$$

As we are working in 1D system, and as $\mathbf{P}$ has the same direction of $\mathbf{E}$, we can write a scalar versions for (12.2) and (12.4). Writing eq.12.2 and eq.12.4 in hyperboloidal coordinates, using eq.2.20, leads to:

$$\begin{aligned} &\partial_\tau^2 P + \Gamma \partial_\tau P + \omega_0^2 P = \epsilon_0 \omega_p^2 E \\ &(\epsilon_0 \mu_0 - y^2) \partial_\tau^2 E + 2y(1-y^2) \partial_y \partial \tau E \\ &+ (1-y^2) \partial_\tau E + 2y(1-y^2) \partial_y E - (1-y^2)^2 \partial_y^2 E \\ &+ \mu_0 \partial_\tau^2 P = 0 \end{aligned} \tag{12.5}$$

Now we introduce two auxiliary scalar fields A and B, where:

$$\begin{aligned} \partial_\tau P &= A \\ \partial_\tau E &= B. \end{aligned} \tag{12.6}$$

Rewritting eq.12.7 using eq.12.6, we get:

$$\begin{aligned} &\partial_\tau A + \Gamma A + \omega_0^2 P = \epsilon_0 \omega_p^2 E \\ &(\epsilon_0\mu_0 - y^2)\partial_\tau B + 2y(1-y^2)\partial_y B \\ &+ (1-y^2)B + 2y(1-y^2)\partial_y E - (1-y^2)^2\partial_y^2 E \\ &+ \mu_0 \partial_\tau A = 0 \end{aligned} \tag{12.7}$$

Considering Fourier transformation (where $\partial_t = \partial_\tau$):

$$\begin{aligned} &i\omega P = A \\ &i\omega E = B \\ &i\omega A = -\Gamma A - \omega_0^2 P + \omega_p^2 \epsilon_0 E, \\ &i\omega(\epsilon_0\mu_0 - y^2)B + i\omega\mu_0 A = -2y(1-y^2)\partial_y B \\ &- (1-y^2)B - 2y(1-y^2)\partial_y E + (1-y^2)^2\partial_y^2 E \end{aligned} \tag{12.8}$$

Now we can write eq.12.8 in the following matricial form:

$$\begin{aligned} &\begin{bmatrix} L1 & L2 & 0 & 0 \\ 0 & 1 & 0 & 0 \\ 0 & 0 & 0 & 1 \\ \omega_p^2\epsilon_0 & 0 & -\omega_0^2 & -\Gamma \end{bmatrix} \begin{bmatrix} E \\ B \\ P \\ A \end{bmatrix} \\ &= i\omega \begin{bmatrix} 0 & \epsilon_0\mu_0 I - y^2 & 0 & \mu_0 \\ 1 & 0 & 0 & 0 \\ 0 & 0 & 1 & 0 \\ 0 & 0 & 0 & 1 \end{bmatrix} \begin{bmatrix} E \\ B \\ P \\ A \end{bmatrix} \end{aligned} \tag{12.9}$$

where

$$\begin{aligned} L1 &= -2y(1-y^2)\partial_y + (1-y^2)^2\partial_y^2 \\ L2 &= -2y(1-y^2)\partial_y - (1-y^2)I \end{aligned} \tag{12.10}$$

Now eq.12.9 is in the form of an eigenvalue problem, but if is written in a compact region in space (the slice does not reach lightlike infinity), so it is still lack boundary conditions. Instead we divide the space in three regions where the cavity region in the middle, and we wrote the same matricial equation in each of the three regions, taking into account the different permittivity parameters. Then we imposed continuity conditions of E and its derivative, no need for imposing any outgoing conditions since we are solving for the whole space and the slices from two external sides will reach to null infinities.

12.2 Numerical implementation

We consider discretizing the grid of y in $N+1$ point, that makes the dimensions of the array $\begin{bmatrix} E & B & P & A \end{bmatrix}^T$ is of $4N+4$. and the two matices multiplied by it in (12.9) are of dimensions $(4N+4)\times(4N+4)$. Let us call these matrices L and M, so we have: $L\begin{bmatrix} E & B & P & A \end{bmatrix}^T = i\omega M \begin{bmatrix} E & B & P & A \end{bmatrix}^T$ now if we want to solve in a specific domain of y so y does not goes from -1 to $+1$, we have to impose some boundary conditions, to do so we make a change in two lines in the matricial equation. We change the lines in the block acting on E corresponding to the positions of the boundaries. As we want to solve in three domains, we will have three matricial equations with the same ω:

$$\begin{aligned} L_{y_1}\begin{bmatrix} E & B & P & A \end{bmatrix}^T_{y_1} &= i\omega M_{y_1}\begin{bmatrix} E & B & P & A \end{bmatrix}^T_{y_1} \\ L_{y_2}\begin{bmatrix} E & B & P & A \end{bmatrix}^T_{y_2} &= i\omega M_{y_2}\begin{bmatrix} E & B & P & A \end{bmatrix}^T_{y_2} \\ L_{y_3}\begin{bmatrix} E & B & P & A \end{bmatrix}^T_{y_3} &= i\omega M_{y_3}\begin{bmatrix} E & B & P & A \end{bmatrix}^T_{y_3} \end{aligned} \tag{12.11}$$

The difference between the three lines of eq.12.11 is the values of permittivity parameters. Assuming that the cavity lies between $x=-a$, and $x=b$, we will consider different grids in each of the three domains:

- $y_1 \in]-1, tanh(-a)]$: we use Chebyshev Right-Radau grid which will exclude the -1 and keep the other domain boundary.
- $y_2 \in [tanh(-a), tanh(b)]$: we use Chebyshev Lobatto grid which takes into account the two domain boundaries.
- $y_3 \in [tanh(b), +1[$: we use Chebyshev Left-Radau grid which will exclude the $+1$ and keep the other domain boundary.

eq.12.11 can be written in one matrix:

$$\begin{aligned} &\begin{bmatrix} L_{y_1} & 0 & 0 & \\ 0 & & L_{y_2} & 0 \\ 0 & 0 & & L_{y_3} \end{bmatrix}\begin{bmatrix} \psi_{y_1} \\ \psi_{y_2} \\ \psi_{y_3} \end{bmatrix} \\ = i\omega &\begin{bmatrix} M_{y_1} & 0 & 0 & \\ 0 & & M_{y_2} & 0 \\ 0 & 0 & & M_{y_3} \end{bmatrix}\begin{bmatrix} \psi_{y_1} \\ \psi_{y_2} \\ \psi_{y_3} \end{bmatrix} \end{aligned} \tag{12.12}$$

where $\psi_i = \begin{bmatrix} E & B & P & A \end{bmatrix}^T_i$, and the resulting matrix is of $12(N+1)\times 12(N+1)$ dimension.

And the last step before implementing the equation using a software is to impose continuity conditions, that is:

$$\begin{aligned} &E_{y_1}(y_1 = tanh(-a)) = E_{y_2}(y_2 = tanh(-a)) \\ &E_{y_2}(y_2 = tanh(b)) = E_{y_3}(y_3 = tanh(b)) \\ &\frac{\mathrm{d}}{\mathrm{dy}_1} E_{y_1}(y_1 = tanh(-a)) = \frac{\mathrm{d}}{\mathrm{dy}_2} E_{y_2}(y_2 = tanh(-a)) \\ &\frac{\mathrm{d}}{\mathrm{dy}_2} E_{y_2}(y_2 = tanh(b)) = \frac{\mathrm{d}}{\mathrm{dy}_3} E_{y_3}(y_3 = tanh(b)) \end{aligned} \tag{12.13}$$

To do that, we replace lines number $N+1$, $4N+5$, $5N+5$, and $8N+9$ in both matrices (considering that the first line is of number 1) by lines which are equivalent to eq.12.13. So line $N+1$ in the matrix on the left becomes all zeros except for the $N+1$ element and for $4N+5$ element, one of these should be $+1$, and the other should be -1. While the corresponding line in the right matrix is all zeros. The same stratigy for line $5N+5$ which is supposed to expess the continuity of E at the $x = b$. Concerning lines $4N+5$, and $8N+9$ we follow the same strategy also, but here to obtain the derivative of E at certain point we have to make sure of that all the E vector is muliplied by the suitable lines in the differentiation matrix (which depends on the position).

Finally we get an eigenvalue problem to be solved.

12.3 Spectrum results

12.3.1 QNM frequencies: Convergence results

Fig.12.3.1 shows the logarithmic relative error $\epsilon_n^{(N)}$ when increasing the number of points in each grid. We mark a fast convergence even with few number of points.

$$\epsilon_N = \log \left| 1 - \frac{\omega^{(N)}}{\omega^{(N_{Max})}} \right|. \tag{12.14}$$

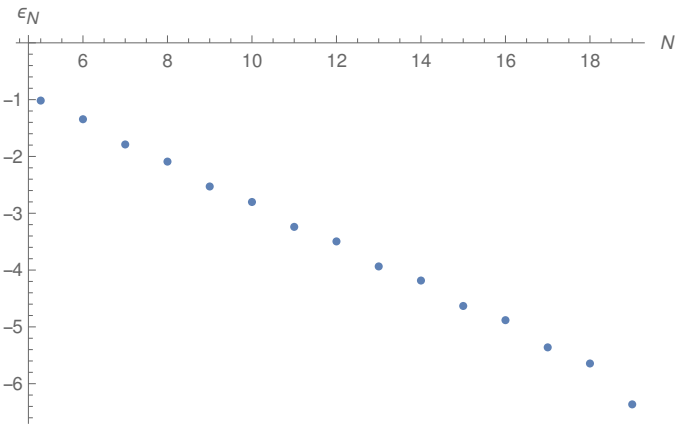

The eigenvalues appear in Fig.12.4 and in Fig.12.4 as the dark spots in the complex plan. The first figure is for a case with a constant permittivity inside the cavity and that does not

depend on the frequency, while the second one is for a case with dispersion with no absorption:

$$\epsilon_{IN}(\omega, x) = \epsilon_\infty - \frac{1}{\omega^2}, \tag{12.15}$$

In this equation the permittivity is constant along the cavity. We mark in both cases the existence of modes with purely imaginary frequencies:

$$\omega_N = ik; k \in \mathcal{N} \tag{12.16}$$

These frequencies have even multiplicities.

12.3.2 QNM eigenfunctions: Normalization

One of the advantages of hyperboloidal slices method is the ability to normalize the fields in the new coordinates. Fig.12.3.2 shows the eigenfunction corresponding to the fundamental mode with respect to the space variable x, note that this mode is going to explode. Fig.12.3.2 shows the eigenfunction corresponding to the fundamental mode with respect to the compactified space variable y, note that this mode is normalizable. An important point to mention is that the field itself differs between normal space-time coordinates (t, x) and (τ, y).

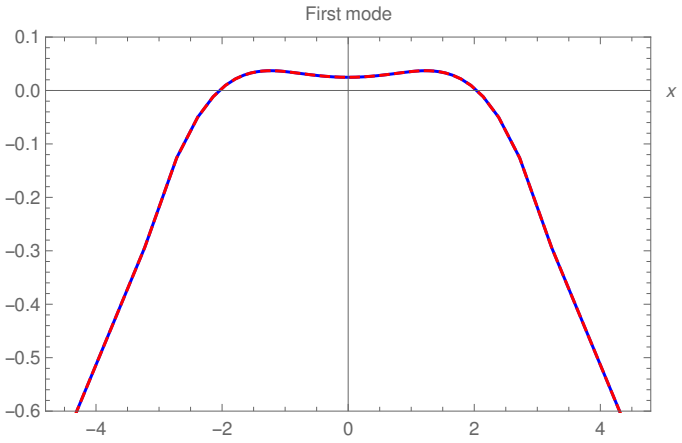

Figure 12.1: Eigenfunction of fundamental mode as a function of the position x. We plot here two identical eigenfunctions related one to the fundamental frequency with a positive real part: ω_f and the other with the fundamental one with a negative real part: $-\omega_f^*$.

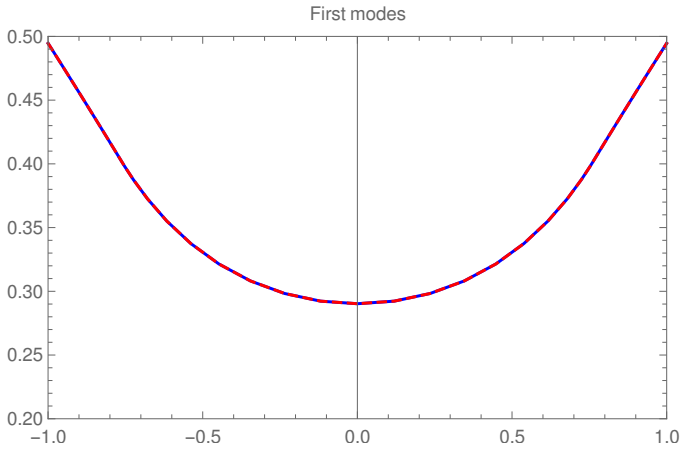

Figure 12.2: Eigenfunction of fundamental mode as a function of the position y. We plot here two identical eigenfunctions related one to the fundamental frequency with a positive real part: ω_f and the other with the fundamental one with a negative real part: $-\omega_f^*$.

Also Fig.12.3.2 shows the eigenfunction corresponding to the first zero mode ($\omega = i$) with respect to the space variable x, note that this mode is going to explode. Fig.12.3.2 shows the eigenfunction corresponding to the fundamental mode with respect to the compactified space. As expected the mode in these coordinates can be normalized.

Zero modes

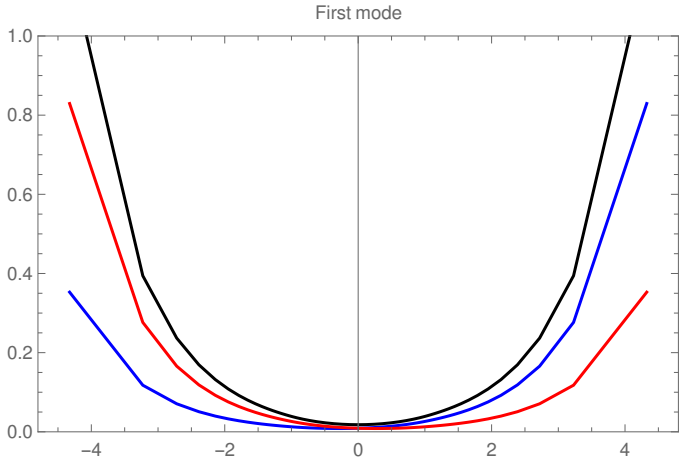

Figure 12.3: Eigenfunctions of the first zero mode as a function of the position x. We plot here two eigenfunctions (in blue and in red) related to the first zero mode which has double multiplicity. The function plotted in black is the sum of both.

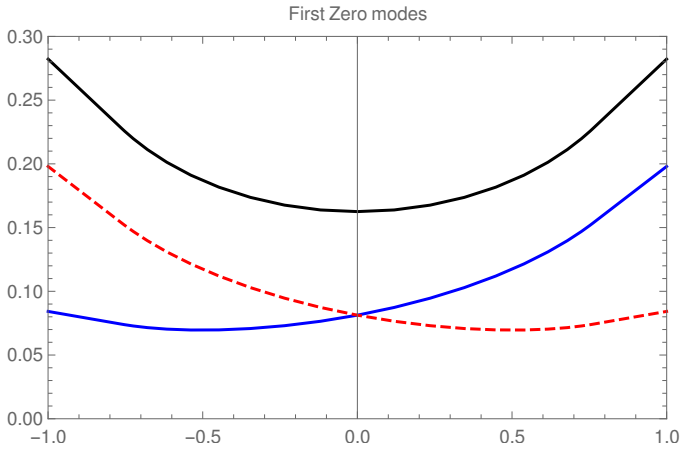

Figure 12.4: Eigenfunction of the first zero mode as a function of the position y. We plot here two eigenfunctions (in blue and in red) related to the first zero mode which has double multiplicity. The function plotted in black line is the sum of both.

12.4 Perturbation and pseudospectrum

Following the same strategy we adopted when studying gravitational waves, here also we calculate the pseudospectrum considering L_2 norm of the eigenfunctions. Fig.12.4 shows a pseudospectrum that is calculated for a case with permittivity inside the cavity: $\epsilon_{IN} = 2.25$. This result shows a potential instability of the higher overtones.

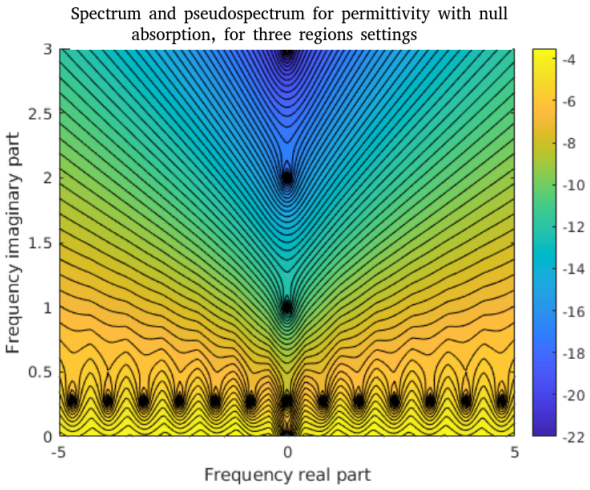

Figure 12.5: Pseudospecturm calculated with L_2-norm for an optical cavity with a constant permittivity inside. Dark areas of the pseudospectrum indicates the existence of eigenvalues. The horizontal eigenvalues correspond to well known and calculated QNM frequencies, while the purely imaginary eigenvalues are detected using hyperboloidal foliation.

Fig.12.4 shows a pseudospectrum calculated for a case with permittivity inside the cavity as: $\epsilon_{IN} = 1 - \frac{1}{\omega^2}$. Also in this case a potential instability appear when having bigger and bigger

imaginary part of the frequency.

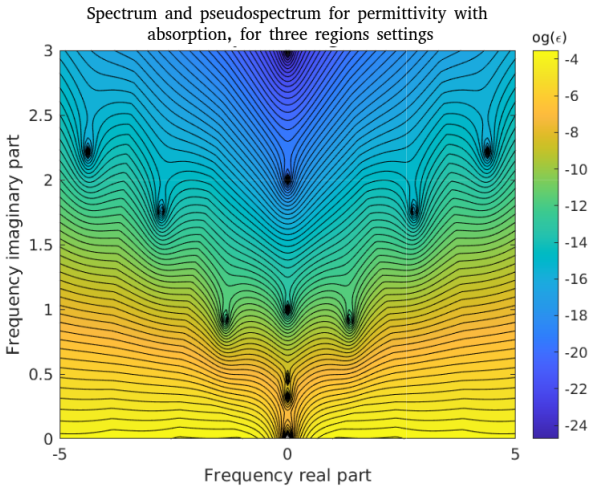

Figure 12.6: Pseudospecturm calculated with L_2-norm for an optical cavity with a permittivity with dispersion and with no absorption inside. Dark areas of the pseudospectrum indicates the existence of eigenvalues. The eigenvalues that falls on logarithmic branches are predictable, while the purely imaginary eigenvalues are detected using hyperboloidal foliation.

This observed instability of overtones marked in both simple cases is due to small perturbation to the studied operator. Keeping in mind that the perturbation that we consider when studying pseudospectrum is of the form: δE, with $||E|| = 1$, we see that this is a general "mathematical" perturbation. On the physical level, we are interested in studying the effect of small perturbations on just the permittivity. For this reason we considered a permittivity as in the second studied case with dispersion and with no absorption and run tests perturbing only the permittivity, The resulting eigenvalues are the same with no displacement at all. This suggests that the branches on which the eigenvalues situated are stable due to physical perturbation of the system.

12.5 QNMs expansion

12.5.1 Normal modes: selfadjoint case

Let us consider the initial data problem of a wave equation on a domain $D \times \mathbb{R}^+$, with $D \subset \mathbb{R}^n$ a compact domain, subject to conservative boundary conditions at the boundaries of D. For concreteness, we consider a scalar wave equation with homogeneous Dirichlet (analogously for Neumann or, more generally, Robin) boundary conditions at ∂D and initial data at D

$$\begin{cases} \left(\partial_t^2 - \Delta + V\right)\phi = 0 \\ \phi(t=0,x) = \varphi_0(x) \\ \partial_t\phi(t=0,x) = \varphi_1(x) \end{cases}, \tag{12.17}$$

where V is a potential that we assume, for simplicity, to satisfy $V(x) > 0$. The initial data problem (12.17) is well-posed, admitting a unique solution $\phi(t,x)$. The goal now is to express this solution in terms of so-called normal modes. We proceed in two equivalent forms.

First version: second-order formulation

Let us proceed first with a (perhaps over-detailed) derivation underlying the relevance of the so-called spectral theorem. We first consider the Fourier transform of Eq. (12.17) or, equivalently, we consider insert the mode $\phi(t,x) = e^{i\omega t}\phi(x)$ in (12.17), leading to the eigenvalue problem

$$(-\Delta + V)\phi(x) = \omega^2\phi(x) \ . \tag{12.18}$$

The key point is that the operator $P_V = -\Delta + V$ is selfadjoint in the scalar product $L^2(D,\mathbb{C})$

$$\langle \varphi, \psi \rangle_2 = \int_D \overline{\varphi}\ \psi\ d^n x \ . \tag{12.19}$$

Under these conditions, the spectral theorem tell us that P_V is unitarily diagonalisable. That is, there exists a (Hilbert) basis in $L^2(D,\mathbb{C})$, namely a complete and orthonormal set of eigenvectors of P_V. To be concrete, we can write

$$P_V\phi_j(x) = (-\Delta + V)\phi_j(x) = \omega_j^2\phi_j(x) \quad , \quad j \in \{1,2,\ldots\} = \mathbb{N}^* \tag{12.20}$$

with $\phi_j(x)|_{\partial D} = 0$ (the discreteness of the label j follows from the compact character of D). The set $\{\phi_{j\in\mathbb{N}^*}\}$ form a Hilbert basis in $L^2(D,\mathbb{C})$:

i) Completeness: we can expand functions in $L^2(D,\mathbb{C})$

$$\psi(x) = \sum_{j=1}^{\infty} a_j\phi_j(x) \quad , \quad \psi \in L^2(D,\mathbb{C}) \ , \tag{12.21}$$

where the symbol $\sum_{j=1}^{\infty}$ denotes a (proper) convergent series in $L^2(D,\mathbb{C})$, that is

$$\lim_{N\to\infty} ||\psi - \sum_{j=1}^{N} a_j\phi_j|| = 0 \ , \tag{12.22}$$

with $||\cdot||$ the norm associated with the scalar product (12.19).

ii) Orthogonality: the eigenfunctions $\phi_{j\in\mathbb{N}^*}$ satisfy

$$\langle \phi_i, \phi_j \rangle_2 = \delta_{ij} \ . \tag{12.23}$$

From (12.21 and (12.21) it follows

$$a_j = \langle \phi_j, \psi \rangle_2 \ . \tag{12.24}$$

Under the hypothesis $V(x) > 0$, the ω_j^2 are non-negative (their reality is assured by the self-adjointness of P_V). For simplicity (and without loss of generality), let us assume that the ω_j^2 are strictly positive

$$0 < \omega_1^2 \leq \omega_2^2 \leq \ldots \omega_j^2 \leq \ldots \tag{12.25}$$

From (12.18) and (12.20) we find the "dispersion relation"

$$\omega^2 = \omega_j^2 \quad \Longrightarrow \omega = \pm\omega_j \ , \tag{12.26}$$

where the two solutions for ω follow from the second-order in time of (12.17). Using now the linear independence of the solutions $e^{i\omega_j t}\phi_j(x)$ and $e^{-i\omega_j t}\phi_j(x)$, the most general solution to the homogeneous equation (12.17) can be written as

$$\phi(t,x) = \sum_{j=1}^{\infty} \left(\alpha_j e^{i\omega_j t}\phi_j(x) + \alpha_{-j} e^{-i\omega_j t}\phi_j(x)\right) \ , \tag{12.27}$$

avec α_j et α_{-j}, with $j \in \mathbb{N}^*$ complex numbers. If we define now

$$\omega_{-j} := -\omega_j \quad , \quad \phi_{-j}(x) := \phi_j(x) \ , \tag{12.28}$$

we can write

$$\phi(t,x) = \sum_{j\in\mathbb{Z}^*}^{\infty} \alpha_j e^{i\omega_j t}\phi_j(x) \ . \tag{12.29}$$

We determine now $\alpha_{j\in\mathbb{Z}^*}$ from the initial data in (12.17), by using critically (12.24). In particular, taking the time derivative in (12.30) we get

$$\partial_t\phi(t,x) = \sum_{j\in\mathbb{Z}^*}^{\infty} i\omega_j\alpha_j e^{i\omega_j t}\phi_j(x) \tag{12.30}$$

Then

$$\begin{aligned}
\phi(t=0,x) &= \sum_{j\in\mathbb{Z}^*}^{\infty} \alpha_j\phi_j(x) = \sum_{j=1}^{\infty} \left(\alpha_j\phi_j(x) + \alpha_{-j}\phi_{-j}(x)\right) \\
&= \sum_{j=1}^{\infty} \left(\alpha_j + \alpha_{-j}\right)\phi_j(x) \\
\partial_t\phi(t=0,x) &= \sum_{j\in\mathbb{Z}^*}^{\infty} i\omega_j\alpha_j\phi_j(x) \\
&= \sum_{j=1}^{\infty} i\left(\omega_j\alpha_j\phi_j(x) + \omega_{-j}\alpha_{-j}\phi_{-j}(x)\right) \\
&= \sum_{j=1}^{\infty} i\omega_j\left(\alpha_j - \alpha_{-j}\right)\phi_j(x)
\end{aligned} \tag{12.31}$$

On the other hand, $\phi_0(x)$ and $\psi_1(x)$ in (12.17) can be expanded in terms of $\phi_j(x)$

$$\begin{aligned}
\varphi_0(x) &= \sum_{j=1}^{\infty} a_j\phi_j(x) \\
\varphi_1(x) &= \sum_{j=1}^{\infty} b_j\phi_j(x) \ ,
\end{aligned} \tag{12.32}$$

so, from (12.17) and the basis character of $\phi_j(x)$ it follows

$$\left\{\begin{array}{rcl} a_j &=& a_j + a_j \\ b_j &=& i\omega_j(a_j - a_j) \end{array}\right. \ , \tag{12.33}$$

from which it follows

$$\alpha_j = \frac{1}{2}\left(a_j - \frac{i}{\omega_j} b_j\right) \ , \forall j \in \mathbb{Z}^* \ . \tag{12.34}$$

On the other hand, from (12.24)

$$a_j = \langle \phi_j, \varphi_0 \rangle_2 \quad , \quad b_j = \langle \phi_j, \varphi_1 \rangle_2 \ , \tag{12.35}$$

so we finally can write, using (12.30), (12.34) and (12.35)

$$\phi(t,x) = \sum_{j\in\mathbb{Z}^*}^{\infty} e^{i\omega_j t} \frac{1}{2}\left(\langle \phi_j, \varphi_0 \rangle_2 - \frac{i}{\omega_j}\langle \phi_j, \varphi_1 \rangle_2\right) \phi_j(x) \tag{12.36}$$

Third version: first-order formulation

Having in mind our discussion of the non-selfadjoint case, that is formulated in a first-order in time setting, we revisit the previous derivation of (12.36). We start by reducing the Eq. (12.17) to a first-order (in time) formulation

$$\psi = \partial_t \phi \quad , \quad u = \begin{pmatrix} \phi \\ \psi \end{pmatrix} \ . \tag{12.37}$$

Then, Eq. (12.17) becomes

$$\partial_t u = iLu \ , \tag{12.38}$$

where the operator L is defined as

$$L = \frac{1}{i}\left(\begin{array}{c|c} 0 & 1 \\ \hline L_1 & 0 \end{array}\right) \ , \tag{12.39}$$

with

$$L_1 = \Delta - V(x) \tag{12.40}$$

and initial data given by

$$u(t=0,x) = \begin{pmatrix} \varphi_0(x) \\ \varphi_1(x) \end{pmatrix} \ . \tag{12.41}$$

The operator L in (12.84) is also selfadjoint, but crucially with respect to a different scalar product that the one in (12.19), namely, with respect to

$$\begin{aligned} &\left\langle \begin{pmatrix} \phi_1 \\ \psi_1 \end{pmatrix}, \begin{pmatrix} \phi_2 \\ \psi_2 \end{pmatrix} \right\rangle_E \\ &= \frac{1}{2}\int_D \left(\overline{\psi_1}\psi_2 + \overline{\nabla\phi_1}\cdot\nabla\phi_2 + V\overline{\phi_1}\phi_2\right) d^n x \ , \end{aligned} \tag{12.42}$$

We address now the resolution of the time evolution problem (12.38) in a spectral approach, but this time we adopt a Laplace transform approach. Specifically, we consider for $\mathrm{Re}(s) > 0$

$$\begin{pmatrix} \hat{\phi}(s;x) \\ \hat{\psi}(s;x) \end{pmatrix} := \mathcal{L} \begin{pmatrix} \phi \\ \psi \end{pmatrix} = \int_0^\infty e^{-st} \begin{pmatrix} \phi \\ \psi \end{pmatrix} dt \ . \tag{12.43}$$

Applying this to Eq. (12.38), we get

$$s \begin{pmatrix} \hat{\phi}(s;x) \\ \hat{\psi}(s;x) \end{pmatrix} - \begin{pmatrix} \phi(t=0,x) \\ \psi(t=0,x) \end{pmatrix} = \left(\begin{array}{c|c} 0 & 1 \\ \hline L_1 & 0 \end{array}\right) \begin{pmatrix} \hat{\phi}(s;x) \\ \hat{\psi}(s;x) \end{pmatrix} \tag{12.44}$$

Dropping the explicit s-dependence and using (12.17) for the initial data, we can write

$$\left(- \left(\begin{array}{c|c} 0 & 1 \\ \hline L_1 & 0 \end{array}\right) + s \right) \begin{pmatrix} \hat{\phi} \\ \hat{\psi} \end{pmatrix} = \begin{pmatrix} \varphi_0 \\ \varphi_1 \end{pmatrix} \tag{12.45}$$

Introducing the self-adjoint operator L in (12.84)

$$\big(L + is\big) \begin{pmatrix} \hat{\phi} \\ \hat{\psi} \end{pmatrix} = i \begin{pmatrix} \varphi_0 \\ \varphi_1 \end{pmatrix} \ , \tag{12.46}$$

namely, using the notation in (12.37)

$$(L + is)u = iS \ , \tag{12.47}$$

where the source S is defined in terms of the initial data

$$S := \begin{pmatrix} \varphi_0 \\ \varphi_1 \end{pmatrix} \ . \tag{12.48}$$

This is a linear non-homogeneous equation. For its resolution, to get the Fourier-transformed $u(\omega;x)$ (or, alternatively, the related Laplace-transformed $u(s;x)$), we proceed in two steps.

In the first step, we consider the homogeneous part of Eq. (12.47. Rewriting the Laplace parameter s in terms of the Fourier one ω by using the relation $s = i\omega$, we can write

$$(L - \omega)u = iS \ , \tag{12.49}$$

whose homogeneous part leads to the eigenvalue problem

$$L \begin{pmatrix} \hat{\phi}_n \\ \hat{\psi}_n \end{pmatrix} = \omega_n \begin{pmatrix} \hat{\phi}_n \\ \hat{\psi}_n \end{pmatrix} \ . \tag{12.50}$$

We notice that this is just the spectral problem of the operator L, that we would have obtained if applying directly the Fourier transform to (12.38), instead of passing through the Laplace one. This is the first-order in time version of the eigenvalue problem (12.18) for the operator P_V. Let

us then relate the eigenfunctions $u_n = \begin{pmatrix} \hat{\phi}_n \\ \hat{\psi}_n \end{pmatrix}$ of the L operator, normalized with respect to scalar product (12.42), to the eingenfunctions ϕ_n's of P_V in (12.20), normalised with respect to (12.42). We first rewrite (12.50) as

$$\left(\begin{array}{c|c} 0 & 1 \\ \hline L_1 & 0 \end{array}\right) \begin{pmatrix} \hat{\phi}_n \\ \hat{\psi}_n \end{pmatrix} = i\omega_n \begin{pmatrix} \hat{\phi}_n \\ \hat{\psi}_n \end{pmatrix} \ . \tag{12.51}$$

This can be rewritten as

$$\hat{\psi}_n = i\omega_n \hat{\phi}_n \ \ , \ \ L_1 \hat{\phi}_n = i\omega_n \hat{\psi}_n \ , \tag{12.52}$$

so, inserting the first one in the second, we find as expected

$$\begin{aligned} L_1 \hat{\phi}_n &= i\omega_n (i\omega_n) \hat{\phi}_n = -\omega_n^2 \tilde{\phi}_n \\ P_V \hat{\phi}_n &= \omega_n^2 \hat{\phi}_n \ , \end{aligned} \tag{12.53}$$

where we have used $P_V = -L_1$. Assuming for simplicity that eigenvalues of P_V are simple (non-degenarate, the general (Fredholm) case can also be treated), it follows

$$\hat{\phi}_n = \alpha \phi_n \ . \tag{12.54}$$

Imposing then the normalization

$$\left\langle \begin{pmatrix} \hat{\phi}_n \\ \hat{\psi}_n \end{pmatrix} , \begin{pmatrix} \hat{\phi}_m \\ \hat{\phi}_m \end{pmatrix} \right\rangle_E = \delta_{nm} \ , \tag{12.55}$$

and using (12.52), (12.54), the integration by parts (with homogeneous boundary conditions) and (12.53) in (12.42), it follows

$$|\alpha| = \frac{1}{\omega_n} \ \ , \ \ \hat{\phi}_n = \frac{1}{\omega_n} \phi_n \tag{12.56}$$

In the second step to the resolution of the Laplace-transformed $u(s;x)$, we need to evaluate the 'resolvent' $(L+is)^{-1}$ of L, so that, using (12.47) we get

$$u(s;x) = i(L+is)^{-1} S \ , \tag{12.57}$$

In order to write the resolvent of L or, equivalently its Green function (integral Kernel of the resolvent), we make of string use of the selfadjointness of L. Explicitly, using again Fourier parameter ω and writing (for $\omega \in \mathbb{R}$ not belonging to the spectrum of L)

$$G_\omega(x',x) = \sum_{j \in \mathbb{Z}^*} \frac{u_j^\dagger(x') u_j(x)}{\omega_j - \omega} \tag{12.58}$$

we can formally write the action of the resolvent, in terms of the integration in the x' variable inside the (energy) scalar product

$$\big((L-\omega)^{-1} S\big)(\omega, x) = \langle G_\omega(\cdot, x), S \rangle_E \tag{12.59}$$

$$:= \sum_{j \in \mathbb{Z}^*} \frac{u_j(x)}{\omega_j - \omega} \langle u_j, S \rangle_E \ . \tag{12.60}$$

This notation is a bit cumbersome and can be made more transparent in the terms of formal "bra's"s and "ket's"

$$(L-\omega)^{-1} = \sum_{j\in\mathbb{Z}^*} \frac{|u_j\rangle\langle u_j|}{\omega_j - \omega} \ , \tag{12.61}$$

where $\langle\,\cdot\,|$ and $|\,\cdot\,\rangle$ must be understood with respect to the energy scalar product (12.42). The sum in (12.61) is associated with actual convergent series, this being to the selfadjointness of L. Namely, expression (12.61) is just the consequence of the completeness of eigenfunctions u_j, together with the "dispersion relation" (12.26).

With these elements we can write the frequency solution to the initial data problem (12.38) as

$$u(\omega;x) = i(L-\omega)^{-1}S = i\sum_{j\in\mathbb{Z}^*} \frac{\langle u_j|S\rangle_E}{\omega_j-\omega}|u_j\rangle \ , \tag{12.62}$$

where the solution can be analytically (actually meromorphically) extended in the ω-complex plane. Writing the Laplace version ($\omega = -is$)

$$u(s;x) = i(L+is)^{-1}S = \sum_{j\in\mathbb{Z}^*} \frac{\langle u_j|S\rangle_E}{s-s_j}|u_j\rangle \ , \tag{12.63}$$

we can recover the time solution by taking the inverse Laplace transform to (12.43), namely

$$u(t,x) = \frac{1}{2\pi i}\int_{c-i\infty}^{c+i\infty} e^{st}u(s;x)ds \ , \tag{12.64}$$

with $c\in\mathbb{R}^+$. Plugging the expression of $U(s;x)$ in (12.63), we find

$$u(t,x) = \frac{1}{2\pi i}\int_{c-i\infty}^{c+i\infty} \sum_{j\in\mathbb{Z}^*} e^{st}\frac{\langle u_j|S\rangle_E}{s-s_j}|u_j\rangle \ . \tag{12.65}$$

Let us consider now a contour C in $s-\mathbb{C}$ formed by the interval $c-iR, c+iR$ and closed on the left half-plane by a circle (of radius R, centered at $c+i0$) and denote by Ω the bounded domain in $\mathbb{C}$ delimited by C, In the context of the operators we are considering, the number of $\omega_j\in\Omega$ is finite, so (using Cauchy theorem) we can safely interchange the sum and the integral we can write (assuming the limit exists)

$$\begin{aligned} u(t,x) &= \lim_{R\to\infty}\frac{1}{2\pi i}\int_{c-iR}^{c+iR}\sum_{j\in\mathbb{Z}^*} e^{st}\frac{\langle u_j|S\rangle_E}{s-s_j}|u_j\rangle \\ &= \lim_{L\to\infty}\left(\sum_{\omega_j\in\Omega}\frac{1}{2\pi i}\oint_C e^{st}\frac{\langle u_j|S\rangle_E}{s-s_j} + (\text{circle part})\right) , \end{aligned} \tag{12.66}$$

The "(circle part)" vanish by standard arguments at the $R\to\infty$ and, applying the Cauchy theorem, we can write

$$u(t,x) = \lim_{R\to\infty}\sum_{\omega_j\in\Omega} e^{s_jt}a_ju_j \ , \tag{12.67}$$

with

$$a_j = \langle u_j | S \rangle_{_E} = \left\langle \begin{pmatrix} \hat{\phi}_j \\ \hat{\psi}_j \end{pmatrix} , \begin{pmatrix} \varphi_0 \\ \varphi_1 \end{pmatrix} \right\rangle_{_E} \tag{12.68}$$

As commented, the number of terms in the sum in (12.68) is finite, so we are considering the existence of the limit of a sequence of partial sums. It is a remarkable feature of self-adjoint operators, namely the existence of a spectral theorem, that such limit exists in the norm associated with the Hilbert scalar product, so finally we can actually write

$$u(t,x) = \sum_{j\in\mathbb{Z}^*} e^{s_j t} a_j u_j = \sum_{j\in\mathbb{Z}^*} e^{i\omega_j t} a_j u_j \ , \tag{12.69}$$

in the sense of a convergent series. The constant a_j can be more explicity expressed as

$$a_j = \frac{1}{2}\int_D \left(\overline{\hat{\psi}_j}\varphi_1 + \overline{\nabla\hat{\phi}_j}\cdot\nabla\varphi_0 + V\overline{\hat{\phi}_j}\varphi_0 \right) d^n x \ ,$$

and using $\psi_j = i\omega_j \phi_j$

$$\begin{aligned} a_j &= \frac{1}{2}\Big(-i\omega_j \int_D \overline{\hat{\phi}_j}\varphi_1 d^n x + \int_D \left(\overline{\nabla\hat{\phi}_j}\cdot\nabla\varphi_0 + V\overline{\hat{\phi}_j}\varphi_0 \right) d^n x \Big) \ , \\ &= \frac{1}{2}\Big(\langle \hat{\phi}_j, \varphi_0 \rangle_{H^2_V} - i\omega_j \langle \hat{\phi}_j, \varphi_1 \rangle_{_2} \Big) \end{aligned} \tag{12.70}$$

with the (Sobolev's) H^1_V scalar product

$$\langle \phi_1, \phi_2 \rangle_{H^2_V} := \int_D \left(\overline{\nabla\phi_1}\cdot\nabla\phi_2 + V\overline{\phi_1}\phi_2 \right) d^n x \tag{12.71}$$

Therefore, we can finally write

$$u(t,x) = \sum_{j\in\mathbb{Z}^*} e^{i\omega_j t} \frac{1}{2}\Big(\langle \hat{\phi}_j, \varphi_0 \rangle_{H^2_V} - i\omega_j \langle \hat{\phi}_j, \varphi_1 \rangle_{_2} \Big) u_j \ , \tag{12.72}$$

This is the general normal mode expansion, expressed in terms of the quantities natural in the first-order in time formulation. In order to make contact with expression (12.36) in the second-order in time formulation, we rewrite

$$\begin{pmatrix} \phi \\ \psi \end{pmatrix} = \sum_{j\in\mathbb{Z}^*} e^{i\omega_j t} \frac{1}{2}\Big(\langle \hat{\phi}_j, \varphi_0 \rangle_{H^2_V} - i\omega_j \langle \hat{\phi}_j, \varphi_1 \rangle_{_2} \Big) \begin{pmatrix} \hat{\phi}_j \\ \hat{\psi}_j \end{pmatrix} , \ , \tag{12.73}$$

Now, noticing $\hat{\phi}_j = \alpha_j \phi_j$ and $\hat{\psi}_j = \alpha_j \psi_j$, we can write

$$\begin{pmatrix} \phi \\ \psi \end{pmatrix} = \sum_{j\in\mathbb{Z}^*} e^{i\omega_j t} \frac{|\alpha_j|^2}{2}\Big(\langle \phi_j, \varphi_0 \rangle_{H^2_V} - i\omega_j \langle \phi_j, \varphi_1 \rangle_{_2} \Big) \begin{pmatrix} \phi_j \\ \psi_j \end{pmatrix} , \tag{12.74}$$

and evaluating from (12.56)

$$\begin{pmatrix} \phi \\ \psi \end{pmatrix} = \sum_{j\in\mathbb{Z}^*} e^{i\omega_j t} \frac{1}{2}\Big(\frac{1}{\omega_j^2}\langle \phi_j, \varphi_0 \rangle_{H^2_V} - \frac{i}{\omega_j}\langle \phi_j, \varphi_1 \rangle_{_2} \Big) \begin{pmatrix} \phi_j \\ \psi_j \end{pmatrix} \ . \tag{12.75}$$

Finally, writing

$$\begin{aligned}\langle\phi_j,\varphi_0\rangle_{H^2_V} &= \int_D\big(\overline{\nabla\phi_j}\cdot\nabla\varphi_0+V\overline{\phi_j}\varphi_0\big)\,d^nx\\ &= \int_D\big(-\overline{\Delta\phi_j}\varphi_0+V\overline{\phi_j}\varphi_0\big)\,d^nx=\int_D\overline{P_V\phi_j}\varphi_0 d^nx\\ &= \omega_j^2\int_D\phi_j\varphi_0 d^nx=\omega_j^2\langle\phi_j,\varphi_0\rangle_2\end{aligned}\tag{12.76}$$

we recover

$$\begin{pmatrix}\phi\\ \psi\end{pmatrix}=\sum_{j\in\mathbb{Z}^*}e^{i\omega_j t}\frac{1}{2}\Big(\langle\phi_j,\varphi_0\rangle_2-\frac{i}{\omega_j}\langle\phi_j,\varphi_1\rangle_2\Big)\begin{pmatrix}\phi_j\\ \psi_j\end{pmatrix}\ ,\tag{12.77}$$

whose first component corresponds exactly to the normal mode expansion (12.36). As in (12.36), the sum here corresponds to a convergent series, for each fixed t. Certainly this second derivation of the normal mode expansion based on the resolvent (Green's function) is significantly more cumbersome than the first derivation using directly the completeness of the eigenfunctions of P_V. However, in contrast with the latter, it has the virtue of generalizing directly to the non-selfadjoint case.

12.5.2 QNM modes: non-selfadjoint case, Keldysh expansion

The normal mode expansion in section 12.5.1 has made explicit use of the completeness and orthogonality properties of the eigenfunctions of a selfadjoint operator. The second derivation in section 12.5.1 also makes critical use of the selfadjointness in the construction of the explicit resolvent (12.61) but, avoiding the explicit use of Hilbert basis and orthogonal projections, it provides an approach whenever we can explictly write the resolvent $(L-\omega)^{-1}$ of an operator L. This precisely what Keldysh's asymptotic expansion of the resolvent provides in the case of non-selfadjoint operators [102, 103, 129, 28, 29].

Let us consider again 5.1.6. If we relax the condition $\langle u_n,v_n\rangle=-1$, we can rewrite expression (5.51) as

$$(L-\lambda)^{-1} \sim \sum_{\lambda_n\in\Omega}\frac{|v_n\rangle\langle w_n|}{\langle w_n,v_n\rangle}\frac{-1}{\lambda-\lambda_n}\tag{12.78}$$

$$= \sum_{\lambda_n\in\Omega}\frac{|v_n\rangle\langle w_n|}{\langle w_n,v_n\rangle}\frac{1}{\lambda_n-\lambda}\ .\tag{12.79}$$

Introducing now the condition number κ_n associated to the eigenvalue λ_n

$$\kappa_n:=\frac{||w_n||\ ||v_n||}{\langle w_n,v_n\rangle}\ ,\tag{12.80}$$

we can write

$$(L-\lambda)^{-1}\sim\sum_{\lambda_n\in\Omega}\kappa_n\frac{|v_n\rangle\langle w_n|}{||w_n||\ ||v_n||}\frac{1}{\lambda_n-\lambda}\ ,\tag{12.81}$$

and, in terms of the normalized left- and right-eingvectors

$$\hat{w}_n = \frac{w_n}{||w_n||} \quad , \quad \hat{v}_n = \frac{v_n}{||v_n||} \ , \tag{12.82}$$

we can finally write

$$(L-\lambda)^{-1} \sim \sum_{\lambda_n \in \Omega} \kappa_n \frac{|\hat{v}_n\rangle\langle\hat{w}_n|}{\lambda_n - \lambda} \ . \tag{12.83}$$

Note that this expression formally recovers the form of Eq. (12.61) in the selfadjoint (more generally, 'normal') case in which $\hat{w}_n = \hat{v}_n$ and $\kappa_n = 1$. However, the statement in (12.61) is much stronger, since the sum there indicatates a series convergence. In the selfadjoint case, expression (12.83) can indeed be extended to the whole $\mathbb{C} \setminus \sigma(L)$ in a convergent sense, but this requires other (Hilbert space) techniques.

In this setting we can repeat the steps followed in 12.5.1, taking care at the proper places of the differences between (12.83) and (12.61), in order to write a QNM resonant expansion in the hyperboloidal approach. The starting point is the first-order (in time) evolution equation in the hyperboloidal approach, namely Eq. (12.38) with the operator L now given by

$$L = \frac{1}{i}\left(\begin{array}{c|c} 0 & 1 \\ \hline L_1 & L_2 \end{array}\right) \ , \tag{12.84}$$

where the L_2 operator accounts for radiation damping. Specifically, following [98] we keep the energy scalar product (12.42), demonstrating that L is non-selfadjoint due precisely to this L_2 term. Taking Laplace transform we get again the non-homogeneous equation (12.47), or Eq. (12.49) in terms of the Fourier spectral parameter. However, the operator L now is not selfadjoint. The relevant spectral problem of the homogeneous part involves both left- and right-eigenvectors, cf. (5.48), that in terms of time frequency ω_n writes

$$L\hat{v}_n = \omega_n \hat{v}_n \quad , \quad L^\dagger \hat{w}_n = \overline{\omega}_n \hat{w}_n \tag{12.85}$$

where we choose right and left-eigenctors $\hat{v}_n$ and $\hat{w}_n$ normalized with respect to the energy scalar (12.42)

$$\hat{v}_n = \begin{pmatrix} \hat{\phi}_n^{\mathrm{R}} \\ \hat{\psi}_n^{\mathrm{R}} \end{pmatrix} \quad , \quad \hat{w}_n = \begin{pmatrix} \hat{\phi}_n^{\mathrm{L}} \\ \hat{\psi}_n^{\mathrm{L}} \end{pmatrix} \tag{12.86}$$

From this spectral problem, the resolvant $(L-\omega)^{-1}$ can be constructed in a bounded $\Omega_\omega \in \mathbb{C}$ as in (12.83) so, for $\lambda \in \Omega_\omega$, we can write

$$u(\omega; x) = i(L-\omega)^{-1} S \sim i \sum_{\omega_j \in \Omega_\omega} \kappa_n \frac{\langle \hat{w}_j | S \rangle_E}{\omega_j - \omega} |\hat{v}_j\rangle \ , \tag{12.87}$$

or, in terms of the Laplace spectral parameters with $s \in \Omega_s$ with $s = i\omega$ and reinserting the analytic part of the resolvent in (12.83), we have

$$u(s; x) = \sum_{s_j \in \Omega_s} \kappa_n \frac{\langle \hat{w}_j | S \rangle_E}{s - s_j} |\hat{v}_j\rangle + iH(s)(S) \ . \tag{12.88}$$

Writing now

$$u(t,x) = \lim_{R\to\infty}\frac{1}{2\pi i}\int_{c-iR}^{c+iR} e^{st}u(s;x)ds = \lim_{R\to\infty}\frac{1}{2\pi i}\int_{c-iR}^{c+iR} e^{st}\Big(\sum_{s_j\in\Omega_s}\kappa_n\frac{\langle\hat{w}_j|S\rangle_{_E}}{s-s_j}|\hat{v}_j\rangle + iH(s)(S)\Big)ds\ ,$$

and using the semi-circular contour C in Eq. (12.66) we can write

$$u(t,x) = \lim_{R\to\infty}\left(\sum_{\omega_j\in\Omega}\frac{1}{2\pi i}\oint_C e^{st}\kappa_n\frac{\langle\hat{w}_j|S\rangle_{_E}}{s-s_j}|\hat{v}_j\rangle + \frac{1}{2\pi}\oint_C e^{st}H(s)(S)ds + (\text{circle part})\right) \quad (12.89)$$

The contour C integral involving the analytic expression $e^{st}H(s)(S)$ vanishes, but nothing guarantees that its integral along the semi-circle vanishes, this depending on the specific dependence of the function $H(\lambda)$, that is not fixed by Keldysh expansion. In general, the last term gives a term $C_R(t;S)$. Using now Cauchy theorem, we can write

$$u(t,x) = \lim_{R\to\infty}\Big(\sum_{\omega_j\in\Omega} e^{s_jt}\kappa_n\langle\hat{w}_j|S\rangle_{_E}\hat{v}_j + C_R(t;S)\Big)\ . \quad (12.90)$$

In contrast with (12.67), nothing guarantees that this limits exists. On the one hand, for strongly non-selfadjoint (more generally non-normal) operators the condition number κ_n can grow without bound and, on the hand, the $C_R(t;S)$ does not need to converge as R goes to infinity, in particular not needing to vanish. In this context we cannot write $u(t,x)$ in terms of an actual convergent series, but we can still an asymptotic QNM resonant expansion

$$u(t,x) \sim \sum_n e^{s_jt}\kappa_n\langle\hat{w}_j|S\rangle_{_E}\hat{v}_j\ , \quad (12.91)$$

or, in the Fourier spectral-parameter

$$u(t,x) \sim \sum_n e^{i\omega_jt}\kappa_n\langle\hat{w}_j|S\rangle_{_E}\hat{v}_j\ , \quad (12.92)$$

meaning by this that, for a bounded domain Ω with $R = \max\{\text{Im}(\omega), \omega\in\Omega\}$, the number of QNMs in finite and we can write

$$u(t,x) = \sum_{\omega_j\in\Omega} e^{i\omega_jt}\kappa_n\langle\hat{w}_j|S\rangle_{_E}\hat{v}_j + E_R(t;S) \quad (12.93)$$

where the structure of the term $e^{st}H(s)(S)$ in the circle part of (12.89) permits to bound the "error" $E_L(t;S)$ in the estimation of $u(t,x)$ by the (finite) resonant expansion. Explicitly, there exists a constant C_R depending on R and the operator L (but not on the initial data), such that

$$||E_L(t;S)||_{_E} \leq C_Re^{-Rt}||S||_{_E}\ . \quad (12.94)$$

This is essentially the content of Lax-Phillips resonant expansion [115, 176, 194, 68], here expressed in terms of normalizable QNM functions and providing an explicit prescription for the evaluation of the associated coefficient explicitly

$$u(t,x) \sim \sum_n e^{s_jt}a_n\hat{v}_j \quad (12.95)$$

with

$$a_n = \kappa_n \langle \hat{w}_j | S \rangle_{_E} \ . \tag{12.96}$$

Notice the formal recovery of the normal mode expansion (12.69), with (12.68), in the self-adjoint case in which $\hat{w}_j = \hat{v}_j$ and $\kappa_j = 1$. Of course, as explained, the sum has a different meaning, although in this case both expressions can be actually shown to the same. Expressing this in terms of the components of normalized vectors (12.86)

$$\begin{pmatrix} \phi \\ \psi \end{pmatrix} \sim \sum_n e^{i\omega_j t} a_n \begin{pmatrix} \hat{\phi}_j^R \\ \hat{\psi}_j^R \end{pmatrix} \tag{12.97}$$

with

$$a_j = \kappa_j \langle \hat{w}_j | S \rangle_{_E} = \kappa_j \Big\langle \begin{pmatrix} \hat{\phi}_j^L \\ \hat{\psi}_j^L \end{pmatrix} , \begin{pmatrix} \varphi_0 \\ \varphi_1 \end{pmatrix} \Big\rangle_{_E} \tag{12.98}$$

$$a_j = \frac{\kappa_n}{2} \int_D \Big(\overline{\hat{\psi}_j^L} \varphi_1 + \overline{\nabla \hat{\phi}_j^L} \cdot \nabla \varphi_0 + V \overline{\hat{\phi}_j^L} \varphi_0 \Big) \, d^n x \ ,$$

and using now $\hat{\psi}_j^L = i\overline{\omega} \hat{\phi}_j^L$ **[justify from the explicit expression of $L_2^\dagger$!]**, we have

$$\begin{aligned} a_j &= \frac{\kappa_n}{2} \Big(\int_D \overline{i\omega_j \hat{\phi}_j^L} \varphi_1 d^n x + \int_D \Big(\overline{\nabla \hat{\phi}_j^L} \cdot \nabla \varphi_0 + V \overline{\hat{\phi}_j^L} \varphi_0 \Big) \, d^n x \Big) \ , \\ &= \frac{\kappa_n}{2} \Big(- i\omega_j \int_D \overline{\hat{\phi}_j^L} \varphi_1 d^n x + \int_D \Big(\overline{\nabla \hat{\phi}_j^L} \cdot \nabla \varphi_0 + V \overline{\hat{\phi}_j^L} \varphi_0 \Big) \, d^n x \Big) \qquad (12.99) \\ &= \frac{\kappa_n}{2} \Big(\langle \hat{\phi}_j^L , \varphi_0 \rangle_{H_V^1} - i\omega_j \langle \hat{\phi}_j^L , \varphi_1 \rangle_2 \Big) \ . \qquad (12.100) \end{aligned}$$

This recovers the selfadjoint case (12.70) when making $\hat{\phi}_j^L \to \hat{\phi}_j$ and $\kappa_n \to 1$. But, more inportantly, it recovers the correct dependence in ω_j. Indeed, from Eqs. (12.97) and (12.99) we can write the QNM resonant expansion for the $\phi(t, x)$ field

$$\phi(t, x) \sim \sum_n e^{i\omega_j t} a_n \hat{\phi}_j^R \ , \tag{12.101}$$

with

$$a_j = \frac{\kappa}{2} \Big(\langle \hat{\phi}_j^L , \varphi_0 \rangle_{H_V^1} - i\omega_j \langle \hat{\phi}_j^L , \varphi_1 \rangle_2 \Big) \tag{12.102}$$

This is the version in the Keldysh setting of the Lax-Philip's asymptotic resonant expansion. This crucially recovers the correct dependence in ω_j, and not in the conjugated $\overline{\omega_j}$ (cf. e.g. Eq.(2.50) in [194]; note the sign change in the convention for the spectral parameter). Finally, in contrast with the self-adjoint case, the expression of a_n cannot be further reduced to purely L^2 scalar products, since $\hat{\phi}_j^L$ is not the eigenfunction of the operator P_V. Of course, (12.36) expression (12.36) is recovered in the selfadjoint case (with the sum now understood in terms of a convergent series), exactly as in Eq. (2.52) in [194].

QNM modes: non-selfadjoint case, Keldysh expansion, optical case

To find the analog expansion for an optical case with a generic permittiviy (does not necessarily follow Lorentz model), we will write the problem in another way using one hyperboloidal slices letting the information about different permittivity in different regions of the space, and for different frequencies impeded in the permittivity function $\epsilon(\omega, x)$. Considering a scalar field in one dimension:

$$(\epsilon(t,x) * \partial_t^2 - \partial_x^2)\phi(t,x) = 0 \tag{12.103}$$

Applying the same Hyperboloidal transformations in eq.2.20, we get:

$$(\epsilon(\tau,y)*\partial_\tau^2 - y^2\partial_\tau^2 + 2y(1-y^2)\partial_\tau\partial_y + (1-y^2)\partial_\tau + 2y(1-y^2)\partial_y - (1-y^2)^2\partial_y^2)\phi(\tau,y) = 0 \tag{12.104}$$

Performing Fourier transformation with respect to τ, and considering an auxiliary field $\psi(\tau, y) = \partial_\tau$, we can write the problem in the following matricial way:

$$\left(\begin{array}{c|c} 0 & 1 \\ \hline L_1 & L_2 \end{array}\right)\begin{pmatrix}\phi\\ \psi\end{pmatrix} = i\omega\left(\begin{array}{c|c} 1 & 0 \\ \hline 0 & \epsilon(\omega,y) - y^2 \end{array}\right)\begin{pmatrix}\phi\\ \psi\end{pmatrix} \tag{12.105}$$

with $L_1 = (1-y^2)((1-y^2)\partial_y^2 - 2y\partial_y)$,
and $L_2 = -(1-y^2)(2y\partial_y + 1)$. Hence the problem can be expressed as: $T(\omega, y)u(\omega, y) = 0$, where:

$$T(\omega,y) = \left(\begin{array}{c|c} 0 & 1 \\ \hline L_1 & L_2 \end{array}\right) - i\omega\left(\begin{array}{c|c} 1 & 0 \\ \hline 0 & \epsilon(\omega,y) - y^2 \end{array}\right) \tag{12.106}$$

It follows that:

$$T'_\omega = -i\left(\begin{array}{c|c} 1 & 0 \\ \hline 0 & \epsilon(\omega,y) - y^2 + \omega\frac{\partial\epsilon}{\partial\omega} \end{array}\right). \tag{12.107}$$

Calculating T'_ω, we can impose that the product:

$$\langle w_n, T'_\omega|_{\omega_n}, v_n\rangle = -1, \tag{12.108}$$

where $w_n = \begin{pmatrix}\phi_{1n}\\ \psi_{1n}\end{pmatrix}$, and $v_n = \begin{pmatrix}\phi_{2n}\\ \psi_{2n}\end{pmatrix}$, then

$$\langle w_n, T'_\omega|_{\omega_n}, v_n\rangle = \langle\begin{pmatrix}\phi_{1n}\\ \psi_{1n}\end{pmatrix}, -i\begin{pmatrix}\phi_{2n}\\ (\epsilon(\omega_n,y) - y^2 + \omega_n\frac{\partial\epsilon}{\partial\omega}|_{\omega_n})\psi_{2n}\end{pmatrix} \tag{12.109}$$

So: Coming back to the approximation of Keldysh expansion, in this case eq.12.78 will be written as:

$$(L-\lambda)^{-1} \sim \sum_{\lambda_n\in\Omega}\frac{|v_n\rangle\langle w_n|}{\langle w_n, T'_\omega|_{\omega_n}, v_n\rangle}\frac{1}{\lambda-\lambda_n} \tag{12.110}$$

$$= \sum_{\lambda_n\in\Omega}\frac{|v_n\rangle\langle w_n|}{\langle w_n, T'_\omega|_{\omega_n}, v_n\rangle}\frac{1}{\lambda-\lambda_n}\,. \tag{12.111}$$

Taking into account eq.12.80, we can write:

$$(L-\lambda)^{-1} \sim \sum_{\lambda_n \in \Omega} \kappa_n \frac{\langle w_n, v_n \rangle}{\langle w_n, T'_\omega|_{\omega_n}, v_n \rangle} \frac{|v_n\rangle\langle w_n|}{||w_n||\ ||v_n||} \frac{1}{\lambda - \lambda_n} \ , \tag{12.112}$$

and, in terms of the normalized left- and right-eingvectors

$$\hat{w}_n = \frac{w_n}{||w_n||} \quad , \quad \hat{v}_n = \frac{v_n}{||v_n||} \ , \tag{12.113}$$

we can finally write

$$(L-\lambda)^{-1} \sim \sum_{\lambda_n \in \Omega} \kappa'_n \frac{|\hat{v}_n\rangle\langle\hat{w}_n|}{\lambda - \lambda_n} \ , \tag{12.114}$$

where $\kappa'_n = \kappa_n \frac{\langle w_n, v_n \rangle}{\langle w_n, T'_\omega|_{\omega_n}, v_n \rangle}$. If we define: where $\kappa'_n = -\kappa_n \frac{\langle w_n, v_n \rangle}{\langle T'_\omega|_{\omega_n} v_n, w_n \rangle}$, then:

$$(L-\lambda)^{-1} \sim \sum_{\lambda_n \in \Omega} \kappa'_n \frac{|\hat{v}_n\rangle\langle\hat{w}_n|}{\lambda_n - \lambda} \ , \tag{12.115}$$

Note that 12.115 was obtained without defining a specific scalar product although the contribution of different poles to the resolvent in a relation with the scalar product choice.

12.6 Conclusions

- Introducing hyperboloidal slicing approach in scattering electro-magnetic problems. This was made assuming a Lorentz model of a permittivity in an cavity.
- Calculated QNMs are normalizable, that is due to the use of hyperboloidal slices approach.
- Introducing pseudospectrum notions and tool to study stability issues in optics.
- Using Chebyshev spectral methods to solve numerically QNM problem with three domains using different grids. The problem was casted as an eigenvalue problem, with continuity conditions to be imposed.
- Identification the existence of purely imaginary eigenvalues: $\omega_n = in$, these are not resonant frequencies while it contribute to the field decay with time.
- Asymptotic resonant expansion in terms of QNMs in the case of permittivity follows Lorentz model with zero absorption in analogy with the case of compact potential as in Lax & Phillips theorem.
- Calculation of excitation coefficients in terms of conditioning number, by re-writing Keldysh expansion as the resonant expansion.

Chapter 13

Conclusions

Contents

The general context of this PhD deals with a scattering problem in which the propagating field is lost at the infinities and, in the presence of a black hole, through its horizon. Such a system can be cast as a non-unitary time evolution problem, therefore in which an infinitesimal generator of time evolution is a non-self-adjoint operator. In a first step we have cast such a problem in an appropriate Hilbert space setting by choosing a hyperboloidal slicing and a suitable scalar product. Specifically, in order to address the spectral instability of the operator, we have chosen a scalar product associated with the energy of the field. In the related energy norm, non-unitarity is just the mathematical translation of non-conservative physical system. From a methodological perspective, the relevant point is that we have translated the discussion of the scattering problem into the spectral properties of a non-self-adjoint operator characteristics, namely the Keldysh expansion, the notion of the pseudospectrum and related concepts as the particular role of random perturbations.

13.1 Main results

The main results we have achieved can be divided in three main topics:

i) *Spectrum, pseudospectrum and scalar product*

- In this thesis we have introduced the pseudospectrum notion to gravitational and optical physics. Dueling in a scattering problem, a pseudospectrum analysis of the *unperturbed* operator infinitesimal time translation generator provides a global picture of QNM spectral (in)stability [98], with the QNM problem cast as an eigenvalue problem of the non-self-adjoint operator.
- We have introduced an energy scalar product as the appropriate one to assess the stability problem under external physical disturbances. Other scalar products could be necessary to assess other QNM problems, A scalar product in Gevrey classes in order to address the problem of defining the QNMs.

- The (energy) pseudospectrum structure of the scattering problems presents a seemingly universal structure. In particular the asymptotics for large real part of frequencies are logarithmic, consistently with the asymptotic of QNM free regions [68].
- The distribution of the perturbed eigenvalues attain logarithmic pseudospectrum contour lines for C^p perturbations in the potential or permittivity case according to Zworski's theorem [192]. We observed that perturbed QNM frequencies associated to regular deterministic perturbations approach the contour lines as the frequency increases. We conjecture that the pseudospectrum contour lines are attained in the infinite frequency limit following a pattern given by Regge QNMs branches.
- Perturbed branches are stable under further perturbations and share basic features with generic compact object QNMs: we conjecture a universality of QNMs of generic compact objects, either matter compact objects or perturbed vacuum (black holes) ones.

ii) *Gravity*

- Fundamental BH QNMs are stable under high-frequency small perturbations, while the overtones are unstable under these kind of perturbations.
- Distinction between axial and polar GW parities: isospectrality loss While both QNM spectra coincide for the Schwarzschild BH, parity loss of generacy is a natural consequence when the system is slightly perturbed. We identify three regimes of the isospectrality loss under perturbation characterized by (ϵ, k), where ϵ is the size of perturbation and k is its frequency, actually the wave number.
- The opening of perturbed QNMs branches opening is assessed by introducing a new parameter: $\mathcal{G} = \lim_{n\to\infty} \omega_n^{\mathrm{R}}/|\omega_n|$. Schwarzschild QNMs have $\mathcal{G} = 0$, whereas Regge branches yields $\mathcal{G} = 1$. The tendency $\mathcal{G} \to 1$ as $k \to \infty$ indicates QNMs migrating to $\epsilon-$pseudospectra log-lines in the large wave-number limit. We propose this parameter as a measure of the loss of regularity in the potential. See Regge QNM conjecture 13.1.
- Reverberation at Regge's length scales $L^R(\epsilon, k)$ is proposed as underlying mechanism, with multiple reflections decreasing QNM damping.
- A BH QNM Weyl's law has been introduced, with hints into classical/quantum BH physics, expressing the 'reverberation scale' in terms of a Weyl's length $L^W(\epsilon, k)$. We propose this parameter as an indication of small structure.

iii) *Optics*

- Introduction hyperboloidal slicing approach in scattering electro-magnetic problems, specifically this has been made assuming a Lorentz model of a permittivity in an cavity.
- Normalization of QNMs due to the use of hyperboloidal slices approach.

– Systematic use of pseudospectrum notion and tool to study stability issues in optics.

- Implementation of multi Chebyshev grids to solve numerically QNM problem. This is fundamental in studying systems configured with jumps in optical properties, where continuity conditions to be imposed.

- Identification the existence of purely imaginary eigenvalues: $\omega_n = in$ for compactly supported potential or permittivity. These are not resonant frequencies while it contribute to the field decay with time.
- Asymptotic resonant expansion in terms of QNMs in the permittivity case we implement this assuming Lorentz model with zero absorption extending Lax & Phillips theorem.
- Calculation of excitation coefficients in terms of conditioning number, by re-writing Keldysh expansion as the resonant expansion.

In order to assess the work of this thesis we compare with the initial objectives:

i) *First objective: Resonant expansion.* We have suggested to write the studied problem in hyperboloidal slices. Defining an appropriate scalar product (energy scalar product for the potential case) allowed re-write the problem as a one in a Hilbert space. Having the problem in a Hilbert space and using Keldysh expansion, we could write an asymptotic resonant expansion in terms of normalizable QNMs eigenfunctions, with a certain prescription for the excitation coefficients. Moreover we have investigated this resonance expansion in relation with the one in Lax-Phillips results. In the self-adjoint case we have shown that this expansion can be reduced to an expansion of normal modes where the system of eigenfunctions is complete.
Thus, the first objective has been partially achieved. Howeve no general assessment of completeness in terms of convergent series has been done.

ii) *Second objective: Instability and scalar product.* We have assessed the (in)-stability of the eigenvalues due to a small perturbation of the studied potentials or permittivity. In order to achieve that, we have introduced:

   – Energy scalar product for problems with potential. While we used L_2-norm for the case of optical problem, but since we found that the eigenvalues in optical case are stable under permittivity perturbation using L_2-norm, the essential goal of assessing its stabilities is achieved.
   – Pseudospectrum notion to scattering optical and gravitational problems.

iii) *Third objective: Introduction diagnosis parameters.* We have introduced quantities that helps in assessing the behaviour of the open perturbed branches of QNMs. These quantities can help in application in the gravitational scattering problems and it can also be used to characterize the QNM eigenvalues of optical systems. The fact of re-writing the QNM optical problem as a problem in a Hilbert space allows to have a new expression for calculating the mode volume and thus the Purcell factor.
The third objective has been achieved in the sense of making a first step in the construction of diagnosis parameters, but much further investigations is needed to consider the third objective is fully achieved.

13.2 Perspectives

This work has led to many open questions. The most important in my opinion are:

i) *General directions:*

- Is it possible to use QNMs of unperturbed operator as a basis for perturbed problem?.
- Can we find the suitable perturbation in order to get a certain form of a perturbed spectrum. This question is particularly relevant in optical settings design.
- What are the parameters on which the structure of pseudospectrum depends?.
- Following the same methodology to study other dissipative systems with outgoing boundary conditions, such as in oceanography waves problems.
- Following the same methodology to study problems with energy loss in the bulk.

ii) *Particular questions:*

- Numerical investigations of a scattered field expansion in terms of QNMs, using the prescribed excitation coefficients we deduced.
- How to practically use the results of isospectrality loss in order to detect the perturbation size to a gravitational Schwarzschild potential?.
- Study the effect of a quantum dot or a molecule on the resonant frequencies of a nanoparticle using pseudospectrum.
- Investigation the effect of purely imaginary frequencies in the compactly support potential or permittivity.
- Calculation the pseudospectrum in optical case with energy scalar product in order to detect any inconsistency.
- Calculation pseudospectrum using other foliations of space-time.
- Calculating pseudospectrum in Cauchy slices, using an L_2 scalar product defined just on the cavity.

Chapter 14

Appendix A: Energy scalar product: Gram matrix G^E

Let us first consider the integral

$$I_\mu(f,g) = \int_{-1}^{1} f(x)g(x)d\mu(x) \ , \tag{14.1}$$

with $d\mu(x) = \mu(x)dx$. We can get a quadrature approximation $I_\mu^N(f,g)$ to $I_\mu(f,g)$ by using expression (7.36) for N-interpolants (7.13) f_N and g_N, combined with the particular expression (17.22) for coefficients in the Chebyshev-Lobatto grid and the grid multiplication. We obtain then

$$I_\mu^N(f,g) = f_N^t \cdot C_\mu^N \cdot g_N \ , \tag{14.2}$$

with $f_N^t = (f(x_0),\ldots,f(x_N))^t$, $g_N^t = (g(x_0),\ldots,g(x_N))^t$ the $(N+1)$-grid approximates of f and g, respectively, and C_μ^N the diagonal matrix given by

$$\begin{aligned} (C_\mu^N)_{ij} &= (C_\mu^N)_i \, \delta_{ij} \\ (C_\mu^N)_i &= \frac{2\mu(x_i)}{\alpha_i N}\left(1 - \sum_{k=1}^{\lfloor \frac{N}{2} \rfloor} T_{2k}(x_i)\frac{2-\delta_{2k,N}}{4k^2-1}\right) \ , \end{aligned} \tag{14.3}$$

where we have used $T_0(x) = 1$, $T_k(1) = 1$ and $T_k(-1) = (-1)^k$. Then, dropping the indices N, we can write the discrete version of the scalar product $\langle \cdot,\cdot \rangle_E$ in (8.22) as

$$\begin{aligned} \langle u_1, u_2 \rangle_E &= \left\langle \begin{pmatrix} \phi_1 \\ \psi_1 \end{pmatrix}, \begin{pmatrix} \phi_2 \\ \psi_2 \end{pmatrix} \right\rangle_E \\ &= \frac{1}{2}\Big(\psi_1^* \cdot C_w \cdot \psi_2 + (\mathbb{D}\phi_1)^* \cdot C_p \cdot \mathbb{D}\phi_1 + \phi_1^* \cdot C_{\tilde{V}_\ell} \cdot \phi_2\Big) \ , \end{aligned} \tag{14.4}$$

that can be rewritten in matrix form as

$$\begin{aligned} \langle u_1, u_2 \rangle_E &= u_1^* \cdot G^E \cdot u_2 \\ &= (\bar{\phi}_1, \bar{\psi}_1) \left(\begin{array}{c|c} G_1^E & 0 \\ \hline 0 & G_2^E \end{array}\right) \begin{pmatrix} \phi_2 \\ \psi_2 \end{pmatrix} \ , \end{aligned} \tag{14.5}$$

with (here, the matrices $C_{\tilde{V}_\ell}$, C_p and C_w are given by (14.3), for the respective functions $\mu(x) = \tilde{V}_\ell(x), p(x), w(x)$)

$$\begin{aligned} G_1^E &= \frac{1}{2}\left(C_{\tilde{V}_\ell} + \mathbb{D}^t \cdot C_p \cdot \mathbb{D}\right) \\ G_2^E &= \frac{1}{2} C_w \ . \end{aligned} \tag{14.6}$$

These expressions define the Gram matrix G^E for the discretised version of the energy scalar product (8.22), in the basis determined from the Chebyshev-Lobatto spectral grid.

Grid interpolation

An important aspect to observe when performing the numerical integration is that 7.36 is exact whenever the original function $f(x)$ is a polynomial of order $\leq N$. With this in mind, and assuming that $f(x)$ and $g(x)$ are polynomials, Eq. (14.2) is exact only for the case where the product $(fg)(x)$ yields polynomials of order $\leq N$. In practical terms, the procedure described above hampers the accuracy of the scalar product's numerical integration whenever the order gets $> N$.

As an illustrative example, take $f(x) = P_\ell(x)$ and $g(x) = P_{\ell'}(x)$, with $P_\ell(x)$ the Legendre polynomials. Then the integral (14.1) — with $\mu(x) = 1$ omitted of the expression — yields $I(f,g) = 2\delta_{\ell,\ell'}/(2\ell+1)$. If we now consider the discrete version $I^N(f,g)$ given by Eq. (14.2), one observes that the exact result is obtained only for the cases $\ell + \ell' \leq N$, even though each individual function $f(x)$ and $g(x)$ is exactly represented for $\ell \leq N$ and $\ell' \leq N$, respectively.

To mitigate this issue, we modify the integration matrix C_μ^N — or equivalently the Gram matrix G^E — by incorporating the following interpolation strategy.

Given an interpolant vector $f_N(x_i)$ associated with a Chebyshev-Lobatto grid $\{x_i\}_{i=0}^N$, one can obtain a second interpolant vector $f_{\bar{N}}(\bar{x}_i)$ associated with another Chebyshev-Lobatto grid $\{\bar{x}_i\}_{i=0}^{\bar{N}}$ with a resolution $N \neq \bar{N}$ via

$$f_{\bar{N}}(\bar{x}_i) = \sum_{i=0}^{N} \mathbb{I}_{\bar{i}i}\, f_N(x_i) \ . \tag{14.7}$$

Components $\mathbb{I}_{\bar{i}i}$ of the interpolation matrix $\mathbb{I}$ are obtained by evaluating 7.13 at the grid $\{\bar{x}_i\}_{i=0}^{\bar{N}}$, with the coefficients $\{c_i\}_{i=0}^N$ expressed in terms of $f_N(x_i)$ via Eq. (17.22). Then

$$\mathbb{I}_{\bar{i}i} = \frac{1}{\alpha_i N}\left(1 + \sum_{j=1}^{N}(2-\delta_{j,N})T_j(\bar{x}_i)T_j(x_i)\right) \ . \tag{14.8}$$

Note that the interpolation matrix $\mathbb{I}$ has size $\bar{N} \times N$, which reduces to a square matrix only if $\bar{N} = N$. In this case, Eq. (14.8) is actually the identity matrix as expected.

Then, for a fixed N, we consider the discrete integration (14.2) in terms of a higher resolution $\bar{N} = 2N$ and interpolate the expression back to the original resolution N. In other words, defining $\mathcal{I}_\mu^N(f,g) := I_\mu^{\bar{N}}(f,g)$, we can consider the grid-interpolated new discrete integration

$$\mathcal{I}_\mu^N(f,g) = f_N^t \cdot \mathcal{C}_\mu^N \cdot g_N \ , \tag{14.9}$$

where $\mathcal{C}_\mu^N = \mathbb{I}^t \cdot C_\mu^{\bar{N}} \cdot \mathbb{I}$ or, in terms of its components

$$(\mathcal{C}_\mu^N)_{ij} = \sum_{\bar{i}=0}^{\bar{N}} \sum_{\bar{j}=0}^{\bar{N}} (\mathbb{I}^t)_{i\bar{i}} \, (C_\mu^{\bar{N}})_{\bar{i}\bar{j}} \, \mathbb{I}_{\bar{j}j} \ . \tag{14.10}$$

Going back to the illustrative example where $f(x) = P_\ell(x)$ and $g(x) = P_{\ell'}(x)$, we now obtain $\mathcal{I}^N(f,g) = 2\delta_{\ell,\ell'}/(2\ell+1)$ exactly whenever $\ell, \ell' \leq N$.

In the same way, we grid-interpolate the Gram matrices

$$\mathcal{G}_1^E = \mathbb{I}^t \cdot G_1^E \cdot \mathbb{I}, \quad \mathcal{G}_2^E = \mathbb{I}^t \cdot G_2^E \cdot \mathbb{I} \ , \tag{14.11}$$

that allows to perform the scalar product (14.5) via

$$\begin{aligned} \langle u_1, u_2 \rangle_E &= u_1^* \cdot \mathcal{G}^E \cdot u_2 \\ &= (\bar{\phi}_1, \bar{\psi}_1) \left(\begin{array}{c|c} \mathcal{G}_1^E & 0 \\ \hline 0 & \mathcal{G}_2^E \end{array} \right) \begin{pmatrix} \phi_2 \\ \psi_2 \end{pmatrix} . \end{aligned} \tag{14.12}$$

Chapter 15

Appendix B: Pöschl-Teller QNMs and regularity

We give here the derivation of Pöschl-Teller QNM frequencies (and QNM eigenfunctions in our setting). This is done for completeness and, more importantly, to illustrate with an explicit example the role of regularity in the enforcement of outgoing boundary conditions in the hyperboloidal scheme.

We start from the Fourier transform in time of the Pöschl-Teller wave equation in Bizoń-Mach coordinates, i.e. Eq. (10.12)

$$\Big((1-x^2)\frac{d^2}{dx^2} - 2(i\omega+1)x\frac{d}{dx} - i\omega(i\omega+1) - 1\Big)\phi = 0\ . \tag{15.1}$$

This equation can be solved in terms of hypergeometric functions. Making the change $x = 1-2z$, it is rewritten as

$$\begin{aligned}&\Big(z(1-z)\frac{d^2}{dz^2} \\ &+\big((1+i\omega) - 2(1+i\omega)z\big)\frac{d}{dz} - \big(i\omega(i\omega+1)+1\big)\Big)\phi = 0\ ,\end{aligned} \tag{15.2}$$

namely Euler's hypergeometric differential equation

$$\Big(z(1-z)\frac{d^2}{dz^2} + \big(c-(a+b+1)z\big)\frac{d}{dz} - ab\Big)\phi = 0\ , \tag{15.3}$$

for the values

$$\begin{aligned} c &= 1+i\omega \\ a &= \frac{(2i\omega+1)\pm i\sqrt{3}}{2} \\ b &= (2i\omega+1) - a = \frac{(2i\omega+1)\mp i\sqrt{3}}{2}\ . \end{aligned} \tag{15.4}$$

For each choice of ω, this equation admits two linearly independent solutions that can be built from the Gauss hypergeometric function ${}_2F_1(a,b;c;z)$. It is only when we enforce some regularity in the solution, that the spectral parameter ω is discretised and we recover the QNM frequencies. In this particular case, it is when we truncate the hypergeometric series ${}_2F_1(a,b;c;z)$ to a

polynomial, that we recover Pöschl-Teller QNM frequencies. Such truncation occurs when either a or b is a non-positive integer. From (15.4) we can write

$$\omega = \mp\frac{\sqrt{3}}{2} + i\Big(-a+\frac{1}{2}\Big) = \pm\frac{\sqrt{3}}{2} + i\Big(-b+\frac{1}{2}\Big)\ . \tag{15.5}$$

Therefore, imposing either $a=-n$ or $b=-n$, with $n\in\mathbb{N}\cup\{0\}$, we finally get

$$\omega_n^{\pm} = \pm\frac{\sqrt{3}}{2} + i\Big(n+\frac{1}{2}\Big)\ . \tag{15.6}$$

Choosing the $a=-n$ version, the corresponding eigenvectors can be written as Jacobi polynomials $P_n^{(\alpha,\beta)}(x)$, defined as

$$P_n^{(\alpha,\beta)}(x) = \frac{(\alpha+1)_n}{n!}\,{}_2F_1(-n,1+\alpha+\beta;\alpha+1;\frac{1-x}{2})\ , \tag{15.7}$$

with $(y)_n$ the Pochhammer symbol (i.e. $(y)_n = \prod_{k=0}^{n-1}(y-k)$). Inserting, for a given $n\in\mathbb{N}\cup\{0\}$, the values (15.4) and (15.6) into ${}_2F_1(a,b;c;z)$ we get, upon comparison with (15.7)

$$\alpha = \beta = i\omega_n\ , \tag{15.8}$$

so that Pöschl-Teller QNM eigenfunctions write, in Bizoń-Mach coordinates, as

$$\phi_n^{\pm}(x) = P_n^{(i\omega_n^{\pm},i\omega_n^{\pm})}(x)\ ,\ x\in[-1,1]\ . \tag{15.9}$$

Chapter 16

Appendix C: Differential geometry notations prerequisites

In this appendix we shall remind of some basic definitions from differential geometry that are necessary to understand Einstein equation and its solutions.

- Topology, When studying a function, one of its important properties to look at is its continuity. Similarly when studying spatial structures (formally topological spaces) we need formal notions to look at its connectivity. Topology studies the properties of topological spaces that are preserved under stretching and twisting (such as connectivity) with no respect to a distance. One of basic examples that is a circle is homeomorphic to an ellipse.
  Definition:
  Let M be a set, The power set of M is the set $P(M)$ that contains all the possible subsets of M including Φ and M. Then T
  $subset P(M)$ is called a topology on M if:

  - Both the empty set and M are elements of T.
  - $\forall X \subset M, and Y \subset M, \Rightarrow X \cup Y \subset M$. It follows that any union of elements of T is an element of T
  - $\forall X \subset M, and Y \subset M, \Rightarrow X \cap Y \subset M$. Any union of elements of T is an element of T. It follows that any intersection of finitely many elements of T is an element of T.

  If T is a topology on M, then the pair (M, T) is called a topological space.

- Topological Manifolds, The intuitive idea behind manifolds is to have a topological space that has locally the structure of R^n, where n (Cartesian structure) is the dimension of the manifold, Fig.16. Definition:
  Formally, a (topological) manifold is a Hausdorff space, with a countable basis, that is locally homeomorphic to Euclidean space, which means that each point p in the manifold M has an open neighborhood homeomorphic to an open neighborhood in Euclidean space. This leads to the notion of *local chart*, that is simply a way of parameterizing an open set $U \subset M$ by an open set $\tilde{U} \subset \mathbb{R}^n$:

$$\begin{aligned} \varphi : U \subset M &\rightarrow \tilde{U} \subset \mathbb{R}^n \\ p &\mapsto x^\mu \equiv (x^0, \ldots, x^{n-1}) \end{aligned} \tag{16.1}$$

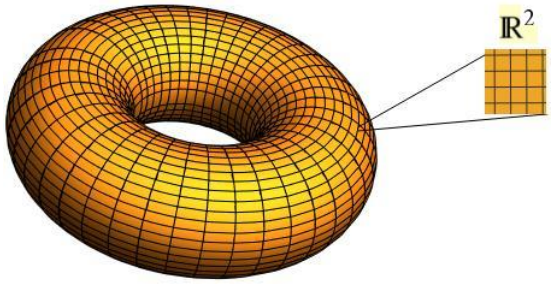

We require that φ is an homeomorphism (continuous with continuous inverse), so that at the local level the topology of M is that of $\mathbb{R}^n$. We do not have "access" directly to p, but to its coordinate representation $x^\mu = (x^0, \ldots, x^{n-1})$. The coordinate representation has no physical/geometrical content, and different labeling are possible:

$$\begin{array}{rcl} \varphi_1 : U_1 \subset M & \to & \tilde{U}_1 \in \mathbb{R}^n \\ p & \mapsto & (x^0, \ldots, x^{n-1}) \end{array} \quad , \quad \begin{array}{rcl} \varphi_2 : U_2 \subset M & \to & \tilde{U}_2 \in \mathbb{R}^n \\ p & \mapsto & (y^0, \ldots, y^{n-1}) \end{array} \tag{16.2}$$

so that

$$\begin{array}{rcl} \phi_2 \circ \phi_1^{-1} : \phi_1(U_1 \cap U_2) \subset \tilde{U}_1 \subset \mathbb{R}^n & \to & \phi_2(U_1 \cap U_2) \subset \tilde{U}_2 \in \mathbb{R}^n \\ (x^0, \ldots, x^{n-1}) & \mapsto & (y^0, \ldots, y^{n-1}) \end{array} \tag{16.3}$$

$$y^i \;=\; y^i(x^0, \ldots, x^{n-1}) \;\;,\;\; i \in \{1, \ldots, n-1\} \;. \tag{16.4}$$

- Vectors:
  - tangent vectors, Let L be a curve on a manifold M (which is a connected subset of M), so L can be represented by a parametrization $\gamma : I \subset \mathrm{R} \Rightarrow \mathrm{L} \subset M$. Let f be a scalar field on M (a function $f : M \longrightarrow \mathrm{R}$). At $p \in M$: $p = \gamma(0) \in \mathrm{L}$. The tangent vector v associated with γ at p is such that:

$$v(f) = \frac{df}{d\lambda}|_p = \frac{df}{dx^\mu}\frac{x^\mu}{d\lambda}|_p = \partial_\mu(f)\frac{x^\mu}{d\lambda}|_p = v^\mu \partial_\mu|_p(f) \tag{16.5}$$

    So $v = v^\mu \partial_\mu|_p$. Note that physicists normally are interested in v^μ. Here as we are studying general relativity it is of highly importance to consider how to relate an infinitesimal change of chart coordinates with an infinitesimal change of λ which could be different for each point of the curve in curved topological manifolds.
    As we have seen we introduced notions of differentiation to the manifolds, and this required the chart coordinates to be differentiable. We will consider just differentiable manifolds in what follows. Indeed the tangent vectors at a point p of a manifold form a vector space called "tangent space" at this point (T_pM). The elements of T p M are simply called vectors at p. The basis (∂_μ) is called the natural basis associated with the coordinates (x^μ). And the union of the tangent vectors at all points of a manifold is called a "tangent bundle" (TM).
  - A vector field is a mapping from M into the tangent bundle TM.

- Cotangent space (T_p^*M): It is the dual space of the tangent space T_pM. It is a set of linear forms $w : T_pM \longrightarrow \mathrm{R}$ Its basis are $\mathbf{d}x^\mu$ such that:

$$\langle \mathbf{d}x^\nu, \partial_\mu \rangle = \delta^\nu_\mu \tag{16.6}$$

The notation (dx) stems from the fact that if we apply the linear form $\mathbf{d}x^\nu$ to the infinitesimal displacement vector $\mathrm{d}x$, we get nothing but the number $\mathrm{d}x^\nu$:

$$\langle \mathbf{d}x^\nu, \mathrm{d}\mathbf{x} \rangle = \langle \mathbf{d}x^\nu, \mathrm{d}x\partial_\mu \rangle = \mathrm{d}x^\nu \tag{16.7}$$

- Tensors: we can define the space $\mathcal{T}^n_m(M)$ of n-times contravariant and m-covariant tensor fields as the ensemble of $C^\infty(M)$-multilinear smooth applications

$$\boldsymbol{T} : \mathcal{T}^*M \times \ldots^n \times \mathcal{T}^*M \times \mathcal{T}M \times \ldots^m \times \mathcal{T}M \to C^\infty(M) \ . \tag{16.8}$$

$\mathcal{T}^n_m(M)$ is also denoted as $\binom{n}{m}$. We note that $\mathcal{T}M = \mathcal{T}^1_0(M)$ and $\mathcal{T}^*M = \mathcal{T}^0_1(M)$. Using the notion of tensor product (over the module $C^\infty(M)$), we can write $\mathcal{T}^n_m(M)$ as

$$\mathcal{T}^n_m(M) = \mathcal{T}M \otimes \ldots^n \mathcal{T}M \otimes \mathcal{T}^*M \times \ldots^m \mathcal{T}^*M = \mathcal{T}M^{\otimes n} \otimes \mathcal{T}^*M^{\otimes m} \tag{16.9}$$

This characterization has the advantage of providing directly a local chart basis in $\mathcal{T}^n_m(M)$, in terms of tensor products of the basis. In brief, we can write

$$\boldsymbol{T} = T^{\mu_1\mu_2\ldots\mu_n}{}_{\nu_1\nu_2\ldots\nu_m} \partial_{\mu_1} \otimes \partial_{\mu_2} \ldots \otimes \partial_{\mu_n} \otimes dx^{\nu_1} \otimes dx^{\nu_2} \ldots \otimes dx^{\nu_m} \ , \ \forall \boldsymbol{T} \in \mathcal{T}^n_m(M) \ . \tag{16.10}$$

This permits us to write the transformation rule of tensors under a change of coordinates. If we write in two coordinate systems

$$\mathbf{T} = T^{i_1\ldots i_n}{}_{j_1\ldots j_m} \frac{\partial}{\partial x^{i_1}} \otimes \ldots \otimes \frac{\partial}{\partial x^{i_n}} \otimes dx^{j_1} \otimes \ldots \otimes dx^{j_m}$$

and

$$\mathbf{T} = T'^{i_1\ldots i_n}{}_{j_1\ldots j_m} \frac{\partial}{\partial x'^{i_1}} \otimes \ldots \otimes \frac{\partial}{\partial x'^{i_n}} \otimes dx'^{j_1} \otimes \ldots \otimes dx'^{j_m} \ ,$$

then it follows from multilinearity

$$T'^{i_1\ldots i_n}{}_{j_1\ldots j_m} = \left(\frac{\partial x'^{i_1}}{\partial x^{k_1}}\right) \ldots \left(\frac{\partial x'^{i_n}}{\partial x^{k_n}}\right) \left(\frac{\partial x^{l_1}}{\partial x'^{j_1}}\right) \ldots \left(\frac{\partial x^{l_m}}{\partial x'^{j_m}}\right) T^{k_1\ldots k_n}{}_{l_1\ldots l_m} \ .$$

- Fields on a manifold: A tensor field of type $\binom{k}{l}$ is a map which associates to each point $p \in M$ a tensor of type $\binom{k}{l}$. A scalar field is a tensor field of type $\binom{0}{0}$. A frame field or moving frame is a n-uplet of vector fields (e_α) such that at each point $p \in M$, $(e_\alpha(p))$ is a basis of the tangent space T_pM . If $n = 4$, a frame field is also called a tetrad and if $n = 3$, it is called a triad

Till now we have seen mathematical definition to enter in general relativity these notions should be dressed with considering points of a manifold as events in the universe. Considering the universe as a manifold shows the absence of a priori geometric meaning in the coordinates. All structures in the theory of in general relativity must be determined dynamically. In particular, this means that the a priori notion of (global) inertial reference frame is absent. Still, in order to have an analytical description, we need to associate to a physical event p some "labels" (t, x, y, z).

However, now the "coordinates" (t, x, y, z) are completely devoid of geometric or physical meaning. They do not have intrinsic meaning. Physical statements must be also independent of the choice of coordinates.

Although to describe things In particular, we require that space-time events to be locally parametrized by coordinates. We require that M can be locally patched to open sets in $\mathbb{R}^4$ (Manifold - with charts).

Still this structure have to have the notions of a measure between different events and what are the light directions, timelike, and spacelike too. Here we come to introducing a metric tensor.

16.0.1 Metric tensor

The metric tensor introduces the notion of measure and scalar product on a smooth manifold. It is a bilinear form that satisfies:

- $\boldsymbol{g}$ is a 2-times covariant tensor

$$\boldsymbol{g} = g_{\mu\nu} dx^\mu \otimes dx^\nu \tag{16.11}$$

- Symmetry: $g_{\mu\nu} = g_{\nu\mu}$.
- Non-degenercy: if $\boldsymbol{V}$ is such that $\boldsymbol{g}(\boldsymbol{V}, \boldsymbol{W}) = 0$, $\forall \boldsymbol{W}$, then $\boldsymbol{V} = 0$

The signature is a feature of the metrics, according to Sylvester's law of inertia, the metric which is diagonalizable has negative diagonal elements and positive onse such as the number of all is n. If at each T_pM, a basis can be chosen such that the first component is negative and the rest are positive, then we name it a Lorentzian metric

$$\boldsymbol{g}_p = \begin{pmatrix} -1 & & & \\ & 1 & & \\ & & 1 & \\ & & & 1 \end{pmatrix} \tag{16.12}$$

. And the signature is (-, +,+,+). The squared-norm of a vector is given by

$$V^2 = \boldsymbol{g}(\boldsymbol{V}, \boldsymbol{V}) = g_{\mu\nu} V^\mu V^\nu = V^\mu V_\mu \tag{16.13}$$

The Lorentzian nature of $g_{\mu\nu}$ permit to classify the vectors in three cathegories

i) Spacelike vectors: $g_{\mu\nu} V^\mu V^\nu > 0$.

ii) Timelike vectors: $g_{\mu\nu} V^\mu V^\nu < 0$.

iii) Lightlike or null vectors: $g_{\mu\nu} V^\mu V^\nu = 0$.

This could be figured as attaching to every point of the manifold a "Light cone" as vectors in T_pM of zero norm, on which the light moves. If a particle is moving faster than light then its trajectory will be outside the light cone and called spacelike trajectory, which if less than light it is called a timelike one.

Measuring distances: element of line.

This small section is fully taken from [99].
The light cone structure of the space-time allows us to structural the space-time in spacelike, timelike and lightlike directions. But the metric has more structure (actually very little more, just a scale), permitting us to measure distances spacelike curves and time intervals along timelike curves. This is provided by the notion of *element of line* associated to the metric in a given coordinate system, simply a quadratic form on infinitesimal displacements in space-time:

$$ds^2 = g_{\mu\nu} dx^\mu dx^\mu \tag{16.14}$$

This can be seen as a generalization of Pythagoras theorem for infinitesimal triangles.

If we consider a spacelike curve $\gamma(\lambda)$ parametrized by λ in coordinates $\{x^\mu\}$, i.e. $(x^\mu(\lambda))$, the evaluation of (16.14) on $\gamma(\lambda)$ gives

$$ds^2 = g_{\mu\nu}(\gamma(\lambda)) \frac{dx^\mu}{d\lambda} \frac{dx^\mu}{d\lambda} d\lambda^2 \quad . \tag{16.15}$$

For a spacelike curves the *arc length* can be simply written as

$$ds = \sqrt{g_{\mu\nu}(\gamma(\lambda)) \frac{dx^\mu}{d\lambda} \frac{dx^\nu}{d\lambda}} d\lambda \tag{16.16}$$

With our convention for the space-time signature $(-1, 1, 1, 1)$, the element of proper time along timelike curves is given by $-c^2 d\tau = ds^2$, that is

$$d\tau = \frac{1}{c} \sqrt{\left| g_{\mu\nu}(\gamma(\lambda)) \frac{dx^\mu}{d\lambda} \frac{dx^\nu}{d\lambda} \right|} d\lambda \tag{16.17}$$

.

Levi−Civita tensor Orientable manifolds means that there is a n-form ϵ such that for any orthonormal basis (regarding the metric) e_i it gives: $\epsilon(e_1, e_2, ...e_n) = \pm 1$ The singes indicate the orientation, choosing an orientation we call ϵ as Levi−Civita tensor.

16.0.2 Derivatives

Covariant derivative − metric dependence

We have seen notions of scalar product between two vectors, but to estimate the change of a vector from point to another we have to be more careful since the tangent vector at a point belongs only to the tangent space at this point and not to other tangent vector spaces. Hence one should find an extra-structure to relate vectors from two different tangent spaces. This structure is called an affine connection ∇, and the $\nabla_u v$ is called the covariant derivative of v along u, and defined as the following:

$$\begin{aligned} &\nabla : \mathfrak{X}(M) \times \mathfrak{X}(M) \to \mathfrak{X}(M) \\ &(u, v) \mapsto \nabla_u(v) \end{aligned} \tag{16.18}$$

- ∇ is bilinear.

- For any scalar field f:
$$\nabla_{fu} v = f \nabla_u v \tag{16.19}$$
- Leibniz rule
$$\nabla_u f v = \langle u, \nabla f \rangle v + f \nabla_u v \tag{16.20}$$
where ∇f is the differential of f.

The variation of a vector from point to another is the covariant derivative along the cotangent vectors $\mathrm{d}v \nabla_{\mathrm{d}x} v$. A vector v is parallelly transported with respect to the affine connection if $\mathrm{d}v = 0$. Having e_α, e_β, e_γ elements from a bases at a certain point, the variation of one of them along another is:

$$\nabla_{e_\alpha} e_\beta = \Gamma^\gamma_{\alpha\beta} e_\gamma \tag{16.21}$$

Levi−Civita connection This connection is:

- Torsion free, i.e.
$$\nabla_\alpha \nabla_\beta f = \nabla_\beta \nabla_\alpha f \tag{16.22}$$
- $\nabla \mathrm{g} = 0$

$\Gamma^\mu_{\alpha\beta}$ for this connection is called Christoffel symbols, and it is given by:

$$\Gamma^\gamma_{\alpha\beta} = \frac{1}{2} \mathrm{g}^{\gamma\mu} \left(\frac{\partial \mathrm{g}_{\mu\beta}}{\partial x^\alpha} + \frac{\partial \mathrm{g}_{\alpha\mu}}{\partial x^\beta} - \frac{\partial \mathrm{g}_{\alpha\beta}}{\partial x^\mu} \right) \tag{16.23}$$

This leads to an important way to look at the variation of a vector:

$$\nabla \mathrm{v} = \nabla_\mu \mathrm{v}^\mu = \frac{1}{\sqrt{|\mathrm{g}|}} \frac{\partial}{\partial x^\mu} \left(\sqrt{|\mathrm{g}|} \mathrm{v}^\mu \right) \tag{16.24}$$

Lie derivative

The extra−structure here is a reference vector field, let it be u, then:

$$\begin{aligned} \mathcal{L}_\mathrm{u} \mathrm{v} &= [\mathrm{u}, \mathrm{v}] \\ &= \mathrm{u}^\mu \frac{\partial \mathrm{v}^\alpha}{\partial x^\mu} - \mathrm{v}^\mu \frac{\partial \mathrm{u}^\alpha}{\partial x^\mu} \end{aligned} \tag{16.25}$$

Exterior derivative

This derivative only concerns the differential forms. The exterior derivative of a $q-$form ω is a $(q+1)-$form which is denoted $\mathrm{d}\omega$. For example if ω is a $2-$form:

$$(\mathrm{d}\omega)_{\alpha\beta\gamma} = \frac{\partial \omega_{\alpha\beta}}{\partial x^\gamma} + \frac{\partial \omega_{\beta\gamma}}{\partial x^\alpha} + \frac{\partial \omega_{\gamma\alpha}}{\partial x^\beta} \tag{16.26}$$

This derivative satisfies always: $\mathrm{dd}\omega = 0$

16.0.3 Curvature

Actually all the previous definition has been written in order to be able to enlight the curvature. For a torsion free affine connection the curvature is defined as:

$$R^{\mu}_{\gamma\alpha\beta}\omega^{\gamma} = (\nabla_{\alpha}\nabla_{\beta} - \nabla_{\beta}\nabla_{\alpha})\omega^{\mu} \tag{16.27}$$

Ricci tensor

Ricci tensor is given by:

$$R_{\alpha\beta} = R^{\mu}_{\alpha\mu\beta} \tag{16.28}$$

Ricci scalar is the trace of the Ricci tensor with respect to the metric g, it's given by:

$$R = g^{\mu\nu}R_{\mu\nu} \tag{16.29}$$

16.0.4 Geodesics, geodesic equation

A geodesics line represent the shortest path between two points in a manifold. Note that in a given space-time, geodesic lines represent light (massless particles) trajectories in a space-time. Formally it is defined as the following:
"A smooth curve L of a pseudo-Riemannian manifold (M, g) is called a geodesic iff it admits a parametrization P whose associated tangent vector field v is transported parallelly to itself along L : $\nabla_v v = 0$, where ∇ is the Levi-Civita connection of the metric g. " [84].

Chapter 17

Appendix D: The coefficients for different grids

We explain in this appendix the derivations of Chebyshev coefficients in different grids.

- Coefficients in Gauss grid:
  Having $k, m \in \mathbb{Z}$ let us define q as: $q = e^{\frac{i\pi(k-m)}{2(N+1)}}$, for the grid of Gauss, it is straight forward that:
  $$q^{4(N+1)} = 1 \tag{17.1}$$
  Let us now calculate the following sum: $S1 = \sum_{j=0}^{2N+1} e^{i(k-m)\phi_j}$:
  $$S1 = q \sum_{j=0}^{2N+1} (q^2)^j = \begin{cases} q(2N+2) & q = \pm 1 \\ \dfrac{q^{2N+2}-1}{q^2-1} & q \neq \pm 1 \end{cases} \tag{17.2}$$
  But because of eq.17.1, and taking into account that $-N < k, m < N$, then:
  $$S1 = 2(N+1)\delta_{mk} \tag{17.3}$$
  and
  $$\sum_{j=0}^{2N+1} \chi_j e^{-im\phi_j} = \sum_{j=0}^{2N+1} \sum_{k=-N}^{+N} \gamma_k e^{ik\phi_j} e^{-im\phi_j} = \sum_{k=-N}^{+N} \gamma_k \sum_{j=0}^{2N+1} e^{i(k-m)\phi_j} \tag{17.4}$$
  $$\sum_{j=0}^{2N+1} \chi_j e^{-im\phi_j} = \sum_{k=-N}^{+N} \gamma_k (2N+2)\delta_{mk} = 2(N+1)\gamma_m \tag{17.5}$$
  The last equation is a formula for calculating the coefficients as the following:
  $$c_m = 2\gamma_m = \frac{1}{N+1} \sum_{j=0}^{2N+1} \chi_j e^{-im\phi_j} = \frac{1}{N+1} (\sum_{j=0}^{N} \chi_j e^{-im\phi_j} + \sum_{l=1}^{N+1} \chi_{N+l} e^{-im\phi_{N+l}}) \tag{17.6}$$
  For $0 \leqslant l \leqslant N$:
  $$\phi_{N+l} = \frac{\pi}{N+1}(N+l+\frac{1}{2}) = 2\pi - \frac{\pi}{N+1}(N+1-l+\frac{1}{2}) = 2\pi - \phi_{N+1-l}, \tag{17.7}$$

it follows that: $e^{-im\phi_{N+l}} = e^{im\phi_{N+1-l}}$ and $\chi_{N+l} = \chi_{N+1-l}$ inserting this in eq.17.6, one gets:

$$c_m = 2\gamma_m = \frac{1}{N+1}(\sum_{j=0}^{N} \chi_j e^{-im\phi_j} + \sum_{l=1}^{N+1} \chi_{N+1-l} e^{im\phi_{N+1-l}}) \tag{17.8}$$

This leads to:

$$c_m = \frac{1}{N+1}\sum_{j=0}^{N} \chi_j (e^{-im\phi_j} + e^{im\phi_j}) = \frac{2}{N+1}\sum_{j=0}^{N} \chi_j \cos(m\phi_j) \tag{17.9}$$

and finally:

$$c_m = \frac{2}{N+1}\sum_{j=0}^{N} \psi(x_j) T_m(x_j) \tag{17.10}$$

- Coefficients in Lobatto grid:
  I am following here exactly the same procedure as in Gauss grid, adapted to Lobatto one. Having $k, m \in \mathbb{Z}$ let us define q as: $q = e^{\frac{i\pi(k-m)}{N}}$, for the grid of Lobatto, it is straight forward that:

$$q^{2N} = 1 \tag{17.11}$$

Now calculating the following sum: $S2 = \sum_{j=0}^{2N-1} e^{i(k-m)\phi_j}$:

$$S2 = \sum_{j=0}^{2N-1} q^j = \begin{cases} 2N & q = 1 \\ 0 & q \neq 1 \end{cases} \tag{17.12}$$

then

$$S2 = \begin{cases} 2N & m - k = 2N\, p; p \in \mathbb{Z} \\ 0 & \text{otherwise} \end{cases} \tag{17.13}$$

So for $-N \leq k \leq N$

$$S2 = 2N \times \begin{cases} \delta_{mk} & 0 < m < N \\ \delta_{Nk} + \delta_{(-N)k} & m = N \end{cases} \tag{17.14}$$

Now looking at the sum:

$$\sum_{j=0}^{2N-1} \chi_j e^{-im\phi_j} = \sum_{j=0}^{2N-1} \sum_{k=-N}^{+N} \gamma_k e^{ik\phi_j} e^{-im\phi_j} = \sum_{k=-N}^{+N} \gamma_k \sum_{j=0}^{2N-1} e^{i(k-m)\phi_j} \tag{17.15}$$

Using eq.17.14, then:

$$\sum_{j=0}^{2N-1} \chi_j e^{-im\phi_j} = 2N \times \begin{cases} \gamma_m & 0 < m < N \\ \gamma_{-N} + \gamma_N = 2\gamma_N & m = N \end{cases} \tag{17.16}$$

so for $0 \leq m \leq N$ one can write:

$$\gamma_m = \frac{2 - \delta_{mN}}{4N} \sum_{j=0}^{2N-1} \chi_j e^{-im\phi_j} \tag{17.17}$$

The last equation is a formula for calculating the coefficients as the following:

$$c_m = 2\gamma_m = \frac{2-\delta_{mN}}{4N}\sum_{j=0}^{2N-1}\chi_j e^{-im\phi_j} = \frac{2-\delta_{mN}}{4N}(\chi_0+\sum_{j=1}^{N-1}\chi_j e^{-im\phi_j}+\sum_{l=1}^{N-1}\chi_{N+l}e^{-im\phi_{N+l}}+\chi_N e^{-im\phi_N}) \tag{17.18}$$

For $0 \leqslant l \leqslant N$:

$$\phi_{N+l} = \frac{\pi(N+l)}{N} = 2\pi - \frac{\pi(N-l)}{N} = 2\pi - \phi_{N-l}, \tag{17.19}$$

it follows that: $e^{-im\phi_{N+l}} = e^{im\phi_{N-l}}$ and $\chi_{N+l} = \chi_{N-l}$ inserting this in eq.17.18, one gets:

$$c_m = 2\gamma_m = \frac{2-\delta_{mN}}{4N}(\chi_0 + (-1)^m\chi_N + \sum_{j=1}^{N-1}\chi_j e^{-im\phi_j} + \sum_{l=1}^{N-1}\chi_{N-l}e^{im\phi_{N-l}} \tag{17.20}$$

This leads to:

$$c_m = \frac{2-\delta_{mN}}{4N}(\chi_0+(-1)^m\chi_N+\sum_{j=1}^{N-1}\chi_j(e^{-im\phi_j}+e^{im\phi_j}) = \frac{2-\delta_{mN}}{4N}(\chi_0+(-1)^m\chi_N+2\sum_{j=1}^{N-1}\chi_j\cos(m\phi_j)) \tag{17.21}$$

and finally:

$$c_m = \frac{2-\delta_{mN}}{4N}(\psi(1) + (-1)^m\psi(-1) + 2\sum_{j=1}^{N-1}\psi(x_j)T_m(x_j)) \tag{17.22}$$

- Coefficients in Right-Radau grid:
  In this grid: $\phi_j = \frac{2\pi j}{2N+1}$ Having $k, m \in \mathbb{Z}$ i define q as: $q = e^{\frac{i2\pi(k-m)}{2N+1}}$, then:

$$q^{2N+1} = 1 \tag{17.23}$$

Now calculating the following sum: $S3 = \sum_{j=0}^{2N} e^{i(k-m)\phi_j}$:

$$S3 = \sum_{j=0}^{2N} q^j = \begin{cases} 2N+1 & q = 1 \\ \dfrac{q^{2N+1}-1}{q-1} = 0 & q \neq 1 \end{cases} \tag{17.24}$$

then

$$S3 = \begin{cases} 2N+1 & m-k = 2N\,p; p \in \mathbb{Z} \\ 0 & \text{otherwise} \end{cases} \tag{17.25}$$

So for $-N \leq k \leq N$

$$S3 = (2N+1)\delta_{mk} \tag{17.26}$$

Now looking at the sum:

$$\sum_{j=0}^{2N+1}\chi_j e^{-im\phi_j} = \sum_{j=0}^{2N+1}\sum_{k=-N}^{+N}\gamma_k e^{ik\phi_j}e^{-im\phi_j} = \sum_{k=-N}^{+N}\gamma_k\sum_{j=0}^{2N+1}e^{i(k-m)\phi_j} \tag{17.27}$$

Using eq.17.26, then:

$$\sum_{j=0}^{2N+1}\chi_j e^{-im\phi_j} = (2N+1)\gamma_m \tag{17.28}$$

then

$$\gamma_m = \frac{1}{2N+1}\sum_{j=0}^{2N+1}\chi_j e^{-im\phi_j} \tag{17.29}$$

The last equation is a formula for calculating the coefficients as the following:

$$c_m = 2\gamma_m = \frac{2}{2N+1}\sum_{j=0}^{2N+1}\chi_j e^{-im\phi_j} = \frac{2}{2N+1}(\chi_0 + \sum_{j=1}^{N}\chi_j e^{-im\phi_j} + \sum_{l=1}^{N}\chi_{N+l}e^{-im\phi_{N+l}}) \tag{17.30}$$

For $1 \leqslant l \leqslant N$:

$$\phi_{N+l} = \frac{2\pi(N+l)}{2N+1} = 2\pi - \frac{2\pi(N+1-l)}{2N+1} = 2\pi - \phi_{N+1-l}, \tag{17.31}$$

it follows that: $e^{-im\phi_{N+l}} = e^{im\phi_{N+1-l}}$ and $\chi_{N+l} = \chi_{N+1-l}$ inserting this in eq.17.30, one gets:

$$c_m = 2\gamma_m = \frac{2}{2N+1}(\chi_0 + \sum_{j=1}^{N}\chi_j e^{-im\phi_j} + \sum_{l=1}^{N}\chi_{N+1-l}e^{im\phi_{N+1-l}} \tag{17.32}$$

This leads to:

$$c_m = \frac{2}{2N+1}(\chi_0 + \sum_{j=1}^{N}\chi_j(e^{-im\phi_j} + e^{im\phi_j}) = \frac{4}{2N+1}(\frac{\chi_0}{2} + \sum_{j=1}^{N}\chi_j\cos(m\phi_j)) \tag{17.33}$$

and finally:

$$c_m = \frac{4}{2N+1}(\frac{\psi(1)}{2} + \sum_{j=1}^{N}\psi(x_j)T_m(x_j)) \tag{17.34}$$

- Coefficients in Left-Radau grid:
  In this grid: $\phi_j = \pi - \frac{2\pi j}{2N+1}$, and $x_j = -\cos\frac{2\pi j}{2N+1}$ It is more efficient to find the relation of this grid's coefficient in term of right-Radau grid ones. So let us use the auxiliary function: $\eta(x) = -\psi(x)$, and the points $\tilde{x_j} = -x_j$ correspond to the right-Radau grid points. Using the property of: $T_m(-x) = (-1)^m T_m(x)$, one can relate the expansion in the two Radau grids:

$$\psi_N(x) = \eta_N(x) = \frac{\tilde{c_0}}{2} + \sum_{m=1}^{N}\tilde{c_m}T_m(-x) = \frac{\tilde{c_0}}{2} + \sum_{m=1}^{N}(-1)^m\tilde{c_m}T_m(x) \tag{17.35}$$

then we get: $c_m = (-1)^m\tilde{c_m}$ Using eq.17.34:

$$\tilde{c_m} = \frac{4}{2N+1}(\frac{\eta(1)}{2} + \sum_{j=1}^{N}\eta(\tilde{x_j})T_m(\tilde{x_j})) = \frac{4}{2N+1}(\frac{\psi(-1)}{2} + \sum_{j=1}^{N}\psi(x_j)(-1)^m T_m(x_j)) \tag{17.36}$$

using the relation between the coefficients of the two grids:

$$c_m = \frac{4}{2N+1}(\frac{(-1)^m\,\psi(-1)}{2} + \sum_{j=1}^{N}\psi(x_j)T_m(x_j)) \tag{17.37}$$

Chapter 18

Appendix E: Chebyshev differential matrix

We show here the derivation of coefficients in Chebyshev differential matrices for different grids.

18.0.1 Right Radau

Considering right Radau grid, From eq.7.20 one can write:

$$\bar{\chi}_N(\phi) = \sum_{-N}^{+N} \bar{\gamma}_k^{\chi} e^{ik\phi} \tag{18.1}$$

where from eq.17.29, we have:

$$\bar{\gamma}_k^{\chi} = \frac{1}{2N+1} \sum_{0}^{2N} \chi(\phi_j) e^{-ik\phi_j} \tag{18.2}$$

Taking the derivative of $\bar{\chi}_N(\phi)$, gives:

$$\begin{aligned} \bar{\chi'}_N(\phi_m) &= \sum_{-N}^{+N} ik\bar{\gamma}_k^{\chi} e^{ik\phi_m} \\ &= \sum_{-N}^{+N} ike^{ik\phi_m} (\frac{1}{2N+1} \sum_{j=0}^{2N} \chi(\phi_j) e^{-ik\phi_j}) \\ &= \sum_{j=0}^{2N} \Delta_{mj}^1 \chi(\phi_j) \end{aligned} \tag{18.3}$$

and the second derivative of $\bar{\chi}_N(\phi)$, gives:

$$\begin{aligned} \bar{\chi''}_N(\phi_m) &= \sum_{-N}^{+N} -k^2\bar{\gamma}_k^{\chi} e^{ik\phi_m} \\ &= \sum_{-N}^{+N} -k^2 e^{ik\phi_m} (\frac{1}{2N+1} \sum_{j=0}^{2N} \chi(\phi_j) e^{-ik\phi_j}) \\ &= \sum_{j=0}^{2N} \Delta_{mj}^2 \chi(\phi_j) \end{aligned} \tag{18.4}$$

where:

$$\begin{aligned}\Delta^1_{mj} =& \frac{i}{2N+1}\sum_{k=-N}^{+N} k e^{ik(\phi_m-\phi_j)}\\ =& \frac{i}{2N+1}\sum_{k=-N}^{+N} k e^{\frac{2\pi ik(m-j)}{2N+1}}\\ =& \frac{i}{2N+1}\sum_{k=-N}^{+N} k q^k\end{aligned} \tag{18.5}$$

and

$$\begin{aligned}\Delta^2_{mj} =& \frac{-1}{2N+1}\sum_{k=-N}^{+N} k^2 e^{ik(\phi_m-\phi_j)}\\ =& \frac{-1}{2N+1}\sum_{k=-N}^{+N} k^2 e^{\frac{2\pi ik(m-j)}{2N+1}}\\ =& \frac{-1}{2N+1}\sum_{k=-N}^{+N} k^2 q^k\\ =& \frac{-1}{2N+1}\sum_{k=-N}^{+N} k^2 q^k\end{aligned} \tag{18.6}$$

where $q = e^{\frac{2\pi i(m-j)}{2N+1}}$, to calculate the last sum, let us define:

$$f(q) = \sum_{k=-N}^{+N} q^k = \frac{q^{N+1} - q^{-N}}{q-1} \tag{18.7}$$

so:

$$f'(q) = \sum_{k=-N}^{+N} k q^{k-1} = \frac{q^{-N-1}[(N(q-1)-1)q^{2N+1} + N(q-1) + q]}{(q-1)^2} \tag{18.8}$$

$$\begin{aligned}f''(q) =& \sum_{k=-N}^{+N} k(k-1)q^{k-2}\\ =& \frac{N^2q^{N+1} - (N+1)(2N-1)q^N + N(N+1)q^{N-1} - (N+1)^2q^{-N} + N(2N+3)q^{-N-1} - N(N+1)q^{-N-2}}{(q-1)^2}\end{aligned} \tag{18.9}$$

and because of $q^{2N+1} = 1$ and $q \neq 1$ (17.23), then:

$$f'(q) = \frac{(2N+1)q^{-N-1}}{q-1} \tag{18.10}$$

$$f''(q) = \frac{(2N+1)(q^N - q^{-N})}{(q-1)^2} \tag{18.11}$$

thus for $m \neq j$:

$$\Delta^1_{mj} = \frac{iq}{2N+1} \sum_{k=-N}^{+N} kq^{k-1} = \frac{iq}{2N+1} f'(q) = \frac{iq^{-N}}{q-1} \tag{18.12}$$

and

$$\begin{aligned} \Delta^2_{mj} &= \frac{-q^2}{2N+1} \sum_{k=-N}^{+N} k^2 q^{k-2} \\ &= \frac{-1}{2N+1}[q^2 \sum_{k=-N}^{+N} k(k-1)q^{k-2} + q^1 \sum_{k=-N}^{+N} kq^{k-1}] \\ &= \frac{-1}{2N+1}[q^2 f''(q) + q^1 f'(q)] = \end{aligned} \tag{18.13}$$

developing it, one gets:

$$\Delta^1_{mj} = \frac{1}{2} \frac{(-1)^{m-j}}{\sin[\frac{\pi}{2N+1}(m-j)]} \tag{18.14}$$

and

$$\Delta^2_{mj} = \frac{-1}{2} \frac{(-1)^{m-j} \cos[\frac{\pi}{2N+1}(m-j)]}{\sin^2[\frac{\pi}{2N+1}(m-j)]} \tag{18.15}$$

for $m = j$ (then $q = 1$):

$$\Delta^1_{mj} = 0 \tag{18.16}$$

$$\Delta^2_{mj} = -\frac{1}{3} N(N+1) \tag{18.17}$$

Therefore:

$$\bar{\chi'}_N(\phi_m) = \sum_{j=0}^{2N} \Delta^1_{mj} \chi(\phi_j) = \frac{1}{2} \sum_{j=0, j\neq m}^{2N} \frac{(-1)^{m-j}}{\sin[\frac{\pi}{2N+1}(m-j)]} \chi(\phi_j) \tag{18.18}$$

In the same way, one gets $\bar{\chi''}$:

$$\bar{\chi''}_N(\phi_m) = \sum_{j=0}^{2N} \Delta^2_{mj} \chi(\phi_j) = -\frac{1}{2} \sum_{j=0, j\neq m}^{2N} \frac{(-1)^{m-j} \cos[\frac{\pi}{2N+1}(m-j)]}{\sin^2[\frac{\pi}{2N+1}(m-j)]} \chi(\phi_j) - \frac{1}{3} N(N+1) \chi(\phi_m) \tag{18.19}$$

In his notes Ansorg started by defining $\chi_N(\phi) = \psi_N(\cos\phi)$, in order to find the relation between the derivation matrix elements in Fourier series with the corresponding ones using Chebyshev polynomials.

$$\begin{aligned} \frac{\partial \chi_N}{\partial \phi} &= -\sqrt{1-x^2}\psi'_N(x) \\ \frac{\partial^2 \chi_N}{\partial \phi^2} &= -x\psi'_N(x) + (1-x^2)\psi''_N(x) \\ \frac{\partial^4 \chi_N}{\partial \phi^4} &= x\psi'_N(x) + (7x^2-4)\psi''_N(x) - 6x(1-x^2)\psi'''_N(x) + (1-x^2)^2 \psi^{(}(4))_N(x) \end{aligned} \tag{18.20}$$

It follows that:

$$\psi'_N(x) = \begin{cases} -\dfrac{1}{\sqrt{1-x^2}}\dfrac{\partial \chi_N}{\partial \phi} & x \neq \pm 1 \\ \pm \dfrac{\partial^2 \chi_N}{\partial \phi^2} & x = \pm 1. \end{cases} \tag{18.21}$$

$$\psi''_N(x) = \begin{cases} -\dfrac{1}{(1-x^2)}(\dfrac{\partial^2 \chi_N}{\partial \phi^2} + x\psi'_N(x)) & x \neq \pm 1 \\ \dfrac{1}{3}(\dfrac{\partial^4 \chi_N}{\partial \phi^4} - x\psi'_N(x)) & x = \pm 1. \end{cases} \tag{18.22}$$

Because of $\chi_N(\phi_{N+l}) = \chi_N(\phi_{N+1-l})$, one can writes:

$$\frac{\partial^\nu \chi_N}{\partial \phi^\nu}(\phi_m) = \Delta^\nu_{m0}\chi_N(\phi_0) + \sum_{j=1}^{N}(\Delta^\nu_{mj} + \Delta^\nu_{m,(2N+1-j)})\chi_N(\phi_j) = \Delta^\nu_{m0}\chi_N(\phi_0) + \sum_{j=1}^{N}(\Delta^\nu_{mj} + \Delta^\nu_{m,(-j)})\chi_N(\phi_j). \tag{18.23}$$

The last equality is because:

$$\begin{aligned} \sin\frac{\phi_{k-(2N+1)}}{2} &= \sin(\frac{\phi_k}{2} - \pi) = -\sin\frac{\phi_k}{2} \\ \cos\frac{\phi_{k-(2N+1)}}{2} &= \sin(\frac{\phi_k}{2} - \pi) = -\cos\frac{\phi_k}{2} \end{aligned} \tag{18.24}$$

using eq.18.14 and eq.18.16, the last equations lead to:

$$\Delta^1_{m,2N+1-j} = \Delta^1_{m,(-j)}. \tag{18.25}$$

On the other hand

$$\begin{aligned} \sin\frac{\phi_k}{2} &= \frac{1}{\sqrt{2}}\sqrt{1-x_k} \\ \cos\frac{\phi_k}{2} &= \frac{1}{\sqrt{2}}\sqrt{1+x_k} \end{aligned} \tag{18.26}$$

where $x_k = \cos\phi_k$ this leads to:

$$\begin{aligned} \sin\frac{\phi_m \pm \phi_j}{2} &= \frac{1}{2}[\sqrt{1-x_m}\sqrt{1+x_j} \pm \sqrt{1+x_m}\sqrt{1-x_j}] \\ \cos\frac{\phi_m \pm \phi_j}{2} &= \frac{1}{2}[\sqrt{1+x_m}\sqrt{1+x_j} \mp \sqrt{1-x_m}\sqrt{1-x_j}] \end{aligned} \tag{18.27}$$

and thus for $j = 0, 1, ...N$:

$$\Delta^1_{mj} + \Delta^1_{m,(-j)} = \begin{cases} (-1)^{m-j}\dfrac{\sqrt{1-x_m}\sqrt{1+x_j}}{x_j - x_m} & j \neq m \\ \dfrac{1}{2\sqrt{1-x_m^2}} & j = m \neq 0 \end{cases} \tag{18.28}$$

$$\Delta^2_{mj}+\Delta^2_{m,(-j)}=\begin{cases}(-1)^{m-j}\dfrac{\sqrt{1+x_m}\sqrt{1+x_j}}{(x_j-x_m)^2}(x_j+x_m-2) & j\neq m\\ -\dfrac{N}{3}(N+1)-\dfrac{x_m}{2(1-x_m^2)} & j=m\neq 0\end{cases} \tag{18.29}$$

and for $j=1,2,....N$:

$$\Delta^4_{0j}+\Delta^4_{0,(-j)}=(-1)^{j+1}\sqrt{2}\frac{\sqrt{1+x_j}}{(1-x_j)^2}[5+x_j-2N(N+1)(1-x_j)] \tag{18.30}$$

and finally the first, and the second derivatives are:

$m\neq 0$, $x_m\neq 1$:

$$\begin{aligned}\psi'_N(x_m)=&-\frac{1}{\sqrt{1-x_m^2}}(\frac{(-1)^m}{\sqrt{2(1-x_m)}}\chi_N(\phi_0)\\ &+\sum_{j=0,j\neq m}^{N}(-1)^{m-j}\frac{\sqrt{1-x_m}\sqrt{1+x_j}}{(x_j-x_m)^2}\chi_N(\phi_j)\\ &+\frac{\chi_N(\phi_m)}{2\sqrt{1-x_m^2}}).\end{aligned} \tag{18.31}$$

$$\begin{aligned}\psi''_N(x_m)=&-\frac{1}{1-x_m^2}[\frac{\partial^2\chi_N}{\partial\phi^2}(\phi_m)+x_m\psi'_N(x_m)]\\ =&-\frac{1}{1-x_m^2}[(\Delta^2_{00}+x_m\Delta^1_{m0})\chi_N(\phi_0)+\sum_{j=0,j\neq m}^{N}(\Delta^2_{mj}+\Delta^2_{m,(-j)}+x_m\Delta^1_{mj})\chi_N(\phi_j)]\end{aligned} \tag{18.32}$$

$m=0$, $x_m=1$:

$$\begin{aligned}\psi'_N(x_0)=&-\frac{\partial^2\chi_N}{\partial\phi^2}(\phi_0)\\ =&-\Delta^2_{00}\chi_N(\phi_0)-\sum_{j=0}^{N}(\Delta^2_{0j}+\Delta^2_{0,(-j)})\chi_N(\phi_j)\\ =&\frac{N}{3}(N+1)\chi_N(\phi_0)+\sum_{j=1}^{N}(-1)^j\frac{\sqrt{2(1+x_j)}}{(1-x_j)}\chi_N(\phi_j).\end{aligned} \tag{18.33}$$

$$\begin{aligned}\psi''_N(x_0)=&-\frac{1}{3}[\frac{\partial^2\chi_N}{\partial\phi^2}(\phi_0)-\psi'_N(x_0)]\\ =&-\frac{1}{3}[(\Delta^4_{00}-\Delta^1_{00})\chi_N(\phi_0)+\sum_{j=1}^{N}(\Delta^4_{0j}+\Delta^4_{0,(-j)}-\Delta^1_{0j})\chi_N(\phi_j)]\end{aligned} \tag{18.34}$$

Now one can deduce the elements of the first order differentiation matrix:

$$D^1_{mj} = \begin{cases} \frac{N}{3}(N+1) & m = j = 0 \\ (-1)^j \frac{\sqrt{2(1+x_j)}}{(1-x_j)} & m = 0, j \neq 0 \\ \frac{(-1)^{m+1}}{\sqrt{2}(1-x_m)\sqrt{1+x_m}} & m \neq 0, j = 0 \\ \frac{-1}{2(1-x_m^2)} & m = j \neq 0 \\ \frac{(-1)^{m-j}}{x_m - x_j}\sqrt{\frac{1+x_j}{1+x_m}} & 0 \neq m \neq j \neq 0 \end{cases} \tag{18.35}$$

and those of the second order differentiation matrix:

$$D^2_{mj} = \begin{cases} \frac{1}{15}(N-1)N(N+1)(N+2) & m = j = 0 \\ (-1)^j \frac{2\sqrt{2}\sqrt{1+x_j}}{3(1-x_j)^2}[N(N+1)(1-x_j) - 3] & m = 0, j \neq 0 \\ \frac{(-1)^{m+1}(2x_m+1)}{\sqrt{2}(1-x_m)^2(1+x_m)^{\frac{3}{2}}} & m \neq 0, j = 0 \\ \frac{-N(N+1)}{3(1-x_m^2)} - \frac{x_m}{(1-x_m^2)^2} & m = j \neq 0 \\ \frac{(-1)^{m-j}(2x_m^2 - x_m + x_j - 2)}{(x_m - x_j)^2(1-x_m^2)}\sqrt{\frac{1+x_j}{1+x_m}} & 0 \neq m \neq j \neq 0 \end{cases} \tag{18.36}$$

18.0.2 Left Radau

Comparing this grid with the right one:

$$x_{jL} = \cos(\pi - \frac{2\pi j}{2N+1}) = -\cos(\frac{2\pi j}{2N+1}) = -x_{jR} \tag{18.37}$$

where x_{jL}, x_{jR} correspond to the points in left Radau, and right Radau respectively. and:

$$\psi_L(x_{jL}) = \psi_R(-x_{jL}) = \psi_R(x_{jR}) \tag{18.38}$$

thus the differentiation relations are:

$$\begin{aligned} \psi'_L(x_{jL}) &= \psi'_R(-x_{jL}) = -\psi'_R(x_{jR}) \\ \psi''_L(x_{jL}) &= \psi''_R(-x_{jL}) = \psi''_R(x_{jR}) \end{aligned} \tag{18.39}$$

So $(D^1_{mj})_L = -(D^1_{mj})_R$, and $(D^2_{mj})_L = (D^2_{mj})_R$, thus

$$D^1_{mj} = \begin{cases} \frac{-N}{3}(N+1) & m = j = 0 \\ (-1)^{j+1}\frac{\sqrt{2(1+x_j)}}{(1-x_j)} & m = 0, j \neq 0 \\ \frac{(-1)^m}{\sqrt{2}(1-x_m)\sqrt{1+x_m}} & m \neq 0, j = 0 \\ \frac{1}{2(1-x_m^2)} & m = j \neq 0 \\ \frac{(-1)^{m-j}}{x_j - x_m}\sqrt{\frac{1+x_j}{1+x_m}} & 0 \neq m \neq j \neq 0 \end{cases} \tag{18.40}$$

and those of the second order differentiation matrix:

$$D^2_{mj} = \begin{cases} \frac{1}{15}(N-1)N(N+1)(N+2) & m = j = 0 \\ (-1)^j \frac{2\sqrt{2}\sqrt{1+x_j}}{3(1-x_j)^2}[N(N+1)(1-x_j) - 3] & m = 0, j \neq 0 \\ \frac{(-1)^{m+1}(2x_m+1)}{\sqrt{2}(1-x_m)^2(1+x_m)^{\frac{3}{2}}} & m \neq 0, j = 0 \\ \frac{-N(N+1)}{3(1-x_m^2)} - \frac{x_m}{(1-x_m^2)^2} & m = j \neq 0 \\ \frac{(-1)^{m-j}(2x_m^2 - x_m + x_j - 2)}{(x_m - x_j)^2(1-x_m^2)}\sqrt{\frac{1+x_j}{1+x_m}} & 0 \neq m \neq j \neq 0 \end{cases} \tag{18.41}$$

18.0.3 Gauss

Considering Gauss grid, From eq.7.20 one can write:

$$\bar{\chi}_N(\phi) = \sum_{-N}^{+N} \bar{\gamma}^{\chi}_k e^{ik\phi} \tag{18.42}$$

where from eq.17.5 (for $-N \leq k \leq N$), we have:

$$\bar{\gamma}^{\chi}_k = \frac{1}{2(N+1)} \sum_{j=0}^{2N+1} \chi_j e^{-ik\phi_j} \tag{18.43}$$

Taking the derivative of $\bar{\chi}_N(\phi)$, gives:

$$\begin{aligned}\bar{\chi'}_N(\phi_m) &= \sum_{-N}^{+N} ik\bar{\gamma}_k^{\chi} e^{ik\phi_m} \\ &= \sum_{k=-N}^{+N} ike^{ik\phi_m} \frac{1}{2(N+1)} \sum_{j=0}^{2N+1} \chi_j e^{-ik\phi_j} \\ &= \sum_{j=0}^{2N+1} \Delta_{mj}^1 \chi(\phi_j)\end{aligned} \tag{18.44}$$

and the second derivative of $\bar{\chi}_N(\phi)$, gives:

$$\begin{aligned}\bar{\chi''}_N(\phi_m) &= \sum_{-N}^{+N} -k^2\bar{\gamma}_k^{\chi} e^{ik\phi_m} \\ &= \sum_{-N}^{+N} -k^2 e^{ik\phi_m} (\frac{1}{2(N+1)} \sum_{j=0}^{2N+1} \chi_j e^{-ik\phi_j}) \\ &= \sum_{j=0}^{2N} \Delta_{mj}^2 \chi(\phi_j)\end{aligned} \tag{18.45}$$

where:

$$\begin{aligned}\Delta_{mj}^1 =& i \sum_{k=-N}^{+N} \frac{1}{2(N+1)} ke^{ik(\phi_m - \phi_j)} \\ =& \frac{i}{2(N+1)} \sum_{k=-N}^{+N} ke^{\frac{2i\pi k(m-j)}{2(N+1)}} \\ =& \frac{i}{2(N+1)} \sum_{k=-N}^{+N} kq^k\end{aligned} \tag{18.46}$$

and

$$\Delta_{mj}^2 = \frac{-1}{2(N+1)} \sum_{k=-N}^{+N} k^2 q^k \tag{18.47}$$

where $q = e^{\frac{\pi i(m-j)}{N+1}}$, to calculate the last sum, let us define:

$$f(q) = \sum_{k=-N}^{+N} q^k = \frac{q^{N+1} - q^N}{q-1} \tag{18.48}$$

so:

$$f'(q) = \sum_{k=-N}^{+N} kq^{k-1} = \frac{Nq^{N+1} - (N+1)q^N + (N+1)q^{-N} - Nq^{-N-1}}{(q-1)^2} \tag{18.49}$$

$$f''(q) = \sum_{k=-N}^{+N} k(k-1)q^{k-2}$$
$$= \frac{N(N-1)q^{N+1} - 2(N+1)(N-1)q^N + N(N+1)q^{N-1} - (N+1)(N+2)q^{-N} + 2N(N+2)q^{-N-1} - N(N+}{(q-1)^3} \tag{18.50}$$

and because of $q^{2(N+1)} = 1$ and $q \neq 1$ (note that in eq.17.23 it needs the power $4(N+1)$ to compensate the $\frac{1}{2}$ in ϕ but as we are subtracting here $\phi_m - \phi_j$ it needs just $2(N+1)$), then:

$$f'(q) = (N+1)q^N \frac{(q+1)}{(q-1)} \tag{18.51}$$

$$\begin{aligned} f''(q) =& \frac{(N(N-1) + 2N(N+2))q^{N+1} - (N(N+1) + 2(N+1)(N-1)q^N + N(N+1)q^{N-1} - (N+1)(N+2}{(q-1)^3} \\ =& \frac{-(N^2+3N+2)q^{N+2} + (3N^2+3N)q^{N+1} - (3N^2+N-2)q^N + (N^2+N)q^{N-1}}{(q-1)^3} \\ =& (N+1)q^{N-1} \frac{-(N+2)q^3 + 3Nq^2 - (3N-2)q + N}{(q-1)^3} \\ =& (N+1)q^{N-1} \frac{N(q-1)^3 - 2q(q^2-1)}{(q-1)^3} \\ =& (N+1)q^{N-1}[N - 2q\frac{q+1}{(q-1)^2}] \end{aligned} \tag{18.52}$$

thus for $m \neq j$:

$$\Delta^1_{mj} = \frac{i}{2} q^{N+1} \frac{q+1}{q-1} \tag{18.53}$$

and

$$\begin{aligned} \Delta^2_{mj} =& \frac{-1}{2(N+1)} \sum_{k=-N}^{+N} k^2 q^k \\ =& \frac{-1}{2(N+1)}[q^2 \sum_{k=-N}^{+N} k(k-1)q^{k-2} + q^1 \sum_{k=-N}^{+N} kq^{k-1}] \\ =& \frac{-1}{2(N+1)}[q^2 f''(q) + q f'(q)] \end{aligned} \tag{18.54}$$

developing it, one gets:

$$\Delta^1_{mj} = \frac{1}{2} \frac{(-1)^{m-j} \cos[\frac{\pi}{2(N+1)}(m-j)]}{\sin[\frac{\pi}{2(N+1)}(m-j)]} \tag{18.55}$$

and

$$\Delta^2_{mj} = \frac{-(-1)^{m-j}}{2}[N + \frac{(q+1)^2}{(q-1)^2}] = \frac{-(-1)^{m-j}}{2}[N - (\frac{\cos[\frac{\pi}{2(N+1)}(m-j)]}{\sin[\frac{\pi}{2(N+1)}(m-j))]})^2] \tag{18.56}$$

for $m = j$ (then $q = 1$):

$$\Delta^1_{mj} = 0 \tag{18.57}$$

$$\Delta^2_{mj} = -\frac{(2N^2+1)}{6} \tag{18.58}$$

In his notes Ansorg started by defining $\chi_N(\phi) = \psi_N(\cos\phi)$, in order to find the relation between the derivation matrix elements in Fourier series with the corresponding ones using Chebyshev polynomials.

$$\begin{aligned}
\frac{\partial\chi_N}{\partial\phi} &= -\sqrt{1-x^2}\psi'_N(x) \\
\frac{\partial^2\chi_N}{\partial\phi^2} &= -x\psi'_N(x) + (1-x^2)\psi''_N(x) \\
\frac{\partial^4\chi_N}{\partial\phi^4} &= x\psi'_N(x) + (7x^2-4)\psi''_N(x) - 6x(1-x^2)\psi'''_N(x) + (1-x^2)^2\psi^{(}(4))_N(x)
\end{aligned} \tag{18.59}$$

It follows that:

$$\psi'_N(x) = \begin{cases} -\dfrac{1}{\sqrt{1-x^2}}\dfrac{\partial\chi_N}{\partial\phi} & x \neq \pm 1 \\ \pm\dfrac{\partial^2\chi_N}{\partial\phi^2} & x = \pm 1. \end{cases} \tag{18.60}$$

$$\psi''_N(x) = \begin{cases} -\dfrac{1}{(1-x^2)}\left(\dfrac{\partial^2\chi_N}{\partial\phi^2} + x\psi'_N(x)\right) & x \neq \pm 1 \\ \dfrac{1}{3}\left(\dfrac{\partial^4\chi_N}{\partial\phi^4} - x\psi'_N(x)\right) & x = \pm 1. \end{cases} \tag{18.61}$$

Because of $\chi_N(\phi_{2(N+1)-l}) = \chi_N(\phi_l)$, one can writes:

$$\frac{\partial^\nu\chi_N}{\partial\phi^\nu}(\phi_m) = \sum_{j=0}^{N}(\Delta^\nu_{mj} + \Delta^\nu_{m,(-j)})\chi_N(\phi_j). \tag{18.62}$$

The last equality is because:

$$\begin{aligned}
\sin\frac{\phi_{2(N+1)-k}}{2} &= \sin(2\pi + \frac{\phi_{(-k)}}{2}) = \sin\frac{\phi_{(-k)}}{2} \\
\cos\frac{\phi_{2(N+1)-k}}{2} &= \cos(2\pi + \frac{\phi_{(-k)}}{2}) = \cos\frac{\phi_{(-k)}}{2}
\end{aligned} \tag{18.63}$$

using eq.18.55 and eq.18.57, the last equations lead to:

$$\Delta^1_{m,2(N+1)-j} = \Delta^1_{m,(-j)}. \tag{18.64}$$

On the other hand

$$\begin{aligned}
\sin\frac{\phi_k}{2} &= \frac{1}{\sqrt{2}}\sqrt{1-x_k} \\
\cos\frac{\phi_k}{2} &= \frac{1}{\sqrt{2}}\sqrt{1+x_k}
\end{aligned} \tag{18.65}$$

where $x_k = \cos\phi_k$ this leads to:

$$\begin{aligned}\sin\frac{\phi_m \pm \phi_j}{2} &= \frac{1}{2}[\sqrt{1-x_m}\sqrt{1+x_j} \pm \sqrt{1+x_m}\sqrt{1-x_j}] \\ \cos\frac{\phi_m \pm \phi_j}{2} &= \frac{1}{2}[\sqrt{1+x_m}\sqrt{1+x_j} \mp \sqrt{1-x_m}\sqrt{1-x_j}]\end{aligned} \tag{18.66}$$

and thus for $j \neq m$:

$$\Delta^1_{mj} + \Delta^1_{m,(-j)} = (-1)^{m-j}\frac{\sqrt{1-x_j^2}}{(x_m - x_j)\sqrt{1-x_m^2}} \tag{18.67}$$

$$\Delta^2_{mj} + \Delta^2_{m,(-j)} = -\frac{(-1)^{m-j}}{2}[2N - \frac{2-x_j^2-x_m^2}{(x_m-x_j)^2}] \tag{18.68}$$

and for $j = m$:

$$\Delta^1_{mj} + \Delta^1_{m,(-j)} = \frac{x_m}{2(1-x_m^2)} \tag{18.69}$$

$$\Delta^2_{mj} + \Delta^2_{m,(-j)} = \frac{-1}{2}[N - \frac{x_m^2}{1-x_m^2}] \tag{18.70}$$

Then by running some calculations as in the previous subsection one can conclude the differentiation matrix:

$$D^1_{mj} = \begin{cases} \dfrac{x_m}{2(1-x_m^2)} & m = j \\ (-1)^{m-j}\dfrac{\sqrt{1-x_j^2}}{(x_m-x_j)\sqrt{1-x_m^2}} & m \neq j \end{cases} \tag{18.71}$$

and those of the second order differentiation matrix:

$$D^2_{mj} = \begin{cases} \dfrac{x_m}{(1-x_m^2)^2} - \dfrac{N(N+2)}{3(1-x_m^2)} & m = j \\ (-1)^{m-j}\dfrac{\sqrt{1-x_j^2}}{(x_m-x_j)\sqrt{1-x_m^2}}(\dfrac{x_m}{(1-x_m^2)} - \dfrac{2}{x_m-x_j}) & m \neq j \end{cases} \tag{18.72}$$

18.0.4 Lobatto

Considering Lobatto grid, From eq.7.20 one can write:

$$\bar{\chi}_N(\phi) = \sum_{-N}^{+N} \bar{\gamma}_k^{\chi} e^{ik\phi} \tag{18.73}$$

where from eq.17.17 (for $-N \leq k \leq N$), we have:

$$\bar{\gamma}_k^{\chi} = \frac{2 - \delta_{kN} - \delta_{k(-N)}}{4N} \sum_{j=0}^{2N-1} \chi_j e^{-ik\phi_j} \tag{18.74}$$

Taking the derivative of $\bar{\chi}_N(\phi)$, gives:

$$\begin{aligned}\bar{\chi'}_N(\phi_m) &= \sum_{-N}^{+N} ik\bar{\gamma}_k^{\chi} e^{ik\phi_m} \\ &= \sum_{k=-N}^{+N} ike^{ik\phi_m} \frac{2-\delta_{kN}-\delta_{k(-N)}}{4N} \sum_{j=0}^{2N-1} \chi_j e^{-ik\phi_j} \\ &= \sum_{j=0}^{2N} \Delta_{mj}^1 \chi(\phi_j)\end{aligned} \tag{18.75}$$

and the second derivative of $\bar{\chi}_N(\phi)$, gives:

$$\begin{aligned}\bar{\chi''}_N(\phi_m) &= \sum_{-N}^{+N} -k^2\bar{\gamma}_k^{\chi} e^{ik\phi_m} \\ &= \sum_{-N}^{+N} -k^2 e^{ik\phi_m} (\frac{2-\delta_{kN}-\delta_{k(-N)}}{4N} \sum_{j=0}^{2N-1} \chi_j e^{-ik\phi_j}) \\ &= \sum_{j=0}^{2N} \Delta_{mj}^2 \chi(\phi_j)\end{aligned} \tag{18.76}$$

where:

$$\begin{aligned}\Delta_{mj}^1 =& i \sum_{k=-N}^{+N} \frac{2-\delta_{kN}-\delta_{k(-N)}}{4N} ke^{ik(\phi_m-\phi_j)} \\ =& \frac{i}{2N} \sum_{k=-N}^{+N} ke^{\frac{\pi ik(m-j)}{N}} - \frac{i}{4N} Nq^N - \frac{i}{4N}(-N)q^{-N} \\ =& \frac{i}{2N} \sum_{k=-N}^{+N} kq^k\end{aligned} \tag{18.77}$$

and

$$\Delta_{mj}^2 = \frac{-1}{2N} \sum_{k=-N}^{+N} k^2 q^k + \frac{N}{4}(q^N + q^{-N}) \tag{18.78}$$

where $q = e^{\frac{\pi i(m-j)}{N}}$, to calculate the last sum, let us define:

$$f(q) = \sum_{k=-N}^{+N} q^k = \frac{q^{N+1} - q^N}{q-1} \tag{18.79}$$

so:

$$f'(q) = \sum_{k=-N}^{+N} kq^{k-1} = \frac{Nq^{N+1} - (N+1)q^N + (N+1)q^{-N} - Nq^{-N-1}}{(q-1)^2} \tag{18.80}$$

$$
\begin{aligned}
f''(q) &= \sum_{k=-N}^{+N} k(k-1)q^{k-2} \\
&= \frac{N(N-1)q^{N+1} - 2(N+1)(N-1)q^N + N(N+1)q^{N-1} - (N+1)(N+2)q^{-N} + 2N(N+2)q^{-N-1} - N(N+}{(q-1)^3}
\end{aligned}
\tag{18.81}
$$

and because of $q^{2N} = 1$ and $q \neq 1$ (17.23), then:

$$
f'(q) = \frac{Nq^N(q+1)}{q(q-1)} \tag{18.82}
$$

$$
f''(q) = q^{N-2}[N^2 - \frac{4Nq}{(q-1)^2}] \tag{18.83}
$$

thus for $m \neq j$:

$$
\begin{aligned}
\Delta^1_{mj} &= \frac{i}{2N} q \sum_{k=-N}^{+N} k q^{k-1} \\
&= \frac{i}{2} q^N \frac{q+1}{q-1}
\end{aligned}
\tag{18.84}
$$

and

$$
\begin{aligned}
\Delta^2_{mj} &= \frac{-1}{2N} \sum_{k=-N}^{+N} k^2 q^k + \frac{N}{4}(q^N + q^{-N}) \\
&= \frac{-1}{2N}[q^2 \sum_{k=-N}^{+N} k(k-1)q^{k-2} + q^1 \sum_{k=-N}^{+N} k q^{k-1}] + \frac{N}{4}(q^N + q^{-N}) \\
&= \frac{-1}{2N}[q^2 f''(q) + q f'(q)] + \frac{N}{4}(q^N + q^{-N})
\end{aligned}
\tag{18.85}
$$

developing it, when $m - j \neq 2Np; p \in \mathrm{Z}$, one gets:

$$
\Delta^1_{mj} = \frac{1}{2} \frac{(-1)^{m-j} \cos[\frac{\pi}{2N}(m-j)]}{\sin[\frac{\pi}{2N}(m-j)]} \tag{18.86}
$$

and

$$
\Delta^2_{mj} = \frac{-1}{2} \frac{(-1)^{m-j}}{\sin^2[\frac{\pi}{2N}(m-j)]} \tag{18.87}
$$

In his notes Ansorg started by defining $\chi_N(\phi) = \psi_N(\cos\phi)$, in order to find the relation between the derivation matrix elements in Fourier series with the corresponding ones using Chebyshev polynomials.

$$
\begin{aligned}
\frac{\partial \chi_N}{\partial \phi} &= -\sqrt{1-x^2}\psi'_N(x) \\
\frac{\partial^2 \chi_N}{\partial \phi^2} &= -x\psi'_N(x) + (1-x^2)\psi''_N(x) \\
\frac{\partial^4 \chi_N}{\partial \phi^4} &= x\psi'_N(x) + (7x^2-4)\psi''_N(x) - 6x(1-x^2)\psi'''_N(x) + (1-x^2)^2\psi^{(}(4))_N(x)
\end{aligned}
\tag{18.88}
$$

It follows that:

$$\psi'_N(x) = \begin{cases} -\dfrac{1}{\sqrt{1-x^2}}\dfrac{\partial \chi_N}{\partial \phi} & x \neq \pm 1 \\ \pm \dfrac{\partial^2 \chi_N}{\partial \phi^2} & x = \pm 1. \end{cases} \tag{18.89}$$

$$\psi''_N(x) = \begin{cases} -\dfrac{1}{(1-x^2)}(\dfrac{\partial^2 \chi_N}{\partial \phi^2} + x\psi'_N(x)) & x \neq \pm 1 \\ \dfrac{1}{3}(\dfrac{\partial^4 \chi_N}{\partial \phi^4} - x\psi'_N(x)) & x = \pm 1. \end{cases} \tag{18.90}$$

Because of $\chi_N(\phi_{2N+l}) = \chi_N(\phi_l)$, one can writes:

$$\frac{\partial^\nu \chi_N}{\partial \phi^\nu}(\phi_m) = \sum_{j=0}^{N} (\Delta^\nu_{mj} + \Delta^\nu_{m,(-j)})\chi_N(\phi_j). \tag{18.91}$$

The last equality is because:

$$\begin{aligned} \sin\frac{\phi_{(2N)-k}}{2} &= \sin(\frac{\phi_{(-k)}}{2} - \pi) = -\sin\frac{\phi_{(-k)}}{2} \\ \cos\frac{\phi_{(2N)-k}}{2} &= \cos(\frac{\phi_{(-k)}}{2} - \pi) = -\cos\frac{\phi_{(-k)}}{2} \end{aligned} \tag{18.92}$$

using eq.18.86, the last equations lead to:

$$\Delta^1_{m,2N-j} = \Delta^1_{m,(-j)}. \tag{18.93}$$

On the other hand

$$\begin{aligned} \sin\frac{\phi_k}{2} &= \frac{1}{\sqrt{2}}\sqrt{1-x_k} \\ \cos\frac{\phi_k}{2} &= \frac{1}{\sqrt{2}}\sqrt{1+x_k} \end{aligned} \tag{18.94}$$

where $x_k = \cos\phi_k$ this leads to:

$$\begin{aligned} \sin\frac{\phi_m \pm \phi_j}{2} &= \frac{1}{2}[\sqrt{1-x_m}\sqrt{1+x_j} \pm \sqrt{1+x_m}\sqrt{1-x_j}] \\ \cos\frac{\phi_m \pm \phi_j}{2} &= \frac{1}{2}[\sqrt{1+x_m}\sqrt{1+x_j} \mp \sqrt{1-x_m}\sqrt{1-x_j}] \end{aligned} \tag{18.95}$$

and thus for $j, m = 1, ...N-1$ and $j \neq m$:

$$\Delta^1_{mj} + \Delta^1_{m,(-j)} = [(-1)^{m-j}][\frac{\sqrt{1-x_m^2}}{x_j - x_m}], \tag{18.96}$$

so in this case

$$D^1_{mj} = \frac{(-1)^{m-j}}{(x_m - x_j)}. \tag{18.97}$$

For $m = 1, ...N-1$ and $j = m$:

$$\begin{aligned}\Delta^1_{mj} + \Delta^1_{m,(-j)} =& \frac{i}{2N}\sum_{k=-N}^{+N} k + \frac{i}{2N}\sum_{k=-N}^{+N} k e^{\frac{2im\pi k}{N}} \\ =& 0 + \frac{i}{2}\frac{e^{\frac{2im\pi}{N}}+1}{e^{\frac{2im\pi}{N}}-1} \\ =& \frac{1}{2}\frac{\cos(\frac{m\pi}{N})}{\sin(\frac{m\pi}{N})} \\ =& \frac{1}{2}\frac{x_m}{\sqrt{1-x_m^2}},\end{aligned} \tag{18.98}$$

so in this case

$$D^1_{mj} = \frac{-1}{2}\frac{x_m}{1-x_m^2}. \tag{18.99}$$

For $m = j = 0$ (then $q = 1$):

$$\Delta^2_{00} = -\frac{-1}{2N}\sum_{k=-N}^{+N} k^2 + \frac{N}{4}(2) = -\frac{2N^2+1}{6}, \tag{18.100}$$

so $D^1_{00} = -\frac{2N^2+1}{6}$ Then by running more computations, we get:

$$D^1_{mj} = \begin{cases} -\dfrac{2N^2+1}{6} & m = j = 0 \\ \dfrac{2N^2+1}{6} & m = j = N \\ \dfrac{-x_j}{2(1-x_j^2)} & m = j \neq 0, N \\ \dfrac{\kappa_m}{\kappa_j}\dfrac{(-1)^{m-j}}{(x_m - x_j)} & m \neq j \end{cases} \tag{18.101}$$

and those of the second order differentiation matrix:

$$D^2_{mj} = \begin{cases} \dfrac{N^2-1}{15} & m = j = 0, N \\ \dfrac{-1}{(1-x_j^2)^2} - \dfrac{N^2-1}{3(1-x_j^2)} & m = j \neq 0, N \\ \dfrac{2}{3}\dfrac{(-1)^j}{\kappa_j}\dfrac{(2N^2+1)(1-x_j)-6}{(1-x_j)^2} & 0 = m \neq j \\ \dfrac{2}{3}\dfrac{(-1)^{N+j}}{\kappa_j}\dfrac{(2N^2+1)(1+x_j)-6}{(1+x_j)^2} & N = m \neq j \\ \dfrac{(-1)^{m-j}}{\kappa_j}\dfrac{x_m^2+x_m x_j-2}{(x_m-x_j)^2(1-x_m^2)} & 0 \neq m \neq N, j \neq m \end{cases} \tag{18.102}$$

where:

$$\kappa_j = \begin{cases} 1 & 0 < j < N \\ 2 & j = 0, N \end{cases} \tag{18.103}$$

Bibliography

[1] J. Aguilar & J. M. Combes, *A class of analytic perturbations for one-body Schrödinger Hamiltonians*, Communications in Mathematical Physics (1971).

[2] I. Agullo, V. Cardoso, A. del Rio, M. Maggiore, & J. Pullin, *Gravitational-wave signatures of quantum gravity*, (7 2020).

[3] L. Al Sheikh & J. L. Jaramillo, *A geometric approach to QNMs in optics: application to pseudospectrum and structural stability*, In preparation. .

[4] V. Aldaya, C. Barceló, & J. Jaramillo, *Spanish Relativity Meeting (ERE 2010): Gravity as a Crossroad in Physics*, Journal of Physics: Conference Series **314** (09 2011).

[5] H. Ammari, P. Millien, M. Ruiz, & H. Zhang, *Mathematical analysis of plasmonic nanoparticles: the scalar case*, arXiv preprint arXiv:1506.00866 (2015).

[6] H. Ammari, M. Ruiz, S. Yu, & H. Zhang, *Mathematical analysis of plasmonic resonances for nanoparticles: the full Maxwell equations*, Journal of Differential Equations **261**(6), 3615–3669 (2016).

[7] A. Anderson & R. H. Price, *Intertwining of the equations of black hole perturbations*, Phys. Rev. **D43**, 3147–3154 (1991).

[8] K. Ando & H. Kang, *Analysis of plasmon resonance on smooth domains using spectral properties of the Neumann–Poincaré operator*, Journal of Mathematical Analysis and Applications **435**(1), 162–178 (2016).

[9] M. Ansorg, *Spektrale Verfahren in der Theoretischen Physik*, page 187 (2013).

[10] M. Ansorg & R. Panosso Macedo, *Spectral decomposition of black-hole perturbations on hyperboloidal slices*, Phys. Rev. **D93**(12), 124016 (2016).

[11] Y. Ashida, Z. Gong, & M. Ueda, *Non-Hermitian Physics*, (6 2020).

[12] A. Ashtekar, *Asymptotic Structure of the Gravitational Field at Spatial Infinity*, in *General Relativity and Gravitation II*, edited by A. Held, volume 2, page 37, Jan. 1980.

[13] A. Ashtekar, *Asymptotic properties of isolated systems: recent developments*, in *General Relativity and Gravitation*, edited by B. Bertotti, F. de Felice, & A. Pascolini, page 37, D. Reidel Publishing Company, 1984.

[14] S. ATTAL, *Lecture notes: OPERATOR AND SPECTRAL THEORY*, Institut Camille Jordan, Université Lyon 1, France .

[15] E. Balslev & J. M. Combes, *Spectral properties of many-body Schrödinger operators with dilatation-analytic interactions*, Communications in Mathematical Physics (1971).

[16] E. Barausse, V. Cardoso, & P. Pani, *Can environmental effects spoil precision gravitational-wave astrophysics?*, Phys. Rev. **D89**(10), 104059 (2014).

[17] R. W. Batterman, *The Devil in the Details: Asymptotic Reasoning in Explanation, Reduction, and Emergence*, Oxford University Press, 2001.

[18] J.-P. Berenger, *A perfectly matched layer for the absorption of electromagnetic waves*, Journal of Computational Physics **114**(2), 185–200 (1994).

[19] J.-P. Berenger, *Three-Dimensional Perfectly Matched Layer for the Absorption of Electromagnetic Waves*, Journal of Computational Physics **127**(2), 363–379 (1996).

[20] M. Berger, *A panoramic view of Riemannian geometry*, Springer, Berlin, 2003.

[21] M. Berkani, *B-Fredholm elements in rings and algebras*, arXiv preprint arXiv:1609.07995 (2016).

[22] M. V. Berry, *Semiclassically weak reflections above analytic and non-analytic potential barriers*, Journal of Physics A: Mathematical and General **15**(12), 3693–3704 (dec 1982).

[23] M. V. Berry & K. E. Mount, *Semiclassical approximations in wave mechanics*, Reports on Progress in Physics **35**(1), 315–397 (jan 1972).

[24] E. Berti, (Personal Website).

[25] E. Berti, V. Cardoso, & A. O. Starinets, *Quasinormal modes of black holes and black branes*, Class. Quant. Grav. **26**, 163001 (2009).

[26] H. R. Beyer, *On the completeness of the quasinormal modes of the Poschl-Teller potential*, Commun. Math. Phys. **204**, 397–423 (1999).

[27] H. Beyer, *The spectrum of radial adiabatic stellar oscillations*, Journal of Mathematical Physics 36 (9), 4815-4825 (1995).

[28] W.-J. Beyn, Y. Latushkin, & J. Rottmann-Matthes, *Finding eigenvalues of holomorphic Fredholm operator pencils using boundary value problems and contour integrals*, arXiv e-prints , arXiv:1210.3952 (Oct. 2012).

[29] W.-J. Beyn, *An integral method for solving nonlinear eigenvalue problems*, Linear Algebra and its Applications **436**(10), 3839–3863 (2012), Special Issue dedicated to Heinrich Voss's 65th birthday.

[30] D. Bindel & M. Zworski, *Theory and computation of resonances in 1d scattering.*

[31] P. Bizoń, T. Chmaj, & P. Mach, *A toy model of hyperboloidal approach to quasinormal modes*, arXiv:2002.01770 (2020).

[32] P. Bizoń & P. Mach, *Global dynamics of a Yang-Mills field on an asymptotically hyperbolic space*, Trans. Am. Math. Soc. **369**(3), 2029–2048 (2017), [Erratum: Trans. Am. Math. Soc.369,no.4,3013(2017)].

[33] P. Bizoń & M. Maliborski, *Dynamics at the threshold for blowup for supercritical wave equations outside a ball*, arXiv:1909.01626 (2019).

[34] J.-F. Bony, S. Fujiie, T. Ramond, & M. Zerzeri, *An example of resonance instability*, arXiv:2005.10035 (2020).

[35] P. Boonserm & M. Visser, *Quasi-normal frequencies: Key analytic results*, JHEP **03**, 073 (2011).

[36] W. Bordeaux Montrieux, *Loi de Weyl presque sûre et résolvante pour des opérateurs non-autoadjoints*, Theses, Ecole Polytechnique X, 2008.

[37] W. Bordeaux Montrieux, *Almost sure Weyl law for a differential system in dimension 1*, Annales Henri Poincaré **1** (01 2011).

[38] C. Canuto, M. Y. Hussaini, A. Quarteroni, & T. A. Zang, *Spectral methods: fundamentals in single domains*, 2007.

[39] V. Cardoso, (Personal Website).

[40] V. Cardoso, J. a. L. Costa, K. Destounis, P. Hintz, & A. Jansen, *Quasinormal Modes and Strong Cosmic Censorship*, Phys. Rev. Lett. **120**, 031103 (Jan 2018).

[41] V. Cardoso, E. Franzin, & P. Pani, *Is the gravitational-wave ringdown a probe of the event horizon?*, Phys. Rev. Lett. **116**(17), 171101 (2016), [Erratum: Phys.Rev.Lett. 117, 089902 (2016)].

[42] V. Cardoso, M. Kimura, A. Maselli, E. Berti, C. F. B. Macedo, & R. McManus, *Parametrized black hole quasinormal ringdown: Decoupled equations for nonrotating black holes*, Phys. Rev. **D99**(10), 104077 (2019).

[43] V. Cardoso & P. Pani, *Testing the nature of dark compact objects: a status report*, Living Rev. Rel. **22**(1), 4 (2019).

[44] R. CARMINATI, *Ondes en milieu complexes*.

[45] S. Chandrasekhar, *The mathematical theory of black holes*, Oxford classic texts in the physical sciences, Oxford Univ. Press, Oxford, 2002.

[46] S. Chandrasekhar & S. Detweiler, *The Quasi-Normal Modes of the Schwarzschild Black Hole*, Proceedings of the Royal Society of London. Series A, Mathematical and Physical Sciences **344**(1639), 441–452 (1975).

[47] E. S. C. Ching, P. T. Leung, A. Maassen van den Brink, W. M. Suen, S. S. Tong, & K. Young, *Quasinormal-mode expansion for waves in open systems*, Rev. Mod. Phys. **70**, 1545–1554 (Oct 1998).

[48] E. S. C. Ching, P. T. Leung, W. M. Suen, & K. Young, *Quasinormal Mode Expansion for Linearized Waves in Gravitational Systems*, Phys. Rev. Lett. **74**, 4588–4591 (Jun 1995).

[49] M. J. Colbrook, B. Roman, & A. C. Hansen, *How to Compute Spectra with Error Control*, Phys. Rev. Lett. **122**, 250201 (Jun 2019).

[50] F. Collino, *Perfectly matched absorbing layers for the paraxial equations*, PhD thesis, INRIA, 1996.

[51] F. Collino & P. Monk, *The perfectly matched layer in curvilinear coordinates*, SIAM Journal on Scientific Computing **19**(6), 2061–2090 (1998).

[52] F. Collino & P. B. Monk, *Optimizing the perfectly matched layer*, Computer methods in applied mechanics and engineering **164**(1-2), 157–171 (1998).

[53] G. B. Cook & M. Zalutskiy, *Purely imaginary quasinormal modes of the Kerr geometry*, Class. Quant. Grav. **33**(24), 245008 (2016).

[54] R. G. Daghigh, M. D. Green, & J. C. Morey, *Significance of Black Hole Quasinormal Modes: A Closer Look*, Phys. Rev. D **101**(10), 104009 (2020).

[55] E. Dahlberg, *On the Completeness of Eigenfunctions of Some Higher Order Operators*, (1973).

[56] T. Damour, *Quelques propriétés mécaniques, électromagnétiques, thermodynamiques et quantiques des trous noirs*, Thèse de doctorat d'État, Université Paris 6, 1979.

[57] T. Damour, *Surface effects in black hole physics*, in *Proceedings of the Second Marcel Grossmann Meeting on General Relativity*, edited by R. Ruffini, page 587, North-Holland, Amsterdam, 1982.

[58] T. Daudé & F. Nicoleau, *Local Inverse Scattering at a Fixed Energy for Radial Schrödinger Operators and Localization of the Regge Poles*, Annales Henri Poincaré **17**(10), 2849–2904 (Dec 2015).

[59] E. B. Davies, *Pseudo-spectra, the harmonic oscillator and complex resonances.*, Proc. R. Soc. Lond., Ser. A, Math. Phys. Eng. Sci. **455**(1982), 585–599 (1999).

[60] E. Davies, *Semi-classical analysis and pseudo-spectra*, Journal of Differential Equations **216**(1), 153–187 (2005).

[61] Y. Decanini, A. Folacci, & B. Raffaelli, *Unstable circular null geodesics of static spherically symmetric black holes, Regge poles and quasinormal frequencies*, Phys. Rev. D **81**, 104039 (2010).

[62] Y. Decanini, A. Folacci, & B. Raffaelli, *Fine structure of high-energy absorption cross sections for black holes*, Class. Quant. Grav. **28**, 175021 (2011).

[63] N. Dencker, J. Sjöstrand, & M. Zworski, *Pseudospectra of semiclassical (pseudo-) differential operators*, Commun. Pure Appl. Math. **57**(3), 384–415 (2004).

[64] M. Dimassi & J. Sjöstrand, *Spectral Asymptotics in the Semi-Classical Limit*, London Mathematical Society Lecture Note Series, Cambridge University Press, 1999.

[65] S. R. Dolan & A. C. Ottewill, *On an Expansion Method for Black Hole Quasinormal Modes and Regge Poles*, Class. Quant. Grav. **26**, 225003 (2009).

[66] R. Donninger & I. Glogić, *Strichartz estimates for the one-dimensional wave equation*, Trans. Am. Math. Soc. **373**(6), 4051–4083 (2020).

[67] M. Dunajski, *Solitons, instantons, and twistors*, Oxford, UK: Univ. Pr. (2010) 359 p, 2010.

[68] S. Dyatlov & M. Zworski, *Mathematical Theory of Scattering Resonances*, Graduate Studies in Mathematics, American Mathematical Society, 2019.

[69] S. Dyatlov, *Quasi-Normal Modes and Exponential Energy Decay for the Kerr-de Sitter Black Hole*, Communications in Mathematical Physics **306**(1), 119–163 (jun 2011).

[70] W. R. Dyksen, E. N. Houstis, R. E. Lynch, & J. R. Rice, *The Performance of the Collocation and Galerkin Methods with Hermite Bi-Cubics*, SIAM Journal on Numerical Analysis **21**(4), 695–715 (1984).

[71] M. Embree & N. Trefethen, (Personal Website).

[72] J. C. Fabris, M. G. Richarte, & A. Saa, *Quasinormal modes and self-adjoint extensions of the Schroedinger operator*, arXiv:2010.10674 (10 2020).

[73] V. Ferrari & B. Mashhoon, *New approach to the quasinormal modes of a black hole*, Phys. Rev. D **30**, 295–304 (Jul 1984).

[74] S. Fortuna & I. Vega, *Bernstein spectral method for quasinormal modes and other eigenvalue problems*, arXiv:2003.06232 (2020).

[75] H. Friedrich, *On the existence of n-geodesically complete or future complete solutions of Einstein's field equations with smooth asymptotic structure*, Comm. Math. Phys. **107**, 587 (1986).

[76] H. Friedrich, *Conformal Einstein evolution*, in *The conformal structure of spacetime: Geometry, Analysis, Numerics*, edited by J. Frauendiener & H. Friedrich, Lecture Notes in Physics, page 1, Springer, 2002.

[77] R. Froese, *Asymptotic Distribution of Resonances in One Dimension*, Journal of Differential Equations **137**(2), 251–272 (1997).

[78] D. Gajic & C. Warnick, *A model problem for quasinormal ringdown on asymptotically flat or extremal black holes*, arXiv:1910.08481 (2019).

[79] D. Gajic & C. Warnick, *Quasinormal modes in extremal Reissner-Nordström spacetimes*, arXiv:1910.08479 (2019).

[80] J. Galkowski & M. Zworski, *Outgoing solutions via Gevrey-2 properties*, (2020).

[81] E. Gasperin & J. L. Jaramillo, *Physical scales and QNM spectral instability: the role of the scalar product*, In preparation. .

[82] R. Geroch, *Asymptotic structure of space-time*, in *Asymptotic structure of spacetime*, edited by E. P. Esposito & L. Witten, Plenum Press, 1976.

[83] K. Glampedakis, A. D. Johnson, & D. Kennefick, *Darboux transformation in black hole perturbation theory*, Phys. Rev. **D96**(2), 024036 (2017).

[84] E. Gourgoulhon, *Geometry and physics of black holes Lecture notes*, (2016).

[85] D. Hafner, P. Hintz, & A. Vasy, *Linear stability of slowly rotating Kerr black holes*, arXiv:1906.00860 (2019).

[86] M. Hager, *Instabilite spectrale semiclassique d'operateurs non-autoadjoints*, Theses, Ecole Polytechnique X, June 2005, Jury: Bony Jean-Michel, Dimassi Mouez, Helffer Bernard, Lerner Nicolas, Zworski Maciej.

[87] M. Hager, *Instabilité spectrale semiclassique d'opérateurs non-autoadjoints. II*, Ann. Henri Poincaré **7**(6), 1035–1064 (2006).

[88] M. Hager, *Instabilité spectrale semiclassique pour des opérateurs non-autoadjoints. I: un modèle*, Ann. Fac. Sci. Toulouse, Math. (6) **15**(2), 243–280 (2006).

[89] M. Hager & J. Sjöstrand, *Eigenvalue asymptotics for randomly perturbed non-selfadjoint operators*, arXiv Mathematics e-prints , math/0601381 (Jan. 2006).

[90] B. Helffer & J. Sjöstrand, *Résonances en limite semi-classique*, Number 24-25 in Mémoires de la Société Mathématique de France, Société mathématique de France, 1986.

[91] P. Hintz & A. Vasy, *Analysis of linear waves near the Cauchy horizon of cosmological black holes*, Journal of Mathematical Physics **58**(8), 081509 (Aug. 2017).

[92] E. N. Houstis, R. E. Lynch, J. Rice, & T. Papatheodorou, *Evaluation of numerical methods for elliptic partial differential equations*, Journal of Computational Physics **27**(3), 323–350 (1978).

[93] (bhptoolkit.org), *Black Hole Perturbation Toolkit*.

[94] L. Hui, D. Kabat, & S. S. C. Wong, *Quasinormal modes, echoes and the causal structure of the Green's function*, JCAP **1912**(12), 020 (2019).

[95] M. Y. Hussaini, C. L. Streett, & T. A. Zang, *Spectral methods for partial differential equations*, (1983).

[96] A. Jansen, *Overdamped modes in Schwarzschild-de Sitter and a Mathematica package for the numerical computation of quasinormal modes*, Eur. Phys. J. Plus **132**(12), 546 (2017).

[97] J. L. Jaramillo, R. P. Macedo, & L. Al Sheikh, *Gravitational wave signatures of black hole quasi-normal mode instability*, In preparation. .

[98] J. L. Jaramillo, R. Panosso Macedo, & L. Al Sheikh, *Pseudospectrum and Black Hole Quasinormal Mode Instability*, Phys. Rev. X **11**(3), 031003 (2021).

[99] J. L. Jaramillo, *A master course on General relativity and black holes*, (2017).

[100] M. Kaashoek & D. Lay, *On operators whose Fredholm set is the complex plane*, Pacific Journal of Mathematics **21**(2), 275–278 (1967).

[101] T. Kato, *Perturbation theory for linear operators. Reprint of the corr. print. of the 2nd ed. 1980.*, Berlin: Springer-Verlag, reprint of the corr. print. of the 2nd ed. 1980 edition, 1995.

[102] M. V. Keldysh, *On the characteristic values and characteristic functions of certain classes of non-self-adjoint equations*, **77**(1), 11–14 (1951).

[103] M. V. Keldysh, *On the completeness of the eigenfunctions of some classes of non-selfadjoint linear operators*, Uspekhi matematicheskikh nauk **26**(4), 15–41 (1971).

[104] G. Khanna & R. H. Price, *Black Hole Ringing, Quasinormal Modes, and Light Rings*, Phys. Rev. **D95**(8), 081501 (2017).

[105] K. D. Kokkotas & B. G. Schmidt, *Quasinormal modes of stars and black holes*, Living Rev. Rel. **2**, 2 (1999).

[106] R. A. Konoplya, *Conformal Weyl gravity via two stages of quasinormal ringing and late-time behavior*, Phys. Rev. D **103**(4), 044033 (2021).

[107] R. A. Konoplya & A. Zhidenko, *Quasinormal modes of black holes: From astrophysics to string theory*, Rev. Mod. Phys. **83**, 793–836 (2011).

[108] R. Konoplya & A. Zhidenko, *Wormholes versus black holes: quasinormal ringing at early and late times*, JCAP **12**, 043 (2016).

[109] H.-O. Kreiss & J. Oliger, *Comparison of accurate methods for the integration of hyperbolic equations*, Tellus **24**(3), 199–215 (1972).

[110] D. Krejčiřík, P. Siegl, M. Tater, & J. Viola, *Pseudospectra in non-Hermitian quantum mechanics*, Journal of Mathematical Physics **56**(10) (Oct. 2015).

[111] J. A. V. Kroon, *Conformal Methods in General Relativity*, Cambridge University Press, Cambridge, 2016.

[112] M. Kuzuoglu & R. Mittra, *Investigation of nonplanar perfectly matched absorbers for finite-element mesh truncation*, IEEE Transactions on Antennas and Propagation **45**(3), 474–486 (1997).

[113] P. Lalanne, *Plasmonics: a few basics.*

[114] P. Lalanne, W. Yan, K. Vynck, C. Sauvan, & J. Hugonin, *Light Interaction with Photonic and Plasmonic Resonances*, Laser & Photonics Reviews **12**(5), 1700113 (2018).

[115] P. D. Lax & R. S. Phillips, *Scattering theory*, volume 26 of *Pure and Applied Mathematics*, Academic Press, Boston, second edition edition, 1989.

[116] P. D. Lax & R. S. Phillips, *Numerical relativity: a review*, Archive for Rational Mechanics and Analysis **40**, 268–280 (1971).

[117] E. Leaver, *An analytic representation for the quasi-normal modes of Kerr black holes*, Proc. R. Soc. London, Ser. A **402**, 285–298 (1985).

[118] P. T. Leung, S. Y. Liu, S. S. Tong, & K. Young, *Time-independent perturbation theory for quasinormal modes in leaky optical cavities*, Phys. Rev. A **49**, 3068–3073 (Apr 1994).

[119] P. T. Leung, S. Y. Liu, & K. Young, *Completeness and orthogonality of quasinormal modes in leaky optical cavities*, Phys. Rev. A **49**, 3057–3067 (Apr 1994).

[120] P. T. Leung, Y. T. Liu, W. M. Suen, C. Y. Tam, & K. Young, *Perturbative approach to the quasinormal modes of dirty black holes*, Phys. Rev. **D59**, 044034 (1999).

[121] J. Li, A. H.-D. Cheng, & C.-S. Chen, *A comparison of efficiency and error convergence of multiquadric collocation method and finite element method*, Engineering Analysis with Boundary Elements **27**(3), 251–257 (2003).

[122] K. Lin & W.-L. Qian, *A Matrix Method for Quasinormal Modes: Schwarzschild Black Holes in Asymptotically Flat and (Anti-) de Sitter Spacetimes*, Class. Quant. Grav. **34**(9), 095004 (2017).

[123] H. Liu, W.-L. Qian, Y. Liu, J.-P. Wu, B. Wang, & R.-H. Yue, *On an alternative mechanism for the black hole echoes*, 4 2021.

[124] E. Maggio, L. Buoninfante, A. Mazumdar, & P. Pani, *How does a dark compact object ringdown?*, (6 2020).

[125] M. Maggiore, *Gravitational Waves: Volume 2: Astrophysics and Cosmology*, OUP Oxford, 2018.

[126] M. Maggiore, *Physical Interpretation of the Spectrum of Black Hole Quasinormal Modes*, Phys. Rev. Lett. **100**, 141301 (Apr 2008).

[127] A. Martinez, *Resonance free domains for non globally analytic potentials*, Ann. Henri Poincaré **3**(4), 739–756 (2002).

[128] A. Medved & D. Martin, *A Note on quasinormal modes: A Tale of two treatments*, Gen. Rel. Grav. **37**, 1529–1539 (2005).

[129] R. Mennicken & M. Möller, *Non-Self-Adjoint Boundary Eigenvalue Problems*, ISSN, Elsevier Science, 2003.

[130] W. B. Montrieux, *Estimation de résolvante et construction de quasimode près du bord du pseudospectre*, 2013.

[131] W. B. Montrieux & J. Sjöstrand, *Almost sure Weyl asymptotics for non-self-adjoint elliptic operators on compact manifolds*, Ann. Fac. Sci. Toulouse, Math. (6) **19**(3-4), 567–587 (2010).

[132] I. G. Moss, *Can you hear the shape of a bell?: Asymptotics of quasinormal modes*, Nuclear Physics B - Proceedings Supplements **104**(1), 181–184 (2002), Proceedings of the International Meeting on Quantum Gravity and Spectral Geometry.

[133] L. Motl, *An Analytical computation of asymptotic Schwarzschild quasinormal frequencies*, Adv. Theor. Math. Phys. **6**, 1135–1162 (2003).

[134] L. Motl & A. Neitzke, *Asymptotic black hole quasinormal frequencies*, Adv. Theor. Math. Phys. **7**(2), 307–330 (2003).

[135] E. Navarro, C. Wu, P. Chung, & J. Litva, *Application of PML superabsorbing boundary condition to non-orthogonal FDTD method*, Electronics Letters **30**(20), 1654–1656 (1994).

[136] A. Nicolet & G. DemÃ©sy, *Finite Elements for Electrodynamics and Modal Analysis of Dispersive Structures*, 2016.

[137] H.-P. Nollert, *Quasinormal modes of Schwarzschild black holes: The determination of quasinormal frequencies with very large imaginary parts*, Phys. Rev. **D47**, 5253–5258 (1993).

[138] H.-P. Nollert, *About the significance of quasinormal modes of black holes*, Phys. Rev. **D53**, 4397–4402 (1996).

[139] H.-P. Nollert, *Topical Review: Quasinormal modes: the characteristic 'sound' of black holes and neutron stars*, Class. Quant. Grav. **16**, R159–R216 (1999).

[140] H.-P. Nollert & R. H. Price, *Quantifying excitations of quasinormal mode systems*, J. Math. Phys. **40**, 980–1010 (1999).

[141] H.-P. Nollert & B. G. Schmidt, *Quasinormal modes of Schwarzschild black holes: Defined and calculated via Laplace transformation*, Phys. Rev. **D45**(8), 2617 (1992).

[142] S. Nonnenmacher & M. Vogel, *Local eigenvalue statistics of one-dimensional random non-selfadjoint pseudo-differential operators*, arXiv:1711.05850 (2018).

[143] S. A. Orszag, *Numerical methods for the simulation of turbulence*, The Physics of Fluids **12**(12), II–250 (1969).

[144] S. A. Orszag, *Comparison of pseudospectral and spectral approximation*, Studies in Applied Mathematics **51**(3), 253–259 (1972).

[145] M. Ould El Hadj, T. Stratton, & S. R. Dolan, *Scattering from compact objects: Regge poles and the complex angular momentum method*, Phys. Rev. D **101**(10), 104035 (2020).

[146] R. Panosso Macedo, *Comment on "Some exact quasinormal frequencies of a massless scalar field in Schwarzschild spacetime"*, Phys. Rev. **D99**(8), 088501 (2019).

[147] R. Panosso Macedo, *Hyperboloidal framework for the Kerr spacetime*, Class. Quant. Grav. **37**(6), 065019 (2020).

[148] R. Panosso Macedo, J. L. Jaramillo, & M. Ansorg, *Hyperboloidal slicing approach to quasi-normal mode expansions: the Reissner-Nordström case*, Phys. Rev. **D98**(12), 124005 (2018).

[149] R. Penrose, *Asymptotic properties of fields and space-times*, Phys. Rev. Lett. **10**, 66 (1963).

[150] R. Penrose, *Zero rest-mass fields including gravitation: asymptotic behaviour*, (1965).

[151] A. Perez & D. Sudarsky, *Dark energy from quantum gravity discreteness*, Phys. Rev. Lett. **122**(22), 221302 (2019).

[152] F. Pled & C. Desceliers, *Review and Recent Developments on the Perfectly Matched Layer (PML) Method for the Numerical Modeling and Simulation of Elastic Wave Propagation in Unbounded Domains*, Archives of Computational Methods in Engineering , 1–48 (2021).

[153] D. Pook-Kolb, O. Birnholtz, J. L. Jaramillo, B. Krishnan, & E. Schnetter, *Horizons in a binary black hole merger II: Fluxes, multipole moments and stability*, (6 2020).

[154] R. H. Price & K. S. Thorne, *Membrane Viewpoint on Black Holes: Properties and Evolution of the Stretched Horizon*, Phys. Rev. D **33**, 915 (1986).

[155] R. H. Price & V. Husain, *Model for the completeness of quasinormal modes of relativistic stellar oscillations*, Phys. Rev. Lett. **68**, 1973–1976 (Mar 1992).

[156] W.-L. Qian, K. Lin, C.-Y. Shao, B. Wang, & R.-H. Yue, *On asymptotical quasinormal mode spectrum for piecewise approximate effective potential*, arXiv:2009.11627 (9 2020).

[157] B. Raffaelli, *Strong gravitational lensing and black hole quasinormal modes: Towards a semiclassical unified description*, Gen. Rel. Grav. **48**(2), 16 (2016).

[158] T. Regge, *Analytic properties of the scattering matrix*, Nuovo Cimento (Italy) Divided into Nuovo Cimento A and Nuovo Cimento B **Vol: (10) 8** (6 1958).

[159] T. Regge & J. A. Wheeler, *Stability of a Schwarzschild Singularity*, Physical Review **108**(4), 1063–1069 (Nov. 1957).

[160] J. A. Roden & S. D. Gedney, *Efficient implementation of the uniaxial-based PML media in three-dimensional nonorthogonal coordinates with the use of the FDTD technique*, Microwave and Optical Technology Letters **14**(2), 71–75 (1997).

[161] C. Runge, *Über empirische Funktionen und die Interpolation zwischen äquidistanten Ordinaten*, Zeitschrift für Mathematik und Physik **46**(224-243), 20 (1901).

[162] C. Sauvan, J.-P. Hugonin, I. Maksymov, & P. Lalanne, *Theory of the spontaneous optical emission of nanosize photonic and plasmon resonators*, Physical Review Letters **110**(23), 237401 (2013).

[163] P. J. Schmid, *Nonmodal Stability Theory*, Annual Review of Fluid Mechanics **39**(1), 129–162 (2007).

[164] B. Schmidt, *On relativistic stellar oscillations*, Gravity Research Foundation essay (1993).

[165] B. Simon, *Resonances in One Dimension and Fredholm Determinants*, Journal of Functional Analysis **178**(2), 396–420 (2000).

[166] J. Sjöstrand, *Lecture notes : Spectral properties of non-self-adjoint operators*, Siminar in journée d'ÉQUATIONS AUX DÉRIVÉES PARTIELLES, (2009) .

[167] J. Sjöstrand, *Lectures on resonances*, version préliminaire, printemps (2002) http://sjostrand.perso. math.cnrs.fr/Coursgbg.pdf .

[168] J. Sjöstrand, *Geometric bounds on the density of resonances for semiclassical problems*, Duke Mathematical Journal **60**, 1–57 (1990).

[169] J. Sjöstrand, *Non-Self-Adjoint Differential Operators, Spectral Asymptotics and Random Perturbations*, Pseudo-Differential Operators, Springer International Publishing, 2019.

[170] J. Sjöstrand, *Weyl law for semi-classical resonances with randomly perturbed potentials*, Number 136 in Mémoires de la Société Mathématique de France, Société mathématique de France, 2014.

[171] J. Sjöstrand & M. Zworski, *Asymptotic distribution of resonances for convex obstacles*, Acta Mathematica **183**(2), 191 – 253 (1999).

[172] J. Sjöstrand & M. Zworski, *Fractal upper bounds on the density of semiclassical resonances*, Duke Mathematical Journal **137**(3), 381 – 459 (2007).

[173] P. Stefanov, *Sharp upper bounds on the number of the scattering poles*, Journal of Functional Analysis **231**(1), 111 – 142 (2006).

[174] L. C. Stein, *qnm: A Python package for calculating Kerr quasinormal modes, separation constants, and spherical-spheroidal mixing coefficients*, J. Open Source Softw. **4**(42), 1683 (2019).

[175] B. Stout, R. Colom, N. Bonod, & R. C. McPhedran, *Spectral expansions of open and dispersive optical systems: Gaussian regularization and convergence*, **23**(8), 083004 (aug 2021).

[176] S.-H. Tang & M. Zworski, *Resonance expansions of scattered waves*, Communications on Pure and Applied Mathematics **53**(10), 1305–1334 (2000).

[177] K. Thorne, R. Price, & D. MacDonald, *Black holes: the membrane paradigm*, Yale University Press, New Haven, 1986.

[178] L. N. Trefethen, *Spectral methods in MATLAB*, SIAM, 2000.

[179] L. N. Trefethen, A. E. Trefethen, S. C. Reddy, & T. A. Driscoll, *Hydrodynamic Stability Without Eigenvalues*, Science **261**(5121), 578–584 (1993).

[180] L. Trefethen & M. Embree, *Spectra and Pseudospectra: The Behavior of Nonnormal Matrices and Operators*, Princeton University Press, 2005.

[181] B. R. Vainberg, *Exterior elliptic problems that depend polynomially on the spectral parameter, and the asymptotic behavior for large values of the time of the solutions of nonstationary problems*, Mat. Sb. (N.S.) **92**(134), 224–241 (1973).

[182] M. Vogel, *Spectral statistics of non-selfadjoint operators subject to small random perturbations*, Séminaire Laurent Schwartz — EDP et applications (2016-2017), talk:19.

[183] R. M. Wald, *General Relativity*, Chicago University Press, 1984.

[184] H. Walther, B. T. H. Varcoe, B.-G. Englert, & T. Becker, *Cavity quantum electrodynamics*, Reports on Progress in Physics **69**(5), 1325–1382 (apr 2006).

[185] N. Warburton & et. al., *The Black Hole Perturbation Toolkit*, In preparation.

[186] C. M. Warnick, *On quasinormal modes of asymptotically anti-de Sitter black holes*, Commun. Math. Phys. **333**(2), 959–1035 (2015).

[187] C. Wu, E. A. Navarro, P. Y. Chung, & J. Litva, *Modeling of waveguide structures using the nonorthogonal FDTD method with a PML absorbing boundary*, Microwave and Optical Technology Letters **8**(4), 226–228 (1995).

[188] J. Yang, *Lecture notes: A primary introduction to spectral theory*, (2019).

[189] A. Zenginoglu, *A Geometric framework for black hole perturbations*, Phys. Rev. **D83**, 127502 (2011).

[190] F. J. Zerilli, *Gravitational Field of a Particle Falling in a Schwarzschild Geometry Analyzed in Tensor Harmonics*, Phys. Rev. D **2**, 2141–2160 (Nov 1970).

[191] Y. J. Zhang, J. Wu, & P. T. Leung, *High-frequency behavior of w-mode pulsations of compact stars*, Phys. Rev. D **83**, 064012 (Mar 2011).

[192] M. Zworski, *Distribution of poles for scattering on the real line*, Journal of Functional Analysis **73**(2), 277 – 296 (1987).

[193] M. Zworski, *Resonances in physics and geometry*, Notices Amer. Math. Soc. **46**, 319–328 (1999).

[194] M. Zworski, *Mathematical study of scattering resonances*, Bulletin of Mathematical Sciences **7**(1), 1–85 (2017).